ANALYSIS AND CONTROL OF LINEAR PERIODICALLY TIME VARYING SYSTEMS

by

NORMAN M. WERELEY

Master of Science in Aeronautics and Astronautics
Massachusetts Institute of Technology (1987)

Bachelor of Mechanical Engineering (Honors)
McGill University (1982)

SUBMITTED TO THE
DEPARTMENT OF AERONAUTICS AND ASTRONAUTICS
IN PARTIAL FULFILLMENT OF THE REQUIREMENTS
FOR THE DEGREE OF

DOCTOR OF PHILOSOPHY

at the

MASSACHUSETTS INSTITUTE OF TECHNOLOGY

February 1991

Signature of Author ____
Department of Aeronautics and Astronautics
November 30, 1990

Certified by _____
Steven R. Hall
Assistant Professor, Department of Aeronautics and Astronautics
Thesis Supervisor

Certified by ____
Norman D. Ham
Professor, Department of Aeronautics and Astronautics

Certified by _____
Andreas H. von Flotow
Associate Professor, Department of Aeronautics and Astronautics

Certified by _____
Wallace E. VanderVelde
Professor, Department of Aeronautics and Astronautics

Accepted by _____
Professor Harold Y. Wachman
Chairman, Department Graduate Committee

[Page Left Blank]

ANALYSIS AND CONTROL OF LINEAR PERIODICALLY TIME VARYING SYSTEMS

by

NORMAN MARK WERELEY

Submitted to the Department of Aeronautics and Astronautics
on November 30, 1990, in partial fulfillment of the
requirements for the degree of
Doctor of Philosophy
in the
Field of Estimation and Control

Abstract

The analysis of linear periodically time varying systems has classically been of interest. However, an analysis and control theory for linear time periodic (LTP) systems has not been developed in an operator theoretic context that is comparable to the theory for linear time invariant (LTI) systems.

The operator theoretic framework developed in this thesis takes advantage of the signal spaces identified in the classical works of Floquet and Hill of *geometrically periodic* (GP) and *(complex) exponentially modulated periodic* (EMP) signals. The linear operator that maps GP input signals to GP output signals is a Fredholm integral operator. Within this integral operator framework, poles, transmission zeroes, principal gains (singular values), and their associated directional properties can be rigorously defined. However, the integral operator approach does not lead to computational methods. The linear operator that maps EMP input signals to EMP output signals is called the *harmonic transfer function*, which can be viewed as an infinite dimensional harmonic balance that maps the Fourier coefficients of the EMP input signals to the Fourier coefficients of the EMP output signals. The harmonic balance approach is most useful in developing computational methods for poles, transmission zeroes, principal gains, and their associated directional properties.

This operator theoretic framework also leads to a generalization of the Nyquist criterion for multivariable LTI systems to LTP systems. An extensive treatment of open loop stability of the Hill equation with sinusoidal parametric excitation (the Mathieu equation), and with rectangular parametric excitation (the Meissner equation), is presented. The LTP Nyquist test is compared to the classical Floquet theory, as well as numerous sufficient conditions presented in the literature, for the Mathieu and Meissner equations.

Generalization of the Nyquist criterion leads to the extension of the Small Gain Theorem, and other stability robustness notions, to LTP systems. Stability robustness properties of the steady state linear quadratic regulator for LTP systems are determined using these tools. In addition, a compensation methodology is developed for weakly periodic systems that treats the periodic effects as a modeling error, and permits the application of LTI synthesis tools to weakly periodic systems.

Thesis Committee: Professor Steven R. Hall, Chairman
Professor Norman D. Ham
Professor Wallace E. Vander Velde
Professor Andreas H. von Flotow

[Page Left Blank]

Acknowledgement

At this final stage of my formal education, it is important to reflect on the individuals and organizations that have contributed so much to my development as a scientist and an engineer. Unfortunately, it is almost impossible to do justice to the vast amounts of emotional, financial, and technical support that I have received over the past three years in as small a space as I have in this acknowledgement.

For any graduate student, the wellspring from which his creativity flows undoubtedly has as its source the advisors that make up his doctoral committee. Prof. Steven R. Hall has worked with me through many a late night preparing conference mats, examining some technical detail, or discussing the relative merits of coffee versus ginger ale. However, coffee has been the crutch by which a multitude of graduate students has written many a journal article, and so I offer no apologies for my addiction. Prof. Hall managed to maintain my research assistantship over most of the course of my tenure as a doctoral student at MIT, notwithstanding various dire threats from my mother, and for that he deserves special note. Prof. Hall provided financial support through an internal MIT grant, and a Boeing Helicopter research grant. Prof. Norman D. Ham is an expert in helicopter rotor aeroelasticity, whereas it remains only an aspiration on my part. As a result, I relied heavily on discussion with Prof. Ham in this area to develop my own understanding of the aeroelasticity of helicopter rotor blades. Prof. Wallace E. Vander Velde provided academic guidance for virtually my entire stay at MIT, but most importantly provided excellent comments on his reading of my thesis. Prof. Andreas von Flotow and I spent a few months studying dynamic instabilities of tethered satellites, active control of machinery mounts, digging a basement and pouring concrete, and installing massive wooden beams (where I believe my weightlifting training was of fundamental value). Prof. von Flotow is responsible for fueling my desire to buy a house so that I could have a construction project of my own.

The doctoral program at MIT is intense, and has many rewards. But probably the greatest reward anyone can have is the love of his wife and family. My wife Jong-on Hahm, sat through many soliloquies on doubly coprime factorizations, Fredholm determinants, quasi–Toeplitz operators, and Nyquist contours, and never batted an eyelash. Of course, she made me sit through several equally long soliloquies about LGN lesions and some weird animal called a hippocampus...

My parents, Duane and Agathe Wereley, and my wife's parents, Doochan and Dong Woo Hahm, deserve a lot of credit for always providing the kind of support only parents can give.

Finally, my office mates have spent numerous hours in argument and debate about every topic in control and estimation theory, and every other topic as well. Mathieu Mercadal and I have spent countless hours drinking coffee, barbequeing on my gas grill, and digging holes in which to plant piers for my deck. It is doubtful that I would have survived MIT without his special brand of humor. Dave Vos taught me the intricacies of the Dutch vernacular, and participated in many technical discussions while we struggled through several courses together. Darryl Pines has sat in many a chalkboard session while new ideas were worked and seemed to always ask just the right question to define the research problem in profound ways. Chris van Schalkwyk and I struggled up the learning curve in TEXand LATEX, the typesetting software used to produce this thesis. But more importantly, Chris was also one of the coffee generation. Finally, Anna Roe let me play LEGO with Hanju for countless enjoyable hours, and let me teach Hanju how to play Godzilla with cement trucks with all of the appropriate sound effects...

Contents

List of Figures

11

List of Tables

Glossary of Acronyms

ARE	Algebraic Riccati Equation
CW	Clockwise
CCW	Counterclockwise
CMRDE	Control Matrix Riccati Differential Equation
DF	Describing Function
EMP	Exponentially Modulated Periodic (signal)
GP	Geometrically Periodic (signal)
HB	Harmonic Balance
HHC	Higher Harmonic Control
HTF	Harmonic Transfer Function
IBC	Individual Blade Control
LQE	Linear Quadratic Estimator (or Kalman filter)
LQG	Linear Quadratic Gaussian
LQR	Linear Quadratic Regulator
LTI	Linear Time Invariant
LTP	Linear Time Periodic
LTV	Linear Time Varying
MIMO	Multi–Input Multi–Output
ODE	Ordinary Differential Equation
SISO	Single–Input Single–Output
SVD	Singular Value Decomposition

Glossary of Symbols

$(\dot{\cdot})$ Temporal derivative

$(\cdot)'$ Spatial or nondimensional derivative

$(\cdot)_n$ Fourier coefficient of $(\cdot)$

$(\cdot)^\sim$ Complex conjugate of $(\cdot)$

$(\cdot)^*$ Hermitian or complex conjugate transpose $(\cdot)$

j $\sqrt{-1}$, an imaginary number

n_p Number of unstable open loop poles

t_0 Initial time

C Field of complex numbers

$\underline{\text{GM}}$ Downward gain margin

$\overline{\text{GM}}$ Upward gain margin

PM Phase margin

R Field of real numbers

T Fundamental period of an LTP system

Z Set of integers

$\boldsymbol{x}(t)$ State vector

$\boldsymbol{u}(t)$ Control vector

$\boldsymbol{y}(t)$ Measurement or observation vector

$\boldsymbol{A}$ Time invariant dynamics matrix

$\boldsymbol{B}$ Time invariant control distribution matrix

$\boldsymbol{C}$ Time invariant measurement matrix

$\boldsymbol{D}$ Time invariant feedforward matrix

$\boldsymbol{I}$ Identity matrix

$\boldsymbol{Q}$ Exponential rate matrix of Floquet solution

$A(t)$ Time periodic dynamics matrix

$B(t)$ Time periodic control distribution matrix

$C(t)$ Time periodic measurement matrix

$D(t)$ Time periodic feedforward matrix

$P(t,\tau)$ Time periodic portion of Floquet solution

$P(t)$ Time periodic portion of Floquet solution for $t_0 = 0$

$P_c(t)$ Time periodic solution of matrix Riccati ODE

$Q_c(t)$ Time periodic state weighting matrix

$R_c(t)$ Time periodic control weighting

$\bar{A}$ Dynamic integral operator (or monodromy matrix, $\Phi(T,0)$)

$\bar{B}$ Control distribution integral operator

$\bar{C}$ Measurement integral operator

$\bar{D}$ Feedforward integral operator

$\bar{I}$ Identity integral operator

$\mathcal{A}$ Toeplitz form of the time periodic dynamics matrix

$\mathcal{B}$ Toeplitz form of the time periodic control distribution matrix

$\mathcal{C}$ Toeplitz form of the time periodic measurement matrix

$\mathcal{D}$ Toeplitz form of the time periodic feedforward matrix

$\widehat{\mathcal{G}}(s)$ Harmonic transfer function

$\mathcal{I}$ Toeplitz form of the identity matrix

$\mathcal{N}$ Modulation frequency matrix

$\mathcal{P}$ Toeplitz form of the time periodic portion of Floquet solution

$\mathcal{P}_c$ Toeplitz form of the time periodic solution of CMRODE

$\mathcal{X}$ Harmonics of state vector in block vector form

$\mathcal{U}$ Harmonics of control vector in block vector form

$\mathcal{Y}$ Harmonics of measurement vector in block vector form

$\Delta(s)$ Open loop Hill determinant

$\Delta_{cl}(s)$ Closed loop Hill determinant

ω Frequency variable

ω_p Pumping or fundamental frequency of an LTP system

ξ_0 Initial condition on the states

ζ Damping ratio

$\Phi(t, \tau)$ State transition matrix

$\Phi(t + T, t)$ Monodromy matrix at time t

$\Phi(T, 0)$ (Fundamental) monodromy matrix

$\circ$ Schur product or element-by-element matrix multiply [53, page 646]

$\mathrm{Im}(\cdot)$ Imaginary part of $(\cdot)$

$\mathrm{Re}(\cdot)$ Real part of $(\cdot)$

Chapter 1

Introduction

In this thesis, plants that are modeled by linear differential equations with periodically time varying parameters are examined. The canonical form of the *Hill equation*, which is the most pervasive periodic differential equation used in modeling physical processes, is a second order oscillator of the form

$$\ddot{x}(t) + [a - 2q\psi(t)]x(t) = 0 \tag{1.1}$$

in which $\psi(t) = \psi(t + T)$ and T is the fundamental period. The time periodic parameter, $\psi(t)$, is often referred to as the *parametric excitation*. The primary motivation for studying such equations is due to the fact that they model important physical processes, such as the flapping of the helicopter rotor blade in forward flight.

The primary thrust of this thesis is to develop analysis tools for linear time periodic (LTP) systems, such as the one above, that rely on an operator representation of the periodic differential equation. Once the appropriate operator has been identified, its properties will be discussed and quantified. The feedback control of the LTP system can then be developed in this context.

1.1 Linear Time Periodic Systems

One class of linear time periodic systems is called a parametrically excited system, due to one or several parameters of the problem varying with time. Parametrically excited systems are widespread, and very often this parametric excitation takes the form of a periodically time varying coefficient.

Many physical systems can be modeled as a Hill equation having a sinusoidal parametric excitation, that is, $\psi(t) = \cos \omega_p t$, which results in the canonical form of the Mathieu equation

$$\ddot{x}(t) + (a - 2q \cos \omega_p t) x(t) = 0 \qquad (1.2)$$

where classically the *pumping frequency*, $w_p = 2$, implying a *pumping period* of $T = \pi$. Here, a represents the constant portion of the time periodic coefficient of $x(t)$, and q represents the amplitude of the time periodic variation. Clearly, the Mathieu equation reduces to a simple harmonic oscillator for $q = 0$. The parameter q is often referred to as the *pumping amplitude* or the *amplitude of parametric excitation*. Dissipation is added to the Mathieu equation in the usual way, resulting in the canonical form of the lossy Mathieu equation

$$\ddot{y}(t) + 2\zeta \dot{y}(t) + (\bar{a} - 2q \cos \omega_p t) y(t) = 0 \qquad (1.3)$$

where ζ is the damping ratio. The Mathieu equation can be obtained from the lossy Mathieu equation using the transformation [67,72,83]

$$x(t) = e^{\zeta t} y(t) \qquad (1.4)$$

such that $a = \bar{a} - \zeta^2$. In much of the literature, the Mathieu equation is studied in lieu of the lossy Mathieu equation due to this transformation. Both the damped and undamped forms of the Mathieu equation are frequently encountered in the literature. The Mathieu equation was originally discovered in the study of the vibrations of stretched elliptical membranes [68], and subsequently in the study of elliptical waveguides [72], gravitationally stabilized earth pointing satellites [51,89], quadrupole mass spectrometry [20], the rolling motion of ships [1], the dynamics of a micromechanical tuning fork gyroscope [57], and in other applications too numerous to mention here. A comprehensive historical review and discussion of experimental results associated with the Mathieu equation has been provided by McLachlan [72], with an updated treatment by Richards [83]. It is certainly curious that in spite of the simple form of the parametric excitation in the Mathieu equation, a closed form solution has eluded the best efforts of a considerable number of researchers. Most have relied on approximate analyses such as those outlined by Richards [83].

Hill [46,47] encountered a similar form of equation,

$$\ddot{x}(t) + p(t) x(t) = 0 \qquad (1.5)$$

18

in his study of the motion of lunar perigee, where $p(t) = p(t+T)$, and developed an infinite determinant methodology for determining the stability of this equation. Hill's work was of profound importance and provides a fundamental building block in the analysis of LTP systems as presented in this thesis. Also, the above equation is of the same form as (1.1), from which the Hill equation derives its name. Linear time periodic systems have continued to be of interest in the study of spacecraft and orbital dynamics, and is well documented by Hughes [51], and Szebehely [98].

In his study of the motion of the side rods of locomotives, Meissner [74] encountered a Hill equation of the form (1.1) where $\psi(t)$ is a unit rectangular wave. The dissipative, or lossy, Meissner equation can also be transformed to a Hill equation via a transformation similar to that in (1.4). The lossy Meissner equation is useful because it can be viewed as a pair of constant coefficient second order oscillators with known analytical solutions, each applicable in alternating time intervals. Approximate numerical techniques for the stability analysis of Hill equations have been developed using the lossy Meissner equation [80], which Richards [85] later refined.

An important class of LTP systems are those modeling rotating machinery, especially rotors. The rigid out-of-plane flapping of a helicopter blade can be modeled as a second order oscillator with time periodic stiffness and damping terms in forward flight, as shown in a textbook by Johnson [52, page 602], and in work at MIT by McKillip [70,71]. The *advance ratio*, a parameter that is of fundamental importance to helicopter dynamics and increases with the speed of forward flight, can be interpreted as the pumping amplitude. The control of helicopter vibrations was the original motivation for the work in this thesis [41,42,43]. A second type of rotating machine that is described by a time periodic model is the wind turbine [27,94].

All of the linear time periodic systems described above have time periodic parametric excitation due to the underlying physics of the problem. However, a second class of linear time periodic systems arises when the requirements of a control system introduce time periodic effects.

A *multirate system* is a continuous time linear time invariant system model to which a base sampling interval, T, applies. The sampling intervals of the multirate system's control and output signals are assumed to be integer multiples of the base sampling interval. If we follow the lead of Araki and Yamamoto [2], and define the *model rate sampling interval,*

T_0, as the sampling period to which all of the sampling devices are synchronized, then a periodically time varying *discrete* time equivalent of the linear time invariant system model results. Some of the analysis results that have been developed for this type of system model resemble those developed in this thesis for linear (continuous) time periodic systems.

In some cases, the actuation requirements induce periodically time varying terms on the system model. For example, if a helicopter pilot sits in a nonrotating reference frame with respect to inertial space, then the control of blade pitch of a rotating helicopter blade takes place in a rotating reference frame. In order for the pilot to introduce a change in longitudinal and lateral cyclic blade pitch from the nonrotating to the rotating reference frames, a device called a *swashplate* is used; a detailed discussion is presented by Johnson [52]. Essentially, the swashplate introduces control distribution terms that are proportional to sinusoids, so that the pilot's constant lateral and longitudinal cyclic pitch commands are *wobbled* (or modulated by sine and cosine) by the swashplate in order to induce the required cyclic pitch variations.

In some cases, the swashplate can actually improve the bandwidth characteristics of the actuator. In a study by Ham, Wereley and von Ellenreider [42,43] of a three bladed tilt rotor application, it was determined that the third in-plane cyclic bending mode had a natural frequency in close proximity to the 4/rev frequency. It was shown that the disturbance spectrum was essentially harmonic due to interference effects as the rotor blade passed the wing, and these interference effects contributed to a significant 4/rev harmonic airload. This situation can cause undesirable vibrations to occur, so that active vibration control was proposed, using the individual-blade-control methodology. At the time of the study, the highest bandwidth actuator that was suitable for this application had a bandwidth of only 3/rev. However, by wobbling 3/rev cyclic pitch control signals using the swashplate, it may be possible to inject sufficient control energy at the 4/rev frequency to significantly reduce these vibration levels. Thus, the periodic effects of the swashplate must be included in the system model in order to achieve the desired performance. This particular study was a primary motivation for the work in this thesis.

Linear time periodic dynamics are often imposed by the design of a sensor. In a thesis by King [57], a micromechanical tuning fork gyroscope was designed for which the gyroscopic response to an input rate about the longitudinal axis between the tines of the tuning fork is described by a second order linear time periodic system model. King showed that the

20

linear time periodic effects are substantial for high frequency operating points of the tuning fork gyroscope, mainly by comparing the responses of the LTP simulation to a simulation where the underlying dynamics were time invariant. Thus, in order to exploit some of the beneficial effects that might be realized by operating the gyroscope in the high frequency range, these periodic effects must be included in the sensor model.

Without a doubt, LTP systems have a vast number of applications in the engineering sciences, especially in the aerospace sciences. Thus, in this thesis, the analysis and control of linear periodically time varying systems will be studied. Although several analysis methods and control strategies have been developed in the past, none of these methodologies have been developed in an operator theoretic context, which will be a central theme of this thesis.

1.2   Linear Operators for LTP Systems

The term *operator* is usually reserved in this thesis to denote the map from an input signal space to an output signal space. The notion of the operator is of fundamental importance in control theory. Properties of linear systems such as stability, controllability, and observability, can be viewed as properties of the operator.

The analysis of linear time periodic (LTP) systems has long suffered from the lack of a clearly defined linear operator that relates signals of fundamental importance to LTP systems. For linear time invariant (LTI) systems, the signal of fundamental importance is the *complex exponential* signal

$$u(t) = u_0 e^{j\omega t} \tag{1.6}$$

which is often referred to as a sinusoidal signal. When a complex exponential input signal is injected into an LTI system, the *total output response* is the superposition of two responses. The first is due to the excitation of the system internal modes, so that this *transient output response* occurs at the system eigenfrequencies. The transient output response can be eliminated from the total system response if the initial condition of the states is specified in a certain way that will be described in the sequel. The second response is the *steady state output response* or *complex exponential response* which leads to the concept of the *frequency response*. The frequency response concept can be stated quite succinctly: *when a complex exponential input signal of a given frequency is injected into an LTI system, the steady state output response is a complex exponential signal of the same frequency, but with*

possibly different amplitude and phase.

The Bode gain and phase diagrams are plots, versus frequency, of the change between the input and output signals' amplitude and phase. The linear operator of interest is then the *transfer function*, and relates complex exponential input signals to complex exponential output signals; that is, the input and output signal spaces are equal. The notion of frequency response can easily be extended to multi–input multi–output LTI systems with a few caveats related to directional properties of the *transfer function matrix*. The concepts of stability, controllability, observability, poles, transmission zeroes, principal gains (singular values), and their associated directional properties, can be described in terms of the transfer function matrix.

Richards [83] attempts to develop an operator based analysis theory for LTP systems by examining the response of an LTP system to a complex exponential input. Many authors including McLachlan [72], and D'Angelo [18], have discussed a similar analysis. This approach, although seemingly the obvious extension of the LTI theory, does not lead to a linear operator that maps complex exponential input signals to complex exponential output signals. Instead, this approach leads to a map from a complex exponential input signals to complex exponential output signals modulated by a periodic signal that may contain an infinite number of harmonics of the pumping frequency. By approximating the response of an LTP system by a linear operator that maps complex exponential input signals to complex exponential output signals, the describing function [61] or the harmonic balance [26] approaches were developed. Leonhard showed that attempting to enforce the LTI behavior on an LTP system can lead to grossly inaccurate results. By increasing the number of harmonics that are included in the periodic portion of the output signal, more accurate results can be obtained. The usual procedure is to include only two or three prevalent harmonics.

However, classical treatments of linear time periodic systems have several clues which can lead us to the fundamental input signal space of interest.

In 1883, Floquet [29], in his celebrated theorem on linear time periodic systems, stated that searching for signals that increase geometrically from a given time, to a time a full period away, determines stability of an LTP system. This leads to the notion of a signal that changes geometrically over one period,

$$x(t + T) = zx(t) \quad z \in C \tag{1.7}$$

where T is the fundamental period of the signal $x(t)$. Floquet then demonstrates that a necessary and sufficient condition for stability can be stated in terms of this type of signal. The Floquet results are stated in more modern terminology in Chapter 2. Floquet theory has been the cornerstone of a multitude of papers and textbooks analyzing linear time periodic systems including extensively cited monographs and a textbook by Magnus and Winkler [67,66], McLachlan [72], and textbooks by Richards [83], and D'Angelo [18].

Probably the most significant of the early papers on systems with periodically time varying parameters is the work of Hill [46], which developed an alternative stability theory to that of Floquet. Hill developed an infinite determinant representation of a linear time periodic system based on the notion that periodic solutions of (1.1) could be determined by assuming a solution of the form

$$x(t) = \sum_{n=-\infty}^{\infty} x_n e^{[\mu + j(\omega + n\omega_p)]t} \tag{1.8}$$

where ω_p is the fundamental period of the parametric excitation. Here, $x(t)$ is represented by a complex Fourier series that is modulated by a complex exponential. The determinants involved here are called Hill determinants and have been the object of intense scrutiny in the literature [30,72,83].

The Floquet theory and the Hill determinant theory will be reviewed in detail in Chapter 2. Both of these analysis methodologies are cornerstones in the theory to be developed in this thesis. Moreover, the signals of fundamental interest were apparently discovered over one hundred years ago by Floquet and Hill: *geometrically periodic signals* (1.7), and *complex exponentially modulated periodic signals* (1.8), respectively. However, to the knowledge of the author, no operator theoretic framework, comparable to that of the linear time invariant transfer function, has been developed for linear time periodic systems using these types of signals.

Thus, a primary objective of this thesis is to develop an operator theoretic framework in which to build an analysis and control theory for linear time periodic systems.

1.3 Control of LTP Systems

Few methodologies have been suggested for dealing with the feedback control of LTP systems. The time periodic coefficients in an LTP system render classical frequency domain

approaches based on the Bode frequency response unusable. However, several approaches have been developed using the calculus of variations and parameter optimization procedures.

During the past decade, methodologies have been suggested for actively suppressing helicopter rotor vibrations due to the time periodic aerodynamic effects of the main rotor. Since these vibrations occur at frequencies that are integer multiples of the rotor frequency, these methods are known collectively as *Higher Harmonic Control* (HHC).

The basic notion behind higher harmonic control is to control rotor blades at harmonics of the rotor frequency such that unsteady airloads are canceled. If the swashplate is used, as is usually the case, the swashplate must be controlled at the N/rev frequency. One of the earliest HHC algorithms was suggested by McHugh and Shaw [69] and Shaw and Albion [92]. It is assumed that the control response matrix, $\mathbf{T}$, is known. This matrix relates the sine and cosine components of the N/rev swashplate inputs to the sine and cosine components of the N/rev response of the helicopter. At each step of the algorithm, a harmonic analysis of the measured quantity (either mast forces or accelerations at some fuselage location) is performed. The result is the quadrature components of the force (or acceleration) at the N/rev frequency. The vector of N/rev components is then multiplied by a decoupling matrix, which is the inverse of the control response matrix, to produce the change in commanded N/rev swashplate motion. Under the assumption that the response of the helicopter to N/rev inputs is essentially quasi–steady, this algorithm should eliminate N/rev vibrations in one step (that is, this method should produce *deadbeat* control). It has been shown [41] that the structure of the HHC compensator is essentially a high gain narrow band filter, that is, a high-Q filter, centered at the N/rev frequency, which is the classical compensator that would be implemented if the plant were linear time invariant. This type of compensator produces a notch in the closed loop Bode gain diagram that rejects harmonic inputs at the N/rev frequency. In addition, the HHC compensator was shown to have excellent stability robustness properties. However, further performance gains in HHC cannot be obtained until the quasi–steady assumption is relaxed so that time periodic dynamics can be introduced into the design plant model.

Many methodologies are available that can take into account linear time periodic dynamics. Several pole placement methodologies have been developed that incorporate the Floquet theory. In addition, methodologies based on calculus of variations and parameter optimization approaches have been developed. However, none of these methods directly

address stability robustness issues, nor do they address specific frequency domain design criteria.

Several methodologies have been developed for *pole placement* in linear time periodic systems [56,106,108,109]. Webb, Calico, and Wiesel [106] and others [108,109] developed a methodology to shift the characteristic exponents (that is, the exponential part of the plant pole). Two modes are taken at a time, and constant feedback gains are chosen to improve stability characteristics, that is, to move the characteristic exponents to a more desirable location in the *s*-plane. Kern [56] takes a slightly different approach to achieve essentially the same goal. First a desired stability characteristic is selected by specifying the exponential rate matrix in the Floquet solution. Then, time periodic feedback gains are computed by applying the Floquet result that a linear time periodic system with time periodic dynamics can be transformed to a similar linear time periodic system with time invariant dynamics. The method requires the identification of this time periodic similarity transformation. Several sufficient conditions are stated for the existence of these time periodic feedback gains.

However, these methods have the same drawbacks as their counterparts for LTI systems. Pole placement does not directly design for usual closed loop specifications such as bandwidth, stability robustness (as manifested by gain and phase margin), and other performance specifications in the frequency domain, nor does it directly account for performance specifications in the time domain such as rise time, peak overshoot, etc.

Alternatively, methodologies based on the state space model and the calculus of variations have been applied to linear time periodic systems. The most well known of these is the linear quadratic regulator (LQR) [59], which has been used quite extensively in the control of linear time periodic systems such as in the control of helicopter vibrations [70,71]. The LQR theory formulates the control problem as the constrained optimization of a scalar cost function, which is a quadratic function of the dynamic states and control variables. The optimization is constrained by the dynamic equations of motion which incorporate the effects of the control variables, and the time periodic coefficients, on the plant under consideration. In principle, the LQR methodology can account for the multi–input multi–output nature of the some LTP systems.

The solution of the LQR problem requires the solution of the control matrix Riccati differential equation (CMRDE). The geometric theory of the CMRDE equation was originally

developed by Rodriguez–Canabal [86,87]. A complete theory on the Floquet representation was concurrently developed by Bucy [11], with a lengthy treatise by Bekir and Bucy [4] that includes a FORTRAN computer listing for a general Hamiltonian system. The procedure is relatively straightforward. First the transition matrix of the Hamiltonian system is computed over a complete period of the LTP system. The steady state solution of an equivalent discrete time control Riccati equation is then computed, and is used as the initial condition for the time periodic control matrix Riccati ODE. Thus, the steady state solution of the equivalent discrete time control Riccati equation serves as a periodic generator [87] for the time periodic solution of the CMRDE. The time periodic solution is the steady state solution in this case, and provides a state feedback implementation.

Several authors including Kano and Nishimura [54,55], Bittanti *et al* [8], and Hernandez and Jodar [45], subsequently developed similar procedures and were apparently unaware of the pioneering work of the mid-1970's. Much of the work cited in these papers revolves around detectability (observability) and stabilizability (controllability) conditions for existence of periodic solutions.

However, the LQR methodology does not account for the relative importance of different frequency ranges in closed loop performance. It may be desirable to have high gain over only a small range of frequency, and then accept low gain everywhere else. However, the LQR methodology essentially weights all frequencies equally in the cost function. For example, the helicopter vibration is due predominantly to harmonic disturbances at integer multiples of the rotor frequency, Ω. Therefore, a possible approach might be to weight control lightly, that is, cheap control, at these frequencies, and/or to weight the states heavily at these harmonics of the rotor frequency. Several methods for achieving this have been suggested for the LTI case of the LQR methodology including frequency shaped cost functionals developed by Gupta [40]. The basic approach in [40] to achieve the desired frequency dependent control and state weighting is to augment the plant with second order oscillators that resonate at the appropriate harmonics. This procedure was applied to an LTI model that approximately describes the time periodic dynamics associated with the helicopter vibration problem [24,25]. Interestingly, the structure of the compensator suggested in [24] is essentially the same as that suggested by Shaw [93], as shown in [41].

A second disadvantage of the LQR methodology is that the frequency response of the LTP system is not shaped directly, as is the case for classical Bode compensation of an LTI

26

plant.

The linear quadratic estimator (LQE, or Kalman filter) is the dual problem to the LQR problem, and has essentially the same characteristics as the LQR problem. The LQR and LQE solutions, both at steady state, together with the separation principle, form the basis of the linear quadratic gaussian (LQG) design methodology for time periodic systems. However, the frequency domain properties of the LQG have not been examined, so that there is no systematic approach for incorporating stability robustness ideas into the LQG procedure.

A third basic approach to the control of linear time periodic systems is that of parameter optimization. For example, in a recent article by Calise *et al* [12], static output feedback (that is, feedback using constant gain on the output signals) was used to reduce vibrations due to a periodically time varying helicopter rotor. The basic approach was to optimize a quadratic cost function similar to that of the LQR cost, except the controlled variables are the states associated with the linear time invariant representation of the state dynamics, obtained using the Floquet theory. A numerical method is then developed to optimize the choice of feedback gains, with the constraint that the feedback gains must be constants. However, this article does not address the possibility that a set of time periodic gains might reduce the cost even further, and possibly improve stability robustness properties. Again, the method does not address the importance of designing a feedback control system so that specific stability robustness properties (such as gain and phase margin) result in the closed loop system.

1.4 Scope of Current Research

In this thesis, a frequency domain representation of the LTP system model is developed and its properties derived. Control synthesis techniques can then be developed in the context of this new frequency domain operator in the hope of developing improved insight into the implications of feedback control for LTP systems. In order to characterize open loop behavior, clear notions of poles and transmission zeroes, as well as their associated directional interpretations, must be stated. A clear notion of open loop gain must be introduced, and phase quantified. Notions of stability robustness such as phase and gain margin, especially as reflected by a Nyquist-like criterion would be desirable. Finally, feedback control systems

can be designed, in the context of these operators, so that stability robustness and other performance issues can be dealt with directly and explicitly.

First some comments on the structure of the document. Definitions, theorems, corollaries, and lemmas are numbered using the same counter, with the chapter number as a prefix. For example, Definition 2.1 might be followed by Theorem 2.2, etc. Equations and examples are numbered consecutively, and separately, within a chapter with the chapter number as a prefix.

In Chapter 2, a summary of the elements of linear system theory applicable to periodically time varying systems is presented. In addition, a review of the classical analysis techniques of Floquet and Hill are discussed in the context of modern linear system theory. The first point of view to be taken in determining an operator for LTP systems is an extension of the Floquet theory, and requires a review of applicable integral operator theory. The second methodology that will be used to develop an operator for LTP systems is a generalization of the harmonic balance methodology. Since the complex Fourier series and Toeplitz forms will play a central role in the application of harmonic balance presented in this thesis, relevant areas will be reviewed in detail.

In Chapter 3, a frequency domain representation of the LTP system model is proposed and several of its properties are derived in the context of linear system theory. The fundamental signal of interest is a *geometrically periodic* or *exponentially modulated periodic* signal, and forms the basis for the theoretical development of the chapter. Two approaches developed for describing the frequency response are presented. The first relies on the integral operator theory and is used primarily for analytical work. The second approach is a generalization of the harmonic balance approach and is useful mainly for numerical work. Basic notions such as the transient state response, steady state response, transient output response, and steady state output response are stated in both contexts. Definitions of LTP poles and zeroes and methods for their computation are presented. Finally, methods for plotting the gain of the frequency response are presented using the singular value decomposition of the steady state output response.

In Chapter 4, a Nyquist criterion for LTP systems is presented. The Nyquist criterion is developed using the *eigenloci* of the LTP frequency response obtained from the integral operator approach. The Nyquist criterion is an essential building block in the LTP control theory since it provides a systematic methodology for stability analysis in the frequency do-

main. The Nyquist criterion also provides the motivation for extending stability robustness ideas to LTP systems.

In Chapter 5, stability robustness notions based on the small gain theorem are restated in terms of the LTP frequency response. The LQR methodology is re-examined for LTP systems in order to determine its stability margins, and its dual problem (the Kalman filter or LQE) is also examined. An LTI compensation methodology is suggested for weakly periodic systems using the LTI model embedded in the LTP state space model (that is, the average state space model), where a sufficient condition is used to guarantee stability in the presence of the time periodic effects.

In Chapter 6, conclusions and recommendations for future research are presented.

[Page Left Blank]

Chapter 2

Linear Time Periodic Systems

In this chapter, the mathematical background required for the study of linear time periodic systems is introduced. First, time domain function spaces that will prove to be useful in this research are introduced. In addition, complex Fourier series and their properties are reviewed and the Toeplitz transform, which has some useful properties in this context, is introduced. Basic notions of linear system theory are presented for the specific case of linear time periodic (LTP) systems. No introduction to linear time periodic systems would be complete without a presentation of the classical analysis techniques of Floquet and Hill, and this chapter reviews these procedures with a somewhat more control theoretic flavor than is available in the literature. However, the methodologies of Floquet and Hill will have new and useful interpretations once the linear operator theoretic approaches are developed.

2.1 Mathematical Preliminaries

In this section, some of the basic mathematics that will be used in this thesis are briefly reviewed. A knowledge of basic matrix algebra is presumed, such as the basic operations of matrix algebra, spectral decomposition (eigenstructure), the singular value decomposition, and basic matrix norms.

The set of integers will be denoted by Z. The field of complex numbers will be denoted by C, and the field of real numbers by R. The complex conjugate of $(\cdot)$ will be denoted by $(\cdot)^\sim$. A complex (real) matrix of dimension $n \times m$ will be denoted by $C^{n \times m}$ ($R^{n \times m}$). The transpose of a matrix, $(\cdot)$, will be denoted by $(\cdot)^T$, and the complex conjugate transpose or Hermitian by $(\cdot)^*$.

2.1.1 The Fourier series

First, define a time domain function space that will be of central importance in this thesis.

Definition 2.1 *Consider a matrix function, $A(t)$, defined on the interval $t \in [a,b]$, that takes values in $C^{n \times m}$. If $A(t)$ has the property that $L_2[0,T]$ norm given by the integral*

$$\int_a^b |A(t)|^2 \, dt = \int_a^b A^*(t)A(t)dt \tag{2.1}$$

exists, then $A(t) \in L_2^{n \times m}[a,b]$. □

The above definition can be specialized to vector and scalar functions. The following discussion of orthogonal systems closely follows that of Churchill [16].

Here, the *inner product* of two scalar functions, $\phi_n(t)$ and $\phi_m(t)$, is denoted by $< \phi_m, \phi_n >$, and is defined to be

$$< \phi_m(t), \phi_n(t) > = \int_a^b \phi_m(t)\phi_n^*(t)dt \tag{2.2}$$

The two functions, $\phi_n(t)$ and $\phi_m(t)$, are defined to be *orthogonal* in the interval $t \in [a,b]$ when the inner product

$$< \phi_m, \phi_n > = 0 \tag{2.3}$$

A system of functions, $\{\phi_n(t) | \, n \in Z\}$, where $\phi_n(t) \in L_2[a,b]$, is *orthonormal* in $t \in [a,b]$ if

$$< \phi_m, \phi_n > = \int_a^b \phi_m(t)\phi_n^*(t)dt = \delta_{mn} \quad \forall \, n, m \in Z \tag{2.4}$$

and δ_{mn} is the *Kronecker delta function*. In this thesis, it is generally more convenient to let the indices n and m to run over all integers from $-\infty$ to ∞, that is, the set of all integers Z.

Let $A(t)$ be a matrix function such that $A(t) \in L_2^{n \times m}[a,b]$. The *Fourier coefficients* of $A(t)$, with respect to the orthonormal system $\{\phi_n(t)\}$ are defined as

$$A_n = \int_a^b A(t)\phi_n^*(t)dt \quad \forall \, n \in Z \tag{2.5}$$

The resulting set of Fourier coefficients, $\{A_n | \, n \in Z\}$ constitute the coefficients of the *generalized Fourier series* of $A(t)$,

$$A(t) = \sum_{n=-\infty}^{\infty} A_n \phi_n(t) \tag{2.6}$$

32

The system of functions, $\{\phi_n(t)|\ n \in Z\}$, is said to be *complete* if no other function exists that is orthogonal to all of the functions in the system. If such an orthogonal function exists, then the system is said to be *incomplete*. If the orthonormal system is complete, then the system forms an orthonormal basis in $L_2[a,b]$.

In this thesis, the functions in $L_2[0,T]$ are of primary interest. It is a well known fact [16, page 77] that the system of functions, $\left\{\frac{1}{\sqrt{T}}e^{jn\omega_p t}\middle|\ n \in Z\right\}$, where $\omega_p = 2\pi/T$, form an *orthonormal basis* in $L_2[0,T]$. We refer to ω_p as the *pumping frequency*. The interval $t \in [0,T]$ will be referred to as the *fundamental interval*. The complex exponential associated with the nth basis function, $e^{jn\omega_p t}$, is referred to as the *nth harmonic* or the *n/rev harmonic*. The index n is referred to as the *harmonic number*. Consider a matrix function, $A(t) \in L_2^{n \times m}[0,T]$. The complex Fourier series is given by

$$A(t) = \sum_{n=-\infty}^{\infty} A_n e^{jn\omega_p t} \tag{2.7}$$

where

$$A_n = \frac{1}{T}\int_0^T A(t)e^{-jn\omega_p t}dt \quad \forall n \in Z \tag{2.8}$$

Each A_n can be expressed as the sum of a real and imaginary number,

$$A_n = \begin{cases} A_{nc} + jA_{ns} & n > 0 \\ A_0 & n = 0 \\ A_{nc} - jA_{ns} & n < 0 \end{cases} \tag{2.9}$$

The constant term in the complex Fourier series occurs for $n = 0$,

$$A_0 = \frac{1}{T}\int_0^T A(t)dt \tag{2.10}$$

and represents the mean or average value of $A(t)$. For $n \in Z$ but $n \neq 0$,

$$\begin{aligned} A_{nc} &= \frac{2}{T}\int_0^T A(t)\cos n\omega_p t\, dt \\ A_{ns} &= \frac{2}{T}\int_0^T A(t)\sin n\omega_p t\, dt \end{aligned} \tag{2.11}$$

Thus,

$$A_n = A_{-n}^{\sim} \tag{2.12}$$

Consider a matrix function, $A(t)$, defined for all time, $t \in (-\infty, \infty)$, that takes values in $C^{n \times m}$. If $A(t)$ has the property that

$$A(t+T) = A(t) \quad \forall t \in (-\infty, \infty) \tag{2.13}$$

33

then $A(t)$ is *periodic* with period T, or T-*periodic*. If we consider only that portion of the matrix function defined over the fundamental interval, then we refer to $A(t)$ as bounded if $A(t) \in L_2^{n \times m}[0, T]$.

When the complex Fourier series of $A(t) \in L_2[0, T]$ converges to $A(t)$ on the fundamental interval, it converges to a matrix function of period T that coincides with $A(t)$ on the fundamental interval. This implies that the complex Fourier series represents the *periodic extension* [16] of $A(t)$ for all $t \in (-\infty, \infty)$. In the case where $A(t)$ is T-periodic, and the complex Fourier series is convergent for t in the fundamental interval, then the complex Fourier series represents $A(t)$ for all values of t. We will denote the periodic extension of $A(t) \in L_2^{n \times m}[0, T]$, or a T-periodic matrix function $A(t)$ for which the function defined over the fundamental interval is an $L_2^{n \times m}[0, T]$ function, as $A(t) \in P^{n \times m}[T]$.

The convergence properties of the complex Fourier series form a large body of research, so that only a brief review of convergence properties is presented below.

Theorem 2.2 *Consider the orthonormal basis in $L_2[0, T]$ formed from the complex exponentials, $\frac{1}{\sqrt{T}} e^{j n \omega_p t}$. If $A(t) \in L_2^{n \times m}[0, T]$, then the Fourier series of $A(t)$ converges to $A(t)$ in the $L_2[0, T]$ norm sense.*

Proof: See Theorem 2.3.11 in Rees *et al* [82, page 99]. □

Essentially, the above theorem implies that if $A(t) \in L_2^{n \times m}[0, T]$ then the Fourier series is absolutely convergent. However, a much stronger statement of convergence can be made, if the behavior of $A(t)$ is restricted.

Theorem 2.3 *Let $A(t) \in L_2^{n \times m}[0, T]$ be piecewise smooth, that is, $A(t)$ is continuous and its first derivative is piecewise continuous. Also, assume that $A(0) = A(T)$. Then the convergence of the complex Fourier series*

$$A(t) = \sum_{n=-\infty}^{\infty} A_n e^{j n \omega_p t} \tag{2.14}$$

to $A(t)$ on the fundamental interval is absolute and uniform with respect to t on the fundamental interval.

Proof: See Churchill [16, page 104].

In practice, the above theorem is not very restrictive since the periodically time varying parameters in most engineering systems can be described by a sum of sinusoids of relatively

34

low harmonic number, that is, a truncated Fourier series. However, in the case where $A(t)$ is not continuous, uniform convergence cannot be guaranteed on an interval where $A(t)$ is discontinuous. This lack of uniform convergence for piecewise continuous $A(t)$ is known as *Gibbs phenomenon*.

Many of the convergence properties of the complex Fourier series have been extended to $L_1[0,T]$ (absolutely integrable) functions of bounded variation. The $L_1[0,T]$ functions are a more general class of functions that contains $L_2[0,T]$ functions. For a review of these results, see Chapter 3 in [82].

Here, a very brief review of the Fourier theory has been presented. However, a vast amount of research has been done in this area and the reader is referred to Rees, Shah, and Stanojevic [82] or Churchill [16] for a complete treatment.

2.1.2 The Toeplitz transform

In many instances the manipulation of complex Fourier series is inconvenient, so that an alternative representation of the complex Fourier series would be useful. Thus, the Toeplitz transform is introduced below.

Definition 2.4 (The Toeplitz transform and Toeplitz forms) *Consider the T-periodic matrix function, $A(t) \in L_2^{n \times m}[0,T]$, with associated fundamental period, T, and fundamental frequency, ω_p. $A(t)$ can be expanded in an absolutely convergent complex Fourier series*

$$A(t) = \sum_{n=-\infty}^{\infty} A_n e^{jn\omega_p t} \qquad (2.15)$$

The Toeplitz transform *of $A(t)$, denoted by $T\{A(t)\}$, maps the set of complex Fourier coefficients, $\{A_n | n \in Z\}$, into a doubly infinite block Toeplitz matrix, $\mathcal{A}$, of the form*

$$T\{A(t)\} = \mathcal{A} = \begin{bmatrix} \ddots & \vdots & \vdots & \vdots & \vdots & \vdots & \\ \cdots & A_0 & A_{-1} & A_{-2} & A_{-3} & A_{-4} & \cdots \\ \cdots & A_1 & A_0 & A_{-1} & A_{-2} & A_{-3} & \cdots \\ \cdots & A_2 & A_1 & A_0 & A_{-1} & A_{-2} & \cdots \\ \cdots & A_3 & A_2 & A_1 & A_0 & A_{-1} & \cdots \\ \cdots & A_4 & A_3 & A_2 & A_1 & A_0 & \cdots \\ & \vdots & \vdots & \vdots & \vdots & \vdots & \ddots \end{bmatrix} \qquad (2.16)$$

The Hermitian form, A, is called the **Toeplitz form** *associated with the matrix function,* $A(t)$.   □

An interesting feature of the Toeplitz form of $A(t)$ is that the element in the nth block row and the mth block column depends only on the difference between the two indices, and will thus be denoted by A_{n-m}.

The Toeplitz transform is introduced so that algebraic manipulations associated with sums and products of complex Fourier series of matrix functions can be simplified. It is also useful in transforming time periodic ordinary differential or algebraic equations into time invariant infinite dimensional algebraic equations. The Toeplitz transform has some useful properties in this regard.

Theorem 2.5 (Properties of the Toeplitz transform) *The Toeplitz transform exhibits the following properties:*

1. *Consider the two conformable time periodic matrix functions, $A(t)$ and $B(t)$, with corresponding absolutely convergent complex Fourier series on the fundamental interval. The Toeplitz transform of the product is the product of its transforms,*

$$
\begin{aligned}
\mathcal{T}\{A(t)B(t)\} &= \mathcal{T}\{A(t)\}\mathcal{T}\{B(t)\} \\
&= \mathcal{A}\mathcal{B}
\end{aligned}
\tag{2.17}
$$

2. *Consider the two T-periodic matrices of the same dimension, $C(t)$ and $D(t)$. The Toeplitz transform of the sum of these two matrices is the sum of its transforms*

$$
\begin{aligned}
\mathcal{T}\{C(t) + D(t)\} &= \mathcal{T}\{C(t)\} + \mathcal{T}\{D(t)\} \\
&= \mathcal{C} + \mathcal{D}
\end{aligned}
\tag{2.18}
$$

3. *Consider the T-periodic square matrix function, $P(t) \in L_2^{n \times n}[0,T]$. Suppose that $\dot{P}(t) \in L_2^{n \times n}[0,T]$. The Toeplitz transform of $P(t)$, is given by*

$$
\begin{aligned}
\mathcal{T}\{\dot{P}(t)\} &= \mathcal{N}\mathcal{P} - \mathcal{P}\mathcal{N} \\
&= \mathcal{N}\mathcal{P} + \mathcal{P}\mathcal{N}^*
\end{aligned}
\tag{2.19}
$$

where

$$
\mathcal{N} = \text{blkdiag}\{jn\omega_p I\}
\tag{2.20}
$$

36

Proof: The proof of (1) is an application of *Cauchy's Rule* [58, page 122]. Since the complex Fourier series associated with the matrix functions are absolutely convergent, their product is also absolutely convergent. Since the series are absolutely convergent, then Cauchy's Rule implies that

$$\sum_{n=-\infty}^{\infty} A_n \sum_{m=-\infty}^{\infty} B_m = \sum_{n=-\infty}^{\infty} \left(\sum_{m=-\infty}^{\infty} A_{n-m} B_m \right) \tag{2.21}$$

It is also a well known fact [58, page 122] that the sum of two absolutely convergent series is absolutely convergent, so that (2) follows directly.

The proof of (3) may not seem straightforward, and is presented below. The time periodic square matrix, $P(t)$, can be expanded in the complex Fourier series,

$$P(t) = \sum_{n=-\infty}^{\infty} P_n e^{jn\omega_p t} \tag{2.22}$$

so that its derivative is given by

$$\dot{P}(t) = \sum_{n,=-\infty}^{\infty} jn\omega_p P_n e^{jn\omega_p t} \tag{2.23}$$

The above series is absolutely convergent since it was assumed that $\dot{P}(t) \in L_2^{n \times n}[0,T]$. The element of $T\{\dot{P}(t)\}$ in the nth row block and mth column block, is given by

$$[\dot{P}(t)]_{n-m} = j(n-m)\omega_p P_{n-m} \tag{2.24}$$

Now, $\mathcal{N}$ is a block diagonal matrix. The nth block row of $\mathcal{N}$, when multiplied into the mth block column of $\mathcal{P}$, picks off the block element P_{n-m}. Similarly, multiplying the nth block row of $\mathcal{P}$ into the mth block column of $\mathcal{N}$ picks off the block element P_{n-m}, so that

$$\begin{aligned} [\mathcal{NP} - \mathcal{PN}]_{n,m} &= jn\omega_p I P_{n-m} - P_{n-m} jm\omega_p I \\ &= j(n-m)\omega_p P_{n-m} \end{aligned} \tag{2.25}$$

as required. $\qquad\qquad\qquad\qquad\qquad\qquad\qquad\qquad\qquad\qquad\qquad\qquad\qquad\qquad\square$

2.1.3 Eigenvalues and eigenvectors

The basic results of spectral theory for matrices are presented below in order to establish terminology.

Theorem 2.6 (Similarity transformation) *A matrix $A \in R^{n \times n}$ can be reduced to a diagonal matrix Λ by the similarity transformation $\Lambda = WAV$ if and only if A has a linearly*

independent set of n right eigenvectors. These right eigenvectors are the columns of V, with corresponding left eigenvectors that are the rows of $W = V^{-1}$, and corresponding eigenvalues that are the diagonal entries of Λ. Also, the original matrix A can be reconstructed from its eigenvalues and eigenvectors using the formula, $A = V\Lambda W$.

Proof: See Noble and Daniel [78]. The above decomposition is often called the spectral decomposition of a matrix. □

However, not all square matrices are diagonalizable as described above.

Definition 2.7 (Defective matrices) *A matrix $A \in R^{n \times n}$ that does not have a set of n linearly independent eigenvectors is said to be* **defective.**

This is not, in practice, a limitation since it is always possible to reduce a matrix to Jordan canonical form [78].

2.2 Linear Time Periodic System Theory

In this thesis, the state space plays a fundamental role, so that some of the basic notions are reviewed in this section.

Definition 2.8 (Linear time periodic state space model) *The* **state space model (SSM)** *of a linear time periodic system, S, can be represented by a linear ordinary differential equation called the* **state dynamic equation**

$$\dot{x}(t) = A(t)x(t) + B(t)u(t) \tag{2.26}$$

and a **measurement** *or* **output equation**

$$y(t) = C(t)x(t) + D(t)u(t) \tag{2.27}$$

where the **dynamic matrix,** $A(t) \in P^{n \times n}[T]$, *the* **control distribution matrix,** $B(t) \in P^{n \times m}[T]$, *the* **measurement matrix,** $C(t) \in P^{m \times n}[T]$, *and the* **feed forward matrix,** $D(t) \in P^{m \times m}[T]$, *are all T-periodic. The state vector, $x(t) \in R^n$, the control vector, $u(t) \in R^m$, and the output vector, $y(t) \in R^p$. The state space model, S, is* **square** *if $p = m$. Here, the notation,*

$$S = \left[\begin{array}{c|c} A(t) & B(t) \\ \hline C(t) & D(t) \end{array} \right] \tag{2.28}$$

or $S = [A(t), B(t), C(t), D(t)]$, is adopted to denote the LTP state space model. □

An LTP system, S, is *strictly proper*, if $D(t) \equiv 0 \; \forall t$. The period of the LTP state space model, T, is called the *pumping period* or the *fundamental period*, and corresponds to a *pumping frequency* or *fundamental frequency*, ω_p. It was assumed that $A(t)$ is the periodic extension of an $L_2[0,T]$ matrix function, and similarly for $B(t)$, $C(t)$, and $D(t)$. However, this assumption is somewhat restrictive, and was imposed so that each of these matrices could be expanded in an absolutely convergent complex Fourier series.

Now, let us consider the solution of the homogeneous linear time periodic state dynamic equation, for which the following result is presented in [10].

Theorem 2.9 (State transition matrix and the homogeneous response) *Consider the homogeneous state dynamic equation,*

$$\dot{x}(t) = A(t)x(t) \tag{2.29}$$

If $A(t) \in P^{n \times n}[T]$, then (2.29) always has a solution, called the **homogeneous response,** *of the form,*

$$x_h(t) = \Phi(t, t_0)\xi_0 \tag{2.30}$$

where $\xi_0 = x(0)$. The state transition matrix, $\Phi(t, t_0)$ is the solution of the matrix differential equation,

$$\frac{d}{dt}\Phi(t, t_0) = A(t)\Phi(t, t_0); \quad \Phi(t_0, t_0) = I \tag{2.31}$$

where I is the identity matrix. Since the dynamics matrix is T-periodic, the state transition matrix is also T-periodic, that is,

$$\Phi(t + T, \tau + T) = \Phi(t, \tau) \tag{2.32}$$

Proof: See Brockett [10, page 20].

Remark: The sequence of matrices, M_k, defined recursively by

$$M_0 = I$$
$$M_k = I + \int_{t_0}^{t} A(\tau)M_{k-1}(\tau)d\tau \tag{2.33}$$

is instrumental in the development of the transition matrix. In fact, the sequence of matrices, M_k, converges on the given interval, and has the transition matrix as its limit function. This recursion is often expressed as the *Peano–Baker series*

$$\Phi(t, t_0) = I + \int_{t_0}^{t} A(\tau_1)d\tau_1 + \int_{t_0}^{t} A(\tau_1)\int_{t_0}^{\tau_1} A(\tau_2)d\tau_2 d\tau_1 + \cdots \tag{2.34}$$

39

The fact that the state transition matrix is T-periodic can be deduced from the series solution

$$\Phi(t + T, t_0 + T) = I + \int_{t_0+T}^{t+T} A(\tau_1)d\tau_1 + \int_{t_0+T}^{t+T} A(\tau_1) \int_{t_0+T}^{\tau_1} A(\tau_2)d\tau_2 d\tau_1 + \cdots \quad (2.35)$$

Successive application of the change of variable, $\eta_k = \tau_k - T$, and the fact that $A(t + T) = A(t)$, leads to the desired result. $\quad\quad\Box$

For an arbitrary linear time periodic system, the state transition matrix, $\Phi(t, t_0)$, is rarely obtained in analytical form, but is almost always obtained via a numerical integration of the defining ordinary differential equation (2.31). Procedures for numerical integration are discussed in [33,83].

The transition matrix posesses the following properties [59,110], which will prove to be useful in the sequel.

Theorem 2.10 (Properties of the state transition matrix) *The state transition matrix of the linear state differential equation in (2.27), has the following properties:*

1. $\Phi(t_2, t_1)\Phi(t_1, t_0) = \Phi(t_2, t_0)$

2. $\Phi(t, t_0)$ is nonsingular $\forall t, t_0$

3. $\Phi^{-1}(t, \tau) = \Phi(\tau, t)$ $\forall t, \tau$

4. $\frac{d}{dt}\Phi^T(t_0, t) = -A^T(t)\Phi^T(t_0, t)$

where the superscript T denotes the transpose. $\quad\quad\Box$

The first three properties will be used extensively in subsequent analyses. The general linear state differential equation has a forced response, as well as a homogeneous response, and the total solution is provided by [59,110].

Theorem 2.11 (Total state response and the superposition integral) *Consider the linear time periodic state dynamic equation*

$$\dot{x}(t) = A(t)x(t) + B(t)u(t) \quad (2.36)$$

*Assume that $A(t) \in P^{n \times n}[T]$, $B(t) \in P^{n \times m}[T]$, and $u(t)$ is piecewise continuous for $t \in [t_0, t]$. The solution of the state dynamic equation, is the sum of the **homogeneous** response, $x_h(t)$, in (2.30) and the **forced response**, $x_f(t)$, given by*

$$x_f(t) = \int_{t_0}^{t} \Phi(t, \tau)B(\tau)u(\tau)d\tau \quad (2.37)$$

40

Thus, the **total response,** *x(t), is given by the well known* **superposition integral,**

$$x(t) = \Phi(t, t_0)\xi_0 + \int_{t_0}^{t} \Phi(t, \tau)B(\tau)u(\tau)d\tau \tag{2.38}$$

for all t.

Proof: This result can be easily verified by direct substitution into (2.27). □

2.3 The Floquet Theory

A classical result in the analysis of linear time periodic systems was developed by Floquet [29] in 1883, and continues to be virtually one of only two analysis procedures presented in most textbooks [9,18,72,83] concerned with linear time periodic systems. The Floquet theorem has been utilized in many areas including the buckling of beams under periodic axial forces [28], the stability analysis of helicopter rotor blade dynamics [44,95], and many others. Many numerical procedures for the analysis of open loop stability have been developed that are completely based on application of the Floquet theorem, such as in [33,36].

In the Floquet Theorem, the state transition matrix, $\Phi(t + T, t)$, plays a fundamentally important role.

Definition 2.12 (Monodromy matrices) *The state transition matrix given by $\Phi(t + T, t)$, where T is the pumping period of the LTP state space model, is called a* **monodromy matrix at time** *t. The constant matrix, $\Phi(t_0 + T, t_0)$, is called the* **(fundamental) monodromy matrix.**

It is customary to assume that $t_0 = 0$, so that the monodromy matrix can be expressed as $\Phi(T, 0)$. This will be assumed throughout the remainder of this thesis. Thus, we proceed to the main results of the Floquet theory as it is called here. However, these results are generally attributed to Floquet, or Liapunov, or both.

Theorem 2.13 (Floquet) *Consider the state space model of the linear time periodic system in Definition 2.8. If the monodromy matrix, $\Phi(T, 0)$, is nondefective, then the following results hold:*

1. **State transition matrix.** *The state transition matrix of (2.26) can always be expressed as*

$$\Phi(t, \tau) = P(t)e^{Q(t-\tau)}P^{-1}(\tau) \tag{2.39}$$

41

where $P(t)$ is a nonsingular T-periodic matrix of dimension $n \times n$, and Q is a constant, possibly complex, matrix of dimension $n \times n$.

2. **Similarity transformation.** *The state transformation*

$$x(t) = P(t)v(t) \tag{2.40}$$

transforms $x(t)$ into a set of periodically time varying system of coordinates, $v(t)$, such that the dynamics matrix in the new state space is linear time invariant, that is,

$$
\begin{aligned}
\dot{v}(t) &= Qv(t) + \bar{B}(t)u(t) \\
y(t) &= \bar{C}(t)v(t) + D(t)u(t)
\end{aligned}
\tag{2.41}
$$

where

$$
\begin{aligned}
Q &= P^{-1}(t)\left\{A(t)P(t) - \dot{P}(t)\right\} \\
\bar{B}(t) &= P^{-1}(t)B(t) \\
\bar{C}(t) &= C(t)P(t)
\end{aligned}
\tag{2.42}
$$

3. **Stability.** *A necessary and sufficient condition for stability is that all eigenvalues of the monodromy matrix lie on the open unit disk, that is,*

$$\lambda\left\{\Phi(T,0)\right\} \in D_o \tag{2.43}$$

where $D_o = \{z \mid |z| < 1\}$.

Proof: (1) State transition matrix. From the defining ODE of the state transition matrix,

$$\dot{\Phi}(t+T,0) = A(t+T)\Phi(t+T,0) \tag{2.44}$$

Since $A(t+T) = A(t)$, it follows that

$$\dot{\Phi}(t+T,0) = A(t)\Phi(t+T,0) \tag{2.45}$$

Clearly, $\Phi(t+T,0)$, also satisfies the defining ODE of the state transition matrix. From the properties of the state transition matrix

$$
\begin{aligned}
\Phi(t+T,0) &= \Phi(t+T,T)\Phi(T,0) \\
&= \Phi(t,0)\Phi(T,0)
\end{aligned}
\tag{2.46}
$$

42

Since the monodromy matrix, $\Phi(T,0)$, is a real, constant, and non-singular matrix, it can be expressed as the matrix exponential function

$$\Phi(T,0) = e^{QT} \tag{2.47}$$

Note, however, that Q might be complex. Thus, (2.46) can be expressed as

$$\Phi(t+T,0) = \Phi(t,0)e^{QT} \tag{2.48}$$

Assume a solution of the form

$$\Phi(t,0) = P(t)e^{Qt} \tag{2.49}$$

so that

$$P(t) = \Phi(t,0)e^{-Qt} \tag{2.50}$$

Now, the inverse of the state transition matrix, $\Phi(t,0)$, always exists. The exponential term is always positive and nonzero, so that its inverse always exists. Thus, the matrix $P(t)$ is nonsingular. Note that

$$
\begin{aligned}
P(t+T) &= \Phi(t+T,0)e^{-Q(t+T)} \\
&= \Phi(t,0)e^{QT}e^{-QT}e^{-Qt} \\
&= \Phi(t,0)e^{-Qt}
\end{aligned}
\tag{2.51}
$$

Comparing (2.50) and (2.51) demonstrates that

$$P(t+T) = P(t) \tag{2.52}$$

that is, $P(t)$ is T-periodic. From the properties of the transition matrix

$$
\begin{aligned}
\Phi(0,\tau) &= \Phi^{-1}(\tau,0) \\
&= e^{-Q\tau}P^{-1}(\tau)
\end{aligned}
\tag{2.53}
$$

so that

$$
\begin{aligned}
\Phi(t,\tau) &= \Phi(t,0)\Phi(0,\tau) \\
&= P(t)e^{Qt}e^{-Q\tau}P^{-1}(\tau)
\end{aligned}
\tag{2.54}
$$

which completes the proof of the first result.

(2) Similarity transformation. The similarity transformation utilized here is

$$x(t) = P(t)v(t) \tag{2.55}$$

so that

$$\dot{x}(t) = \dot{P}(t)v(t) + P(t)\dot{v}(t)$$
$$= A(t)x(t) + B(t)u(t)$$

Solving the above two equations for $\dot{v}(t)$ yields

$$\dot{v}(t) = P^{-1}(t)\left\{A(t)P(t) - \dot{P}(t)\right\}v(t) + B(t)u(t) \tag{2.56}$$

From (2.39),

$$P(t) = \Phi(t)e^{-Qt} \tag{2.57}$$

so that

$$\dot{P}(t) = \dot{\Phi}(t,0)e^{-Qt} - \Phi(t,0)e^{-Qt}Q$$
$$= \dot{\Phi}(t,0)e^{-Qt} - P(t)Q$$

Solving for Q in the above expression yields

$$Q = P^{-1}(t)\left\{A(t)P(t) - \dot{P}(t)\right\} \tag{2.58}$$

Thus, (2.56) can be simplified, which concludes the proof of the second result.

(3) Stability. The monodromy matrix describes the state transition over one full period, so that

$$x(kT) = \Phi(kT,0)\xi_0$$
$$= \Phi^k(T,0)\xi_0 \tag{2.59}$$

From the monodromy matrix eigenvalue problem,

$$\Phi(T,0) = V\Lambda W \tag{2.60}$$

Hence,

$$x(kT) = V\Lambda^k W\xi_0 \tag{2.61}$$

44

The state vector, $x(kT)$, will be asymptotically stable as k grows large, only if the eigenvalues of the monodromy matrix contained in Λ are on the open unit disk, $\lambda_i \in D_0$ $\forall i$. Conversely, if the eigenvalues of the monodromy matrix are all on the open unit disk, then the state vector will be asymptotically stable as $k \to \infty$.

Remark: An interesting observation can be made about LTP systems as a result of the proof of the Floquet Theorem. Recall that

$$\Phi(T,0) = e^{QT} \qquad (2.62)$$

Thus

$$Q = \frac{1}{T} \log \Phi(T,0) \qquad (2.63)$$

If $\Phi(T,0)$ has a negative real eigenvalue, say λ_i, then $\log \lambda_i$ is complex (with no complex conjugate), so that Q is also complex. However, $\Phi(t,0)$ must be a real matrix. This implies that $P(t)$ must be complex such that the resulting product of $P(t)$ and e^{Qt} is real. $\square$

The above statement of the Floquet Theorem is somewhat more comprehensive than that provided in the majority of textbooks dealing with LTP systems. However, all of the above results are directly or indirectly derivative of Floquet's original work. A slightly more general Floquet Theorem can be stated if the more general case of a Jordan canonical form is assumed for the monodromy matrix. However, this extension unnecessarily complicates the algebra, and is omitted for brevity and clarity.

Given a state space representation of an LTP system, either open or closed loop, the monodromy matrix $\Phi(T,0)$ can be determined by integrating its defining ordinary differential equation. However, this results in a yes or no answer to the question of stability. Determination of the monodromy matrix is straightforward using a numerical integration technique where the periodically time varying coefficients of $A(t)$ are approximated using either a staircase or trapezoidal waveform [80,83,84,85]. Alternative numerical procedures have been developed by Friedmann *et al* [33]. However, the Floquet theory only presents a methodology for the analysis of a closed loop system, and in particular, only provides the z-plane locations of the eigenvalues of the monodromy matrix. Thus, Floquet theory can only serve as an analysis tool, and not as a compensator synthesis tool.

Suppose that the initial condition, ξ_0, of the LTP system is chosen such that it is a right eigenvector, v, of the monodromy matrix, $\Phi(T,0)$. Then,

$$x(T) \quad = \quad \Phi(T,0)\xi_0$$

$$= z\xi_0 \tag{2.64}$$

Alternatively, if an arbitrary initial time with the same property is selected,

$$x(t+T) = zx(t) \tag{2.65}$$

then an interesting observation can be made. Floquet Theory can be viewed as the search for signals, $x(t)$, that increase *geometrically* from period to period. This observation will form the basis for defining a class of input signals that have a geometrical variation from period to period, so that a linear operator can be developed to describe the input–output characteristics of LTP systems.

The Floquet theorem also permits us to dispense with the study of LTP systems with periodically time varying dynamics in the open loop, and consider instead the completely general case of a periodically time varying state space representation with a time invariant dynamics matrix, Q. However, as soon as feedback is introduced, time periodic dynamics must be reconsidered, as will be discussed in the sequel.

2.4 The Hill Theory and Harmonic Balance

A classical dynamic analysis method for systems with time periodic parameters is the method of *harmonic balance*. This procedure was originally introduced in 1878 by Hill [47,46] in his landmark paper on the infinite determinant approach for stability analysis of LTP systems. Since that time, the harmonic balance approach has been extended to the study of nonlinear systems, such as described by Nayfeh and Mook [77], and is an integral part of the describing function methodology [35].

Harmonic balance refers to the series expansion of the periodic parts of the solution to the dynamic equations using a trigonometric or complex Fourier series. The Fourier series involves the expansion of the parametric excitation into a set of basis functions, namely, sinusoids, that are orthonormal over the fundamental period using an L_2 norm. The dynamic equations of motion are then expanded in terms of these Fourier series and all terms are grouped by harmonic number. Since the sinusoids form an orthonormal basis in the fundamental interval, the coefficients multiplying each basis function (sinusoid or harmonic) must vanish for each and every harmonic number independently. This is often referred to as either the *principle of harmonic balance*, or *linear independence*. In principle,

46

a generalized Fourier series can be used; that is, a Fourier series for which an arbitrary set of orthonormal functions is developed. In this thesis, however, only the orthonormal basis formed from the complex exponentials will be considered.

The harmonic balance approach has been used in many forms. Nayfeh and Mook [77] express the periodic portion of the state vector as a truncated trigonometric Fourier series of the form

$$x(t) = \sum_{n=0}^{N} x_n \cos (n\omega_p t + n\beta_0) \qquad (2.66)$$

Others, including Leonhard [61], and Dugundji [27], typically use a truncated trigonometric Fourier series of the form

$$x(t) = \sum_{n=0}^{N} \{x_{nc} \cos n\omega_p t + x_{ns} \sin n\omega_p t\} \qquad (2.67)$$

However, the above trigonometric forms of the Fourier series are inconvenient because they lead to asymmetrical linear operators in the frequency domain, although the results obtained using the trigonometric and complex forms of the Fourier series are exactly equivalent. This will become clear in the next chapter. Meirovitch [73] utilizes the complex Fourier series

$$x(t) = \sum_{n=-\infty}^{\infty} x_n e^{jn\omega_p t} \qquad (2.68)$$

Hill essentially used the same complex Fourier series modulated by the complex exponential in order to make the connection with the assumed Floquet solution, so that

$$x(t) = e^{st} \sum_{n=-\infty}^{\infty} x_n e^{jn\omega_p t} \qquad (2.69)$$

In the above form of series expansion, the dependence of the assumed solution on the complex exponential rates is explicit. In fact, this type of series expansion will lead to linear operators in the frequency domain that have desirable symmetry properties.

Several authors call the *method of harmonic balance* the approach whereby only a single harmonic is included in the series expansion [61,99,101]. Several authors permit many harmonics to be included in the series expansion, and have called this the *generalized harmonic balance* methodology [61,99,101]. However, Hill formulated his lunar perigee problem including an infinite number of harmonics, and then truncated the resulting infinite determinants to obtain approximate results. Thus, all harmonic balance methods are derivative of Hill's original approach, the only difference being that Hill included the complex exponential portion of the Floquet solution explicitly, as opposed to the former harmonic balance

47

methods, where the complex exponential portion of the Floquet solution remains implicit in the state vector.

The only relatively recent work that utilized the complete Floquet solution is Schweizer [90,91]. However, his use of the trigonometric Fourier series form of the Floquet solution leads to an inconvenient form. Also, several of the results obtained were cumbersome in the extreme, probably due to the fact that the geometric approaches currently commonplace in the study of multivariable LTI systems, were not commonly available in the early 1960's.

At this point, let us review the classical Hill determinant methodology. The connection between Hill's original work and the harmonic balance approaches will be discussed more thoroughly in the context of the linear operators developed in the next chapter.

The classical development of the Hill determinant is straightforward and is outlined below. Here, a second order Hill equation with no dissipative terms will be considered,

$$\ddot{x}(t) + [a - 2q\psi(t)]x(t) = 0 \tag{2.70}$$

where $\psi(t)$ is T–periodic, so that $\psi(t)$ can be expressed as a complex Fourier series,

$$\psi(t) = \sum_{n=-\infty}^{\infty} \psi_n e^{jn\omega_p t} \tag{2.71}$$

where the ψ_n are the complex Fourier coefficients, and ω_p is the *pumping* or *fundamental frequency*. (By convention, $T = \pi$, so that $\omega_p = 2$.) The Hill determinant analysis rests on the assumed Floquet solution of the form

$$x(t) = e^{st} \sum_{n=-\infty}^{\infty} x_n e^{jn\omega_p t} \tag{2.72}$$

Substituting (2.71) and (2.72) into (2.70), we have

$$0 = e^{st} \sum_{n=-\infty}^{\infty} (s + jn\omega_p)^2 x_n e^{jn\omega_p t} + e^{st} \left(a - 2q \sum_{m=-\infty}^{\infty} \psi_m e^{jm\omega_p t} \right) \sum_{n=-\infty}^{\infty} x_n e^{jn\omega_p t} \tag{2.73}$$

Multiplying through by e^{-st} and grouping terms yields

$$
\begin{aligned}
0 &= \sum_{n=-\infty}^{\infty} [(s + jn\omega_p)^2 + a] x_n e^{jn\omega_p t} - 2q \sum_{m,n=-\infty}^{\infty} \psi_m x_n e^{j(m+n)\omega_p t} \\
&= \sum_{n=-\infty}^{\infty} [(s + jn\omega_p)^2 + a] x_n e^{jn\omega_p t} - 2q \sum_{m,n=-\infty}^{\infty} \psi_m x_{n-m} e^{jn\omega_p t} \\
&= \sum_{n=-\infty}^{\infty} \left\{ [(s + jn\omega_p)^2 + a] x_n - 2q \sum_{m=-\infty}^{\infty} \psi_m x_{n-m} \right\} e^{jn\omega_p t} \tag{2.74}
\end{aligned}
$$

48

Since the system of functions, $\{e^{jn\omega_p t} | n \in Z\}$, form a set of orthonormal basis functions in $L_2[0,T]$, the principle of harmonic balance can be applied to obtain the infinite set of simultaneous equations below:

$$0 = [(s + jn\omega_p)^2 + a]x_n - 2q \sum_{m=-\infty}^{\infty} \psi_m x_{n-m}, \quad \forall n \in Z \tag{2.75}$$

In order for the above system of equations to have a nontrivial solution, we require that the determinant,

$$\phi(s) = \det \begin{bmatrix} \ddots & \vdots & \vdots & \vdots & \vdots & \vdots & \\ \cdots & \rho_{-2} & k_1 & k_2 & k_3 & k_4 & \cdots \\ \cdots & k_{-1} & \rho_{-1} & k_1 & k_2 & k_3 & \cdots \\ \cdots & k_{-2} & k_{-1} & \rho_0 & k_1 & k_2 & \cdots \\ \cdots & k_{-3} & k_{-2} & k_{-1} & \rho_1 & k_1 & \cdots \\ \cdots & k_{-4} & k_{-3} & k_{-2} & k_{-1} & \rho_2 & \cdots \\ & \vdots & \vdots & \vdots & \vdots & \vdots & \ddots \end{bmatrix} \tag{2.76}$$

be zero, where

$$\rho_n = (s + jn\omega_p)^2 + k_0 \tag{2.77}$$

and

$$k_n = \begin{cases} a - 2q\psi_0, & n = 0 \\ -2q\psi_n, & \forall n \in Z, \; n \neq 0 \end{cases} \tag{2.78}$$

The above determinant, which does not converge, is usually presented in the literature as a precursor to the Hill determinant, or a pre–Hill determinant [83]. Consider the following result for the absolute convergence of infinite determinants.

Lemma 2.14 (Absolute convergence of infinite determinants) *An infinite determinant is absolutely convergent if*

(a) the product of the elements on the main diagonal is absolutely convergent, and

(b) the sum of the non-diagonal elements is absolutely convergent.

Proof: See McLachlan [72] for an exposition of the Hill determinant. The above lemma is proved in [107]. □

A simple way to satisfy the conditions in the above lemma is to divide every row n by ρ_n, so that the Hill determinant defined by

$$\Delta(s) = \det \begin{bmatrix} \ddots & \vdots & \vdots & \vdots & \vdots & \vdots & \\ \cdots & 1 & \frac{k_1}{\rho_{-2}} & \frac{k_2}{\rho_{-2}} & \frac{k_3}{\rho_{-2}} & \frac{k_4}{\rho_{-2}} & \cdots \\ \cdots & \frac{k_{-1}}{\rho_{-1}} & 1 & \frac{k_1}{\rho_{-1}} & \frac{k_2}{\rho_{-1}} & \frac{k_3}{\rho_{-1}} & \cdots \\ \cdots & \frac{k_{-2}}{\rho_0} & \frac{k_{-1}}{\rho_0} & 1 & \frac{k_1}{\rho_0} & \frac{k_2}{\rho_0} & \cdots \\ \cdots & \frac{k_{-3}}{\rho_1} & \frac{k_{-2}}{\rho_1} & \frac{k_{-1}}{\rho_1} & 1 & \frac{k_1}{\rho_1} & \cdots \\ \cdots & \frac{k_{-4}}{\rho_2} & \frac{k_{-3}}{\rho_2} & \frac{k_{-2}}{\rho_2} & \frac{k_{-1}}{\rho_2} & 1 & \cdots \\ & \vdots & \vdots & \vdots & \vdots & \vdots & \ddots \end{bmatrix} \qquad (2.79)$$

is absolutely convergent. The fact that the infinite determinant is absolutely convergent is very useful from a numerical standpoint. However, by normalizing the pre–Hill determinant, the structure inherent to the pre-Hill determinant is destroyed. This structure will be examined in detail in the next chapter.

The Hill determinant is most commonly used to to develop stability diagrams that describe stable regions in a parameter space associated with the system under consideration. For example, the canonical form of the Mathieu equation,

$$\ddot{x}(t) + (a - 2q\cos\omega_p t)x(t) = 0 \qquad (2.80)$$

has two parameters, a and q, for which stability boundaries are often sought. The stability boundaries are plotted in the (a, q) plane. The resulting stability diagram for the Mathieu equation (that is, with no damping) is called the Strutt diagram [72,83], and is shown in Figure 2.1.

2.5 Summary

In this chapter, the basic mathematical preliminaries for the study of LTP systems were described. The complex Fourier series and a brief discussion of its convergence properties was presented. The Toeplitz form and the Toeplitz transform was introduced. Application of the state space to LTP systems was reviewed, and applicable results from the linear system theory were presented. Finally, the classical theories of Floquet and Hill were reviewed.

The above preliminaries will serve as the starting point for the developments in the next chapter.
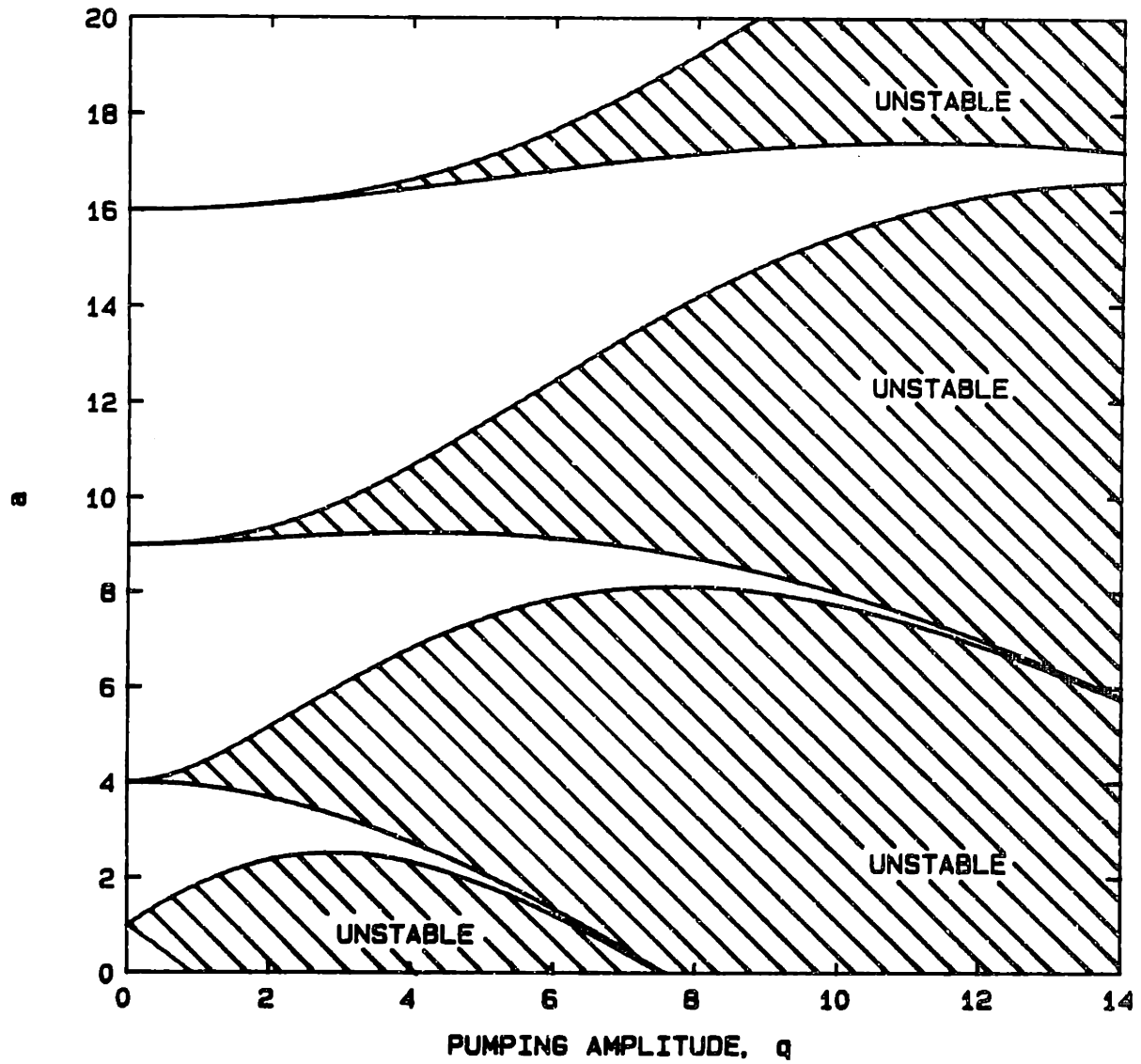
Figure 2.1: Classical stability (Strutt) diagram for the Mathieu equation. The Strutt diagram is symmetrical about the a axis. Unstable regions are shaded. This diagram was produced from data in Appendix 2 of [72].

[Page Left Blank]

Chapter 3

Frequency Response of LTP Systems

It is interesting to note that neither a transfer function notion, nor a frequency response notion, has ever been developed for linear time periodic systems that is completely analogous to the LTI transfer function. The objective of this chapter is to develop a linear operator or transfer function for LTP systems that is analogous to the LTI transfer function. The transfer properties of the LTP system can be deduced in terms of the LTP transfer function. Properties of LTP systems such as poles, transmission zeroes, principal gains, and their associated directional properties, are then described in terms familiar to the multivariable control theory.

3.1   Introduction

The dynamics of an LTI system can be described in the time domain by a nth order matrix differential equation with constant coefficients called the LTI state space model. In steady state, the response of a linear time invariant (LTI) system to a complex exponential (sinusoidal) input signal of a given frequency, is a complex exponential output signal of the same frequency, but with possibly different amplitude and phase. This leads to the notion of the LTI frequency response and the LTI transfer function. The Laplace transform can be applied to the LTI state space model with trivial initial conditions to obtain the LTI transfer function. The Bode diagrams are then determined by computing the magnitude and phase of the complex valued LTI transfer function over the frequency range of interest (with
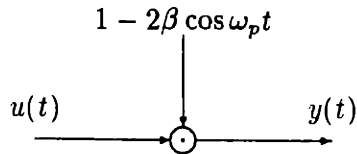
$$1 - 2\beta \cos \omega_p t$$

$$u(t) \quad\quad\quad\quad\quad y(t)$$

Figure 3.1: Simple LTP system. A signal, $u(t)$, passes through a time periodic gain, which is an amplitude modulation by a periodic signal, $1 - 2\beta \cos \omega_p t$, to obtain the output, $y(t)$.

some caveats concerning directional properties in the multivariable case). An important characteristic of the LTI transfer function is that it is an operator for which the input and the output signal spaces are equal, that is, the space of complex exponential signals. In the sequel, these notions will be made more precise.

However, the complex exponential input signal does not lead to such a convenient frequency response notion for LTP systems even in the simplest of cases. To illustrate this, consider the simple LTP system represented by the amplitude modulation of a signal, as shown in Figure 3.1. The frequency at which the amplitude modulation takes place is called the *pumping frequency*, ω_p. For a complex exponential input signal, $u(t) = e^{st}$, the output signal is the sum of three complex exponentials,

$$y(t) = e^{st} - \beta e^{(s-j\omega_p)t} - \beta e^{(s+j\omega_p)t} \tag{3.1}$$

Thus, when a complex exponential input is injected into an LTP system, several harmonics of the pumping frequency may appear in the output signal, all modulated by the input complex exponential. Thus, the input and output signal spaces are not equal. As a result, the notion of a transfer function for LTP systems has been elusive.

It is well understood that the steady state response of an LTP system may contain several harmonics of the pumping frequency, and was a motivation for the development of the describing function (DF) [61] or equivalently, the harmonic balance technique [27, for example] as applied to LTP systems. The fundamental assumption behind these approaches is that the fundamental harmonic of an oscillation in a closed loop LTP system is not influenced by higher harmonics. Essentially, the LTI frequency response notion is used to approximate the LTP response, which can lead to grossly inaccurate results. Leonhard suggested [61] that this problem can be mitigated by including as many harmonics as influence the fundamental harmonic, but an infinite number of harmonics may influence the fundamental. However, arguments analogous to high frequency roll–off in LTI systems

can be used to limit the number of harmonics that must be included in the DF approaches. Leonhard also presents examples suggesting that satisfactory results can be obtained by including only two or three prevalent harmonics in some cases. Since the harmonic balance method is essentially identical to the DF approach in this context, the same discussion applies.

However, neither the DF, nor the harmonic balance approach, has led to a notion of an operator for LTP systems comparable to the transfer function for LTI systems. As a result, Schweizer [90,91], proposed a frequency domain operator based on the trigonometric Fourier series expansion of a single–input single–output LTP system. However, Schweizer's operator requires the computation of infinite continued fractions which would be impractical and cumbersome for a multivariable system. As a result, this particular operator has not received widespread acceptance in the study of LTP systems. In addition, many of the results that are currently accepted practice in the analysis of the transfer function matrix for multivariable LTI systems were not available to Schweizer.

Invariably in the fields of signal processing and control theory, time periodic signals are expanded in complex Fourier series in order to understand their harmonic content. A similar procedure is advocated here, so that the parametric excitation embedded in the description of an LTP system can be examined systematically, and a corresponding transfer function and frequency response clearly stated. Several useful analysis tools in the multivariable control theory can then be extended to this LTP transfer function. Feedback compensation techniques can then be developed in this context to improve open loop characteristics of the LTP system.

The chapter is organized as follows. The response of an LTI system to a complex exponential test signal is reviewed in order to establish terminology and to provide a basis for comparison with the LTP system theory developed in the sequel. The response of an LTP system to a complex exponential signal is also reviewed in detail in order to substantiate the claim that the complex exponential test signal does not result in a complex exponential steady state response. This analysis leads to the identification of a fundamental signal space for LTP systems. The LTP frequency response is derived utilizing integral operators, and poles and transmission zeroes are defined in this context. However, the integral operator approach is not very convenient for numerical calculations. Hence, a generalization of the harmonic balance approach is introduced in order to characterize the LTP frequency

response, and methods for calculating poles, zeroes, and their associated directional properties, are presented. The principal gains, associated directions, and the LTP principal gain diagram are then introduced. The relationship of the generalized harmonic balance approach developed here to the traditional application of harmonic balance, such as described by Dugundji [27], and its relationship to the classical Hill theory, is also discussed. The chapter closes with some applications of the above techniques to some interesting linear time periodic state space models.

3.2   LTI Frequency Response

In order to compare the LTI theory with the theory to be developed for LTP systems in the sequel, a brief review of the LTI frequency response is provided to establish terminology.

The test signal of fundamental interest in the study of LTI systems is the *complex exponential* or the *exponentially modulated sinusoid*,

$$u(t) = u_0 e^{st} \quad s \in C, \; u_0 \in C^m \tag{3.2}$$

It is desired to determine the response of the LTI state space model,

$$
\begin{aligned}
\dot{x}(t) &= Ax(t) + Bu(t) \\
y(t) &= Cx(t) + Du(t)
\end{aligned}
\tag{3.3}
$$

to this complex exponential. At the same time, associated transient responses will also be determined due to their importance in developing the notion of transmission zeroes.

Recall that the total state response, $x(t)$, associated with (3.3) is given by the convolution form of the variation of constants formula,

$$x(t) = e^{At}\xi_0 + \int_0^t e^{A(t-\tau)} Bu(\tau) d\tau \tag{3.4}$$

The first term is traditionally called the *homogeneous state response*, $x_h(t)$, and the second term the *forced response*, $x_f(t)$, or the *particular solution*. Now, let's determine the response of LTI system to the complex exponential in (3.2):

$$
\begin{aligned}
x(t) &= e^{At}\xi_0 + \int_0^t e^{A(t-\tau)} Bu_0 e^{s\tau} d\tau \\
&= e^{At}\xi_0 - e^{At}(sI - A)^{-1} Bu_0 + (sI - A)^{-1} Bu_0 e^{st}
\end{aligned}
$$

Grouping terms yields the *total state response*,

$$x(t) = e^{At} \left[\xi_0 - (sI - A)^{-1} B u_0 \right] + (sI - A)^{-1} B u_0 e^{st} \qquad (3.5)$$

The total state response can be separated into the sum of the *transient response*, or that portion of the total response corresponding to a relaxation of the system modes,

$$x_{tr}(t) = e^{At} \left[\xi_0 - (sI - A)^{-1} B u_0 \right] \qquad (3.6)$$

and the *steady state response*, or *complex exponential response*, or that portion of the total state response that does not correspond to a relaxation of the system modes,

$$x_{ss}(t) = (sI - A)^{-1} B u_0 e^{st} \qquad (3.7)$$

The *transient output response* is given by

$$y_{tr}(t) = C e^{At} \left[\xi_0 - (sI - A)^{-1} B u_0 \right] \qquad (3.8)$$

and the *steady state output response* or the *complex exponential output response* by

$$y_{ss}(t) = \left[C(sI - A)^{-1} B + D \right] u_0 e^{st} \qquad (3.9)$$

The LTI *transfer function matrix* is then given by the term in square brackets, or

$$\hat{G}(s) = C(sI - A)^{-1} B + D \qquad (3.10)$$

In the above discussion, the steady state or complex exponential response was determined directly from the total response. However, the steady state response can be determined by taking a slightly different point of view, that is, to search for the initial condition, ξ_0, that produces no relaxation of the system modes such that the total response consists of only the complex exponential response. Fortunately, by inspection of (3.6), this initial condition is easily identified,

$$\xi_0 = (sI - A)^{-1} B u_0 \qquad (3.11)$$

so that the transient response vanishes. This choice of an initial condition can then be substituted into the convolution integral to obtain the steady state output (or complex exponential) response.

The steady state output response in (3.9) leads to the usual LTI frequency response concept, which is depicted in Figure 3.2. From the steady state response, we can deduce

$$u(t) = u_0 e^{j\omega t} \qquad \hat{G}(s) \qquad y(t) = \hat{G}(j\omega)u_0 e^{j\omega t}$$
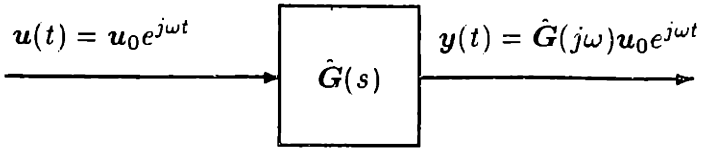
Figure 3.2: LTI frequency response. In steady state, an LTI system maps a sinusoidal input signal of frequency ω, into a sinusoidal output signal of the same frequency, but with possibly different amplitude and phase.

the frequency response: *in steady state, an LTI system maps a sinusoidal input signal of frequency ω, into a sinusoidal output signal of the same frequency, but with possibly different amplitude and phase.* This statement is true for both SISO and multivariable systems. As a practical matter, the steady state response is determined by evaluating the transfer function matrix at the frequency of interest, ω, to obtain the complex valued matrix, $\hat{G}(j\omega)$, which is then multiplied by the complex valued input direction (vector), u_0, to obtain the output direction (vector), y_0. Thus, the mathematical operations of interest are multiplications of complex matrices.

The poles and transmission zeroes can be easily identified using this approach. The poles of the LTI system are simply those locations in the complex s-plane for which the transfer function (linear operator) is not analytic. Thus, the LTI poles are determined using the eigenvalue problem,

$$[sI - A]v = 0 \tag{3.12}$$

where the mode shapes are the eigenvectors, v. The transmission zeroes are determined by recognizing that the choice of initial condition in (3.11) results in the transient output response vanishing for all time. Rearranging yields

$$(sI - A)\xi_0 - Bu_0 = 0 \tag{3.13}$$

Then, substituting (3.11) into (3.9) yields

$$(C\xi_0 + Du_0)e^{st} = 0 \tag{3.14}$$

Since the complex exponential is never zero, the above equation can only be satisfied if

$$C\xi_0 + Du_0 = 0 \tag{3.15}$$

58

Table 3.1: **Summary of LTI system responses.** The LTI frequency response is deduced by injecting a complex exponential test signal into an LTI state space model, and using the convolution integral to determine the system response.

Concept	Symbol	Formulation
Test signal	$u(t)$	$u_0 e^{st}$
Responses		
Homogeneous	$x_h(t)$	$e^{At}\xi_0$
Forced	$x_f(t)$	$\left(e^{st}I - e^{At}\right)(sI - A)^{-1}Bu_0$
Transient	$x_{tr}(t)$	$e^{At}\left[\xi_0 - (sI - A)^{-1}Bu_0\right]$
Steady State	$x_{ss}(t)$	$(sI - A)^{-1}Bu_0 e^{st}$
Transient Output	$y_{tr}(t)$	$Ce^{At}\left[\xi_0 - (sI - A)^{-1}Bu_0\right]$
Steady State Output	$y_{ss}(t)$	$\left[C(sI - A)^{-1}B + D\right]u_0 e^{st}$
Transfer function	$\widehat{G}(s)$	$C(sI - A)^{-1}B + D$

Hence, (3.13) and (3.15) can be expressed as the LTI transmission zero generalized eigenvalue problem,

$$\begin{bmatrix} sI - A & -B \\ -C & -D \end{bmatrix} \begin{bmatrix} \xi_0 \\ u_0 \end{bmatrix} = 0 \tag{3.16}$$

All of the properties derived above for an LTI system are based on the fundamental input signal space consisting of complex exponential signals, and are summarized in Table 3.1. The derivations of the various responses are straightforward and do not require any specialized mathematics except the fundamental notions of the convolution integral form of the variation of constants formula and the defining ODE of the state transition matrix. Moreover, the complex exponential input signal produces a complex exponential output signal via the steady state output response, and it is this steady state response that is the transfer function of the LTI system. This linear map can be analyzed using linear algebra involving norms, singular values and eigenvalues, and their associated directional properties.

Finally, for LTI systems, the connection between the time domain and the frequency domain is obtained via the Fourier transform. The complex exponential is a basis function for the time domain function space of square integrable signals denoted by $L_2(-\infty, \infty)$ with

the inner product

$$< x,y >= \int_{-\infty}^{\infty} x(t)^* y(t) dt \tag{3.17}$$

The frequency domain is obtained by application of the Fourier transform to obtain the frequency domain function space L_2, with inner product

$$< x,y >= \frac{1}{2\pi} \int_{-\infty}^{\infty} x(j\omega)^* y(j\omega) dt \tag{3.18}$$

The point here is that the Fourier transform is a Hilbert space isomorphism, that is, a map that is continuous, preserves the L_2 norm, and has a continuous inverse. This is an extremely useful property that is used frequently in the control theory.

3.3 LTP System Response to a Complex Exponential

Richards [83] and others have attempted to describe a map, similar to that of the LTI transfer function, for LTP systems using the complex exponential signal. However, the complex exponential test signal is inappropriate for LTP systems, so that the resulting map cannot be analyzed via the algebra described above. In this section, the response of the LTP system to a complex exponential signal is examined in detail, in the hope of gaining insight into the character of the test input signal for LTP systems that is analogous to the complex exponential signal for LTI systems.

Here, we consider the response of the LTP state space model

$$\begin{aligned}
\dot{x}(t) &= A(t)x(t) + B(t)u(t) \\
y(t) &= C(t)x(t) + D(t)u(t)
\end{aligned} \tag{3.19}$$

to a complex sinusoid of the form

$$u(t) = u_0 e^{st} \tag{3.20}$$

Similar analyses are presented by Richards [83, page 41] and D'Angelo [18, page 200], although not in the same form as developed here.

The total response is given by the superposition integral,

$$x(t) = \Phi(t,0)\xi_0 + \int_0^t \Phi(t,\tau)B(\tau)u(\tau)d\tau \tag{3.21}$$

The first part, as before, is called the homogeneous response,

$$x_h(t) = \Phi(t,0)\xi_0 \tag{3.22}$$

and the second part is called the forced response,

$$
\begin{aligned}
x_f(t) &= \int_0^t \Phi(t,\tau)B(\tau)u(\tau)d\tau \\
&= \int_0^t \Phi(t,\tau)B(\tau)u_0 e^{s\tau}d\tau \\
&= \int_0^t \Phi(t,\tau)B(\tau)e^{s\tau}d\tau\, u_0 \qquad (3.23)
\end{aligned}
$$

From the properties of the state transition matrix,

$$
\begin{aligned}
\Phi(t,\tau) &= \Phi(t,0)\Phi(0,\tau) \\
&= \Phi(t,0)\Phi^{-1}(\tau,0) \qquad (3.24)
\end{aligned}
$$

we have

$$
x_f(t) = \Phi(t,0)\int_0^t \Phi^{-1}(\tau,0)B(\tau)e^{s\tau}d\tau\, u_0 \qquad (3.25)
$$

Using the Floquet result from Theorem 2.13,

$$
\Phi(t,0) = P(t)e^{Qt} \qquad (3.26)
$$

$$
\Phi^{-1}(\tau,0) = e^{-Q\tau}P^{-1}(\tau) \qquad (3.27)
$$

the forced response can be expressed as

$$
\begin{aligned}
x_f(t) &= \Phi(t,0)\int_0^t e^{-Q\tau}P^{-1}(\tau)B(\tau)e^{s\tau}d\tau\, u_0 \\
&= \Phi(t,0)\int_0^t e^{(sI-Q)\tau}P^{-1}(\tau)B(\tau)d\tau\, u_0 \qquad (3.28)
\end{aligned}
$$

To simplify the algebra, let

$$
\bar{B}(\tau) = P^{-1}(\tau)B(\tau) \qquad (3.29)
$$

Now, $\bar{B}(\tau)$ is a T-periodic matrix, and can be expanded in a complex Fourier series,

$$
\bar{B}(\tau) = \sum_{m=-\infty}^{\infty} \bar{B}_m e^{jm\omega_p \tau} \qquad (3.30)
$$

Substituting,

$$
x_f(t) = \Phi(t,0)\sum_{m=-\infty}^{\infty}\int_0^t e^{(s_m I - Q)\tau}\bar{B}_m d\tau u_0 \qquad (3.31)
$$

where

$$
s_m = s + jm\omega_p \qquad (3.32)
$$

61

Evaluating the integral,

$$
\begin{aligned}
x_f(t) &= \Phi(t,0) \sum_{m=-\infty}^{\infty} e^{(s_m I - Q)\tau}(s_m I - Q)^{-1}\Big|_{\tau=0}^{t} \bar{B}_m u_0 \\
&= P(t)e^{Qt} \sum_{m=-\infty}^{\infty} \left[e^{(s_m I - Q)t} - I \right] (s_m I - Q)^{-1} \bar{B}_m u_0
\end{aligned}
\tag{3.33}
$$

Finally, the forced response becomes

$$
x_f(t) = P(t) \sum_{m=-\infty}^{\infty} (s_m I - Q)^{-1} \bar{B}_m u_0 e^{s_m t} - \Phi(t,0) \sum_{m=-\infty}^{\infty} (s_m I - Q)^{-1} \bar{B}_m u_0
\tag{3.34}
$$

The total response is the sum of the homogeneous and forced responses,

$$
\begin{aligned}
x(t) &= \Phi(t,0) \left\{ \xi_0 - \sum_{m=-\infty}^{\infty} (s_m I - Q)^{-1} \bar{B}_m u_0 \right\} \\
&\quad + P(t) \sum_{m=-\infty}^{\infty} (s_m I - Q)^{-1} \bar{B}_m u_0 e^{s_m t}
\end{aligned}
\tag{3.35}
$$

The transient response, which is that part of the total response corresponding to the relaxation of the system modes, is given by the first term in the total response,

$$
x_{tr}(t) = \Phi(t,0) \left\{ \xi_0 - \sum_{m=-\infty}^{\infty} (s_m I - Q)^{-1} \bar{B}_m u_0 \right\}
\tag{3.36}
$$

The transient response vanishes for $t \to \infty$ if the system is strictly stable. The steady state forced response is then the second term in the total response, and is given by

$$
x_{ss}(t) = P(t) \sum_{m=-\infty}^{\infty} (s_m I - Q)^{-1} \bar{B}_m u_0 e^{s_m t}
\tag{3.37}
$$

Although the test input signal considered here is a complex exponential, the steady state forced response contains, in general, an infinite number of harmonics of the fundamental or pumping frequency ω_p, all modulated by the complex exponential input signal. To complete this discussion, the transient output response is given by

$$
\begin{aligned}
y_{tr}(t) &= C(t)x_{tr}(t) \\
&= C(t)\Phi(t,0) \left\{ \xi_0 - \sum_{m=-\infty}^{\infty} (s_m I - Q)^{-1} \bar{B}_m u_0 \right\}
\end{aligned}
\tag{3.38}
$$

and the steady state output response is given by

$$
y_{ss}(t) = C(t)P(t) \sum_{m=-\infty}^{\infty} (s_m I - Q)^{-1} \bar{B}_m u_0 e^{s_m t} + \sum_{n=-\infty}^{\infty} D_n u_0 e^{s_n t}
\tag{3.39}
$$

62

Several important conclusions can be drawn from the above analysis of the response of an LTP system to a complex exponential input. In the LTI case, the test input signal was a complex exponential, as was steady state output response. This steady state response provided the representation of the transfer function matrix. On the other hand, the steady state response of an LTP system to a complex exponential test input signal can contain many frequency components, including the input frequency, but excluding the pumping frequency, except when $\omega = 0$ and when ω is commensurate with ω_p. However, every frequency component in the steady state response is the complex exponential modulation of a harmonic of the pump frequency. In general, the steady state response of an LTP system to a complex exponential test input where the complex exponent is on the imaginary axis, $s = j\omega$, is aperiodic

$$y(t + T) \neq y(t) \tag{3.40}$$

unless the input frequency, ω, and the pump frequency, ω_p, are commensurate or $\omega = \dot{0}$. For example, if $\omega_p = 2\omega$, then the steady state response will be periodic with frequency ω. The relative amplitudes of the various harmonic components can be easily deduced from the steady state output response, although this is not done here explicitly.

In the remainder of this chapter, descriptions of an LTP system that are analogous to the LTI frequency response will be developed using a different test input signal that is of fundamental importance to LTP systems, namely, *geometrically periodic* or *(complex) exponentially modulated periodic* signals.

3.4 Fundamental Signal Spaces for LTP Systems

The objective of performing the analysis in the previous section was to develop insight into what class of input signals might lead to a linear map for LTP systems. It was shown in the previous section that the LTP system maps a complex exponential to a complex exponential modulation of a possibly infinite number of harmonics of the pumping frequency, so that it makes sense to include all harmonics of the pumping frequency in the test signal. It was stated previously that both Floquet and Hill have provided clear insight into what these signal spaces ought to be, and here the definitions of these signal spaces are formalized.

Recall from the Floquet theory that the homogeneous state response at time t, is related to the state state response a full period away, by a complex scalar,

$$x(t + T) = zx(t); \quad z \in C \tag{3.41}$$

At time $t + NT$, the state vector is related to the state vector at time t in similar fashion

$$x(t + NT) = z^N x(t) \tag{3.42}$$

Thus, in order to achieve the desired linear map, it is clear that a test input signal of the same form as (3.42) must be selected. This leads to the concept of a *geometrically periodic* signal.

Definition 3.1 (Geometrically periodic signals) *A geometrically periodic (GP) signal, $u(t)$, with fundamental frequency, ω_p, and corresponding fundamental period T, has the property that*

$$u(t + NT) = z^N u(t) \tag{3.43}$$

where $z \in C$. □

Note that this signal is fundamentally different from a periodic signal for which $|z| \equiv 1$. The notion of the geometrically periodic (GP) test signal will be most useful in the development of the LTP frequency response using an integral operator approach in the next section. A geometrically periodic signal can be expressed as a complex exponential modulation of a periodic signal. When the periodic portion of the GP signal is expressed as a complex Fourier series, the GP signal is referred to as an *exponentially modulated periodic signal* [83].

Definition 3.2 (Exponentially modulated periodic signals) *A (complex) exponentially modulated periodic (EMP) signal can be expressed as the complex Fourier series of a periodic signal of fundamental frequency, ω_p, modulated by a complex exponential (sinusoidal) signal,*

$$\begin{aligned} u(t) &= e^{st} \sum_{n=-\infty}^{\infty} u_n e^{jn\omega_p t} \\ &= \sum_{n=-\infty}^{\infty} u_n e^{s_n t}; \quad t \geq 0 \end{aligned} \tag{3.44}$$

where

$$s_n = s + jn\omega_p \tag{3.45}$$

and $s \in C$. □

The exponentially modulated periodic test signal will be used in the sequel to develop the LTP frequency response using a generalization of the harmonic balance methodology.

Lemma 3.3 *An exponentially modulated periodic signal can be expressed as a geometrically periodic signal, and vice versa.*

Proof: The two points of view, namely *geometrically periodic* (GP) and *exponentially modulated periodic* (EMP) signals, can be reconciled by noting that

$$z = e^{sT} \tag{3.46}$$

The proof follows directly from this fact, and that any periodic signal can be expanded uniquely in a complex Fourier series. □

A strong analogy will be proposed at this point. *Geometrically periodic (or exponentially modulated periodic) signals are to LTP systems as complex exponential signals are to LTI systems.* One difficulty that is introduced by the notion of the EMP signal is the infinite number of Fourier coefficients that might be required to describe a periodic signal. This is certainly a drawback, but one that is inherent to the analysis of LTP systems and cannot be avoided.

Clearly, GP signals for which $|z| < 1$ are $L_2[0,T]$ signals, and have bounded energy. Similarly, EMP signals for which $\text{Re}(s) < 0$, are $L_2[0,T]$ signals. In addition, an orthonormal basis for GP or EMP signals consists of complex exponentials at all multiples of the pump frequency.

Two closely related representations of an LTP system will be introduced. The first representation is based on an integral operator approach, and uses the definition of the geometrically periodic signal. The integral operator approach will permit the exploitation of the many results available in the mathematical literature on the kernels of integral operators [17]. The second approach is a generalization of the harmonic balance or describing function approaches that is more familiar to the theory of dynamics and control, and utilizes the definition of the (complex) exponentially modulated periodic signal. However, the harmonic balance approach has not been stated in the linear operator form as will be done here.

Both approaches are strongly related and this relationship will be discussed and quantified. Also, the benefits and disadvantages of each approach will be discussed in the remainder of this chapter.

3.5 LTP Frequency Response Using Integral Operators

In this section, the notion of the GP test input signal will be used to deduce frequency response notions for LTP systems. First, the response of LTP systems to GP signals will be examined.

Theorem 3.4 (LTP system response to GP signals) *Consider the state space model of an LTP system with time periodic dynamics,* $S = [A(t), B(t), C(t), D(t)]$. *If the input to the LTP system is a geometrically periodic signal,*

$$u(t + NT) = z^N u(t) \tag{3.47}$$

where z is not an eigenvalue of the monodromy matrix, then the total state response is the sum of a geometrically periodic **steady state response,**

$$
\begin{aligned}
x_{ss}(t) &= \Phi(t,0)[zI - \Phi(T,0)]^{-1} \int_0^T \Phi(T,\tau)B(\tau)u(\tau)d\tau \\
&\quad + \int_0^t \Phi(t,\tau)B(\tau)u(\tau)d\tau
\end{aligned}
\tag{3.48}
$$

and a **transient state response** *of the form*

$$x_{tr}(t) = \Phi(t,0)\left\{ \xi_o - [zI - \Phi(T,0)]^{-1} \int_0^T \Phi(T,\tau)B(\tau)u(\tau)d\tau \right\} \tag{3.49}$$

which vanishes as $t \to \infty$ if the system is asymptotically stable. Also, the geometrically periodic **steady state output response** *is given by*

$$
\begin{aligned}
y_{ss}(t) &= C(t)\Phi(t,0)[zI - \Phi(T,0)]^{-1} \int_0^T \Phi(T,\tau)B(\tau)u(\tau)d\tau \\
&\quad + C(t) \int_0^t \Phi(t,\tau)B(\tau)u(\tau)d\tau + D(t)u(t)
\end{aligned}
\tag{3.50}
$$

and the **transient output response** *is given by*

$$y_{tr}(t) = C(t)\Phi(t,0)\left\{ \xi_0 - [zI - \Phi(T,0)]^{-1} \int_0^T \Phi(T,\tau)B(\tau)u(\tau)d\tau \right\} \tag{3.51}$$

Proof: The total state response is given by the superposition equation [110] for initial state condition ξ_o,

$$x(t) = \Phi(t,0)\xi_o + \int_0^t \Phi(t,\tau)B(\tau)u(\tau)d\tau \tag{3.52}$$

66

If the input to the LTP system is GP, then a GP steady state response, $x_{ss}(t)$, exists (unless z is an eigenvalue of the monodromy matrix). To determine this GP solution, recall that

$$x(T) = z\xi_0$$
$$= \Phi(T,0)\xi_0 + \int_0^T \Phi(T,\tau)B(\tau)u(\tau)d\tau$$

Solving the above equations for the initial state, ξ_0, yields

$$\xi_0 = [zI - \Phi(T,0)]^{-1} \int_0^T \Phi(T,\tau)B(\tau)u(\tau)d\tau \tag{3.53}$$

The steady state response is then obtained by substitution of the above initial condition into the superposition equation (3.52), to obtain (3.48). Now, let us verify that the steady state response is indeed a GP signal, that is,

$$x_{ss}(t+T) = zx_{ss}(t) \tag{3.54}$$

To simplify the algebra, set

$$\alpha = [zI - \Phi(T,0)]^{-1} \int_0^T \Phi(T,\tau)B(\tau)u(\tau)d\tau \tag{3.55}$$

so that

$$x_{ss}(t) = \Phi(t,0)\alpha + \int_0^t \Phi(t,\tau)B(\tau)u(\tau)d\tau \tag{3.56}$$

One full period later, the steady state response is given by

$$x_{ss}(t+T) = \Phi(t+T,0)\alpha + \int_0^{t+T} \Phi(t+T,\tau)B(\tau)u(\tau)d\tau$$
$$= \Phi(t+T,0)\alpha + \int_0^T \Phi(t+T,\tau)B(\tau)u(\tau)d\tau$$
$$+ \int_T^{t+T} \Phi(t+T,\tau)B(\tau)u(\tau)d\tau \tag{3.57}$$

Applying a property of the state transition matrix

$$x_{ss}(t+T) = \Phi(t+T,T)\Phi(T,0)\alpha + \int_0^T \Phi(t+T,T)\Phi(T,\tau)B(\tau)u(\tau)d\tau$$
$$+ \int_T^{t+T} \Phi(t+T,\tau)B(\tau)u(\tau)d\tau \tag{3.58}$$

Since the state transition matrix is also periodic, that is,

$$\Phi(t+T,T) = \Phi(t,0) \tag{3.59}$$

a further simplification can be made,

$$
\begin{aligned}
x_{ss}(t+T) &= \Phi(t,0)\Phi(T,0)\alpha + \Phi(t,0)\int_0^T \Phi(T,\tau)B(\tau)u(\tau)d\tau \\
&\quad + \int_T^{t+T} \Phi(t+T,\tau)B(\tau)u(\tau)d\tau
\end{aligned}
\tag{3.60}
$$

The first integral can be expressed in terms of α,

$$
\int_0^T \Phi(T,\tau)B(\tau)u(\tau)d\tau = [zI - \Phi(T,0)]\,\alpha
\tag{3.61}
$$

so that grouping terms multiplied by α,

$$
\begin{aligned}
x_{ss}(t+T) &= \Phi(t,0)\left[\Phi(T,0) + zI - \Phi(T,0)\right]\alpha + \int_T^{t+T} \Phi(t+T,\tau)B(\tau)u(\tau)d\tau \\
&= z\Phi(t,0)\alpha + \int_T^{t+T} \Phi(t+T,\tau)B(\tau)u(\tau)d\tau
\end{aligned}
\tag{3.62}
$$

Let us consider the remaining integral separately. Making the change of variable, $\eta = \tau - T$,

$$
\begin{aligned}
\int_T^{t+T} \Phi(t+T,\tau)B(\tau)u(\tau)d\tau &= \int_0^t \Phi(t+T,\eta+T)B(\eta+T)u(\eta+T)d\eta \\
&= z\int_0^t \Phi(t,\eta)B(\eta)u(\eta)d\eta
\end{aligned}
\tag{3.63}
$$

Thus, grouping terms in z, and making the change of variable $\tau = \eta$,

$$
\begin{aligned}
x_{ss}(t+T) &= z\left(\Phi(t,0)\alpha + \int_0^t \Phi(t,\tau)B(\tau)u(\tau)d\tau\right) \\
&= zx_{ss}(t)
\end{aligned}
\tag{3.64}
$$

Therefore, the steady state response is a GP signal.

The transient response is obtained by noting that it is the difference between the total response from the superposition integral (3.52), and the GP steady state response (3.48),

$$
x_{tr}(t) = x(t) - x_{ss}(t)
\tag{3.65}
$$

The steady state output, $y_{ss}(t)$, is found by substitution of the GP state response into the output equation,

$$
y_{ss}(t) = C(t)x_{ss}(t) + D(t)u(t)
\tag{3.66}
$$

The steady state output is also GP, since

$$
\begin{aligned}
y_{ss}(t+T) &= C(t+T)x_{ss}(t+T) + D(t+T)u(t+T) \\
&= z\left[C(t)x_{ss}(t) + D(t)u(t)\right] \\
&= zy_{ss}(t)
\end{aligned}
\tag{3.67}
$$

The resulting transient output response is found from

$$y_{tr}(t) = C(t)x_{tr}(t) \tag{3.68}$$

concluding the proof.

Remark: The fundamental result shown above is that if a GP test signal, $u(t)$, is the input to an LTP system, then in steady state both the state, $x(t)$, and the output, $y(t)$, are also GP signals.   □

Thus, the steady state output leads to a transfer function for LTP systems.

Definition 3.5 (LTP integral operator representation) *The steady state output response can be expressed as*

$$y(t) = \int_0^T \widehat{G}(z; t, \tau)u(\tau)d\tau \tag{3.69}$$

where $t \in [0, T]$, and the integral operator kernel $\widehat{G}(z; t, \tau)$ is defined as

$$
\begin{aligned}
\widehat{G}(z; t, \tau) = & \ C(t)\Phi(t,0)\left[zI - \Phi(T,0)\right]^{-1}\Phi(T,\tau)B(\tau) \\
& + D(t)\delta(t - \tau) + \begin{cases} 0, & \tau > t \\ \frac{1}{2}C(t)B(t), & \tau = t \\ C(t)\Phi(t,\tau)B(\tau), & \tau < t \end{cases}
\end{aligned} \tag{3.70}
$$

The integral operator defined by (3.69–3.70) will be denoted by $\widehat{G}(z)$, so that (3.69) can be expressed in a more compact form,

$$y(t) = \widehat{G}(z)u(t) \tag{3.71}$$

where $z \in C$.   □

Note that $\widehat{G}(z; t, \tau)$ has been defined, for $t = \tau$, as the average of the integral operator kernel across the discontinuity. Since this is a set of measure zero, it does not affect the value of the integral. However, this choice of $\widehat{G}(z; t, t)$ is necessary to obtain correct limits in certain limiting procedures that will be required in the next chapter. Later, this requirement will be carefully described.

It will be shown that the integral operator $\widehat{G}(z)$ plays a similar role in the study of LTP systems as the transfer function matrix does in the theory of linear time invariant (LTI) multi–input multi–output (MIMO) systems. In order to continue the analogies with LTI systems, the state space model appropriate to the description of LTP systems evolving from period to period will be defined.

69

Definition 3.6 (Integral operator state space model) *A linear time periodic system can be represented by an* **integral operator state space model** *of the form*

$$\tilde{x}_{k+1} = \tilde{A}\tilde{x}_k + \tilde{B}\tilde{u}_k$$
$$\tilde{y}_k = \tilde{C}\tilde{x}_k + \tilde{D}\tilde{u}_k \tag{3.72}$$

Here, $\tilde{x}_k \in R^n$, and describes the state at the beginning of the kth period. The input, $\tilde{u}_k \in L_2^m[0,T]$, and the output $\tilde{y}_k \in L_2^m[0,T]$, are defined over the subinterval k as

$$\tilde{u}_k = u(t + kT)$$
$$\tilde{y}_k = y(t + kT) \tag{3.73}$$

for $k \in Z$ and $t \in [0,T]$. The dynamic integral operator, $\tilde{A}$, maps the state at time kT, denoted by $\tilde{x}_k$, to the state at time $(k+1)T$, denoted by $\tilde{x}_{k+1}$. The control distribution operator, $\tilde{B}$, maps a piece of the continuous time control signal, $\tilde{u}_k$, defined on the kth subinterval, to the state at time $(k + 1)T$. The measurement operator, $\tilde{C}$, maps the state at time kT to a piece of the continuous time measurement signal, $\tilde{y}_k$, defined on the kth subinterval. Finally, the feedforward operator, $\tilde{D}$, maps a piece of the continous time control signal, $\tilde{u}_k$, to a piece of the continuous time output signal, $\tilde{y}_k$, both defined on the kth subinterval. These maps can be expressed in the compact form; $\tilde{A} : C^n \to C^n$, $\tilde{B} : L_2^m[0,T] \to C^n$, $\tilde{C} : C^n \to L_2^m[0,T]$, $\tilde{D} : L_2^m[0,T] \to L_2^m[0,T]$. The operators are defined as

$$\tilde{A} = \Phi(T,0)$$
$$\tilde{B}\tilde{u}_k = \int_0^T \Phi(T,\tau)B(\tau)\tilde{u}_k \, d\tau$$
$$\tilde{C} = C(t)\Phi(t,0)$$
$$\tilde{D}\tilde{u}_k = \int_0^t \{C(t)\Phi(t,\tau)B(\tau) + D(t)\delta(t-\tau)\}\tilde{u}_k \, d\tau \tag{3.74}$$

The integral operator state space model will be denoted by $\tilde{S}$. The notation

$$\tilde{S} = \left[\begin{array}{c|c} \tilde{A} & \tilde{B} \\ \hline \tilde{C} & \tilde{D} \end{array} \right] = \left[\begin{array}{c|c} \Phi(T,0) & \tilde{B} \\ \hline \tilde{C} & \tilde{D} \end{array} \right] \tag{3.75}$$

or $\tilde{S} = [\tilde{A}, \tilde{B}, \tilde{C}, \tilde{D}] = [\Phi(T,0), \tilde{B}, \tilde{C}, \tilde{D}]$, is adopted to denote the the integral operator state space model. □

It should be noted that the above integral operator state space model is reminiscent of the state space models used to develop the discrete time control theory. The above definitions permit us to express the integral operator in a compact form, as stated in the following lemma.

Definition 3.7 (Integral operator transfer function) *The integral operator transfer function,* $\widehat{G}(z)$, *explicitly describes the relationship between the input,* $u(t) \in L_2^m[0,T]$ *and the output,* $y(t) \in L_2^p[0,T]$,

$$y(t) = \widehat{G}(z)u(t) \tag{3.76}$$

where

$$\widehat{G}(z) = \tilde{C}\left(zI - \tilde{A}\right)^{-1}\tilde{B} + \tilde{D} \tag{3.77}$$

where $z \in C$. □

Although the notation, $\tilde{A}$, has been introduced for the monodromy matrix, the notation $\Phi(T,0)$ will be retained for clarity.

The integral operator approach outlined above will prove useful in the development of a generalized Nyquist criterion for linear time periodic systems in Chapter 4 mainly due to the available results on the eigenvalues of integral operators [17], and will be useful primarily in an analytical context. However, the integral operator approach does not easily lend itself to numerical calculations, and alternative procedures will be developed for numerical work.

3.5.1 Poles in the z-plane

The eigenstructure of LTP systems has been examined in the Floquet context. However, the eigenstructure, as well as the transmission zeroes and associated directions, of an LTP system can be examined in the integral operator context to obtain useful insights into LTP system behavior.

The poles of an LTP system can be described in both the z-plane, using Floquet theory or the integral operator form of the LTP frequency response, or in the s-plane, using the generalized harmonic balance representation developed in the sequel. Both approaches lead to equivalent definitions of LTP system poles. Traditionally, the poles of an LTP system have been described in the z-plane as below.

71

Definition 3.8 (LTP poles in the z-plane) *The poles of an LTP system are the locations in the complex z-plane where the integral operator transfer function (3.48) is not analytic.*   □

This definition is based on the analyticity of the integral operator developed above, but the computation of the LTP poles is still the familiar eigenvalue problem from the Floquet theory.

Theorem 3.9 (LTP pole eigenvalue problem in the z-plane) *The z-plane poles of an LTP system, and their associated directions, are computed using the monodromy matrix eigenvalue problem,*

$$\{zI - \Phi(T,0)\}\, v = 0 \tag{3.78}$$

where $z \in C$.

Proof: This is obvious from the Floquet theorem, and is equally clear from the derivation of the steady state response using the integral operator formulation in Theorem 3.4.   □

The usual classification scheme [72,83] for the eigenvalues of the monodromy matrix will be adopted. The eigenvalues of the monodromy matrix are of three types: positive real, negative real, complex conjugate. The corresponding poles and mode shapes will be referred to as P type, N type, and C type, respectively. Each type of z–plane pole corresponds to a specific type of pole and mode shape in the s–plane as well, which will be made clear in the development of an s–plane operator in the sequel.

Definition 3.10 (LTP characteristic polynomial in the z-plane) *An LTP system has a characteristic polynomial, $\phi(z)$, defined by the determinant*

$$\phi(z) = \det\left[zI - \Phi(T,0)\right] \tag{3.79}$$

where $z \in C$.   □

This definition leads to an alternative computational method to the above eigenvalue problem, that is, to compute the roots of the *characteristic polynomial.*

Theorem 3.11 (LTP poles in the z-plane via the characteristic polynomial) *The poles of the LTP system can be determined by finding the roots of the characteristic polynomial, $\phi(z) = 0$.*

Proof: This result is the well known equivalence between the eigenvalue problem and the characteristic polynomial root finding problem.

Remark: The drawback of using the characteristic polynomial root finding problem is that no directional information, that is, the eigenvectors, can be extracted from the analysis. The only information obtained from the characteristic polynomial root finding problem is the pole locations.

□

The eigenvectors or directions of the poles have the standard interpretation associated with the linear system, and represent modes of the integral operator state space model. Alternatively, the eigenvectors represent the invariant subspaces associated with the state vector evolving from period to period.

3.5.2 LTP transmission zeroes in the z-plane

A transmission zero (or blocking zero) of an LTP system is determined from the internal and forced dynamics that lead to all outputs being identically zero (and, hence, all derivatives identically zero) for all $t > 0$. A precise definition is possible in terms of the GP signal.

Definition 3.12 (LTP transmission zeroes in the z-plane) *An LTP transmission zero is a location, z, in the z-plane, along with an initial state condition, ξ_o, and a geometrically periodic signal*

$$u(t + NT) = z^N u(t) \tag{3.80}$$

which when input to an LTP system leads to all outputs being identically zero for all time, that is, $y(t) \equiv 0$ for all $t \geq 0$.

This definition leads to the following theorem.

Theorem 3.13 (LTP transmission zero eigenvalue problem in the z-plane) *The zero locations, directions, and associated initial conditions, are determined using the LTP transmission zero generalized eigenvalue problem*

$$\begin{bmatrix} z\boldsymbol{I} - \boldsymbol{\Phi}(T,0) & -\tilde{\boldsymbol{B}} \\ -\tilde{\boldsymbol{C}} & -\tilde{\boldsymbol{D}} \end{bmatrix} \begin{bmatrix} \xi_o \\ u(t) \end{bmatrix} = 0 \tag{3.81}$$

where the operators $\tilde{\boldsymbol{B}}$, $\tilde{\boldsymbol{C}}$, and $\tilde{\boldsymbol{D}}$ were defined in Definition 3.6.

□

73

Proof: Recall that the total output response is the sum of the steady state response (3.50) and the transient response (3.51). The transient output response will vanish if

$$0 = \xi_0 - [zI - \Phi(T,0)]^{-1} \int_0^T \Phi(T,\tau)B(\tau)u(\tau)d\tau \tag{3.82}$$

The steady state response must also vanish, and noting the above,

$$0 = C(t)\Phi(t,0)\xi_0 + \int_0^t C(t)\Phi(t,\tau)B(\tau)u(\tau)d\tau + D(t)u(t) \tag{3.83}$$

Incorporating the definitions of the operators $\bar{B}$, $\bar{C}$, and $\bar{D}$ into (3.82) and (3.83), and rearranging, yields the system of equations

$$\begin{aligned}
0 &= [zI - \Phi(T,0)]\xi_0 - \bar{B}u(t) \\
0 &= -\bar{C}\xi_0 - \bar{D}u(t)
\end{aligned} \tag{3.84}$$

concluding the proof. $\square$

This integral operator form of the transmission zero generalized eigenvalue problem is completely analogous to its LTI counterpart. In principle, it would be possible to compute the zero locations and the form of the geometrically periodic signal, or direction of the zero, leading to zero output. Iterative methods based on a straightforward application of successive substitutions and a time discretization might be used, such as suggested by Cochran [17, page 103] for the computation of eigenvalues of integral operators. However, this computation is tedious in the time domain, and does not take advantage of the harmonic structure of GP signals. In the next section methods for computing the zeroes will be developed.

3.5.3 Principal gains and directions

The integral operator transfer function is a linear one-to-one map, and as a result, this linear map can be described by a singular value decomposition (SVD) that is analogous to the SVD analysis for the LTI transfer function matrix. The SVD analysis of an integral operator is described by Cochran [17]. The singular values provide the principal gains of the LTP system, and the singular vectors provide the principal directions, associated with the specific input–output relationship under investigation. However, the integral operator formulation as presented thus far, does not provide much insight into how these principal gains and directions are computed. Essentially the only conclusion that can be drawn is

74

that for every value of z on the unit circle (that is, a periodic input), there is a direction of maximal amplification. Alternatively, there is an input direction (signal) that leads to a maximally amplified output direction (signal) for a given z. These maximum input and output directions are a single basis vector of an infinite dimensional domain (input) and range (output) space associated with the particular integral operator transfer function in question. Finally, all of the singular values, input and output directions are parameterized by z.

A more satisfactory interpretation, and methods for computation, of the principal gains (singular values) and the principal directions (singular vectors), will be described in the next section, by utilizing the harmonic balance methodology.

3.6 LTP Frequency Response Using Harmonic Balance

To develop useful numerical calculation techniques, an approach different from that of integral operators is needed. A collection of numerical procedures will be required to compute poles, zeroes, principal gains, and their associated directional properties. The dichotomy of operator theoretic versus practical numerical procedures is not unusual, and in fact this dichotomy exists for the LTI theory as well. The linear operator for LTI systems is the transfer function. The fundamental arithmetic operation between transfer functions is the convolution of matrix polynomials. However, the convolution of matrix polynomials cannot be implemented on the computer very easily since it is a symbolic operation. Thus, virtually all of the numerical procedures developed for LTI systems use state space models where multiplication of matrices, both real and complex, are the fundamental operation of interest, and are easily dealt with by a computer. In fact, many authors, including Francis [31] and Doyle et al [23], concede that although the operator theory leads to many useful and elegant results, in the end the state space is used for computational methods, which are inferred from the operator theoretic results.

The numerical procedures developed here can be motivated by a simple and common observation. The time periodic parametric excitation associated with most physical systems can be expressed by a sum of sinusoids of relatively low harmonic number. This is certainly true of the Mathieu equation [72], the helicopter rotor [52, page 602], wind turbines [94], and satellites of various types in eccentric orbits [50,89], where at most only the first three

75

or four harmonics are required to describe the parametric excitation. Therefore, from an engineering standpoint, a sensible numerical procedure would attempt to exploit this tendency. Instead of attempting to develop methods based on a time discretization approach as suggested in [17], an approach based on the harmonic balance methodology is developed [27,46,47]. The harmonic balance approach offers two primary advantages. The first advantage is that low frequency contributions to the parametric excitation can be more easily captured than with a time discretization approach. Secondly, time periodic parametric excitation, and (complex) exponentially modulated periodic signals, are naturally described by the complex Fourier series.

According to Theorem 2.13, any LTP state space representation with a time periodic dynamics matrix, $A(t)$, can be expressed as a state space representation with a time invariant dynamics matrix, Q, but with possibly time periodic $\bar{B}(t)$, $\bar{C}(t)$, and $D(t)$. This fact will, again, be of central importance in deriving the harmonic balance form of the LTP frequency response. Here, it is desired to determine the frequency response of the state space model of an LTP system to a exponentially modulated periodic signal of the form (3.44), where the set of Fourier coefficients $\{u_m | m \in Z\}$ are constant vectors. This leads to the following theorem.

Theorem 3.14 (LTP system response to EMP signals) *Consider the state space model of an LTP system with time periodic dynamics matrix,* $S = [A(t), B(t), C(t), D(t)]$. *The LTP state space model can always be transformed to a state space model with time invariant dynamics,* $S = [Q, \bar{B}(t), \bar{C}(t), D(t)]$, *where* $\bar{B}(t) = P^{-1}(t)B(t)$ *and* $\bar{C}(t) = C(t)P(t)$. *The time periodic matrix* $\bar{B}(t)$ *can be expanded in a complex Fourier series of the form*

$$\bar{B}(\tau) = \sum_{l=-\infty}^{\infty} \bar{B}_l e^{jl\omega_p \tau} \tag{3.85}$$

and similarly for $\bar{C}(t)$ *and* $D(t)$. *If the input to the LTP system above is an EMP signal,*

$$u(t) = \sum_{m=-\infty}^{\infty} u_m e^{s_m t} \quad t \geq 0 \tag{3.86}$$

where $s_m = s + jm\omega_p$ *and* $s \in C$, *then the state response consists of an exponentially modulated periodic* **steady state response** *given by*

$$x_{ss}(t) = \sum_{n,l,m=-\infty}^{\infty} P_{n-l} (s_l I - Q)^{-1} \bar{B}_{l-m} u_m e^{s_n t} \tag{3.87}$$

76

and a **transient state response** *given by*

$$x_{tr}(t) = \Phi(t,0) \left\{ \xi_0 - \sum_{l,m=-\infty}^{\infty} (s_l I - Q)^{-1} \bar{B}_{l-m} u_m \right\} \qquad (3.88)$$

which vanishes as $t \to \infty$ *if the system is asymptotically stable. In addition, the* **steady state output response** *is an EMP signal of the form*

$$y_{ss}(t) = \sum_{n=-\infty}^{\infty} \left\{ \sum_{l,m=-\infty}^{\infty} \bar{C}_{n-l} (s_l I - Q)^{-1} \bar{B}_{l-m} u_m + \sum_{m=-\infty}^{\infty} D_{n-m} u_m \right\} e^{s_n t} \qquad (3.89)$$

and the **transient output response** *is given by*

$$y_{tr}(t) = C(t)\Phi(t,0) \left\{ \xi_0 - \sum_{l,m=-\infty}^{\infty} (s_l I - Q)^{-1} \bar{B}_{l-m} u_m \right\} \qquad (3.90)$$

Proof: The total state response is given by the superposition integral with initial condition on the states, ξ_0,

$$x(t) = \Phi(t,0)\xi_0 + \int_0^t \Phi(t,\tau)B(\tau)u(\tau)d\tau \qquad (3.91)$$

where the first term is the homogeneous response, $x_h(t)$, and the second term is the forced response, $x_f(t)$. First, let's examine the forced response,

$$x_f(t) = \int_0^t \Phi(t,\tau)B(\tau)u(\tau)d\tau \qquad (3.92)$$

From the properties of the state transition matrix,

$$\begin{aligned} \Phi(t,\tau) &= \Phi(t,0)\Phi(0,\tau) \\ &= \Phi(t,0)\Phi^{-1}(\tau,0) \end{aligned} \qquad (3.93)$$

so that

$$x_f(t) = \Phi(t,0) \int_0^t \Phi^{-1}(\tau,0)B(\tau)u(\tau)d\tau \qquad (3.94)$$

Using the Floquet result from Theorem 2.13,

$$\Phi(t,0) = P(t)e^{Qt} \qquad (3.95)$$

$$\Phi^{-1}(\tau,0) = e^{-Q\tau}P^{-1}(\tau) \qquad (3.96)$$

the forced response can be expressed as

$$x_f(t) = \Phi(t,0) \int_0^t e^{-Q\tau}P^{-1}(\tau)B(\tau)u(\tau)d\tau \qquad (3.97)$$

To simplify the algebra, let

$$\bar{B}(\tau) = P^{-1}(\tau)B(\tau) \tag{3.98}$$

Note that $\bar{B}(\tau)$ is a periodically time varying matrix and can be expanded in a complex Fourier series as in (3.85), and substituting for $u(\tau)$ from (3.86);

$$
\begin{aligned}
x_f(t) &= \Phi(t,0) \int_0^t e^{-Q\tau} \sum_{l=-\infty}^{\infty} \bar{B}_l e^{jl\omega_p\tau} \sum_{m=-\infty}^{\infty} u_m e^{s_m\tau} d\tau \\
&= \Phi(t,0) \int_0^t e^{-Q\tau} \sum_{l,m=-\infty}^{\infty} \bar{B}_l u_m e^{s_{l+m}\tau} d\tau \\
&= \Phi(t,0) \int_0^t e^{-Q\tau} \sum_{l,m=-\infty}^{\infty} \bar{B}_{l-m} u_m e^{s_l\tau} d\tau
\end{aligned}
$$

Interchanging the order of integration and double summation yields

$$
\begin{aligned}
x_f(t) &= \Phi(t,0) \sum_{l,m=-\infty}^{\infty} \int_0^t e^{(s_l I - Q)\tau} d\tau \bar{B}_{l-m} u_m \\
&= \Phi(t,0) \sum_{l,m=-\infty}^{\infty} \left\{ e^{(s_l I - Q)t} - I \right\} (s_l I - Q)^{-1} \bar{B}_{l-m} u_m
\end{aligned}
$$

so that the forced response is

$$x_f(t) = P(t) \sum_{l,m=-\infty}^{\infty} \left\{ e^{s_l t} I - e^{Qt} \right\} (s_l I - Q)^{-1} \bar{B}_{l-m} u_m \tag{3.99}$$

After grouping terms, the total state response is given by

$$
\begin{aligned}
x(t) &= \Phi(t,0) \left\{ \xi_0 - \sum_{l,m=-\infty}^{\infty} (s_l I - Q)^{-1} \bar{B}_{l-m} u_m \right\} \\
&+ P(t) \sum_{l,m=-\infty}^{\infty} (s_l I - Q)^{-1} \bar{B}_{l-m} u_m e^{s_l t}
\end{aligned} \tag{3.100}
$$

The first term in the total state response represents the transient state response,

$$x_{tr}(t) = \Phi(t,0) \left\{ \xi_0 - \sum_{l,m=-\infty}^{\infty} (s_l I - Q)^{-1} \bar{B}_{l-m} u_m \right\} \tag{3.101}$$

and the second term represents the steady state response,

$$x_{ss}(t) = P(t) \sum_{l,m=-\infty}^{\infty} (s_l I - Q)^{-1} \bar{B}_{l-m} u_m e^{s_l t} \tag{3.102}$$

Expanding $P(t)$ in a complex Fourier series,

$$P(t) = \sum_{n=-\infty}^{\infty} P_n e^{jn\omega_p t} \tag{3.103}$$

78

and substituting into (3.102) yields

$$x_{ss}(t) = \sum_{n=-\infty}^{\infty} P_n e^{jn\omega_p t} \sum_{l,m=-\infty}^{\infty} (s_l I - Q)^{-1} \bar{B}_{l-m} u_m e^{s_l t}$$

$$= \sum_{n,l,m=-\infty}^{\infty} P_n (s_l I - Q)^{-1} \bar{B}_{l-m} u_m e^{s_l + n t}$$

Making a change in the index variable produces a more convenient representation, namely,

$$x_{ss}(t) = \sum_{n,l,m=-\infty}^{\infty} P_{n-l} (s_l I - Q)^{-1} \bar{B}_{l-m} u_m e^{s_n t} \qquad (3.104)$$

The transient output response is determined from

$$y_{tr}(t) = C(t) x_{tr}(t)$$

$$= C(t)\Phi(t,0) \left\{ \xi_0 - \sum_{l,m=-\infty}^{\infty} (s_l I - Q)^{-1} \bar{B}_{l-m} u_m \right\} \qquad (3.105)$$

The steady state output response is determined from

$$y_{ss}(t) = C(t) x_{ss}(t) + D(t) u(t)$$

$$= C(t) P(t) \sum_{l,m=-\infty}^{\infty} (s_l I - Q)^{-1} \bar{B}_{l-m} u_m e^{s_l t} + \sum_{n,m=-\infty}^{\infty} D_n u_m e^{s_n + m t}$$

After making appropriate changes of index, the steady state output response becomes

$$y_{ss}(t) = \sum_{n=-\infty}^{\infty} \left\{ \sum_{l,m=-\infty}^{\infty} \bar{C}_{n-l} (s_l I - Q)^{-1} \bar{B}_{l-m} u_m + \sum_{m=-\infty}^{\infty} D_{n-m} u_m \right\} e^{s_n t} \qquad (3.106)$$

concluding the proof.   □

The fundamental result shown above is that when an EMP test signal is injected into an LTP system with a time periodic dynamics matrix, the steady state output response is also an EMP signal. Thus, the steady state output response leads to the concept of a transfer function for LTP systems because the input and output signal spaces are equal. Hence, the LTP frequency response can be stated: *in steady state, an LTP system maps an EMP input signal, to an EMP output signal of the same frequency, but with possibly different amplitude and phase (as long as s is not an eigenvalue of Q).* The LTP frequency response notion is completely analogous to the LTI frequency response notion. Of course, the amplitude in the LTP case refers to the amplitude of all the harmonics in the input and output signals, that is, the LTP system has directional properties that will be quantified in the sequel.

3.6.1 The harmonic transfer function

Manipulation of infinite series is cumbersome, so that an alternative notation is developed. In this section a linear operator, called the harmonic transfer function, is developed to represent the steady state response from Theorem 3.14. The harmonic transfer function relates all of the input harmonics to all of the output harmonics in a systematic way. Here, harmonic balance is applied directly without taking advantage of the Floquet result that transforms an LTP state space model with time periodic dynamics to an LTP state space model with time invariant dynamics, and possibly time periodic control distribution and measurement matrices.

Consider the proper LTP state space model with time periodic dynamics, $S = [A(t), B(t), C(t), D(t)]$. The test signal considered here is an EMP signal of the form,

$$u(t) = \sum_{m=-\infty}^{\infty} u_m e^{s_m t} \quad t \geq 0 \tag{3.107}$$

According to Theorem 3.14, the steady state response is an EMP signal of the form,

$$x(t) = \sum_{m=-\infty}^{\infty} x_m e^{s_m t} \tag{3.108}$$

$$\dot{x}(t) = \sum_{m=-\infty}^{\infty} s_m x_m e^{s_m t} \tag{3.109}$$

The output signal, $y(t)$, is simply a linear combination of the state and the control, so that it may also be expanded in a complex Fourier series,

$$y(t) = \sum_{n=-\infty}^{\infty} y_n e^{s_n t} \tag{3.110}$$

The T-periodic dynamics matrix can be expanded in a complex Fourier series,

$$A(t) = \sum_{m=-\infty}^{\infty} A_m e^{jm\omega_p t} \tag{3.111}$$

and similarly for $B(t)$, $C(t)$, and $D(t)$. Now, expanding the state dynamics equation from the LTP state space model in terms of the above complex Fourier series;

$$
\begin{aligned}
\sum_{n=-\infty}^{\infty} s_n x_n e^{s_n t} &= \sum_{n=-\infty}^{\infty} A_n e^{jn\omega_p t} \sum_{m=-\infty}^{\infty} x_m e^{s_m t} + \sum_{n=-\infty}^{\infty} B_n e^{jn\omega_p t} \sum_{m=-\infty}^{\infty} u_m e^{s_m t} \\
&= \sum_{n,m=-\infty}^{\infty} A_n x_m e^{s_n + m t} + \sum_{n,m=-\infty}^{\infty} B_n u_m e^{s_n + m t} \\
&= \sum_{n,m=-\infty}^{\infty} A_{n-m} x_m e^{s_n t} + \sum_{n,m=-\infty}^{\infty} B_{n-m} u_m e^{s_n t} \tag{3.112}
\end{aligned}
$$

A similar expansion of the measurement equation results in the following:

$$\sum_{n=-\infty}^{\infty} y_n e^{s_n t} = \sum_{n,m=-\infty}^{\infty} C_{n-m} x_m e^{s_n t} + \sum_{n,m=-\infty}^{\infty} D_{n-m} u_m e^{s_n t} \qquad (3.113)$$

Moving all terms to the RHS in equations (3.112—3.113) yields:

$$0 = \sum_{n=-\infty}^{\infty} \left\{ s_n x_n - \sum_{m=-\infty}^{\infty} A_{n-m} x_m - \sum_{m=-\infty}^{\infty} B_{n-m} u_m \right\} e^{s_n t}$$

$$0 = \sum_{n=-\infty}^{\infty} \left\{ y_n - \sum_{m=-\infty}^{\infty} C_{n-m} x_m - \sum_{m=-\infty}^{\infty} D_{n-m} u_m \right\} e^{s_n t} \qquad (3.114)$$

Now, multiplying through by e^{-st}, we note that the complex exponentials, $\{e^{jn\omega_p t} \mid n \in Z\}$, form an orthonormal basis in $L_2[0,T]$. Thus, from the *principle of harmonic balance*, the terms enclosed by braces in the above infinite sets of equations must vanish. Hence, the two equations below hold for all $n \in Z$:

$$s_n x_n = \sum_{m=-\infty}^{\infty} A_{n-m} x_m + \sum_{m=-\infty}^{\infty} B_{n-m} u_m$$

$$y_n = \sum_{m=-\infty}^{\infty} C_{n-m} x_m + \sum_{m=-\infty}^{\infty} D_{n-m} u_m \qquad (3.115)$$

Although the above equations are a concise representation of the input–output relationship between the Fourier coefficients of the input and output signals, manipulating summations can be tedious. Therefore, the Toeplitz form notation developed in Chapter 2 will be utilized as in the following definition.

Definition 3.15 (Harmonic state space model) *The system of equations from (3.115) can be expressed as the doubly infinite matrix equation,*

$$s\mathcal{X} = (\mathcal{A} - \mathcal{N})\mathcal{X} + \mathcal{B}u$$

$$\mathcal{Y} = \mathcal{C}\mathcal{X} + \mathcal{D}u \qquad (3.116)$$

where the doubly infinite vectors representing the harmonics of the state, control, and output

81

signals, are

$$\mathcal{X} = \begin{bmatrix} \vdots \\ x_{-2} \\ x_{-1} \\ x_0 \\ x_1 \\ x_2 \\ \vdots \end{bmatrix}, \quad \mathcal{U} = \begin{bmatrix} \vdots \\ u_{-2} \\ u_{-1} \\ u_0 \\ u_1 \\ u_2 \\ \vdots \end{bmatrix}, \quad \mathcal{Y} = \begin{bmatrix} \vdots \\ y_{-2} \\ y_{-1} \\ y_0 \\ y_1 \\ y_2 \\ \vdots \end{bmatrix}. \tag{3.117}$$

The T-periodic dynamics matrix, $A(t)$, is expressed in terms of its complex Fourier coefficients, $\{A_n | n \in Z\}$, as a doubly infinite block Toeplitz matrix called a **Toeplitz form**,

$$\mathcal{A} = \begin{bmatrix} \ddots & \vdots & \vdots & \vdots & \vdots & \vdots & \\ \cdots & A_0 & A_{-1} & A_{-2} & A_{-3} & A_{-4} & \cdots \\ \cdots & A_1 & A_0 & A_{-1} & A_{-2} & A_{-3} & \cdots \\ \cdots & A_2 & A_1 & A_0 & A_{-1} & A_{-2} & \cdots \\ \cdots & A_3 & A_2 & A_1 & A_0 & A_{-1} & \cdots \\ \cdots & A_4 & A_3 & A_2 & A_1 & A_0 & \cdots \\ & \vdots & \vdots & \vdots & \vdots & \vdots & \ddots \end{bmatrix} \tag{3.118}$$

with a similar definition for B in terms of its Fourier coefficients represented by $\{B_n | n \in Z\}$, C in terms of $\{C_n | n \in Z\}$, and $\mathcal{D}$ in terms of $\{D_n | n \in Z\}$. Finally, define a doubly infinite block diagonal matrix containing all harmonics of the pumping frequency,

$$\mathcal{N} = \text{blkdiag}\{jn\omega_p I\} \quad \forall n \in Z \tag{3.119}$$

This doubly infinite matrix equation (3.116) is called the **harmonic state space model**, *denoted by S. The notation,*

$$S = \left[\begin{array}{c|c} \mathcal{A} - \mathcal{N} & \mathcal{B} \\ \hline \mathcal{C} & \mathcal{D} \end{array} \right] \tag{3.120}$$

or $S = [(\mathcal{A}\text{-}\mathcal{N}), \mathcal{B}, \mathcal{C}, \mathcal{D}]$, is adopted to denote the harmonic state space model. □

The above harmonic state space model is a useful representation of the LTP system, and is very similar to the Toeplitz and circulant systems state space models for spatially invariant linear systems. A Toeplitz system is composed of an infinite number of identical

subsystems [105]. In fact, if the modulation frequency matrix in the harmonic state space model is set to zero, $\mathcal{N} = 0$, then the harmonic state space model is identical to the infinite dimensional Toeplitz system. Toeplitz systems have been studied in great detail by Chu [15], Melzer and Kuo [75], and Wall [105]. The cited research explores the use of the z–transform in the design of optimal feedback controllers for both the centralized and decentralized cases for continuous time Toeplitz systems. Wall [105] developed a transformation to alleviate some of the computational difficulties associated with the infinite dimensionality of Toeplitz systems. Circulant systems are finite dimensional analogs of Toeplitz systems, and are also examined in [105].

Unfortunately, the Toeplitz system results are not directly applicable to the LTP case. The dynamic operator, $(\mathcal{A} - \mathcal{N})$, associated with the harmonic state space model is *quasi-Toeplitz*, that is, the dynamic operator is the difference between a doubly infinite block Toeplitz matrix or Toeplitz form, $\mathcal{A}$, and a doubly infinite block diagonal complex matrix, $\mathcal{N}$. In addition, the harmonic state space model has much more structure than the typical Toeplitz system. The harmonic operators $\mathcal{A}$, $\mathcal{B}$, $\mathcal{C}$, and $\mathcal{D}$, are Toeplitz forms as defined by Grenander [38], and are Hermitian. The harmonics associated with a given system matrix generally grow small as the harmonic number grows large and can be represented by a complex Fourier series. A truncated complex Fourier series suffices for most dynamical systems. Thus, the harmonic operators are effectively banded Toeplitz forms. However, these are not requirements for general Toeplitz systems as described by Wall [105], so that the additional structure in the LTP problem would not be exploited by Wall's results.

The objective of the above analysis was to determine an explicit input-output functional relationship between the Fourier coefficients or harmonics of the input, $\{u_n | n \in Z\}$, and those of the output, $\{y_n | n \in Z\}$. This relationship is represented by the *harmonic transfer function*, $\widehat{\mathcal{G}}(s)$.

Definition 3.16 (Harmonic transfer functions) *The* **harmonic transfer function,** $\widehat{\mathcal{G}}(s)$, *is an infinite dimensional matrix of Fourier coefficients that describes the input–output relationship between the harmonics of the input signal, and those of the output signal, such that*

$$y = \widehat{\mathcal{G}}(s)u \tag{3.121}$$

where

$$\hat{\mathcal{G}}(s) = \mathcal{C} \left[s\mathcal{I} - (\mathcal{A} - \mathcal{N}) \right]^{-1} \mathcal{B} + \mathcal{D} \qquad (3.122)$$

as long as the inverse exists. □

This definition of the harmonic transfer function is obtained by eliminating $\mathcal{X}$ from (3.116), in favor of $\mathcal{Y}$ and $\mathcal{U}$, results in the the desired input—output relationship.

However, there are two problems associated with the harmonic transfer function as stated above. First, it is not clear that the harmonic transfer function, which requires the inversion of a doubly infinite matrix, will always exist. This problem will be dealt with, in general, by application of the Floquet Theorem as was done in Theorem 3.14. This is done in the first example considered below. Second, the harmonic transfer function is a doubly infinite matrix operator, which cannot be implemented on the computer. However, truncation of the harmonic transfer function leads to numerical procedures that can be easily implemented on the computer.

Now, let us consider some simplifying cases of the harmonic transfer function.

Example 3.1 (Transformation to time invariant dynamics) In this example, the Floquet transformation is applied to simplify the doubly infinite block Toeplitz of the dynamics matrix, $\mathcal{A}$, to a simpler doubly infinite block diagonal form. Consider the linear time periodic system, $S = [A(t), B(t), C(t), D(t)]$, with time periodic dynamics and state vector, $x(t)$. Application of the Floquet transformation results in a new realization, $S = [Q, \bar{B}(t), \bar{C}(t), D(t)]$, with a constant dynamics matrix and state vector, $v(t)$. Here, Q is a constant matrix, so that

$$\mathcal{Q} = \text{blkdiag}\{Q\} \qquad (3.123)$$

As a result, the system of equations (3.115) can be simplified after solving for v_l

$$v_l = (s_l I - Q)^{-1} \sum_{m=-\infty}^{\infty} \bar{B}_{l-m} u_m \quad \forall l \in Z$$

$$y_n = \sum_{l=-\infty}^{\infty} \bar{C}_{n-l} v_l + \sum_{m=-\infty}^{\infty} D_{n-m} u_m \quad \forall n \in Z \qquad (3.124)$$

Substituting for v_l in the output equation yields the input—output relationship:

$$y_n = \sum_{m=-\infty}^{\infty} \left\{ \sum_{l=-\infty}^{\infty} \bar{C}_{n-l} (s_l I - Q)^{-1} \bar{B}_{l-m} + D_{n-m} \right\} u_m \quad \forall n \in Z \qquad (3.125)$$

84

Hence, the harmonic transfer function is simply the terms in parentheses and can be expressed as

$$\widehat{\mathcal{G}}_{n,m}(s) = \sum_{l=-\infty}^{\infty} \bar{C}_{n-l} (s_l I - Q)^{-1} \bar{B}_{l-m} + D_{n-m} \quad \forall m, n \in Z \qquad (3.126)$$

Although application of the Floquet transformation has simplified the form of the harmonic transfer function, each block element of $\widehat{\mathcal{G}}(s)$ is evaluated using an infinite summation of Fourier coefficients. This result produces the same EMP steady state output response that was obtained in Theorem 3.14. Finally, the application of the second Floquet result has demonstrated that the inverse $[s\mathcal{I} - (\mathcal{A} - \mathcal{N}]^{-1})$ exists as long as s_n is not an eigenvalue of Q for all $n \in Z$. $\qquad\qquad\qquad\qquad\qquad\qquad\qquad\qquad\qquad\qquad$ $\square$

A large class of problems that are important in the study of periodically time varying systems are those represented by LTI plants with input or output amplitude modulations. These include such things as N-path networks [103, see Chapter 11] and commutated networks [97], as well as a host of communication network applications. The harmonic transfer functions for both these cases simplify markedly as shown in the following two examples.

Example 3.2 (LTI plant with modulated input) Consider the state space models of an amplitude modulated input to an LTI plant, $S = [Q, B(t), C, D(t)]$. Again, Q is a constant matrix, so that Q is an infinite dimensional block diagonal matrix given by equation (3.123). As a result, equations (3.115) can be further simplified after solving for x_n, so that

$$x_n = (s_n I - Q)^{-1} \sum_{m=-\infty}^{\infty} B_{n-m} u_m$$

$$y_n = C x_n + \sum_{m=-\infty}^{\infty} D_{n-m} u_m \qquad (3.127)$$

Substituting for x_n in the output equation yields the input–output relationship

$$y_n = \sum_{m=-\infty}^{\infty} \left\{ C(s_n I - Q)^{-1} B_{n-m} + D_{n-m} \right\} u_m \quad \forall n \in Z \qquad (3.128)$$

Hence, the harmonic transfer function is simply the terms in parentheses,

$$\widehat{\mathcal{G}}_{n,m}(s) = C(s_n I - Q)^{-1} B_{n-m} + D_{n-m} \quad \forall m, n \in Z \qquad (3.129)$$

Here, no infinite sums are required to determine the elements of the harmonic transfer function as was the case in the previous example. $\qquad\qquad\qquad\qquad\qquad\qquad$ $\square$

Example 3.3 (LTI plant with modulated output) Consider the state space model of an amplitude modulated output from an LTI plant, $S = [Q, B, C(t), D(t)]$. Following the identical procedure to Example 3.2 yields the harmonic transfer function

$$\widehat{\mathcal{G}}_{n,m}(s) = C_{n-m}\left(s_m I - Q\right)^{-1} B + D_{n-m} \quad \forall m, n \in Z \qquad (3.130)$$

As in Example 3.2, no infinite sums must be computed. $\qquad\qquad\qquad\qquad \square$

Two different forms of the harmonic transfer function were presented. The first form of the harmonic transfer function developed in Theorem 3.14 and in Example 3.1, corresponds to the harmonic state space model $\mathcal{S} = [(Q\text{-}\mathcal{N}), \bar{B}, \bar{C}, \mathcal{D}]$, and has a block diagonal dynamics matrix in its harmonic balance form. The second form of the harmonic transfer function, as developed in Lemma 3.16, corresponds to the harmonic state space model $\mathcal{S} = [(\mathcal{A}\text{-}\mathcal{N}), \bar{B}, \bar{C}, \mathcal{D}]$, and has a dynamic operator that is a full quasi–Toeplitz matrix. However, both representations of the harmonic transfer function must be related since they describe the same input–output relationship. In the following lemma, a similarity transformation is described that quantifies this relationship.

Lemma 3.17 (A similarity transformation) *Consider the LTP state space model,* $S = [A(t), B(t), C(t), D(t)]$. *Its harmonic state space model, denoted by the 4-tuplet* $\mathcal{S} = [(\mathcal{A} - \mathcal{N}), \mathcal{B}, \mathcal{C}, \mathcal{D}]$, *has a doubly infinite block Toeplitz dynamics matrix,* $\mathcal{A}$:

$$s\mathcal{X} = (\mathcal{A} - \mathcal{N})\mathcal{X} + \mathcal{B}u$$
$$y = \mathcal{C}\mathcal{X} + \mathcal{D}u \qquad (3.131)$$

A similarity transformation is given by

$$\mathcal{X} = \mathcal{P}v \qquad (3.132)$$

where $\mathcal{P}$ is the doubly infinite block Toeplitz matrix formed from the Fourier coefficients of the T-periodic matrix $P(t)$ introduced in the Floquet Theorem. Using the above similarity transformation, the above harmonic state space model can be transformed to a harmonic state space model, denoted by the 4-tuplet $\mathcal{S} = [(Q - \mathcal{N}), \bar{B}, \bar{C}, \mathcal{D}]$, such that Q is a doubly infinite block diagonal dynamics matrix,

$$sv = (Q - \mathcal{N})v + \bar{B}u$$
$$y = \bar{C}v + \mathcal{D}u \qquad (3.13?)$$

86

Here:

$$\begin{aligned}
\mathcal{Q} - \mathcal{N} &= \mathcal{P}^{-1}(\mathcal{A} - \mathcal{N})\mathcal{P} \\
\bar{\mathcal{B}} &= \mathcal{P}^{-1}\mathcal{B} \\
\bar{\mathcal{C}} &= \mathcal{C}\mathcal{P}
\end{aligned}$$
(3.134)

Proof: Recall from the Floquet theorem that the similarity transformation applicable in the time domain is

$$x(t) = P(t)v(t)$$
(3.135)

and led to the relationships in (2.42). Multiplying the first two of these relationships by $P(t)$ yields:

$$\begin{aligned}
P(t)Q &= A(t)P(t) - \dot{P}(t) \\
P(t)\bar{B}(t) &= B(t) \\
\bar{C}(t) &= C(t)P(t)
\end{aligned}$$

Since all of the above matrices are T-periodic, taking the Toeplitz transform of both sides yields:

$$\begin{aligned}
\mathcal{P}\mathcal{Q} &= \mathcal{A}\mathcal{P} - (\mathcal{N}\mathcal{P} - \mathcal{P}\mathcal{N}) \\
\mathcal{P}\bar{\mathcal{B}} &= \mathcal{B} \\
\bar{\mathcal{C}} &= \mathcal{C}\mathcal{P}
\end{aligned}$$

Rearranging yields the relationships in (3.134). $\qquad\qquad\square$

This similarity transformation is analogous to that for LTI systems and has the virtue that it is an algebraic similarity transformation, instead of a time varying similarity transformation requiring the solution of an ODE. Unfortunately, the similarity transformation requires the infinite dimensional Toeplitz form $\mathcal{P}$.

Although several simplifications to the harmonic transfer function have been presented, they are neither essential, nor are they limitations to the harmonic transfer function. The truncated harmonic transfer function can be determined experimentally by inputting a complex exponential, and measuring as many harmonic as desired.

Before discussing truncation of the harmonic transfer function, let us consider the definitions of poles and transmission zeroes, and methods for computing their locations and directions using harmonic balance.

3.6.2 LTP poles in the s-plane

In the discussion of the integral operator representation of an LTP system, the poles of an LTP system were defined in the z-plane. However, an equivalent statement can be made in the s-plane using the generalized harmonic balance formulation.

Definition 3.18 (LTP poles in the s-plane) *The poles of an LTP system are the locations in the complex s-plane where the harmonic transfer function is not analytic.* $\square$

This definition leads to the following theorem.

Theorem 3.19 (LTP pole eigenvalue problem in the s-plane) *The poles of the LTP system, and their associated directions, are computed in the complex s-plane using the eigenvalue problem*

$$\{s\mathcal{I} - (\mathcal{A} - \mathcal{N})\}\nu = 0 \tag{3.136}$$

In the case where the dynamics are similarity transformed to be time invariant, then the poles are given by the union of the eigenvalues from the eigenvalue problems

$$\{sI - (Q - jn\omega_p I)\}v = 0; \quad \forall\, n \in Z \tag{3.137}$$

where $s \in C$.

Proof: This is clear from the development of the harmonic transfer function, and can be deduced for time invariant dynamics from the form of the steady state response and from the similarity transformation derived in Lemma 3.17. $\square$

The definitions of LTP poles in the z-plane and the s-plane are equivalent because all of the s-plane poles map to the Floquet poles in the z-plane according to

$$z = e^{sT} \tag{3.138}$$

so that an infinite folding of poles occurs due to the infinite branches of the complex logarithm function. However, there are only as many unique poles as there are states in the linear time periodic state space model, that is, n unique poles, or the dimension of $A(t)$, or, equivalently, of Q. These unique poles are located in the *fundamental strip*, illustrated in Figure 3.3, defined as that infinite strip region in the s-plane for which

$$\text{Im}(s) \in \left(-\frac{\omega_p}{2}, \frac{\omega_p}{2}\right] \tag{3.139}$$

(a) s-plane **(b)** z-plane
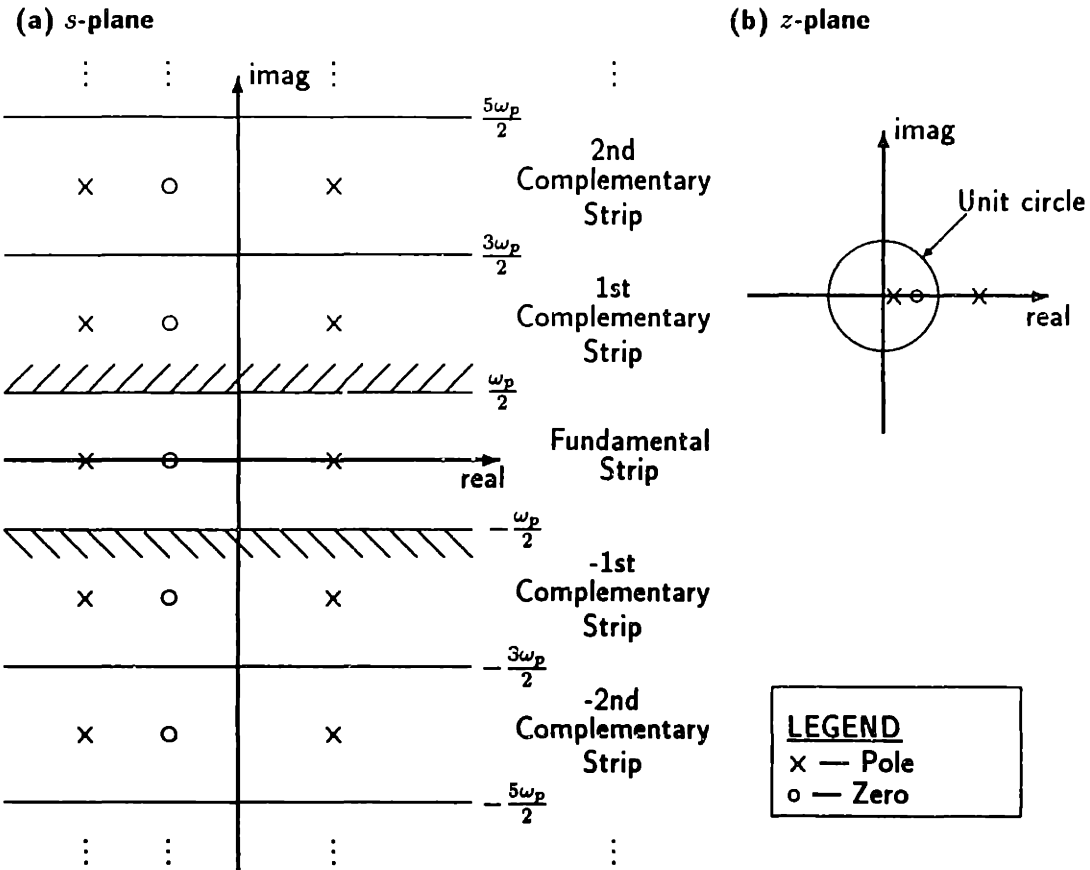
Figure 3.3: LTP pole-zero diagram. LTP systems have infinite folding of poles about the fundamental strip as shown in (a). The fundamental strip provides the unique set of s-plane poles that is transformed into the z-plane pole zero diagram shown in (b).

The branches of the logarithm function fold this set of unique poles about the fundamental strip such that there are n infinite families of poles, which are simply reflections of the poles in the fundamental strip into the complementary strips. The kth complementary strip is defined as that infinite strip region in the s-plane for which

$$\text{Im}(s) \in \left(\frac{(2k-1)\omega_p}{2}, \frac{(2k+1)\omega_p}{2} \right] \qquad k \in \mathbb{Z}, k \neq 0 \qquad (3.140)$$

The fundamental and complementary strips are shown in the pole-zero diagram in Figure 3.3.

This infinite folding of poles is well understood from the classical notion of the *characteristic exponents* of an LTP system [83]. As a practical observation, the pole locations in the complementary strips are obtained by adding $\pm jm\omega_p$, $\forall m \in Z$, to the pole locations in the fundamental strip, as stated in Theorem 3.19. In this thesis, the convention of considering only those pole locations in the fundamental strip of the complex s-plane is adopted, since the fundamental strip poles are a unique set.

Consideration of only a single branch of the logarithm function may lead one to believe that LTP systems do not have complex conjugate poles in the s-plane. In fact, LTP systems always have complex conjugate poles when all branches of the logarithm function are considered. To illustrate this, recall the definition of the complex logarithm [58, page 815],

$$s = \frac{1}{T}\left[\log|z| + j\angle z\right] + jn\omega_p \tag{3.141}$$

where each value of $n \in Z$ defines a different branch. However, since the poles in the z-plane are either real or complex conjugate, then the poles in the s-plane are either real or complex conjugate *when all branches of the logarithm function are considered.*

However, it is entirely possible that a complex pole location in the fundamental strip may not have a corresponding complex conjugate pole that is also in the fundamental strip. Recall that the eigenvalues of the monodromy matrix were classified as N type (negative real), P type (positive real), and C type (complex conjugate), and that they correspond to the z-plane poles of the LTP integral operator transfer function. For a P type z-plane pole,

$$s = \frac{1}{T}\log(a) + jn\omega_p, \quad z = a, \ a > 0, \ \forall \, n \in Z \tag{3.142}$$

that is, a P type pole in the z-plane corresponds to a pole on the real axis in the fundamental strip of the s-plane. For an N type z-plane pole,

$$s = \frac{1}{T}\log(a) + j\frac{(2n+1)\pi}{T}, \quad z = -a, \ a > 0 \tag{3.143}$$

that is, the N type pole in the z-plane corresponds to a pole on the horizontal boundary of the fundamental strip of the s-plane, for which $\mathrm{Im}(s) = j\frac{\omega_p}{2}$. Since the fundamental strip does not include the boundary, $\mathrm{Im}(s) = -j\frac{\omega_p}{2}$, an N type pole cannot have a complex conjugate in the fundamental strip. However, N type poles come in pairs, although not in complex conjugate pairs. Finally, a C type pole is a complex conjugate pole in the z-plane, and as a result, corresponds to complex conjugate pair of poles in the fundamental strip of the complex s-plane.

90

Associated with the pole is a direction that can be expressed as a complex periodic signal, or a mode shape of the LTP system. The pole direction is computed as follows. Associated with the ith pole in the fundamental strip, $s^{(i)}$, is an infinite dimensional right eigenvector, $\mathcal{V}^{(i)}$, both computed using the above LTP pole eigenvalue problem in the s–plane. The block vector elements, $\left\{ v_n^{(i)} \mid n \in Z \right\}$, of the right eigenvector $\mathcal{V}^{(i)}$ are the Fourier coefficients of the complex periodic signal that represents the fundamental mode shape. Thus, the ith mode shape can be expressed as the complex periodic signal

$$v^{(i)}(t) = \sum_{n=-\infty}^{\infty} v_n^{(i)} e^{jn\omega_p t} \tag{3.144}$$

The time response of the ith fundamental mode is given by

$$x^{(i)}(t) = e^{s^{(i)}t} \sum_{n=-\infty}^{\infty} v_n^{(i)} e^{jn\omega_p t} \tag{3.145}$$

Note that the mode shapes are folded just as the pole locations are folded into the complementary strips. To illustrate this, make the change of variable, $n = m + k$, in the above time response of the ith mode,

$$
\begin{aligned}
x^{(i)}(t) &= e^{s^{(i)}t} \sum_{m=-\infty}^{\infty} v_{m+k}^{(i)} e^{j(m+k)\omega_p t} \\
&= e^{\left(s^{(i)}+jk\omega_p\right)t} \sum_{m=-\infty}^{\infty} v_{m+k}^{(i)} e^{jm\omega_p t}
\end{aligned} \tag{3.146}
$$

Thus, the coefficients of the mode shape are shifted by the index k, and the pole is now located in the kth complementary strip.

The type of pole under consideration has some ramifications on the exact nature of the mode shape. For a P type pole, the pole in the fundamental strip of the s–plane is strictly real, so that $s = \alpha$. Hence, the time response of the P type mode is given by

$$x(t) = e^{\alpha t} \sum_{n=-\infty}^{\infty} v_n e^{jn\omega_p t} \tag{3.147}$$

which is the familar EMP signal. However, for an N type pole, the fundamental strip pole is given by $s = \alpha + j\frac{\omega_p}{2}$, so that the time response of the P type mode is given by

$$x(t) = e^{\alpha t} e^{j\frac{\omega_p}{2}} \sum_{n=-\infty}^{\infty} v_n e^{jn\omega_p t} \tag{3.148}$$

Thus, the N type pole also corresponds to an EMP signal. However, a subharmonic of period $2T$ or a $\frac{1}{2}$/rev subharmonic shows up in the modal response. Much of the discussion

91

by Johnson [52] on mode shapes concerns apportioning this $\frac{1}{2}$/rev periodicity in the mode shapes or in the pole. In this thesis, the convention of considering only those poles located in the fundamental strip was adopted. This implies that all $\frac{1}{2}$/rev periodicity is lumped into the pole location, and only the periodicity occuring at integer multiples of the pumping frequency, that is, the T-periodic portion of the modal response, is included in the mode shape. Finally, a C type pole is given by $s = \alpha + \pm j\beta$ in the fundamental strip. The modal response will appear as a complex exponential modulation of two T-periodic mode shapes. Of course, this leads to the well known exponentially modulated double sideband suppressed carrier behavior [83, page 24].

As an aside, if Q is defective, then this gives rise to boundary modes, or t-multiplied modes designated as P, tP, etc. or N, tN, etc. These are sometimes referred to as the Brillouin modes.

The T-periodic portion of the Floquet solution is easily identified using these techniques,

$$P(t) = \left[\begin{array}{cccc} v^{(1)}(t) & v^{(2)}(t) & \cdots & v^{(n)}(t) \end{array} \right] \tag{3.149}$$

The corresponding exponential rate matrix, Q, associated with the above $P(t)$ is given by

$$Q = \text{diag} \left[\begin{array}{cccc} s^{(1)} & s^{(2)} & \cdots & s^{(n)} \end{array} \right] \tag{3.150}$$

It should be noted that the above matrices are unique by convention, since the poles that make up the matrix, Q, are the unique set of s-planes poles from the fundamental strip, and the periodic portion of the Floquet solution, $P(t)$, corresponds to the unique normalized eigenvectors of $(\mathcal{A} - \mathcal{N})$. However, an equally valid Floquet solution can be obtained via any time invariant or time periodic similarity transformation applied to the state vector of the LTP state space model with time invariant dynamics.

The characteristic polynomial for the LTP system can also be defined in the s-plane using an infinite determinant representation. Based our intuition of LTI systems, we would expect the characteristic polynomial to be

$$\phi(s) = \det |s\mathcal{I} - (\mathcal{A} - \mathcal{N})| \tag{3.151}$$

However, the above determinant, which is the state space generalization of the pre-Hill determinant, does not converge.

Again, we resort to a simple normalization to render the above determinant convergent. The normalization is obtained by rewriting the homogeneous dynamics equation in the

92

harmonic state space model as

$$(s\mathcal{I} + \mathcal{N})x = \mathcal{A}x \tag{3.152}$$

so that

$$\left[\mathcal{I} - (s\mathcal{I} + \mathcal{N})^{-1}\mathcal{A} \right] x = 0 \tag{3.153}$$

The above equation has a nontrivial solution if the infinite determinant

$$\Delta(s) = \det \left[\mathcal{I} - (s\mathcal{I} + \mathcal{N})^{-1}\mathcal{A} \right] \tag{3.154}$$

equals zero, as long as the determinant is convergent. Therefore, let us consider the question of convergence. It can be shown that the above infinite determinant belongs to a known class of convergent determinants called *normal determinants*. The determinant

$$\Delta = \det \begin{bmatrix} 1 + c_{11} & c_{12} & c_{13} & \cdots \\ c_{21} & 1 + c_{22} & c_{23} & \cdots \\ c_{31} & c_{32} & 1 + c_{33} & \cdots \\ \vdots & \vdots & \vdots & \ddots \end{bmatrix} \tag{3.155}$$

is *normal* if the double series

$$\sum_{n,m=-\infty}^{\infty} c_{nm} \tag{3.156}$$

is absolutely convergent [9, page 21]. We can apply this result here. The summation over the index m corresponds to the mth block row sum of $(s\mathcal{I}+\mathcal{N})^{-1}\mathcal{A}$, which can be expressed as

$$\frac{1}{s_n} \sum_{m=-\infty}^{\infty} A_{n-m} \tag{3.157}$$

Now, we have assumed that $A(t)$ can be expanded in an absolutely convergent complex Fourier series, so that is can be summed to $\bar{A}$. Thus, each block row sum is absolutely convergent, since it corresponds to the Fourier coefficients of $A(t)$. The summation over the index n sums together all of the block row sums of $(s\mathcal{I} + \mathcal{N})^{-1}\mathcal{A}$, so that if

$$\bar{A} \sum_{n=-\infty}^{\infty} \frac{1}{s + jn\omega_p} \tag{3.158}$$

converges, then the infinite determinant also converges. The above infinite series can be summed in a special way,

$$\begin{aligned}
\sum_{n=-\infty}^{\infty} \frac{1}{s + jn\omega_p} &= \frac{1}{s} + \sum_{n=1}^{\infty} \left[\frac{1}{s + jn\omega_p} + \frac{1}{s - jn\omega_p} \right] \\
&= \frac{1}{s} + \sum_{n=1}^{\infty} \frac{2s}{s^2 + (n\omega_p)^2} \tag{3.159}
\end{aligned}$$

93

From [37], the series expansion of the hyperbolic cotangent is given by

$$\sum_{k=1}^{\infty} \frac{1}{a^2 + k^2} = \frac{\pi}{2a} \left(\coth \pi a - \frac{1}{\pi a} \right) \qquad (3.160)$$

After some simplification,

$$\frac{1}{s} + \sum_{n=1}^{\infty} \frac{2s}{s^2 + (n\omega_p)^2} = \coth \left(\frac{\pi s}{\omega_p} \right) \qquad (3.161)$$

so that the above series is absolutely convergent for s in the fundamental strip. Thus, the infinite determinant, $\Delta(s)$, is a normal determinant, and is the state space interpretation of the Hill determinant.

Thus, we proceed to the following definition.

Definition 3.20 (The open loop Hill determinant) *An LTP system has a Hill determinant, $\Delta(s)$, defined as the convergent infinite determinant*

$$\Delta(s) = \det \left[\mathcal{I} + (s\mathcal{I} + \mathcal{N})^{-1} \mathcal{A} \right] \qquad (3.162)$$

where $s \in C$. □

The above Hill determinant can be expressed in terms of the exponential rate matrix, Q, from the Floquet solution.

Lemma 3.21 *The characteristic polynomial can be expressed as the infinite product of finite dimensional determinants,*

$$\Delta(s) = \prod_{n=-\infty}^{\infty} \det \left[I - \frac{1}{s_n} Q \right] \qquad (3.163)$$

Proof: The proof is an application of the similarity transformation that was derived in Lemma 3.17.

Remark: One difficulty introduced by the normalization that leads to the Hill determinant is the introduction of singularities on the $j\omega$ axis at $s = jn\omega_p$ for all $n \in Z$, including a singularity at the origin. To use the Hill determinant as a numerical method requires that we define a new function that only has singularities at the poles of the LTP system. This can be accomplished using Louisville's theorem as described in [83]. However, the method of choice for determining the open loop poles is the truncated s-plane pole eigenvalue problem, or the z-plane pole eigenvalue problem, so that application of the Hill determinant methodology is not considered further. □

3.6.3 LTP transmission zeroes in the s-plane

As was the case for poles, the zeroes of an LTP system can be determined using both the integral operator (z-plane) and generalized harmonic balance (s-plane) formulations.

Definition 3.22 (LTP transmission zeroes in the s-plane) *An LTP transmission zero is a location in the complex s-plane, s_z, along with an input direction corresponding to an EMP signal*

$$u(t) = \sum_{m=-\infty}^{\infty} u_m e^{(s_z + jm\omega_p)t} \tag{3.164}$$

and an initial condition for the states, ξ_0, which when input to an LTP system with a square LTP state space model, leads to all outputs being identically zero for all time; that is, $y(t) \equiv 0$, for all $t \geq 0$. □

This definition is an extension of the definition for LTP zeroes in the z-plane using the definition of the EMP signal, and leads to the theorem below.

Theorem 3.23 (LTP transmission zero eigenvalue problem in the s-plane) *Consider a square LTP state space model, that is, an LTP state space model with the same number of inputs as outputs. The LTP transmission zero located at $s = s_z$, with input direction u_0 and initial condition v_0, is determined from the infinite dimensional generalized eigenvalue problem*

$$\begin{bmatrix} s_z \mathcal{I} - (\mathcal{Q} - \mathcal{N}) & -\bar{\mathcal{B}} \\ -\bar{\mathcal{C}} & -\mathcal{D} \end{bmatrix} \begin{bmatrix} v_0 \\ u_0 \end{bmatrix} = 0 \tag{3.165}$$

*where ξ_0 is the non-trivial partition of v_0, and complex valued u_0 contains the harmonics of the EMP signal associated with the transmission zero, or the **direction** of the transmission zero.*

Proof: The proof essentially involves expanding the total output response from Theorem 3.14 in harmonics, and selecting the initial condition such that the transient and steady state portions of the output response vanish for all time. Recall the transient output response, from (3.90),

$$\begin{aligned} y_{tr}(t) &= 0 \\ &= C(t)\Phi(t,0)\left\{ \xi_0 - \sum_{l,m=-\infty}^{\infty} (s_l I - Q)^{-1} \bar{B}_{l-m} u_m \right\} \end{aligned}$$

95

which will vanish for all $t > 0$, if

$$\xi_0 = \sum_{l,m=-\infty}^{\infty} (s_l I - Q)^{-1} \bar{B}_{l-m} u_m \qquad (3.166)$$

The above equation can also be expressed as the infinite dimensional matrix equation,

$$\nu_0 = \{s\mathcal{I} - (\mathcal{Q} - \mathcal{N})\}^{-1} \bar{\mathcal{B}} u_0 \qquad (3.167)$$

where it is understood that u_0 contains the harmonics of the EMP signal that must be the system input for trivial output. ν_0 contains the harmonics of the initial condition, for which there is only one non-zero block containing ξ_0. Recall the steady state output response from Eq. (3.89), which must also vanish for all $t > 0$,

$$
\begin{aligned}
y_{ss}(t) &= 0 \\
&= \sum_{n=-\infty}^{\infty} \left\{ \sum_{l,m=-\infty}^{\infty} \bar{C}_{n-l} (s_l I - Q)^{-1} \bar{B}_{l-m} u_m + \sum_{m=-\infty}^{\infty} D_{n-m} u_m \right\} e^{s_n t} \quad .
\end{aligned}
$$

Applying the principle of harmonic balance, we obtain a second infinite dimensional matrix equation,

$$0 = \bar{\mathcal{C}} \{s\mathcal{I} - (\mathcal{Q} - \mathcal{N})\}^{-1} \bar{\mathcal{B}} u_0 + \mathcal{D} u_0 \qquad (3.168)$$

This equation can be simplified using the previous result from (3.167), so that

$$0 = -\bar{\mathcal{C}} \nu_0 - \mathcal{D} u_0 \qquad (3.169)$$

Rearranging (3.167), yields

$$0 = \{s\mathcal{I} - (\mathcal{Q} - \mathcal{N})\} \nu_0 - \bar{\mathcal{B}} u_0 \qquad (3.170)$$

concluding the proof. $\qquad\qquad\qquad\qquad\qquad\qquad\qquad\qquad\qquad\qquad\qquad\square$

It is also possible to compute the transmission zero locations and directions directly from the harmonic state space model of the LTP state space model with time periodic dynamics.

Corollary 3.24 (A similar transmission zero eigenvalue problem in the s-plane)
The LTP transmission zero at $s = s_z$, input direction, u_0, and initial condition x_0, are determined from the infinite dimensional generalized eigenvalue problem

$$\begin{bmatrix} s_z \mathcal{I} - (\mathcal{A} - \mathcal{N}) & -\mathcal{B} \\ -\mathcal{C} & -\mathcal{D} \end{bmatrix} \begin{bmatrix} x_0 \\ u_0 \end{bmatrix} = 0 \qquad (3.171)$$

where ξ_0 is the block sum of x_0, and complex valued u_0 contains the harmonics of the EMP signal associated with the transmission zero, or the direction of the transmission zero.

96

Proof: The above generalized eigenvalue problem can be developed by applying the similarity transformation

$$\begin{bmatrix} x_0 \\ u_0 \end{bmatrix} = \begin{bmatrix} \mathcal{P} & 0 \\ 0 & \mathcal{I} \end{bmatrix} \begin{bmatrix} v_0 \\ u_0 \end{bmatrix} \tag{3.172}$$

to the transmission zero generalized eigenvalue problem in Theorem 3.23. The interpretation of u_0 remains the same. However, an interpretation of x_0 is required.

The similarity transformation is given by

$$x(t) = P(t)v(t) \tag{3.173}$$

and since $x(t)$ and $v(t)$ are EMP signals, and $P(t)$ is a T–periodic matrix, then

$$0 = \sum_{n=-\infty}^{\infty} \left\{ x_n - \sum_{m=-\infty}^{\infty} P_{n-m} v_m \right\} e^{s_n t} \tag{3.174}$$

Applying the principle of harmonic balance,

$$x_n = \sum_{m=-\infty}^{\infty} P_{n-m} v_m; \quad \forall n \in Z \tag{3.175}$$

But from Theorem 3.23, the initial state condition associated with the transmission zero in the kth complementary strip shows up in a single block of v_0, say the kth block, so that

$$\begin{aligned} v_m &= \xi_o \delta_{m-k} \\ &= \begin{cases} \xi_o & \text{for } m = k \\ 0 & \text{otherwise} \end{cases} \end{aligned} \tag{3.176}$$

However, we are only interested in the unique fundamental strip transmission zero, so that $k = 0$, and

$$v_m = \xi_o \delta_m \tag{3.177}$$

The initial condition for the similarity transformed problem becomes

$$\begin{aligned} x_n &= \sum_{m=-\infty}^{\infty} P_{n-m} v_m \\ &= \sum_{m=-\infty}^{\infty} P_{n-m} \xi_o \delta_m \\ &= P_n \xi_o \end{aligned} \tag{3.178}$$

that is, the initial state condition, ξ_o is sifted through the harmonics of $P(t)$. Alternatively if we search for a transmission zero in the kth complementary strip , then $v_m = \xi_o \delta_{m-k}$,

97

and

$$x_n = P_{n-k}\xi_0 \quad \forall n \in Z \tag{3.179}$$

Recall that the state transition matrix for the LTP system can be expressed as

$$\Phi(t,0) = P(t)e^{Qt} \tag{3.180}$$

Since $\Phi(0,0) = I$, evaluating at $t = 0$, determines that $P(0)=I$. Also, since $P(t)$ is T-periodic, evaluating its complex Fourier series for $t = 0$ produces the result

$$
\begin{aligned}
P(0) &= \sum_{n=-\infty}^{\infty} P_n \\
&= I
\end{aligned}
\tag{3.181}
$$

Now, summing both sides of (3.179) over all values of n,

$$
\begin{aligned}
\sum_{n=-\infty}^{\infty} x_n &= \sum_{n=-\infty}^{\infty} P_{n-k}\xi_0 \\
&= \left(\sum_{n=-\infty}^{\infty} P_n \right) \xi_0 \\
&= \xi_0
\end{aligned}
\tag{3.182}
$$

Thus, the initial condition for the transmission zero eigenvalue problem is the block sum of x_0. $\qquad\square$

By again utilizing the generalized harmonic balance methodology, the transmission zero computation can be performed in relatively simple fashion using standard eigenvalue problem software.

The transmission zeroes, and transmission zero directions, are also folded about the fundamental strip in the same manner as the poles, leading to infinite families of transmission zeroes. Again, only zeroes in the fundamental strip will be considered. Consider the ith transmission zero in the fundamental strip, $s_z^{(i)}$. The direction of the transmission zero leads to the form of the EMP signal that must be input to the LTP system, along with the initial condition ξ_0, to obtain trivial output for all time. This transmission zero signal (direction) is computed as follows. The block vector elements, $\left\{ u_{0,n}^{(i)} \mid n \in Z \right\}$, of the infinite dimensional vector $u_0^{(i)}$, are the Fourier coefficients of the input signal, so that the transmission zero direction is given by the EMP signal

$$u_0(t) = e^{s_z^{(i)}t} \sum_{n=-\infty}^{\infty} u_{0,n}^{(i)} e^{jn\omega_p t}; \quad \forall n \in Z \tag{3.183}$$

3.6.4 Pole–zero diagram

Having stated how the poles and zeroes of an LTP system can be computed, the pole-zero diagram can be constructed in both the z-plane and the s-plane. The pole-zero diagram of a typical LTP system is shown in Figure 3.3. In the s-plane, the poles and zeroes are folded about the fundamental strip, which contains the imaginary axis from $\omega \in (-\omega_p/2, \omega_p/2]$, by multiples of the fundamental or pumping frequency, ω_p, as shown in Figure 3.3a. The infinite number of s-plane poles are all mapped to a finite unique set of poles and zeroes in the z-plane, as shown in Figure 3.3b. Clearly, the z-plane representation of the pole–zero diagram is much more convenient than its counterpart in the s-plane for the simple reason that the z-plane poles are finite in number. In addition, consideration of different branches of the logarithm function is not necessary in the z–plane.

3.6.5 Principal gains and directions

In this section, we propose to study the principal gains of the LTP system, by studying the singular value decomposition (SVD) of the truncated harmonic transfer function.

Here, N will denote the number of positive harmonics included in a given analysis, with the implication being that an equal number of negative harmonics and the zero harmonic are also included in the truncated HTF. Hence, the set of integers $Z_N = \{-N, -N+1, \cdots, N-1, N\}$ is defined.

The complex Fourier series associated with the state, input, and output are truncated, as below:

$$
\mathcal{X}_N = \begin{bmatrix} x_{-N} \\ \vdots \\ x_{-1} \\ x_0 \\ x_1 \\ \vdots \\ x_N \end{bmatrix}, \mathcal{U}_N = \begin{bmatrix} u_{-N} \\ \vdots \\ u_{-1} \\ u_0 \\ u_1 \\ \vdots \\ u_N \end{bmatrix}, \mathcal{Y}_N = \begin{bmatrix} y_{-N} \\ \vdots \\ y_{-1} \\ y_0 \\ y_1 \\ \vdots \\ y_N \end{bmatrix}.
\tag{3.184}
$$

Hence, a truncated input-output relationship is formed

$$
\mathcal{Y}_N = \mathcal{G}_N \mathcal{U}_N
\tag{3.185}
$$

99

where the harmonic transfer function has been truncated to have dimension $m(2N + 1) \times m(2N + 1)$, with an equal number of positive and negative harmonics. The implication here is that if enough harmonics are included in the truncated harmonic transfer function, correct answers will be obtained in the principal gain analyses outlined in this section. The dependence of the truncated quantities on the integer N will be suppressed to simplify notation.

Directional properties of LTP systems can be generalized as any property of the harmonic transfer function or geometrically periodic signals that exhibits a miltivariable dependency, that is, in the multi–input multi–output sense, in addition to the frequency dependency shared with scalar LTI transfer functions and scalar sinusoidal signals. The directional properties of the harmonic transfer function are manifested both by the multichannel nature of multivariable systems, and in the infinite number of Fourier coefficients required to characterize EMP signals. Here, the principal gains and their directional properties are described in terms of the singular value decomposition of the truncated harmonic transfer function.

Recall that a GP (EMP) input to an LTP system produces a GP (EMP) output in steady state with possibly differing amplitude and phase, according to Theorems 3.4, and 3.14. Clearly, this map is linear since the underlying dynamics were linear. This suggests that the singular value decomposition will provide useful information because singular values and singular directions lead to useful interpretations of domain and range spaces, and directions of maximal amplification for arbitrary linear maps [32].

The harmonic transfer function maps an EMP input into a EMP output where the plant has m independent inputs and m independent outputs. The input, $u(t)$, is a bounded EMP signal,

$$u(t) = \sum_{n=-\infty}^{\infty} u_n e^{s_n t} \quad u_n \in C^m \ \forall n \tag{3.186}$$

and, provided the internal dynamics represented by $A(t)$ are asymptotically stable (the eigenvalues of the monodromy matrix are on the unit disk, or the eigenvalues of Q are in the LHP), the steady state output signal will also be a bounded EMP signal,

$$y(t) = \sum_{n=-\infty}^{\infty} y_n e^{s_n t} \quad y_n \in C^m \quad \forall n \in Z \tag{3.187}$$

Now, the harmonic transfer function matrix provides the linear map, so that

$$y = \widehat{\mathcal{G}}(s)u \tag{3.188}$$

The harmonic transfer function is a complex matrix that changes value with frequency, ω, where the frequency range of interest is given by

$$\omega \in \Omega_r = \left(-\frac{\omega_p}{2}, \frac{\omega_p}{2} \right] \tag{3.189}$$

Now, for any value of frequency, $\omega \in \Omega_r$, the singular value decomposition (SVD) of the harmonic transfer function can be computed, as given by

$$\widehat{G}_N(j\omega) = \mathbf{U}(j\omega)\Sigma(j\omega)\mathbf{V}^*(j\omega) \tag{3.190}$$

where the superscript $*$ denotes the Hermitian or complex conjugate transpose operation. Each quantity in the SVD is parameterized by frequency in the frequency range of interest, $\omega \in \Omega_r$. For practical reasons, the number of harmonics included in the HTF is finite, say N, and it will be assumed that $\widehat{\mathcal{G}}_N(j\omega)$ is invertible, then

(a) the quantity $\Sigma_N(j\omega)$ is a $m(2N+1) \times m(2N+1)$ complex diagonal matrix consisting of the singular values of the truncated harmonic transfer function such that

$$\sigma_{max}(\omega) = \sigma_1(\omega) \geq \sigma_2(\omega) \geq \cdots \geq \sigma_{2N+1}(\omega) = \sigma_{min}(\omega). \tag{3.191}$$

The minimum singular value $\sigma_{min}(\omega)$ is simply the gain associated with the minimum amplification direction for the number of harmonics included in the harmonic transfer function. However, if more harmonics are included in the truncated harmonic transfer function, a smaller minimum singular value may be found. These singular values are the *principal gains* of the LTP system.

(b) The quantity $\mathbf{V}(j\omega)$ is an $m(2N+1) \times m(2N+1)$ complex matrix whose column vectors $\left\{ v^{(n)}(\omega) \right\}$ are the right singular vectors of $\widehat{\mathcal{G}}_N(j\omega)$ and form a basis for the *domain space*. The right singular vectors are the *principal input directions*.

(c) The quantity $\mathbf{U}(j\omega)$ is an $m(2N+1) \times m(2N+1)$ complex matrix whose column vectors $\left\{ u^{(n)}(\omega) \right\}$ are the left singular vectors of $\mathcal{G}_N(j\omega)$ and form a basis for the *range space*. The left singular directions are the *principal output directions*.

This singular value analysis can be carried out for $\omega \in \Omega_r$ so that these singular values can be plotted versus frequency as a Bode plot (that is, decibels versus frequency, $\omega \in \Omega_r$). This *principal gain diagram* is analogous in many respects to the singular value plot for multivariable LTI systems, although the specific interpretation must be carefully worked as will be done here.

Principal gain diagram

The principal gain diagram provides a useful gain characteristic that is analogous to SV plots for LTI systems. How is the information in the SVD at a given frequency interpreted? At each frequency it is assumed that the input to the asymptotically stable system is a *unit complex periodic signal* of the form

$$u(t) = \sum_{n=-\infty}^{\infty} u_n e^{j(\omega+n\omega_p)t} \tag{3.192}$$

where

$$\|u\|_2 = 1 \tag{3.193}$$

Then assuming that the system is in steady state the resulting output will be

$$y(t) = \sum_{n=-\infty}^{\infty} y_n e^{j(\omega+n\omega_p)t} \tag{3.194}$$

where

$$\|y\|_2 = \left\|\widehat{\mathcal{G}}(j\omega)u\right\|_2 \tag{3.195}$$

The magnitude will depend on the direction of the input signal.

Maximum amplification direction analysis

Consider an SVD analysis at a specified frequency $\omega \in \Omega_r$. The SVD analysis will produce a maximum singular value, $\bar{\sigma}(\omega)$, with a corresponding complex valued right singular vector, $\bar{v}(\omega)$, with $m(2N+1)$ elements, and a corresponding left singular vector, $\bar{u}(\omega)$ with $m(2N+1)$ elements. The maximum right and left singular vectors correspond to the first columns of $V(j\omega)$ and $U(j\omega)$, respectively. The block vector elements of $\bar{v}(\omega)$ can be expressed in polar form as

$$\bar{v}_n(\omega) = \bar{a}_n \circ e^{j\bar{\psi}_n}; \quad \forall n \in Z. \tag{3.196}$$

Here, the $\circ$ denotes the *Schur product* as defined by Kailath [53, page 646], which is an element by element multiplication of compatible matrices (vectors). The quantities $\bar{a}_n$ and $\bar{\psi}_n$ are parameterized by frequency, although this frequency dependence will be implicit to simplify notation. Also, n denotes that portion of $\bar{v}(\omega)$ corresponding to the nth harmonic. Each element of the block vector $\bar{v}(\omega)$ contribute a different amplitude and a different phase. The block vector elements of $\bar{u}(w)$ can also be written in polar form as

$$\bar{u}_n(\omega) = \bar{b}_n \circ e^{j\bar{\phi}_n}; \quad \forall n \in Z. \tag{3.197}$$

Again, the quantities $\bar{u}_n$ and $\bar{\phi}_n$ depend implicitly on frequency.

In steady state, the input and output signals that correspond to the direction of maximum amplification can be reconstructed from the information contained in the maximum SV analysis. First, the input signal corresponding to the maximum amplification direction can be reconstructed from the quantities $\bar{a}_n$ and $\bar{\psi}_n$, for all $n \in Z$, as

$$\bar{u}(t) = \sum_{n=-\infty}^{\infty} \bar{a}_n \circ e^{j\bar{\psi}_n} e^{j(\omega + n\omega_p)t}. \qquad (3.198)$$

The steady state output signal corresponding to the maximum amplification direction, $\bar{y}(t)$, can also be reconstructed using the quantities $\bar{\sigma}$, $\bar{b}_n$, and $\bar{\phi}_n$, as

$$\bar{y}(t) = \bar{\sigma} \sum_{n=-\infty}^{\infty} \bar{b}_n \circ e^{j\bar{\phi}_n} e^{j(\omega + n\omega_p)t}. \qquad (3.199)$$

Thus, the direction of maximum amplification is a complex periodic signal represented by a complex Fourier series, that when input to an LTP system, results in the maximum amplification as determined by the maximum singular value, and with very precise phase and amplitude characteristics for each harmonic of the complex Fourier series associated with the input and output signals.

Note that all of these directional properties vary with frequency in the frequency range of interest, $\omega \in \Omega_r$. In addition, the above analysis can be applied to all of the singular values, σ_n and their corresponding right and left singular vectors, $v^{(n)}(\omega)$ and $u^{(n)}(\omega)$, respectively. In fact, since the right singular vectors, $v^{(n)}(\omega)$, are linearly independent and orthonormal, they form a basis for the domain space of the harmonic transfer function. Also, since the left singular vectors, $u^{(n)}(\omega)$, are linearly independent and orthonormal, they are a basis for the range space of the harmonic transfer function. The amplitude and phase of any periodic input to the LTP system at a frequency $\omega \in \Omega_r$ can be expressed as a linear combination of the right singular vectors at that frequency. The amplitude and phase of the corresponding output can be predicted at steady state by the same linear combination of the left singular vectors. Unfortunately, a SISO LTP system does not have a scalar phase notion comparable to the Bode phase notion for SISO LTI transfer functions, but has a directional phase notion due to the directionality contributed by the harmonics.

3.6.6 Effects of truncation

To this point, the properties developed using the generalized harmonic balance method have glibly dealt with infinite dimensionality of the harmonic state space model, harmonic

103

transfer function, and associated pole and zero eigenvalue problems. Clearly, in order to implement these analyses on the computer, these procedures must be truncated to have only a few harmonics, or at least as many harmonics as the computer memory allows.

The computations described in this section will work better for systems with parametric excitation that can be described exactly by a truncated complex Fourier series (such as a sum of sinusoids of low harmonic number or the sinusoidal parametric excitation of the Mathieu equation) than for parametric excitation that cannot be expressed as a uniformly convergent complex Fourier series (such as a square wave or sawtooth wave).

What constitutes "enough harmonics"? Consider the computation of LTP system poles using the infinite dimensional eigenvalue problem posed in Theorem 3.19. Due to the structure of the poles in the s-plane, that is, the infinite folding of the poles about the fundamental strip, and the fact that the fundamental strip contains all of the unique poles, enough harmonics are included to guarantee convergence of the pole location in some neighborhood in the fundamental strip. In addition, it is hoped that the identification of the poles in the fundamental strip is straightforward, and that as harmonics are added, the fundamental strip continues to contain only the n poles of interest. The pole locations in the complementary strips are then inferred from the pole locations in the fundamental strip. However, the number of harmonics required is problem dependent, so that no global convergence criteria were developed in the course of this research. Thus, based on current knowledge, an examination of convergence of the pole locations tends to degenerate to a numerical exercise for a given example. This is no better, nor any worse, than what is currently available in the literature. Essentially the same discussion applies for the determination of the transmission zero locations, principal gains, etc.

3.7   Connections to Classical Theory

The theory developed thus far has as its underpinnings the signal spaces identified by Floquet and Hill over a century ago. However, it is useful to reiterate in what ways the methods of Floquet, Hill, and of harmonic balance relate to the operator representations of LTP systems developed in the previous sections.

3.7.1 The Floquet theory

The connection between the integral operator representation and the Floquet theory is clear. Floquet theory is the search for solutions to the state dynamic equation that that increase geometrically from period to period. This interpretation is presented in most textbooks that deal with Floquet theory including [83]. This observation spurred the introduction of the geometrically periodic (GP) signal space in a formal manner. However, the GP signal has only been used as the form of the solution of the open–loop homogenous state dynamic equation. In order to develop a frequency domain interpretation for LTP systems, an explicit input–output relationship was developed, namely the integral operator transfer function, $\widehat{G}(z)$. This linear operator maps a GP input signal to a GP output signal when the LTP system is in steady state, and is completely analogous to the LTI transfer function for which the complex exponential is the test input signal of interest.

3.7.2 The Hill theory and harmonic balance

In Chapter 2, the traditional method of formulating the Hill determinant was outlined for a second order Hill equation. Here, the Hill determinant procedure will be interpreted using the notions developed in the previous section. Traditionally the Hill determinant has been used to examine open loop stability of LTP systems described by an ODE of the form,

$$\ddot{x}(t) + [a - 2q\psi(t)]\,x(t) = 0 \qquad (3.200)$$

where the system under consideration has only two free parameters, a and q. Many authors, including Richards [83], have attempted to formulate the Hill determinant methodology for a general order Hill equation by a brute force extension of the formulation used for the second order equation. This is done by using vector valued a and q, but this leads to results that are cumbersome in the extreme.

Here, the state space formulation will be introduced, along with the same complex Fourier series expansions used by Hill, in order to extend the Hill determinant formulation to its most general form in a straightforward manner. Consider the unforced open loop state space model

$$\dot{x}(t) = A(t)x(t) \qquad (3.201)$$

The state vector is assumed to be an EMP signal, so that

$$x(t) = \sum_{m=-\infty}^{\infty} x_m e^{s_m t}$$

$$\dot{x}(t) = \sum_{m=-\infty}^{\infty} s_m x_m e^{s_n t} \qquad (3.202)$$

Since $A(t)$ is T–periodic, it can be expanded in a complex Fourier series,

$$A(t) = \sum_{n=-\infty}^{\infty} A_n e^{jn\omega_p t} \qquad (3.203)$$

Now, expanding (3.201) in terms of these series,

$$\sum_{n=-\infty}^{\infty} s_n x_n e^{s_n t} = \sum_{n=-\infty}^{\infty} A_n e^{jn\omega_p t} \sum_{m=-\infty}^{\infty} x_m e^{s_m t}$$

$$= \sum_{n,m=-\infty}^{\infty} A_{n-m} x_m e^{s_n t} \qquad (3.204)$$

Grouping terms,

$$0 = \sum_{n=-\infty}^{\infty} \left\{ s_n x_n - \sum_{m=-\infty}^{\infty} A_{n-m} x_m \right\} e^{s_n t} \qquad (3.205)$$

multiplying through by e^{-st}, and applying the principle of harmonic balance,

$$\hat{0} = s_n x_n - \sum_{m=-\infty}^{\infty} A_{n-m} x_m \quad \forall n \in Z \qquad (3.206)$$

This infinite set of equations can be expressed in matrix form as

$$\left[\mathcal{I} - (s\mathcal{I} + \mathcal{N})^{-1} \mathcal{A} \right] \chi = 0 \qquad (3.207)$$

As an aside, let us consider the harmonic balance approach as it is traditionally applied in dynamics textbooks, or as described by Dugundji [27]. Here we expand only the periodic portion of the Floquet solution, and leave the complex exponential part of the Floquet solution embedded (implicit) in the state vector, $x(t)$. Then,

$$x(t) = \sum_{m=-\infty}^{\infty} x_m(t) e^{jm\omega_p t}$$

$$\dot{x}(t) = \sum_{n=-\infty}^{\infty} \left\{ \dot{x}_n(t) + jn\omega_p x_n(t) \right\} e^{jn\omega_p t} \qquad (3.208)$$

Expanding (3.201) in terms of the above series

$$\sum_{n=-\infty}^{\infty} \left\{ \dot{x}_n(t) + jn\omega_p x_n(t) \right\} e^{jn\omega_p t} = \sum_{n=-\infty}^{\infty} A_n e^{jn\omega_p t} \sum_{m=-\infty}^{\infty} x_n(t) e^{jm\omega_p t}$$

$$= \sum_{n,m=-\infty}^{\infty} A_{n-m} x_m(t) e^{jn\omega_p t} \qquad (3.209)$$

106

Moving all terms to the LHS

$$0 = \sum_{n=-\infty}^{\infty} \left\{ \dot{x}_n(t) + jn\omega_p x_n(t) - \sum_{m=-\infty}^{\infty} A_{n-m} x_m(t) \right\} e^{jn\omega_p t} \qquad (3.210)$$

and applying the principle of harmonic balance,

$$0 = \dot{x}_n(t) + jn\omega_p x_n(t) - \sum_{m=-\infty}^{\infty} A_{n-m} x_m(t) \quad \forall n \in Z \qquad (3.211)$$

Taking Laplace transforms,

$$\begin{aligned} 0 &= s x_n(s) + jn\omega_p x_n(s) - \sum_{m=-\infty}^{\infty} A_{n-m} x_m(s) \\ &= s_n x_n(s) - \sum_{m=-\infty}^{\infty} A_{n-m} x_m(s) \quad \forall n \in Z \end{aligned} \qquad (3.212)$$

This infinite set of equations can be expressed in matrix form as

$$[\mathcal{I} - (s\mathcal{I} + \mathcal{N})^{-1}\mathcal{A}]\mathcal{X} = 0 \qquad (3.213)$$

which is the same result as determined using the Hill approach of EMP signals. Thus, the only difference between the traditional application of harmonic balance in [27], and the generalized harmonic balance approach advocated here is whether or not the complex exponential part of the Floquet solution is included explicitly in the expansions, as is the case in the Hill theory [46,47,83], or left implicitly as part of the state vector, as is the case in the harmonic balance approaches discussed by Dugundji [27] and others [99,101].

In either case, the above infinite set of equations has a nontrivial solution if the infinite determinant

$$\Delta(s) = \det \left[\mathcal{I} - (s\mathcal{I} + \mathcal{N})^{-1} \mathcal{A} \right] \qquad (3.214)$$

equals zero. Thus, $\Delta(s)$ is the usual form of the Hill determinant, except for the fact that it has been applied here to the unforced LTP state space model.

The Hill determinant procedure usually takes the following form. Suppose that $A(t)$ has a set of parameters $(a_1, a_2, \cdots, a_k)$, for which a characterization of the stability regions is sought. The stability boundaries are characterized by the existence of periodic solutions. The goal of the Hill determinant analysis is then to determine for which values of the parameters $(a_1, a_2, \cdots, a_k)$, the Hill determinant $\Delta(j\omega)$ vanishes. This is a computationally intensive task, involving a search over the parameter space $(a_1, a_2, \cdots, a_k)$, and an examination of the effects of truncation of the Hill determinant.

Let us draw an analogy with LTI systems for clarification. Consider the second order oscillator,

$$\ddot{x}(t) + 2\zeta\omega_n\dot{x}(t) + \omega_n^2 x(t) = 0 \qquad (3.215)$$

where the damping ratio, ζ, and the natural frequency, ω_n, are the free parameters over which the search for periodic solutions will be conducted. The stability boundaries are determined by finding for which combinations of ζ and ω_n the characteristic polynomial vanishes, *and* the roots of the characteristic polynomial are purely imaginary. The characteristic polynomial is given by

$$s^2 + 2\zeta\omega_n s + \omega_n^2 = 0 \qquad (3.216)$$

Since the search is for periodic solutions, set $s = j\omega$, so that

$$-\omega^2 + j2\zeta\omega_n\omega + \omega_n^2 = 0 \qquad (3.217)$$

Clearly, $\zeta = 0$ and $\omega = \omega_n$ produces a periodic solution, and specifies the stability boundary.

Thus, the conclusion to be drawn is that the Hill determinant methodology can be interpreted as a way of evaluating the roots of the characteristic polynomial in the s–plane.

3.8   Some Comments on the Frequency Domain

Up to this point, the notion of the frequency domain has been somewhat imprecise, and in this section, the notion of the frequency domain is developed in terms of the GP and EMP signals, and the linear operators developed above.

3.8.1   The frequency domain and the z-plane

At this point, let us consider the connection between the time and the frequency domain in the z–plane. As in the case of LTI systems, we are concerned with $L_2(-\infty, \infty)$ signals. The usual basis signal for LTI systems is the complex exponential, which can be expressed as the product of a complex exponential signal for which $\text{Im}(s) \in (-\omega_p/2, \omega_p/2]$, that is, a complex exponential in the fundamental strip, and some harmonic of the pumping frequency or the T–periodic portion of the complex exponential. The fundamental strip exponential is then the geometric variation over a period that is extracted from the complex exponential basis signal as the complex parameter z, and describes the effect of the fundamental strip exponential over one period. The remaining T–periodic portion of the complex exponential

basis signal is then an $L_2[0,T]$ signal. Thus, this gives rise to the GP signal, which turns out to be convenient in the study of LTP systems, and is an alternative basis signal for $L_2(-\infty, \infty)$.

By introducing the GP signal, the square integrable signal has been mapped into the z domain. The unit circle in the z-plane is parameterized by $\theta \in (-\pi, \pi]$, since $z = e^{j\theta}$ on the unit circle. The frequency domain is then given by the direct product of the unit circle in the z-plane, denoted by $L_2(-\pi, \pi]$, and all $L_2[0,T]$ signals, that is,

$$L_2(-\infty, \infty) \xrightarrow{z} L_2(-\pi, \pi] \otimes L_2[0,T] \tag{3.218}$$

This is somewhat odd in that the frequency domain is expressed as the direct product of a frequency domain function space, $L_2(-\pi, \pi]$, and a time domain function space, $L_2[0,T]$. However, this is just a consequence of the integral operator formulation, and the fact that the complex exponential was folded down into a product of a fundamental strip exponential and a T-periodic signal.

3.8.2 The frequency domain and the s-plane

In the integral operator formulation, it was deduced that the introduction of the GP signal transformed $L_2(-\infty, \infty)$ signals to a direct product of $L_2(-\pi, \pi]$, that is, the unit circle in the z-plane, and $L_2[0,T]$ signals. It is a well known fact that the unit circle is equivalent to the imaginary axis in the fundamental strip from the map $z = e^{sT}$, so that

$$L_2(-\pi, \pi] \xrightarrow{z=e^{sT}} L_2\left(-\frac{\omega_p}{2}, \frac{\omega_p}{2}\right] \tag{3.219}$$

The class of signals in $L_2[0,T]$ can be expressed as convergent complex Fourier series defined as the class l_2. It is a well known fact that the complex Fourier series is a Hilbert space isomorphism from $L_2[0,T]$ onto l_2 [82, page 101], so that

$$L_2[0,T] \xrightarrow{\mathcal{F}} l_2 \tag{3.220}$$

where $\mathcal{F}$ denotes the Fourier series. Thus, the frequency domain for the s-plane or harmonic balance formulation of the LTP transfer function maps square integrable signals to the direct product of $L_2\left(-\frac{\omega_p}{2}, \frac{\omega_p}{2}\right]$ and complex Fourier series, l_2. This relationship can be described as

$$L_2(-\infty, \infty) \xrightarrow{\mathcal{F}} L_2\left(-\frac{\omega_p}{2}, \frac{\omega_p}{2}\right] \otimes l_2 \tag{3.221}$$

3.8.3 Isomorphism between z-plane and s-plane

Based on this discussion, it follows that the harmonic transfer function is an isomorphic representation of the integral operator transfer function since the underlying test signals are isomorphic, that is, they are both basis signals for $L_2(-\infty, \infty)$.

In the equation below, the relationships between the frequency domain in the LTP s-plane, and the LTP z-plane are depicted.

$$
\begin{array}{ccccc}
z\text{-plane:} & L_2(-\infty,\infty) & \xrightarrow{z} & L_2(-\pi,\pi] & \otimes & L_2[0,T] \\
& \| & & \| & & \downarrow \mathcal{F} \\
s\text{-plane:} & L_2(-\infty,\infty) & \xrightarrow{\mathcal{F}} & L_2\left(-\frac{\omega_p}{2},\frac{\omega_p}{2}\right] & \otimes & l_2
\end{array}
\tag{3.222}
$$

3.9 Analysis Examples

In order to illustrate the utility of the analysis tools that were described above, two examples will be discussed. The first example is a second order LTI oscillator for which the input to the LTI plant is amplitude modulated by a periodic signal. The state space model for this example has a time invariant dynamics matrix, but has a time periodic control distribution matrix. The second example is a form of the lossy Mathieu equation, which has time periodic dynamics and time invariant control distribution and measurement matrices.

3.9.1 LTI oscillator with modulated input

Consider the LTI plant,

$$
G(s) = \left(\frac{\omega_n^2}{|a|}\right) \frac{s-a}{s^2 + 2\zeta\omega_n s + \omega_n^2}
\tag{3.223}
$$

which has an input that is amplitude modulated by the signal, $1 - 2\beta \cos\omega_p t$, as shown in Figure 3.4. The values of the above parameters are $\omega_n = 0.5$, $\zeta = 0.3$, $a = -1$, and $\beta = 0.2$.

The state space model of the LTP system is given by

$$
\begin{aligned}
A_0 &= \begin{bmatrix} 0 & 1 \\ -\omega_n^2 & -2\zeta\omega_n \end{bmatrix} \\[2ex]
B(t) &= \begin{bmatrix} 0 \\ 1 - 2\beta\cos\omega_p t \end{bmatrix} \\[2ex]
C_0 &= \left(\frac{\omega_n^2}{|a|}\right) \begin{bmatrix} 1 & -a \end{bmatrix}
\end{aligned}
\tag{3.224}
$$
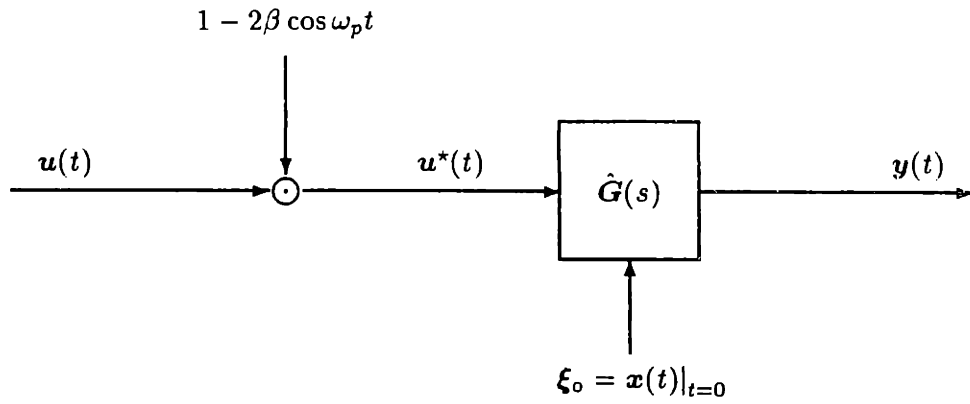
Figure 3.4: Block diagram for LTI plant with amplitude modulated input.

The matrices A_o and C_o are time invariant. However, $B(t)$ is T-periodic and can be expanded in a complex Fourier series as

$$
\begin{aligned}
B(t) &= \{\cdots, 0, B_{-1}, B_0, B_1, 0, \cdots\} \\
&= \left\{\cdots, 0, \begin{bmatrix} 0 \\ -\beta \end{bmatrix}, \begin{bmatrix} 0 \\ 1 \end{bmatrix}, \begin{bmatrix} 0 \\ -\beta \end{bmatrix}, 0, \cdots \right\}
\end{aligned}
\tag{3.225}
$$

Now, following the procedure outlined in Example 3.2, the harmonic transfer function can be determined

$$
\hat{\mathcal{G}}(s) = \begin{bmatrix}
\ddots & \vdots & \vdots & \vdots & \vdots & \vdots & \\
\cdots & G_{-2} & -\beta G_{-2} & 0 & 0 & 0 & \cdots \\
\cdots & -\beta G_{-1} & G_{-1} & -\beta G_{-1} & 0 & 0 & \cdots \\
\cdots & 0 & -\beta G_0 & G_0 & -\beta G_0 & 0 & \cdots \\
\cdots & 0 & 0 & -\beta G_1 & G_1 & -\beta G_1 & \cdots \\
\cdots & 0 & 0 & 0 & -\beta G_2 & G_2 & \cdots \\
& \vdots & \vdots & \vdots & \vdots & \vdots & \ddots
\end{bmatrix}
\tag{3.226}
$$

where

$$
G_n = C_o[(s + jn\omega_p)I - A_o]^{-1} B_0
\tag{3.227}
$$

In Figure 3.5, the system poles are plotted in both the s-plane, as shown in Figure 3.5a, and in the z-plane as shown in Figure 3.5b. In the s-plane, there are only two poles in the
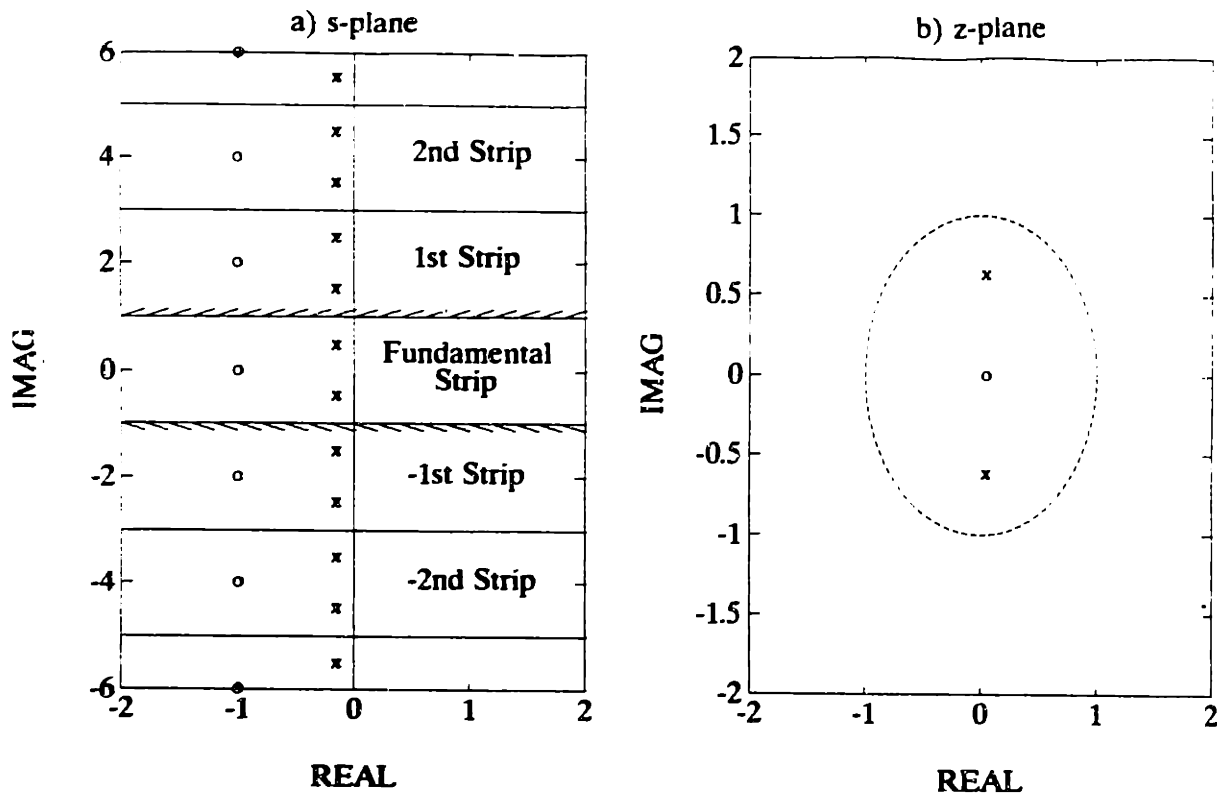
Figure 3.5: Pole-zero diagram of LTI plant with modulated input. The poles and zeroes are plotted in both the s-plane, as shown in (a), and in the z-plane, as shown in (b). In the s-plane, the poles and zeroes are folded about the fundamental strip, so that there are two infinite families of poles. The z-plane representation is somewhat more convenient since there are a finite number of poles and zeroes in the z-plane.

fundamental strip, which are folded into the complementary strips by factors of $\pm jn\omega_p$. As a result, the LTP system has an infinite number of poles in the s-plane, although there are only two infinite families of poles in this example. All of the poles in the s-plane are mapped to a unique set of z-plane poles as shown in Figure 3.5b. These two diagrams illustrate the equivalence between the s-plane and the z-plane poles, which is expected from results of the Floquet theory, and illustrates how the poles in the s-plane are folded about the fundamental strip. The directions associated with the poles have the same interpretation as for LTI systems, so are not considered further.

The example being considered is an LTI plant with a transmission zero, where the input to the LTI plant is amplitude modulated by a signal that has no zero crossings (that is, $\beta < 0.5$). The plant is LTP due only to the amplitude modulation, so that the LTP

transmission zero can be deduced using the LTI theory.

The LTI transmission zero eigenvalue problem is solved for the embedded LTI state space model, $S_o = [A_o, B_o, C_o]$. The solution yields the zero location, $s_z^{(\text{LTI})}$, the initial condition direction, $\xi_o^{(\text{LTI})}$, and the input direction (which will be a scalar value in this case), $u_0^{(\text{LTI})}$, with the following numerical values:

$$s_z^{(\text{LTI})} = -1, \quad \xi_o^{(\text{LTI})} = \begin{bmatrix} -.5615 \\ .5615 \end{bmatrix}, \quad u_0^{(\text{LTI})} = 0.5334. \tag{3.228}$$

Hence, for the above initial condition, if the signal

$$
\begin{aligned}
u^\star(t) &= u_0^{(\text{LTI})} e^{s_z^{(\text{LTI})} t} \\
&= 0.5334 e^{-t} \tag{3.229}
\end{aligned}
$$

is injected at the point indicated in Figure 3.4, then the output signal, $y(t)$, will be zero for all time after the initial time.

Based on purely intuitive arguments and the fact that $\beta < 0.5$ so that the modulating signal has no zero crossings, it is reasonable to expect that the LTP transmission zero will be located at $s_z = -1$, which is in the fundamental strip. The LTP transmission zero will then be folded into the complementary strips. In addition, the initial condition direction should be the same, and the input direction should be the LTI input direction divided by the modulating signal, that is,

$$\xi_0 = \xi_o^{(\text{LTI})} = \begin{bmatrix} -.5615 \\ .5615 \end{bmatrix} \tag{3.230}$$

$$
\begin{aligned}
u(t) &= \left(\frac{1}{1 - 2\beta \cos \omega_p t} \right) u^\star(t) \\
&= \left(\frac{0.5334}{1 - 2\beta \cos \omega_p t} \right) e^{-t} \tag{3.231}
\end{aligned}
$$

Using the LTP transmission zero eigenvalue problem in the s-plane (truncated to $N = 10$ harmonics), the LTP transmission zero can be obtained directly. The transmission zero locations are $s_z = -1 \pm jn\omega_p$ as expected, and the initial condition indicated above is obtained. The transmission zero input direction leads to the computation of an EMP input

signal,

$$u(t) = e^{s_z t} \begin{bmatrix} \vdots \\ u_{-1} \\ u_0 \\ u_1 \\ \vdots \end{bmatrix}^T \begin{bmatrix} \vdots \\ e^{-j\omega_p t} \\ 1 \\ e^{j\omega_p t} \\ \vdots \end{bmatrix} = e^{-t} \begin{bmatrix} \vdots \\ 0.1215 \\ 0.5820 \\ 0.1215 \\ \vdots \end{bmatrix}^T \begin{bmatrix} \vdots \\ e^{-j2t} \\ 1 \\ e^{j2t} \\ \vdots \end{bmatrix} \qquad (3.232)$$

which can be expanded in cosines as

$$u(t) = e^{-t} \{ 0.5820 + 0.2429 \cos 2t + 0.0507 \cos 4t + \cdots \} \qquad (3.233)$$

that is, the transmission zero direction is an EMP signal consisting of a sum of cosines only. For $\beta < 0.5$, the transmission zero input direction provides the complex Fourier coefficients of the leading term in parentheses in (3.231), as expected from intuitive arguments.

For $\beta > 0.5$, the amplitude modulation signal has zero crossings, so that no bounded pre-modulated signal exists that will produce the required LTI transmission zero input direction at the plant input. Therefore, there are no transmission zeroes for $\beta > 0.5$.

To reiterate, the pole-zero diagram in the z-plane is much more convenient than its counterpart in the s-plane for the simple reason that the poles and zeroes in the z-plane are finite in number. However, the s-plane formulations permit determination of directional information in a systematic way, whereas the z-plane formulations do not.

The principal gain diagram is shown in Figure 3.6. The LTP principal gain diagram is plotted over the fundamental strip only, and repeats itself in the complementary strips. The principal gains are analogous to the gain notions for LTI systems, but it should be noted that there are an infinite number of gain curves, although a finite number are shown here.

Let us consider a maximum singular value analysis at $\omega = \omega_p/4 = 0.5$, as indicated by the shaded circle in Figure 3.6. Based on the SVD analysis of the truncated harmonic transfer function, there is a direction of maximum amplification in both the input and output sense. The maximal input direction is given by the right singular vector associated

114

with the maximum singular value,

$$
\bar{u}(t) = e^{j\omega t}
\begin{bmatrix} \vdots \\ \bar{u}_{-1} \\ \bar{u}_0 \\ \bar{u}_1 \\ \vdots \end{bmatrix}^T
\begin{bmatrix} \vdots \\ e^{-j\omega_p t} \\ 1 \\ e^{j\omega_p t} \\ \vdots \end{bmatrix}
= e^{jt/2}
\begin{bmatrix} \vdots \\ 0.1933 \\ -0.9612 \\ 0.1933 \\ \vdots \end{bmatrix}^T
\begin{bmatrix} \vdots \\ e^{-j2t} \\ 1 \\ e^{j2t} \\ \vdots \end{bmatrix}
\tag{3.234}
$$

Note, in this case, that all of the harmonics enter with zero phase. The maximum principal gain is given by the maximum singular value, $\bar{\sigma} = 1.9388$, and indicates how the LTP system amplifies the above signal. The maximum output direction is given by the left singular vector associated with the maximum singular value,

$$
\bar{y}(t) = \bar{\sigma} e^{j\omega t}
\begin{bmatrix} \vdots \\ \bar{y}_{-1} \\ \bar{y}_0 \\ \bar{y}_1 \\ \vdots \end{bmatrix}^T
\begin{bmatrix} \vdots \\ e^{-j\omega_p t} \\ 1 \\ e^{j\omega_p t} \\ \vdots \end{bmatrix}
= 1.9388 e^{jt/2}
\begin{bmatrix} \vdots \\ -0.0150 + j0.0412 \\ -0.4467 + j0.8933 \\ -0.0056 - j0.0214 \\ \vdots \end{bmatrix}^T
\begin{bmatrix} \vdots \\ e^{-j2t} \\ 1 \\ e^{j2t} \\ \vdots \end{bmatrix}
$$

To illustrate the notion of phase for LTP systems, the complex coefficients in the output direction will be expressed in polar form

$$
\bar{y}(t) = 1.9388 e^{jt/2}
\begin{bmatrix} \vdots \\ 0.0442 \angle 110.0^\circ \\ 0.9988 \angle 116.5^\circ \\ 0.0221 \angle 255.3^\circ \\ \vdots \end{bmatrix}^T
\begin{bmatrix} \vdots \\ e^{-j2t} \\ 1 \\ e^{j2t} \\ \vdots \end{bmatrix}
\tag{3.235}
$$

Note that the direction associated with the maximum principal gain consists predominantly of three harmonics, and that each harmonic has a different associated phase change. This is an illustration of how LTP SISO systems have directional phase notions that are comparable to LTI multivariable systems, and not scalar phase notions such as those for LTI SISO systems.

The maximum input direction is shown in Figure 3.7a, and the corresponding output direction is shown in Figure 3.7b, both as predicted from the singular value analysis. The

115

input signal in Figure 3.7a was used as the input to a simulation of the linear time periodic system with zero initial conditions. The resulting output signal is shown in Figure 3.7c. In steady state, the simulated system output and the output as predicted from the singular value analysis coincide. Thus, this serves as an illustration of the LTP frequency response: *if a complex periodic signal is the input to an LTP system, then the output signal is also complex periodic in steady state, but with possibly different gain and phase (as long as $s = j\omega$ is not a pole of the system).*

In the above maximum direction analysis at frequency $\omega = 0.5$, the maximum input direction is a single basis direction in the infinite dimensional domain (input) space, and the maximum output direction is a single basis direction in the infinite dimensional range (output) space. The maximum singular value is the largest gain associated with the harmonic transfer function evaluated at $\omega = 0.5$. All of the principal gains, input and output directions are parameterized by frequency, so that different results will be obtained for every $\omega \in \Omega_r$.

Before commencing a feedback control design, it is important to understand the open loop properties of the linear system or plant under consideration. The above exercise illustrates that basic open loop analyses can be carried out for an LTP plant, that are completely analogous to those for an LTI plant.

3.9.2 Lossy Mathieu equation

The first example had time invariant dynamics and a time periodic control distribution matrix. Here, the time periodic dynamics of the Lossy Mathieu equation are considered. Defining the state vector as

$$x^T = \begin{bmatrix} \theta & \dot{\theta} \end{bmatrix} \tag{3.236}$$

leads to the system matrices

$$A(t) = \begin{bmatrix} 0 & 1 \\ -(1 - 2\beta \cos \omega_p t) & -2\zeta \end{bmatrix}, \quad B = \begin{bmatrix} 0 \\ 1 \end{bmatrix}, \quad C = \begin{bmatrix} 1 & 1 \end{bmatrix} \tag{3.237}$$

Here, the measurement and control distribution matrices are time invariant. It is assumed that the a linear combination of displacement, $x(t)$, and velocity, $\dot{x}(t)$, is measured. The parameter values selected for this example are $\omega_p = 2$, $\zeta = 0.2$, and $\beta = 0.2$. For most of the analyses performed in this section, truncation of the harmonic balance procedures
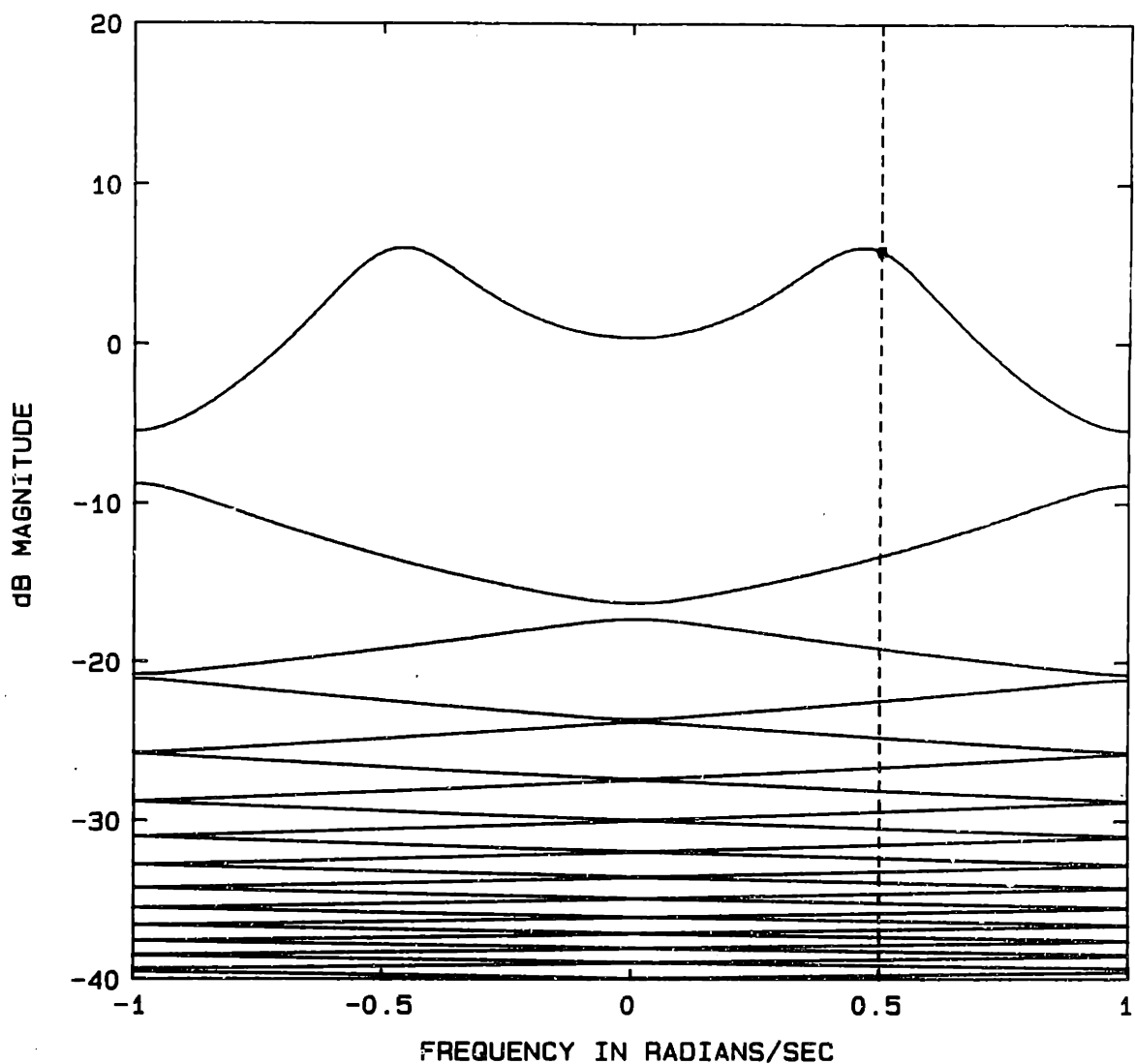
Figure 3.6: **Principal gain diagram for LTI plant with modulated input.** The principal gains of the LTP system are characterized by its singular value plot of the harmonic transfer function over the fundamental strip given by the frequency range $\omega \in \Omega_r$. The shaded circle on the maximum principal gain locus corresponds to the frequency of the maximum direction analysis shown in Figure 3.7.
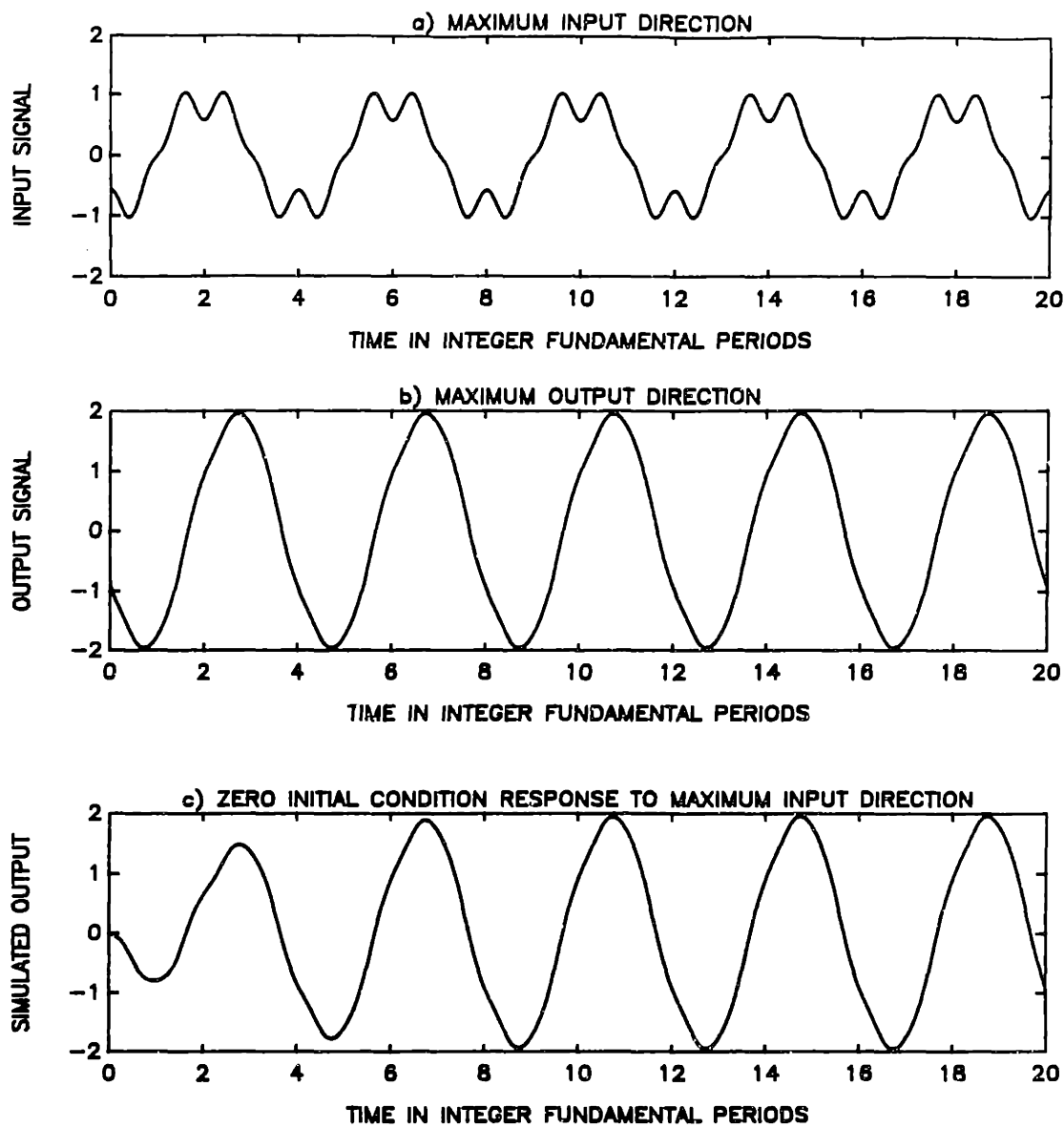
Figure 3.7: Maximum direction analysis of an LTI plant with modulated input. The direction of maximum amplification is the direction associated with the largest singular value of the SVD of the harmonic transfer function at a particular frequency. In this figure, the maximal direction analysis is carried out at $\omega = 0.5$. The maximal input direction, represented by the EMP signal shown in (a), is amplified by the maximum principal gain, and is changed to the maximal output direction, represented by the EMP signal shown in (b). The simulated output for the maximal input direction is shown in (c). The maximal output direction and the simulated signals coincide as t grows large.
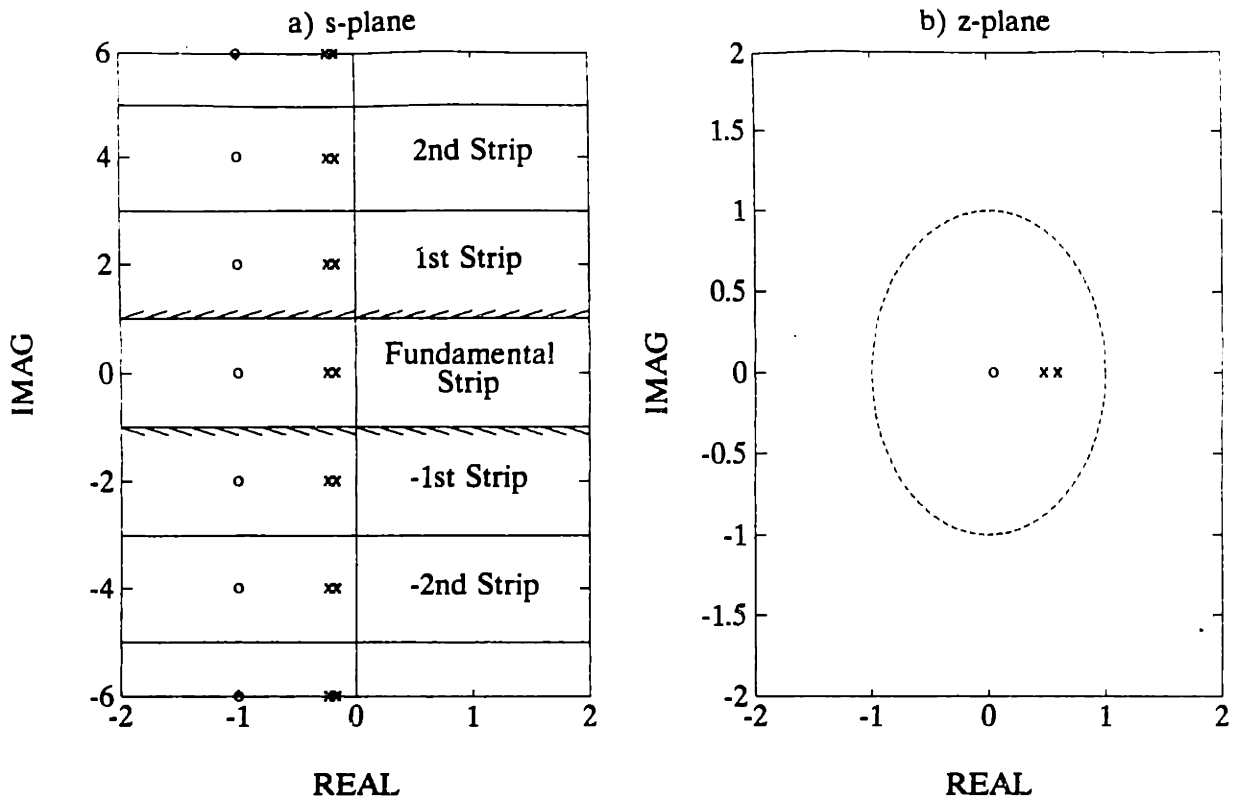
Figure 3.8: Pole-zero diagram for lossy Mathieu equation example The poles and zeroes are plotted in both the s-plane, as shown in (a), and in the z-plane, as shown in (b). In the s-plane, the poles and zeroes are folded about the fundamental strip, so that there are two infinite families of poles, and a single infinite family of zeroes. The harmonic balance procedure was truncated to include only $N = 10$ harmonics in this analysis.

to $N = 10$ harmonics proved to be sufficient to obtain reasonable results. In addition, the harmonic state space model consists of tridiagonal block Toeplitz dynamics matrix, and the Toeplitz forms associated with the input and output matrices are block diagonal.

The pole-zero diagram is shown in Figure 3.8 in both the s-plane and the z-plane. The eigenvalues of $(A$-$\mathcal{N})$ in the s-plane are folded about the fundamental strip, and are mapped to the eigenvalues of the monodromy matrix or the Floquet poles in the z-plane. The transmission zero generalized eigenvalue problem produced a zero in the fundamental strip, located at $s_z = -1$, as shown in Figure 3.8. These transmission zeroes are also folded about the fundamental strip as shown in Figure 3.8.

For the lossy Mathieu equation, the directional properties of the poles and zeroes will be explored in greater detail than the previous example.

The pole directions, or eigenvectors in the s-plane, are actually eigenfunctions in the time domain. Using the harmonic procedures developed above, it is possible to determine these eigenfunctions. The pole directions are complex periodic signals for which the Fourier coefficients are given by the right eigenvectors of the LTP pole eigenvalue problem in the s-plane.

The first mode of the system corresponds to a pole located at $s^{(1)} = -0.2353$, and its associated right direction is given by the complex periodic signal,

$$
\begin{aligned}
v^{(1)}(t) &= \left(\cdots + v^{(1)}_{-1} e^{-j\omega_p t} + v^{(1)}_0 + v^{(1)}_1 e^{j\omega_p t} + \cdots \right) \\
&= \left(\cdots + \begin{bmatrix} 0.0183 - j0.2456 \\ -0.4956 + j0.0211 \end{bmatrix} e^{-j\omega_p t} + \begin{bmatrix} 0.0360 - j0.0083 \\ -0.0085 + j0.0020 \end{bmatrix} \right. \\
&\quad \left. + \begin{bmatrix} -0.0085 + j0.0020 \\ 0.1242 + j0.2128 \end{bmatrix} e^{j\omega_p t} + \cdots \right).
\end{aligned}
\tag{3.238}
$$

Thus, the first system mode will have a time response of

$$
x^{(1)}(t) = e^{s^{(1)}t} v^1(t)
\tag{3.239}
$$

The second mode of the system corresponds to a pole located at $s_2 = -0.1647$, and its associated right direction is given by the complex periodic signal

$$
\begin{aligned}
v^{(2)}(t) &= \left(\cdots + v^{(2)}_{-1} e^{-j\omega_p t} + v^{(2)}_0 + v^{(2)}_1 e^{j\omega_p t} + \cdots \right) \\
&= \left(\cdots + \begin{bmatrix} 0.0184 + j0.2461 \\ 0.4891 - j0.0774 \end{bmatrix} e^{-j\omega_p t} + \begin{bmatrix} 0.0360 + j0.0083 \\ -0.0059 - j0.0014 \end{bmatrix} \right. \\
&\quad \left. + \begin{bmatrix} -0.0059 - j0.0014 \\ 0.1243 - j0.2132 \end{bmatrix} e^{j\omega_p t} + \cdots \right)
\end{aligned}
\tag{3.240}
$$

Thus, the second system mode will have a time response of

$$
x^{(2)}(t) = e^{s^{(2)}t} v^{(2)}(t)
\tag{3.241}
$$

The periodic portion of the Floquet solution is formed from the above two pole directions, so that

$$
P(t) = \begin{bmatrix} v^{(1)}(t) & v^{(2)}(t) \end{bmatrix}
\tag{3.242}
$$
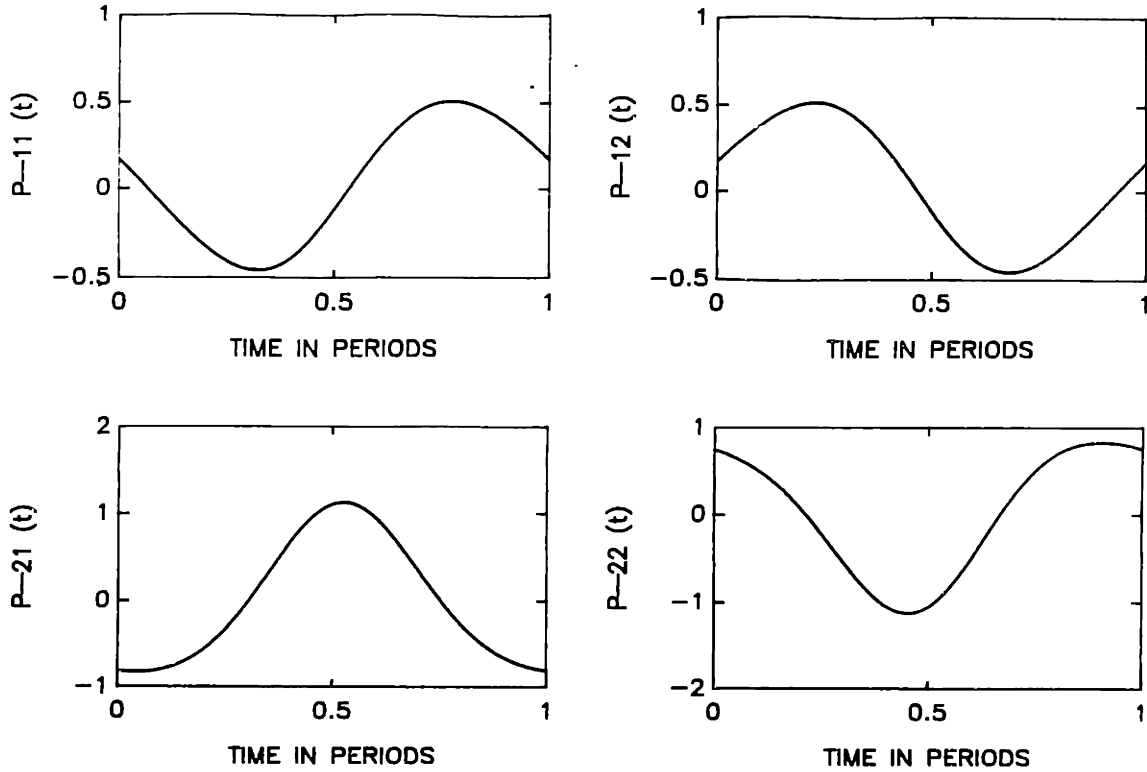
Figure 3.9: Periodic portion of the Floquet solution for the lossy Mathieu equation The directions of the LTP poles are obtained using the LTP pole eigenvalue problem in the s-plane. The above plot is a representation of the time periodic matrix from the Floquet solution, $P(t)$. The columns of $P(t)$ are the mode shapes, which are complex periodic signals, computed from the pole directions associated with the poles in the fundamental strip.

This matrix is plotted in Figure 3.9, and illustrates the periodic nonsingular nature of $P(t)$. The above representation of the Floquet similarity transformation matrix is very simple to compute using the harmonic balance formulation. In addition, $P(t)$ is completely analogous to the right eigenvector matrix for linear time invariant systems.

The LTP transmission zero cannot be deduced by the simple intuitive arguments developed in the previous example. Therefore, the LTP transmission zero eigenvalue problem will be utilized directly. The zero locations are $s_z = -1 \pm jn\omega_p$. The initial condition direction is given by

$$\boldsymbol{\xi_o}^T = \begin{bmatrix} 0.1994 & -0.1994 \end{bmatrix} \tag{3.243}$$

The input direction leads to the EMP signal

$$u(t) = e^{s_z t} \begin{bmatrix} \vdots \\ u_{-1} \\ u_0 \\ u_1 \\ \vdots \end{bmatrix}^T \begin{bmatrix} \vdots \\ e^{-j\omega_p t} \\ 1 \\ e^{j\omega_p t} \\ \vdots \end{bmatrix} = e^{-t} \begin{bmatrix} -0.1994 \\ 0.9170 \\ -0.1994 \end{bmatrix}^T \begin{bmatrix} e^{-j2t} \\ 1 \\ e^{j2t} \end{bmatrix} \qquad (3.244)$$

The transmission zero direction can be expressed as

$$u(t) = e^{-t} \{0.9170 - 0.3988 \cos 2t\} \qquad (3.245)$$

Thus, if the above signal is injected into the system for the above initial conditions, then the system output is identically zero for all time after the initial time.

The principal gain diagram of this system is shown in Figure 3.10. Again, there are an infinite number of principal gain curves corresponding to the infinite dimensional domain and range spaces of the harmonic transfer function, and only a small number are shown in this diagram. The largest gains occur for the zeroth, and first harmonics, which can be concluded by examination of the singular vectors associated with each gain plot.

A maximum amplification analysis is performed in this case, for $\omega = \omega_p/4 = 0.5$, as indicated by the shaded circle in Figure 3.10. Based on the SVD analysis of the truncated harmonic transfer function ($N = 10$ harmonics), there is a direction of maximum amplification in both the input and output sense. The maximal input direction is given by the right singular vector associated with the maximum singular value,

$$\bar{u}(t) = e^{j\omega t} \begin{bmatrix} \vdots \\ \bar{u}_{-1} \\ \bar{u}_0 \\ \bar{u}_1 \\ \vdots \end{bmatrix}^T \begin{bmatrix} \vdots \\ e^{-j\omega_p t} \\ 1 \\ e^{j\omega_p t} \\ \vdots \end{bmatrix} = e^{jt/2} \begin{bmatrix} \vdots \\ 0.8227 - j0.1088 \\ 0.3497 + j0.0572 \\ 0.3319 + j0.2692 \\ \vdots \end{bmatrix}^T \begin{bmatrix} \vdots \\ e^{-j2t} \\ 1 \\ e^{j2t} \\ \vdots \end{bmatrix}$$
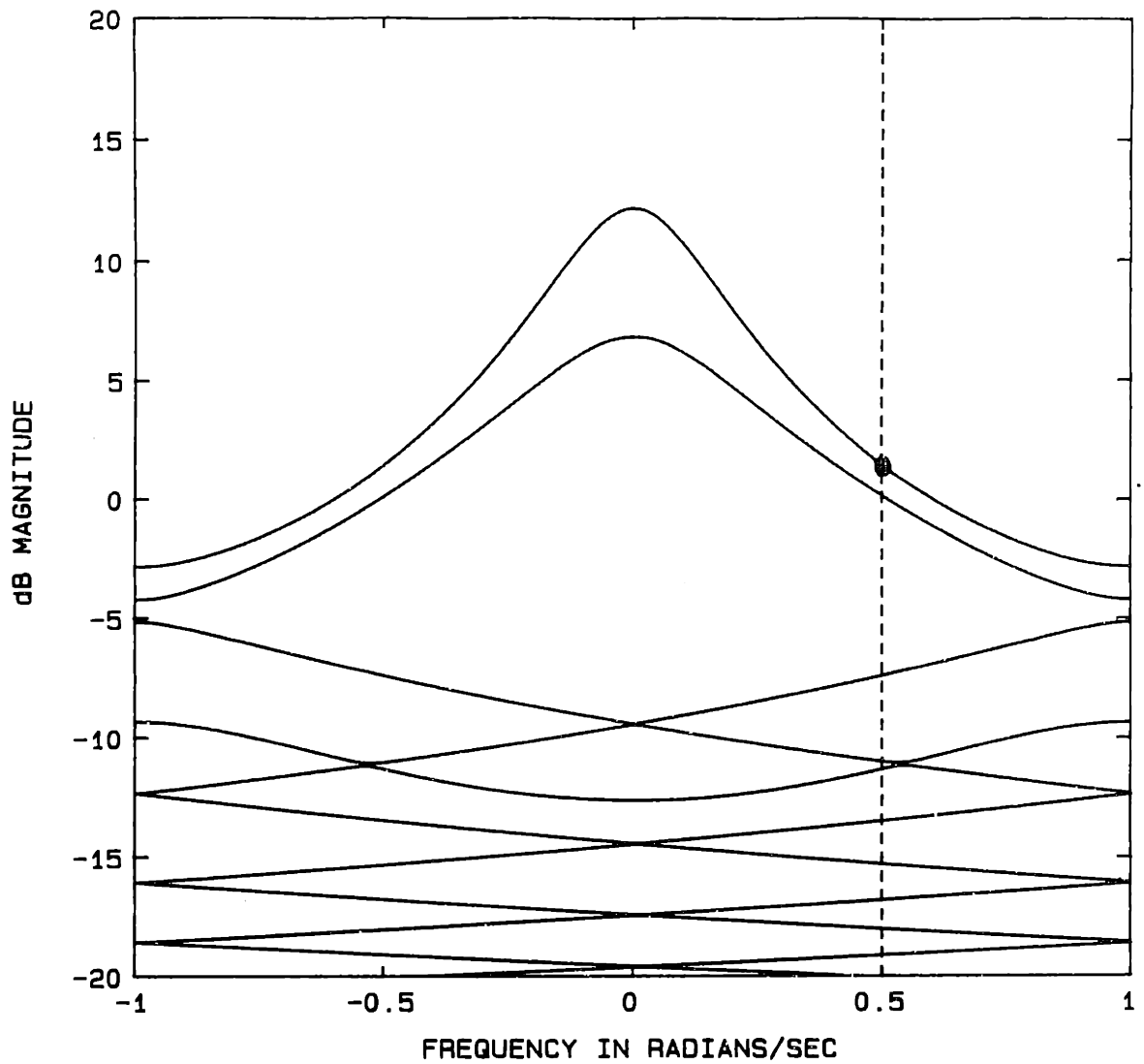
Figure 3.10: Principal gain diagram for lossy Mathieu equation example. The gain of the LTP system at a given frequency is characterized by the principal gains (singular values) of the harmonic transfer function. The principal gain diagram is a graph of these singular values over the imaginary axis in the fundamental strip, given by the frequency range $\omega \in (-\omega_p/2, \omega_p/2]$. The shaded circle on the maximum principal gain locus corresponds to the frequency of the maximum direction analysis shown in Figure 3.11.

It is instructive to express the input direction in polar form,

$$\bar{u}(t) = e^{jt/2} \begin{bmatrix} \vdots \\ 0.8299 \angle -7.534° \\ 0.3544 \angle 9.292° \\ 0.4274 \angle 39.05° \\ \vdots \end{bmatrix}^T \begin{bmatrix} \vdots \\ e^{-j2t} \\ 1 \\ e^{j2t} \\ \vdots \end{bmatrix} \qquad (3.246)$$

Note that in this case all of the harmonics enter with a specific phase. The maximum principal gain is given by the maximum singular value, $\bar{\sigma} = 1.1798$, and indicates how much the LTP system amplifies the above signal. The maximum output (principal) direction is given by left singular vector associated with the maximum singular value,

$$\bar{y}(t) = \bar{\sigma} e^{j\omega t} \begin{bmatrix} \vdots \\ \bar{y}_{-1} \\ \bar{y}_0 \\ \bar{y}_1 \\ \vdots \end{bmatrix}^T \begin{bmatrix} \vdots \\ e^{-j\omega_p t} \\ 1 \\ e^{j\omega_p t} \\ \vdots \end{bmatrix} = 1.1798 e^{jt/2} \begin{bmatrix} \vdots \\ 0.5594 - j0.5626 \\ 0.1664 + j0.0646 \\ 0.2647 - j0.4809 \\ \vdots \end{bmatrix}^T \begin{bmatrix} \vdots \\ e^{-j2t} \\ 1 \\ e^{j2t} \\ \vdots \end{bmatrix}$$

To illustrate the notion of phase for LTP systems, the complex coefficients in the output direction will be expressed in polar form,

$$\bar{y}(t) = 1.1798 e^{jt/2} \begin{bmatrix} \vdots \\ 0.7934 \angle -45.17° \\ 0.1784 \angle 21.21° \\ 0.5490 \angle -61.17° \\ \vdots \end{bmatrix}^T \begin{bmatrix} \vdots \\ e^{-j2t} \\ 1 \\ e^{j2t} \\ \vdots \end{bmatrix} \qquad (3.247)$$

Note that the direction associated with the maximum principal gain consists predominantly of three harmonics, and that each harmonic has a corresponding associated phase change. A phase notion must then reflect the phase *change* between corresponding harmonics in the input and output directions. Thus, the phase is a directional property of the harmonic transfer function.

The maximum input direction is shown in Figure 3.11a, and the corresponding output direction is shown in Figure 3.11b, both as predicted from the singular value analysis. The

124

input signal in Figure 3.11a was used as the input to a simulation of the linear time periodic system with zero initial conditions. The resulting output signal is shown in Figure 3.11c. At steady state, the simulated system output and the output as predicted from the singular value analysis coincide, illustrating the LTP interpretation of the Bode frequency response.

3.10 Summary

In this chapter, a class of signals called geometrically periodic signals, and its Fourier series expansion called exponentially modulated periodic signals, was defined. Frequency response notions for linear time periodic systems were developed using the fact that GP (or EMP) input signals produced GP (or EMP) output signals at steady state. The linear map was described using two approaches: integral operators (on the basis of GP signals), harmonic balance (on the basis of EMP signals).

The integral operator is a finite dimensional time domain operator. Although the integral operator is somewhat novel in the control theory, it posesses analogous properties to the LTI transfer function. The concepts of poles, transmission zeroes, and their directional properties were developed in the integral operator framework. Methods for determining these properties were also presented in terms of their defining eigenvalue problems. In the LTI theory, the transfer function matrix and complex exponential signals lead to simple mathematical manipulations of complex matrices and vectors that can be easily implemented on the computer. In contrast, the fundamental mathematical operation involved in the integral operator approach to LTP system analysis is an integral operator mapping a signal, which does not translate easily into a numerical procedure.

However, the observation was made that most linear time periodic systems are time periodic due to parametric excitation, and that the parametric excitation can often be expressed as a truncated complex Fourier series. It was deemed advantageous to exploit this tendency, so that numerical methods were developed in terms of a harmonic balance of the time periodic state space model.

The harmonic balance operator, here called the harmonic transfer function, describes the explicit input-output relationship between the complex Fourier coefficients of the geometrically periodic input and output signals. It can be interpreted loosely as a demodulated representation of the linear time periodic system, since the Fourier coefficients are modu-

a) MAXIMUM INPUT DIRECTION

TIME IN INTEGER FUNDAMENTAL PERIODS

b) MAXIMUM OUTPUT DIRECTION

TIME IN INTEGER FUNDAMENTAL PERIODS

c) ZERO INITIAL CONDITION RESPONSE TO MAXIMUM INPUT DIRECTION

TIME IN INTEGER FUNDAMENTAL PERIODS
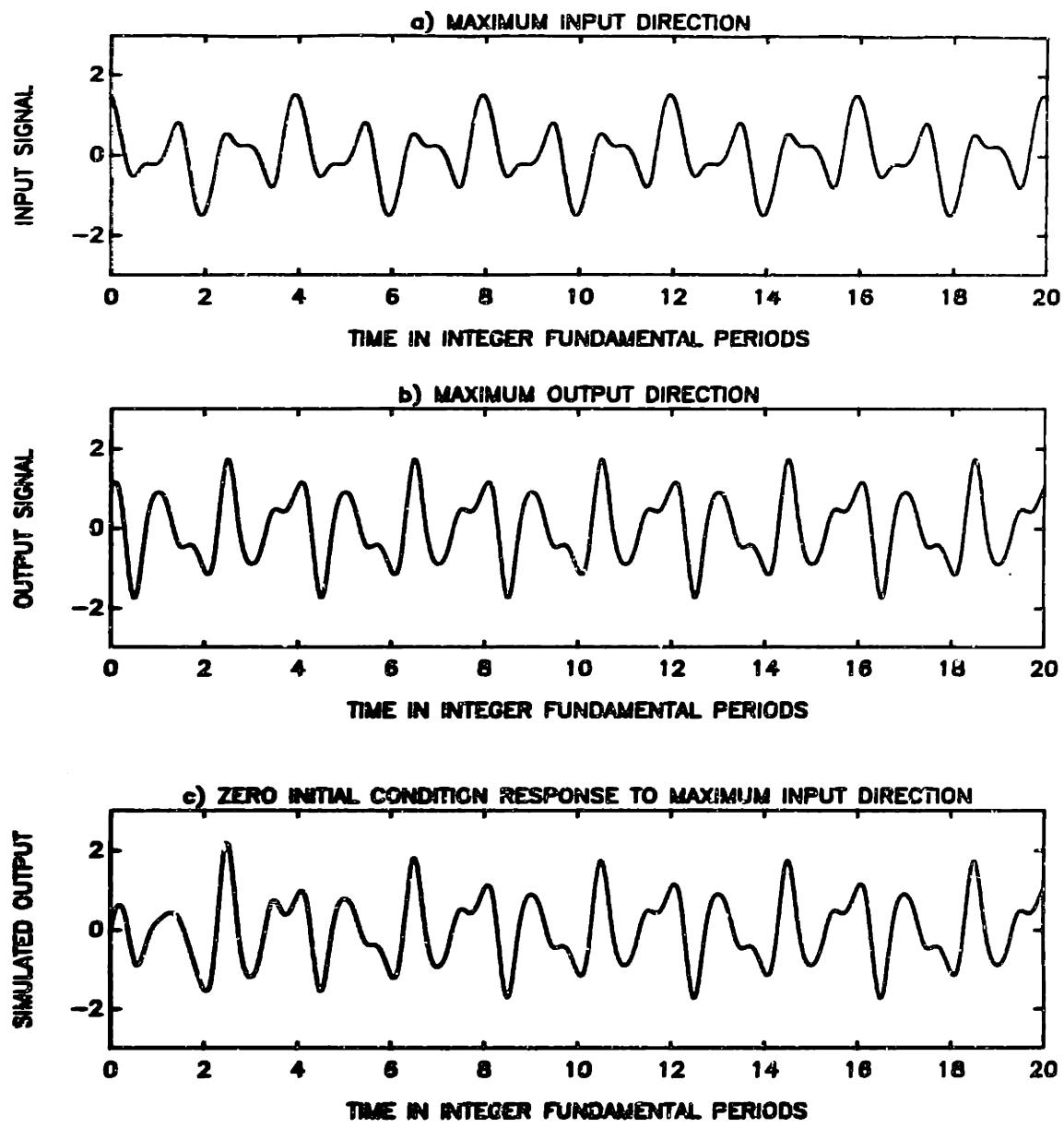
Figure 3.11: Maximum direction analysis for lossy Mathieu equation example. The direction of maximum amplification is the direction associated with the largest singular value of the SVD of the harmonic transfer function at a particular frequency.

lated by the carrier signals, $\{e^{jn\omega_p t} \mid \forall n \in Z\}$. This infinite dimensional representation of the linear time periodic system was called the harmonic state space model. Notions of poles and transmission zeroes were then developed in the context of harmonic balance, and methods for calculating LTP poles, transmission zeroes, and their assocaiated directions, were presented. The singular values or principal gains of the harmonic transfer function were discussed and the LTP principal gain diagram described. Notions of the domain and range spaces were presented.

At the conclusion of the chapter, two examples of LTP systems were analyzed in order to illustrate the benefits of the analysis techniques described above. The first example was a second order LTI plant with an input amplitude modulation. The second example was the lossy Mathieu equation where the embedded LTI state space model $[A_0, B_0, C_0]$ was chosen to have a transmission zero at $s = -1$. In both cases, the analysis procedures developed using harmonic balance were simple to accomplish on the computer using standard software (for example, 386–MATLAB), and provided insight into the open loop characteristics of LTP systems that does not exist in the literature.

[Page Left Blank]

Chapter 4

Nyquist Criterion for LTP Systems

In this chapter, a Nyquist criterion for linear time periodic systems is presented. The Nyquist criterion offers a method of determining closed loop stability of a system as a function of feedback gain. Closed loop stability is determined by inspection (counting encirclements of the $-\frac{1}{k}$ point) of a Nyquist diagram constructed from the eigenloci of the LTP transfer function. The Nyquist criterion is also an important ingredient in the extension of the stability robustness results from the LTI control theory to LTP systems.

4.1 Introduction

The stability of linear time periodic (LTP) systems has classically been of interest, particularly as expressed by Floquet theory and the Hill determinant technique [83]. The Floquet theory has figured prominently in the study of the stability of rotating machinery such as helicopter rotors [27,33], wind turbines [94], and various other systems with parametric excitation [26,101]. LTP system stability has also been examined using Lyapunov theory for autonomous systems [104], various perturbation analyses [77], and describing functions [61]. However, all of the above techniques suffer from the limitation that stability is determined for a specific value of gain, that is, only a yes or no answer is provided to the question of stability.

As a result of this limitation, several sufficient conditions for LTP system stability have been proposed. The stability of fast periodic systems [6] can be examined by an extension

to the basic Floquet stability criterion. In addition, several sufficient conditions have been developed for a specific class of LTP system models, namely, those that can be represented by the (lossy) Mathieu equation [39,81,102]. However, these sufficient stability conditions lead to a conservative characterization of a stability boundary, and, in some cases, lead to inaccurate results for large damping ratios and/or small amplitudes of parametric excitation [83].

All of the above are analysis tools, and are of limited usefulness in the synthesis of feedback controllers.

Hence, the notion of the state space has been applied to the control synthesis problem for LTP systems. Notions of controllability and observability [7,54, among others] have been developed for LTP systems, which [54] demonstrates are equivalent statements of these two properties. The linear quadratic regulator/estimator (LQR/LQE) formulation has been aggressively applied in the LTP context, especially in the study of helicopter vibrations [71,70]. However, the LQR/LQE formulation is basically a time domain design methodology where virtually the only rule of thumb for selecting the quadratic state and control weights is Bryson's Rule. As a result, notions of immense importance to the classical control theory such as bandwidth, stability margins, error constants and the frequency domain transfer function, which are becoming commonplace in the theory of multivariable LTI feedback control, are virtually unknown in the context of a continuous time feedback control theory for LTP systems.

In order to extend the synthesis of feedback controllers for LTP systems into the frequency domain, a generalization of the Nyquist idea for linear time invariant systems, either single–input single–output (SISO) or multi–input multi–output (MIMO), should prove to be a useful starting point.

The classical Nyquist stability criterion [79] developed for SISO systems is one of the most fundamental results in the classical control theory. This Nyquist test reduces the determination of closed loop stability to inspection (by counting encirclements) of a Nyquist diagram. The classical Nyquist stability criterion also provides much of the motivation for the frequency response of SISO systems. This same notion has been extended to systems with delays [19], and to MIMO systems in various ways [3,5,14,13,21,63]. Plotting eigenloci of the open loop transfer function matrix is a powerful methodology due to its ease of numerical implementation and because it permits the verification of stability for a param-

eterization of feedback gain by inspection of a generalized Nyquist diagram. Barman and Katzenelson [3] first presented a rigorous theory for a MIMO Nyquist test, and made much use of the geometric properties of eigenvalues of the open loop transfer function matrix in the s-plane, particularly the graph theoretic properties of eigenloci. Subsequently, MacFarlane and Postlethwaite [63] used Riemann surfaces to develop an equivalent MIMO Nyquist stability criterion for the rational transfer function matrix case. Finally, Desoer and Wang [21] developed a MIMO Nyquist stability criterion based on eigenloci for the rational transfer function case using straightforward proofs that rely on the theory of analytic functions and some elementary mathematical analysis, and then extended these results to distributed systems.

Thus, the primary objective of this chapter is to present a Nyquist criterion for LTP systems that is completely analogous to the Nyquist criterion (based on eigenloci) for linear time invariant (LTI) systems. To date, only the possibility of a Nyquist criterion for continuous time LTP systems has been mentioned in passing [91,90]. However, to date, no comparable Nyquist stability criterion has been developed for LTP systems. One disadvantage of the classical techniques of Floquet and Lyapunov is that stability is determined for a *single value of feedback gain*. The concept of plotting eigenloci of a representation of the open loop LTP system is particularly attractive because closed loop stability can be determined for a *family of gain parameters* using the argument principle. The development of a Nyquist stability criterion for LTP systems based on eigenloci will add a powerful new tool to the study of LTP systems, and will complement the Floquet theory which provides part of the central core of the LTP Nyquist stability criterion.

4.2   The Fredholm-Carleman Integral Operator Theory

In this section, relevant portions of the integral operator theory, originally developed by Fredholm and Carleman, will be presented mainly to establish notation and to provide a framework for the developments of this chapter.

Fredholm [17,48] examined integral equations with continuous (thus, bounded) integral operator kernels. The canonical form of the *Fredholm integral equation of the second kind* is given by

$$\varphi(x) = f(x) + \mu \int_a^b K(x,y)\varphi(y)dy \qquad (4.1)$$

Here, $f(x)$ is a known function, and $\varphi(x)$ is an unknown function, and the objective is to determine the kernel that is inverse to $K(x, y)$, thus, solving the problem. This problem is by no means solvable in general, nor is the solution always guaranteed to exist for arbitrary kernels. For $f(x) = 0$, that is, the *homogenous* integral equation,

$$\varphi(x) - \mu \int_a^b K(x, y)\varphi(y)dy = 0 \tag{4.2}$$

an eigenvalue problem results, where $T = b - a$. The homogenous integral equation is satisfied trivially for $\varphi(x) \equiv 0$, and, in general, nontrivial solutions exist only for specific values of μ. The values μ_k are the *characteristic values*. The inverse values,

$$\lambda_k = \frac{1}{\mu_k} \tag{4.3}$$

are eigenvalues, and along with the associated eigenfunctions, are a direct analogy to the eigenvalues and eigenvectors of a matrix operator.

The *Fredholm determinant* [17,48] of an integral operator with kernel $K(x, y)$ is denoted by $\mathcal{D}_K(\mu)$, which is defined as the limit of the determinant of a sequence of matrices that approximates the operator $[I - \mu K(x, y)]$ as follows:

$$
\begin{aligned}
\mathcal{D}_K(\mu) &= \det\left[I - \mu K(x, y)\right] \\
&= \lim_{n \to \infty} \mathcal{D}_{K(x,y)}^{(n)}(\mu) \\
&= \lim_{n \to \infty}
\begin{vmatrix}
I - \mu h K(x_1, x_1) & -\mu h K(x_1, x_2) & \cdots & -\mu h K(x_1, x_n) \\
-\mu h K(x_2, x_1) & I - \mu h K(x_2, x_2) & \cdots & -\mu h K(x_2, x_n) \\
\vdots & \vdots & \ddots & \vdots \\
-\mu h K(x_n, x_1) & -\mu h K(x_n, x_2) & \cdots & I - \mu h K(x_n, x_n)
\end{vmatrix}
\end{aligned}
\tag{4.4}
$$

where

$$h = \frac{T}{n} \tag{4.5}$$

$$x_i = ih \tag{4.6}$$

This limit exists when the trace of the kernel matrix, $\mathrm{Tr}(K(x, y))$, is well defined.

The Fredholm determinant, $\mathcal{D}_K(\mu)$, can also be expressed as an infinite series [17, page 46]

$$\mathcal{D}_K(\mu) = \sum_{n=0}^{\infty} d_n \mu^n \tag{4.7}$$

132

where

$$d_0 = 1, \quad d_n = -\frac{1}{n} \sum_{m=1}^{n} k_m d_{n-m}. \tag{4.8}$$

Here,

$$k_m = \operatorname{Tr} \{K^m(x,y)\} \tag{4.9}$$

and

$$
\begin{aligned}
K^1(x,y) &= K(x,y) \\
K^m(x,y) &= \int_a^b K(x,z)K^{m-1}(z,y)\,dz
\end{aligned}
\tag{4.10}
$$

The $K^m(x,y)$ are known as the *iterated kernels*.

Finally, it was assumed that the $L_2[a,b]$ kernel has a well defined $k_1 = \operatorname{Tr}\{K(x,y)\}$, so that the Fredholm determinant has a factorization of the form

$$\mathcal{D}_K(\mu) = e^{-k_1\mu} \prod_{n=1}^{\infty} \left(1 - \frac{\mu}{\mu_n}\right) e^{\mu/\mu_n} \tag{4.11}$$

The fundamental point here is that the zeroes of the Fredholm determinant are the characteristic values or inverse eigenvalues of the integral operator kernel. The above form of the Fredholm determinant will provide the fundamental starting point for the development of a Nyquist test using the eigenloci of the integral operator transfer function.

Let us reconsider the integral operator kernel for the LTP system case. In order for the Fredholm determinant in equation (4.4) to have the correct limit, the diagonal entries should be the average of the kernel across the discontinuity, $t = \tau$. Therefore, for strictly proper LTP systems, $\hat{G}(z;t,t)$ must be defined as

$$\hat{G}(z;t,t) = C(t)\Phi(t,0)\left[zI - \Phi(T,0)\right]^{-1}\Phi(T,t)B(t) + \frac{1}{2}C(t)B(t) \tag{4.12}$$

as defined in Definition 3.5. In addition, the integral operator kernel is parametrically dependent on the complex parameter z, that is, the geometric variation of the state vector from the beginning of one period to the beginning of the next.

The Fredholm determinant will play a central role in the development of a generalized Nyquist criterion for LTP systems using the integral operator approach, as will be seen in the next section.

4.3 Nyquist Criterion Via Integral Operators

Consider the block diagram of a feedback servo, as shown Figure 4.1. Here, r is the reference input, e is the servo error, u is the actuator input, and y is the measurement. It is assumed that the integral operator $\widehat{G}(z)$ is square, that is, there are as many inputs as outputs. In addition, it is assumed that the corresponding LTP state space model, $S = [A(t), B(t), C(t)]$, is strictly proper (that is, $D(t) = 0$ for all $t \in [0, T]$). This is not a limiting assumption in practice since all physically realizable systems are strictly proper, that is, all physically realizable systems experience gain roll off at high frequency when sensor and actuator dynamics are considered. We also assume that $r(t)$ is zero, or bounded, so that it need not be considered in an examination of internal stability as will be done here. Assuming that $r(t) = 0$, the linear static output feedback control law is given by

$$
\begin{aligned}
u(t) &= \mu y(t) \\
&= -ky(t)
\end{aligned}
\tag{4.13}
$$

so that $\mu = -k$. The notation μ is customary in the integral operator theory, and the notation k is customary in the linear control theory. The notation μ for the gain parameter will be utilized in the sequel in order to utilize the properties of the Fredholm determinant directly out of the literature. The resulting closed loop dynamics are

$$
\dot{x}(t) = A_{\text{cl}}(t)x(t)
\tag{4.14}
$$

where

$$
\begin{aligned}
A_{\text{cl}}(t) &= A(t) + \mu B(t)C(t) \\
&= A(t) - kB(t)C(t)
\end{aligned}
\tag{4.15}
$$

The stability of the closed loop system is determined from the eigenvalues of the closed loop monodromy matrix $\Phi_{\text{cl}}(T, 0; \mu)$ with obvious definition. Again, however, stability can only be determined for a single value of gain, $\mu \; (= -k)$.

4.3.1 A Nyquist criterion

An approach that introduces the feedback gain as a parameter would provide a more useful closed loop stability analysis. Recall the integral operator state space model from Defini-
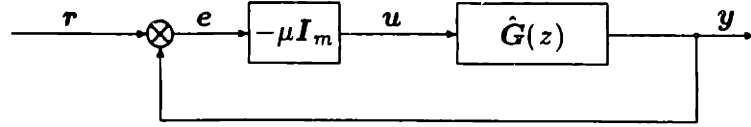
Figure 4.1: LTP feedback system under consideration.

tion 3.6,

$$\tilde{x}_{k+1} = \Phi(T,0)\tilde{x}_k + \tilde{B}\tilde{u}_k \qquad (4.16)$$

$$\tilde{y}_k = \tilde{C}\tilde{x}_k + \tilde{D}\tilde{u}_k \qquad (4.17)$$

Note that the LTP state space model associated with the integral operator transfer function is strictly proper (that is, $D(t) = 0$), so that the feedforward integral operator becomes

$$\tilde{D}\tilde{u}_k = \int_0^t C(t)\Phi(t,\tau)B(\tau)\tilde{u}_k(\tau)d\tau \qquad (4.18)$$

The kernel of the above integral operator is the *impulse response matrix* [59, page 12]

$$K(t,\tau) = C(t)\Phi(t,\tau)B(\tau); \quad t \geq \tau \qquad (4.19)$$

The static output feedback control law is applied

$$\tilde{u}_k = \mu\tilde{y}_k \qquad (4.20)$$

Substituting (4.17) into (4.20)

$$\tilde{u}_k = \mu\tilde{C}\tilde{x}_k + \mu\tilde{D}\tilde{u}_k \qquad (4.21)$$

and solving for $\tilde{u}_k$,

$$\tilde{u}_k = \mu(\tilde{I} - \mu\tilde{D})^{-1}\tilde{C}\tilde{x}_k \qquad (4.22)$$

If the input to the LTP system is a GP signal, then

$$\tilde{x}_{k+1} = z\tilde{x}_k \qquad (4.23)$$

so that from (4.16) and (4.22)

$$0 = [zI - \Phi(T,0)]\tilde{x}_k + \tilde{B}\tilde{u}_k$$

$$0 = -\mu\tilde{C}\tilde{x}_k + (\tilde{I} - \mu\tilde{D})\tilde{u}_k \qquad (4.24)$$

135

These equations can be expressed in matrix form,

$$\begin{bmatrix} zI - \Phi(T,0) & -\tilde{B} \\ -\mu\tilde{C} & \tilde{I} - \mu\tilde{D} \end{bmatrix} \begin{bmatrix} \tilde{x}_k \\ \tilde{u}_k \end{bmatrix} = 0 \tag{4.25}$$

A solution exists when

$$\varphi(z) = \det \begin{bmatrix} zI - \Phi(T,0) & -\tilde{B} \\ -\mu\tilde{C} & \tilde{I} - \mu\tilde{D} \end{bmatrix} = 0 \tag{4.26}$$

where the above determinant is found using a limiting procedure similar to the one used to define the Fredholm determinant. Applying the *Schur formulae* [34] for determinants of partitioned matrices,

$$\varphi(z) = |zI - \Phi(T,0)| \left| \tilde{I} - \mu\tilde{D} - \mu\tilde{C}[zI - \Phi(T,0)]^{-1}\tilde{B} \right| \tag{4.27}$$

Recall from Lemma 3.7 that the integral operator transfer function can be expressed as

$$\widehat{G}(z) = \tilde{C}[zI - \Phi(T,0)]^{-1}\tilde{B} + \tilde{D} \tag{4.28}$$

so that (4.27) can be simplified,

$$\varphi(z) = |zI - \Phi(T,0)| \left| \tilde{I} - \mu\widehat{G}(z) \right| \tag{4.29}$$

Applying the Schur formulae to (4.26) a second time yields

$$\varphi(z) = \left| \tilde{I} - \mu\tilde{D} \right| \left| zI - \Phi(T,0) - \mu\tilde{B}(\tilde{I} - \mu\tilde{D})^{-1}\tilde{C} \right| \tag{4.30}$$

Consider the first determinant in the above product. The kernel of the integral operator associated with $\tilde{D}$ is the impulse response, which is a *Volterra integral operator kernel*. Again, the diagonal entries of the kernel must be the average of the kernel across the discontinuity, so that

$$\tilde{D}(\tau,\tau) = \frac{1}{2}C(\tau)B(\tau) \tag{4.31}$$

According to [48, page 243], the Fredholm determinant of a Volterra integral operator kernel converges to the trace of the Fredholm determinant, so that

$$\begin{aligned} \mathcal{D}_{\tilde{D}}(\mu) &= \left| I - \mu\tilde{D} \right| \\ &= \exp\left\{ -\frac{\mu}{2}\int_0^t C(\tau)B(\tau)d\tau \right\} \end{aligned} \tag{4.32}$$

136

Clearly, $\mathcal{D}_{\tilde{\boldsymbol{D}}}(\mu)$ can never vanish, and is greater than zero for all values of μ, so that the Volterra kernel has no characteristic values.

Now, consider the second determinant of the product in (4.30). If the feedback signal in (4.22) is the input to the dynamic equation (4.16), then

$$\tilde{x}_{k+1} = \tilde{A}_{\mathrm{cl}}\tilde{x}_k \qquad (4.33)$$

where

$$\tilde{A}_{\mathrm{cl}} = \left[\boldsymbol{\Phi}(T,0) + \mu\tilde{B}(\tilde{I} - \mu\tilde{D})^{-1}\tilde{C} \right] \qquad (4.34)$$

However, another connection must be made. Recall that the closed loop transition matrix satisfies the differential equation

$$\dot{\boldsymbol{\Phi}}_{\mathrm{cl}}(t,\tau) = [A(t) + \mu B(t)C(t)]\boldsymbol{\Phi}_{\mathrm{cl}}(t,\tau) \qquad (4.35)$$

Evaluating for $\tau = 0$,

$$\dot{\boldsymbol{\Phi}}_{\mathrm{cl}}(t,0) = [A(t) + \mu B(t)C(t)]\boldsymbol{\Phi}_{\mathrm{cl}}(t,0) \qquad (4.36)$$

The above equation has a Volterra integral equation as a solution,

$$\boldsymbol{\Phi}_{\mathrm{cl}}(t,0) = \boldsymbol{\Phi}(t,0)\boldsymbol{\Phi}_{\mathrm{cl}}(t,0) + \mu\int_0^t \boldsymbol{\Phi}(t,\tau)B(\tau)C(\tau)\boldsymbol{\Phi}_{\mathrm{cl}}(\tau,0)d\tau \qquad (4.37)$$

Now, evaluating the above at $t = T$, and noting that $\boldsymbol{\Phi}(0,0) = I$, yields

$$\begin{aligned} \boldsymbol{\Phi}_{\mathrm{cl}}(T,0) &= \boldsymbol{\Phi}(T,0) + \mu\int_0^T \boldsymbol{\Phi}(T,\tau)B(\tau)C(\tau)\boldsymbol{\Phi}_{\mathrm{cl}}(\tau,0)d\tau \\ &= \boldsymbol{\Phi}(T,0) + \mu\tilde{B}C(t)\boldsymbol{\Phi}_{\mathrm{cl}}(T,0) \end{aligned} \qquad (4.38)$$

Multiplying (4.37) by $C(t)$,

$$C(t)\boldsymbol{\Phi}_{\mathrm{cl}}(t,0) = C(t)\boldsymbol{\Phi}(t,0) + \mu\tilde{D}C(t)\boldsymbol{\Phi}_{\mathrm{cl}}(t,0) \qquad (4.39)$$

so that

$$\begin{aligned} C(t)\boldsymbol{\Phi}_{\mathrm{cl}}(t,0) &= \left(\tilde{I} - \mu\tilde{D}\right)^{-1}C(t)\boldsymbol{\Phi}(t,0) \\ &= \left(\tilde{I} - \mu\tilde{D}\right)^{-1}\tilde{C} \end{aligned} \qquad (4.40)$$

Substituting the above result into (4.38) yields

$$\begin{aligned} \boldsymbol{\Phi}_{\mathrm{cl}}(T,0) &= \boldsymbol{\Phi}(T,0) + \mu\tilde{B}\left(\tilde{I} - \mu\tilde{D}\right)^{-1}\tilde{C} \\ &= \tilde{A}_{\mathrm{cl}} \end{aligned} \qquad (4.41)$$

137

Hence, the above together with (4.32) results in the following simplification of (4.30):

$$\varphi(z) = \mathcal{D}_{\tilde{D}}(\mu)\,|zI - \Phi_{\mathrm{cl}}(T,0;\mu)| \qquad (4.42)$$

Therefore, combining (4.29) and (4.42),

$$\begin{aligned}
\varphi(z) &= |zI - \Phi(T,0)|\,\left|\tilde{I} - \mu\widehat{G}(z)\right| \\
&= \mathcal{D}_{\tilde{D}}(\mu)\,|zI - \Phi_{\mathrm{cl}}(T,0;\mu)|
\end{aligned} \qquad (4.43)$$

produces the following equation,

$$\mathcal{D}_{\widehat{G}(z)}(\mu) = \det\left[\tilde{I} - \mu\widehat{G}(z)\right] = \mathcal{D}_{\tilde{D}}(\mu)\frac{\det\left[zI - \Phi_{\mathrm{cl}}(T,0;\mu)\right]}{\det\left[zI - \Phi(T,0)\right]} \qquad (4.44)$$

Now, $\mathcal{D}_{\widehat{G}(z)}(\mu)$ is analytic in the complex z-plane except at the poles of the open loop system. Therefore, the argument principle can be used to count the number of closed loop poles outside the unit circle using the Nyquist path illustrated in Figure 4.2. An important point to remember is that the Fredholm determinant or the impulse response, $\mathcal{D}_{\tilde{D}}(\mu)$, does not contribute any characteristic values on the Nyquist contour and as a result does not contribute any encirclements. This leads to the following theorem, which is a generalization of the well known result for linear time invariant MIMO systems.

Theorem 4.1 (Stability Theorem based on $\left|\tilde{I} - \mu\widehat{G}(z)\right|$) *Let $\bar{N}_1$ be the Nyquist contour defined in Figure 4.2. The closed loop system (4.14) is asymptotically stable if and only if:*

(1) $\mathcal{D}_{\widehat{G}(z)}(\mu) \neq 0$, *for all* $z \in \bar{N}_1$,

(2) $\mathcal{D}_{\widehat{G}(z)}(\mu)$ *encircles the origin* n_p *times in the counterclockwise sense, where* n_p *is the number of zeroes of the open loop system characteristic polynomial with magnitude greater than or equal to unity, counting multiplicities.*

Remark: The above theorem follows directly from the argument principle, and is the fundamental connection between the Fredholm determinant and the Floquet theory. However, this theorem is of limited utility in the direct determination of closed loop system stability. To utilize the above theorem as a Nyquist test, a value of feedback gain is selected. Then, the Fredholm determinant is computed along the Nyquist contour, and the result plotted in the complex plane. The encirclements of the origin by the Fredholm determinant can then
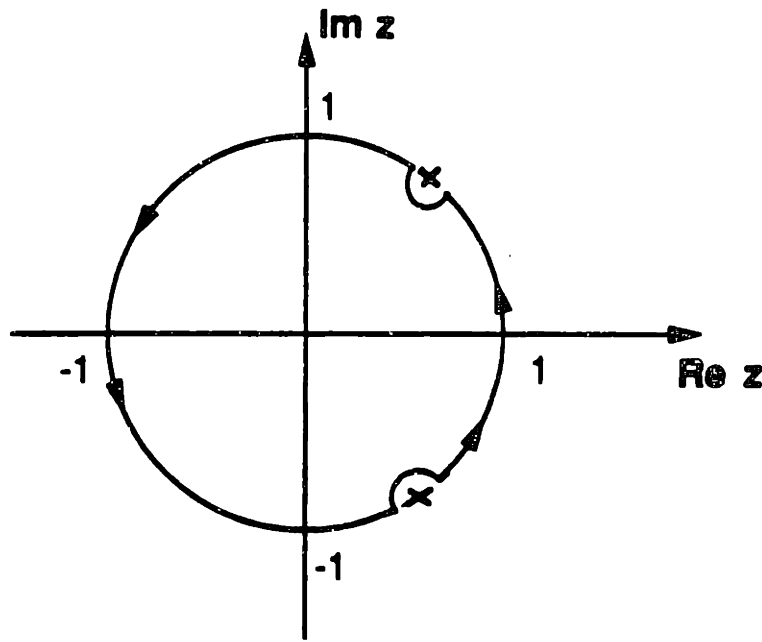
Figure 4.2: The LTP Nyquist contour. The Nyquist path is denoted by $\bar{N}_1$. The "×" denote the poles of $\widehat{G}(z)$, and appropriate indentations are shown such that poles on the unit circle are considered unstable.

be counted and closed loop stability determined for a single value of feedback gain. This is certainly as difficult a computation as computing the closed loop monodromy matrix and its eigenvalues. $\qquad\qquad\qquad\qquad\qquad\qquad\qquad\qquad\qquad\qquad\qquad\qquad\qquad\quad$ □

4.3.2 A Nyquist test using eigenloci

The objective of the following analysis is to generalize the Nyquist stability criterion, so that it may be applied to linear time periodic systems for any $\mu < 0$ $(k > 0)$, or a parameterization of feedback gain, and stability determined by inspection. Using the above Nyquist test, we compute the Fredholm determinant, $\mathcal{D}_{\widehat{G}(z)}(\mu)$, on the Nyquist contour in the z-plane, that is, the unit circle, and count encirclements of the origin. However, by computing the *eigenloci* of $\widehat{G}(z)$, that is, the eigenvalues of $\widehat{G}(z)$ as z is varied along the Nyquist contour in the z-plane, we can count encirclements of the $-\frac{1}{k}$ point by these eigenloci in order to determine stability. Thus, the Nyquist test can be parameterized by feedback gain, so that stability of the closed loop system can be determined for any value

of feedback gain. In this section, the concept of a Nyquist test using eigenloci is developed.

Here, we shall consider the strictly proper feedback system in Figure 4.1 with a square integral operator transfer function, $\widehat{G}(z)$. For each $z \in \bar{N}_1$, $G(\cdot, \cdot; z)$ is an L_2 kernel, and therefore the Fredholm determinant $\mathcal{D}_{\widehat{G}(z)}(\mu)$ is an entire function of μ [48]. Therefore, there are a countable number of zeroes in the μ plane denoted by $\mu_i(z)$ that are the *characteristic values* of $\widehat{G}(z)$. The eigenvalues of the integral operator are given by

$$\lambda_i(z) = \frac{1}{\mu_i(z)} \quad i = 1, 2, 3, \ldots \tag{4.45}$$

Now, the Fredholm determinant can be expressed in terms of the eigenvalues by

$$\mathcal{D}_{\widehat{G}(z)}(\mu) = e^{k_1 \mu} \prod_{i=1}^{\infty} \left(1 - \mu \lambda_i(z)\right) e^{\mu \lambda_i(z)} \tag{4.46}$$

where the product expansion is known to converge absolutely [17].

First, recall the following result on the algebraic dependence of characteristic values [17, see Theorem 12.3-2].

Theorem 4.2 *Let the L_2 kernel $K(x, y, \epsilon)$ depend analytically on ϵ, and consider a simple closed contour C which encloses a single arbitrary characteristic value of $K(x, y, 0)$, of multiplicity N and no others. For small enough ϵ, the characteristic value of $K(x, y, \epsilon)$ within C consists of branches of one or several analytic functions which have at most algebraic singularities of order $1 \le p - 1 \le N - 1$ at $\epsilon = 0$.*

This theorem is instrumental in proving the following lemma.

Lemma 4.3 *The eigenvalues $\lambda_i(z), z \in \bar{N}_1$ approach 0 uniformly on $\bar{N}_1$.*

Proof: The proof is by contradiction. Suppose that the limit is not uniform for $z \in \bar{N}_1$. Then for any ϵ, there exists an infinite sequence $n_1, n_2, \ldots$ and $z_1, z_2, \ldots$ such that

$$|\lambda_{n_i}(z_i)| \ge \epsilon \tag{4.47}$$

or, equivalently,

$$|\mu_{n_i}(z_i)| \le \frac{1}{\epsilon} \tag{4.48}$$

Now, $\bar{N}_1$ is compact. We define the disk $D_\epsilon = \left\{ x \in C : |x| \le \frac{1}{\epsilon} \right\}$, which is also compact. Thus, $\bar{N}_1 \times D_\epsilon$ is also compact, so that the infinite sequence $\{(z_1, \mu_1), (z_2, \mu_2), \ldots\}$ has a

140

limit point in $\bar{N}_1 \times D_\epsilon$, which we will denote by (z_∞, μ_∞). Since $\mathcal{D}_{\widehat{G}(z)}(\mu)$ is continuous in z and μ, and

$$\mathcal{D}_{\widehat{G}(z_i)}(\mu_i) = 0 \qquad (4.49)$$

it follows that

$$\mathcal{D}_{\widehat{G}(z_\infty)}(\mu_\infty) = 0 \qquad (4.50)$$

where μ_∞ is a characteristic value of $\widehat{G}(z_\infty)$. Since (z_∞, μ_∞) is a limit point, in any neighborhood of (z_∞, μ_∞) there are an infinite number of points (z_i, μ_i). Corresponding to each (z_i, μ_i) is the index n_i and the branch $\mu_{n_i}(z)$ of the solution to the characteristic equation $\mathcal{D}_{\widehat{G}(z_i)}(\mu) = 0$. But, this contradicts Theorem 4.2, thus proving the lemma. $\square$

Now, following the example of [21], we define some graph theoretic terms. Let $\gamma(\cdot) :$ $[\alpha, \beta] \to C$, $\alpha \neq \beta$, $[\alpha, \beta] \subset R$, then $\gamma(\cdot)$ is said to be a *path* in the complex plane if $\gamma(\cdot)$ is continuous. A path $\gamma(\cdot)$ is a *loop* if $\gamma(\alpha) = \gamma(\beta)$. A path $\gamma(\cdot)$ is said to be a *road* if $\gamma(\cdot)$ is differentiable except at a finite number of points. A road $\gamma(\cdot)$ is a *circuit* if $\gamma(\alpha) = \gamma(\beta)$. Let $\gamma(\cdot): [\alpha, \beta] \to C$ be a circuit. Let the point $\lambda_0 \notin \gamma$, where $\gamma := \gamma([\alpha, \beta])$. Then $C(p; \gamma)$ denotes the number of counterclockwise (CCW) encirclements of $p \in C$ by the circuit γ [22]

$$C(p, \gamma) = \frac{1}{2\pi j} \int_\gamma \frac{dz}{z - \lambda_0} \qquad (4.51)$$

Now, we are prepared to develop the generalized Nyquist diagram for LTP systems.

To construct the Nyquist diagram, we resort to a stratagem similar to that employed in [21], which deals with the distributed parameter LTI case. Because the eigenvalues of $\widehat{G}(z)$ uniformly converge to the origin on $\bar{N}_1$, some eigenloci, λ_i, form continuous indexed families of paths that lie outside a disk of radius ϵ, namely D_ϵ, centered at the origin in the complex plane. These indexed families of paths begin and end within the disk D_ϵ, an example of which is shown in Figure 4.3 by solid lines. By arbitrarily closing the continuous indexed family of paths within the disk to form families of loops, $\{\lambda_j^* | j = 1, 2, \cdots, p\}$, as shown by a dashed line in Figure 4.3, the number of encirclements of the $-\frac{1}{k}$ point by these loops can be determined. The sum of these encirclements is precisely the number of encirclements of $\mathcal{D}_{\widehat{G}(z)}(\mu)$ about the origin.

Now, we are prepared to state the generalized Nyquist stability criterion for systems with periodically time varying parameters.

limit point in $\bar{N}_1 \times D_\epsilon$, which we will denote by (z_∞, μ_∞). Since $\mathcal{D}_{\widehat{G}(z)}(\mu)$ is continuous in z and μ, and

$$\mathcal{D}_{\widehat{G}(z_i)}(\mu_i) = 0 \tag{4.49}$$

it follows that

$$\mathcal{D}_{\widehat{G}(z_\infty)}(\mu_\infty) = 0 \tag{4.50}$$

where μ_∞ is a characteristic value of $\widehat{G}(z_\infty)$. Since (z_∞, μ_∞) is a limit point, in any neighborhood of (z_∞, μ_∞) there are an infinite number of points (z_i, μ_i). Corresponding to each (z_i, μ_i) is the index n_i and the branch $\mu_{n_i}(z)$ of the solution to the characteristic equation $\mathcal{D}_{\widehat{G}(z_i)}(\mu) = 0$. But, this contradicts Theorem 4.2, thus proving the lemma. $\quad\square$

Now, following the example of [21], we define some graph theoretic terms. Let $\gamma(\cdot)$: $[\alpha, \beta] \to C$, $\alpha \neq \beta$, $[\alpha, \beta] \subset R$, then $\gamma(\cdot)$ is said to be a *path* in the complex plane if $\gamma(\cdot)$ is continuous. A path $\gamma(\cdot)$ is a *loop* if $\gamma(\alpha) = \gamma(\beta)$. A path $\gamma(\cdot)$ is said to be a *road* if $\gamma(\cdot)$ is differentiable except at a finite number of points. A road $\gamma(\cdot)$ is a *circuit* if $\gamma(\alpha) = \gamma(\beta)$. Let $\gamma(\cdot)$: $[\alpha, \beta] \to C$ be a circuit. Let the point $\lambda_0 \notin \gamma$, where $\gamma := \gamma([\alpha, \beta])$. Then $C(p; \gamma)$ denotes the number of counterclockwise (CCW) encirclements of $p \in C$ by the circuit γ [22]

$$C(p, \gamma) = \frac{1}{2\pi j} \int_\gamma \frac{dz}{z - \lambda_0} \tag{4.51}$$

Now, we are prepared to develop the generalized Nyquist diagram for LTP systems.

To construct the Nyquist diagram, we resort to a stratagem similar to that employed in [21], which deals with the distributed parameter LTI case. Because the eigenvalues of $\widehat{G}(z)$ uniformly converge to the origin on $\bar{N}_1$, some eigenloci, λ_i, form continuous indexed families of paths that lie outside a disk of radius ϵ, namely D_ϵ, centered at the origin in the complex plane. These indexed families of paths begin and end within the disk D_ϵ, an example of which is shown in Figure 4.3 by solid lines. By arbitrarily closing the continuous indexed family of paths within the disk to form families of loops, $\{\lambda_j^* | j = 1, 2, \cdots, p\}$, as shown by a dashed line in Figure 4.3, the number of encirclements of the $-\frac{1}{k}$ point by these loops can be determined. The sum of these encirclements is precisely the number of encirclements of $\mathcal{D}_{\widehat{G}(z)}(\mu)$ about the origin.

Now, we are prepared to state the generalized Nyquist stability criterion for systems with periodically time varying parameters.

Figure 4.3: **Loops used in the Nyquist test.** The eigenloci of $\widehat{G}(z)$ are continuous and are uniformly convergent on $\bar{N}_1$, so that an indexed family of paths can be arbitrarily closed within the disk D_ϵ to form a loop. Only those paths that travel outside D_ϵ are considered. The resulting loops can then be used to count encirclements according to the Nyquist stability criterion for LTP systems.

Theorem 4.4 (Generalized Nyquist stability criterion for lumped LTP case)

Consider the feedback system S shown in Figure 4.1. Associated with $\widehat{G}(z)$ and $\left|\frac{1}{k}\right| > \epsilon > 0$ are the eigenloci λ_i. Then the closed-loop system is stable

$$\Longleftrightarrow \begin{cases} \text{i)} \quad -\frac{1}{k} \notin \{\lambda_j^* | j = 1, 2, \cdots, p\} \\ \text{ii)} \quad \sum_{j=1}^{p} C(-\frac{1}{k}; \lambda_j^*) = n_p \end{cases} \tag{4.52}$$

where n_p denotes the number of unstable open loop poles, or zeroes of the open-loop system characteristic polynomial with magnitude greater than or equal to unity counting multiplicities, and λ_j^* denotes any indexed family of loops formed from the eigenloci and arbitrarily closed inside a disk of radius epsilon, D_ϵ, centered on the origin in the complex plane.

142

Remark 1: The proof is essentially similar to the proof of Theorem L3 in Desoer and Wang [21], since the problem has been rendered analogous to the LTI lumped parameter case.

Remark 2: Theorem 4.4 generalizes the multivariable Nyquist stability criterion for LTI systems to systems with periodically time varying parameters. To guarantee closed loop stability, the number of CCW encirclements of the $-\frac{1}{k}$ point by a family of loops, $\{\lambda_j^* | j = 1, 2, \cdots, p\}$, which is formed as z travels around the Nyquist path $\bar{N}_1$ in CCW fashion, must equal the number of open loop unstable poles. Also by only considering those loops that exit the disk, D_ϵ, only a finite number of eigenloci are considered. □

4.4   Nyquist Criterion Via Harmonic Theory

In Chapter 3, the integral operator transfer function was used to describe the explicit relationship between GP input and GP output signals. However, the integral operator approach does not provide numerical techniques directly because the integral operator is essentially a functional operating on vector functions, which cannot be implemented on the computer directly. Numerical methods must be developed that are inferred from the integral operator results, and the usual approach taken is a time discretization of the integral operator kernel [17]. In this thesis, Hill theory or harmonic balance approaches have been developed largely due to the convenient representation of the GP signal as an EMP signal.

By expanding the periodic portion of the GP signal in a complex Fourier series (an application of the Hill theory or harmonic balance), the integral operator transfer function was transformed into a frequency domain operator called the *harmonic transfer function.* The harmonic transfer function is isomorphic in the fundamental strip of the s–plane to the integral operator in the z–plane. Alternatively, the integral operator in the z–plane can be uniquely represented by the harmonic transfer function in the s–plane. Moreover, the eigenloci of the harmonic transfer function can be easily computed using standard eigenvalue software, as long as the harmonic transfer function is truncated.

In this section, the Nyquist criterion is developed from the harmonic balance point of view, and a numerical method is proposed to develop the Nyquist diagram.

4.4.1 A Nyquist criterion

Consider a square strictly proper LTP state space model, $S = [A(t), B(t), C(t)]$. To reiterate, a square LTP state space model has the same number of inputs as outputs. Strictly proper implies that the feedforward matrix, $D(t)$, is identically zero. Corresponding to this LTP state space model is the harmonic state space model of the form

$$(s\mathcal{I} + \mathcal{N})\chi = \mathcal{A}\chi + \mathcal{B}u \tag{4.53}$$

$$y = \mathcal{C}\chi \tag{4.54}$$

Assume that a linear static output feedback law is applied

$$u = -ky$$

$$= -k\mathcal{C}\chi \tag{4.55}$$

Rearranging (4.53) and (4.55) results in two equations

$$0 = [\mathcal{I} - (s\mathcal{I} + \mathcal{N})^{-1}\mathcal{A}]\chi - (s\mathcal{I} + \mathcal{N})^{-1}\mathcal{B}u$$

$$0 = -k\mathcal{C}\chi - \mathcal{I}u \tag{4.56}$$

The above equations can be expressed in matrix form as

$$\begin{bmatrix} \mathcal{I} - (s\mathcal{I} + \mathcal{N})^{-1}\mathcal{A} & -(s\mathcal{I} + \mathcal{N})^{-1}\mathcal{B} \\ -k\mathcal{C} & -\mathcal{I} \end{bmatrix} \begin{bmatrix} \chi \\ u \end{bmatrix} = 0 \tag{4.57}$$

The above infinite set of equations has a solution when

$$\varphi(s) = \det \begin{bmatrix} \mathcal{I} - (s\mathcal{I} + \mathcal{N})^{-1}\mathcal{A} & -(s\mathcal{I} + \mathcal{N})^{-1}\mathcal{B} \\ -k\mathcal{C} & -\mathcal{I} \end{bmatrix} = 0 \tag{4.58}$$

Applying the Schur lemma for determinants of partitioned matrices,

$$\varphi(s) = \left| \mathcal{I} - (s\mathcal{I} + \mathcal{N})^{-1}\mathcal{A} \right| \left| \mathcal{I} + k\mathcal{C} \left[\mathcal{I} - (s\mathcal{I} + \mathcal{N})^{-1}\mathcal{A} \right]^{-1} (s\mathcal{I} + \mathcal{N})^{-1}\mathcal{B} \right| \tag{4.59}$$

Now, the first determinant in the above product is the open loop Hill determinant, $\Delta(s)$. The second determinant can be simplified by noting that

$$(s\mathcal{I} - (\mathcal{A} - \mathcal{N}))^{-1} = (\mathcal{I} - (s\mathcal{I} + \mathcal{N})^{-1}\mathcal{A})^{-1}(s\mathcal{I} + \mathcal{N})^{-1} \tag{4.60}$$

To show this, take the inverse of both sides of the above equation

$$s\mathcal{I} - (\mathcal{A} - \mathcal{N}) = (s\mathcal{I} + \mathcal{N})(\mathcal{I} - (s\mathcal{I} + \mathcal{N})^{-1}\mathcal{A}) \tag{4.61}$$

and simplify. The second determinant is the open loop harmonic transfer function, $\widehat{\mathcal{G}}(s)$, so that (4.59) can be expressed as

$$\varphi(s) = \Delta(s)\left|\mathcal{I} + k\widehat{\mathcal{G}}(s)\right| \tag{4.62}$$

Applying the Schur lemma a second time,

$$\begin{aligned}\varphi(s) &= \left|\mathcal{I} - (s\mathcal{I} + \mathcal{N})^{-1}\mathcal{A} - k(s\mathcal{I} + \mathcal{N})^{-1}\mathcal{B}\mathcal{C}\right| \\ &= \left|\mathcal{I} - (s\mathcal{I} + \mathcal{N})^{-1}(\mathcal{A} - k\mathcal{B}\mathcal{C})\right|\end{aligned} \tag{4.63}$$

Substituting the linear feedback control law into (4.53), the closed loop dynamics can be expressed by

$$(s\mathcal{I} + \mathcal{N})x = (\mathcal{A} - k\mathcal{B}\mathcal{C})x \tag{4.64}$$

Also, the Toeplitz form associated with the closed loop dynamic matrix, $\mathcal{A}_{\mathrm{cl}}(t)$, is given by

$$\mathcal{A}_{\mathrm{cl}} = \mathcal{A} - k\mathcal{B}\mathcal{C} \tag{4.65}$$

Thus, the infinite determinant in (4.63) is the closed loop Hill determinant, which is denoted by $\Delta_{\mathrm{cl}}(s; k)$, so that

$$\varphi(s) = \Delta_{\mathrm{cl}}(s; k) \tag{4.66}$$

Combining (4.62) and (4.66),

$$\begin{aligned}\varphi(s) &= \det\left[\mathcal{I} + k\widehat{\mathcal{G}}(s)\right]\Delta(s) \\ &= \Delta_{\mathrm{cl}}(s; k)\end{aligned}$$

produces the following relationship

$$\begin{aligned}\Delta_{\widehat{\mathcal{G}}(s)}(k) = \det\left[\mathcal{I} + k\widehat{\mathcal{G}}(s)\right] &= \frac{\Delta_{\mathrm{cl}}(s; k)}{\Delta(s)} \\ &= \frac{\det\left[\mathcal{I} - (s\mathcal{I} + \mathcal{N})^{-1}\mathcal{A}_{\mathrm{cl}}\right]}{\det\left[\mathcal{I} - (s\mathcal{I} + \mathcal{N})^{-1}\mathcal{A}\right]} \\ &= \frac{\det[\mathcal{I} - (s\mathcal{I} + \mathcal{N})^{-1}(\mathcal{A} - k\mathcal{B}\mathcal{C})]}{\det[\mathcal{I} - (s\mathcal{I} + \mathcal{N})^{-1}\mathcal{A}]}\end{aligned} \tag{4.67}$$

145

Both the closed and open loop Hill determinants are absolutely convergent, since the Hill determinant was shown to be a member of a class of converging determinants called normal determinants. The infinite determinant, $\Delta_{\widehat{\mathcal{G}}(s)}(k)$, is the quotient of two convergent infinite determinants, and so must itself be convergent as long as $(s\mathcal{I}+\mathcal{N})^{-1}$ exists. The above is the harmonic balance or Hill theory analog to (4.44), and is constructed using Hill determinants.

The expression in (4.67) can be expressed as

$$\Delta_{\widehat{\mathcal{G}}(s)}(k) = \det\left[\mathcal{I} + k\widehat{\mathcal{G}}(s)\right] = \frac{\prod_{n=-\infty}^{\infty} \det[\boldsymbol{I} - \frac{1}{s+jn\omega_p}\boldsymbol{Q}_{\mathrm{cl}}]}{\prod_{n=-\infty}^{\infty} \det[\boldsymbol{I} - \frac{1}{s+jn\omega_p}\boldsymbol{Q}]} \tag{4.68}$$

Again, the conclusion is that zeroes of the infinite determinant, $\Delta_{\widehat{\mathcal{G}}(s)}(k)$ are periodic across the complementary strips, or that the zeroes are reflected from the fundamental strip into the complementary strips.

As in previous discussions of the harmonic theory, we are only concerned with behavior of the above function in the fundamental strip, since s has been restricted to be in the fundamental strip of the complex s-plane. The Hill determinant, $\Delta_{\widehat{\mathcal{G}}(s)}(k)$ is analytic everywhere in the fundamental strip except at the open loop poles of the system. Therefore, the argument principle can be used to count the number of closed loop poles in the right half fundamental strip using the Nyquist contour, $s \in \bar{N}_f$, shown in Figure 4.4.

Thus, the above discussion leads to the statement of a Nyquist stability theorem based on a harmonic theory approach.

Theorem 4.5 (Stability theorem based on the Hill determinant of the harmonic transfer function) *Let $\bar{N}_f$ be the Nyquist contour defined in Figure 4.4. The closed loop system is asymptotically stable if and only if*

(1) $\Delta_{\widehat{\mathcal{G}}(s)}(k) \neq 0$ for all $s \in \bar{N}_f$,

(2) $\Delta_{\widehat{\mathcal{G}}(s)}(k)$ encircles the origin n_p times in the counterclockwise sense, where n_p is the number of zeroes of the open loop Hill determinant in the closed right half plane (that is, the right half plane including the imaginary axis) of the fundamental strip, counting multiplicities.

Remark: In order to use the above Nyquist test, the Hill determinant of the harmonic transfer function must be computed for a given value of k, for a parameterization of s in the complex s-plane, that is, the Nyquist contour $\bar{N}_f$. The encirclements of the origin by

146
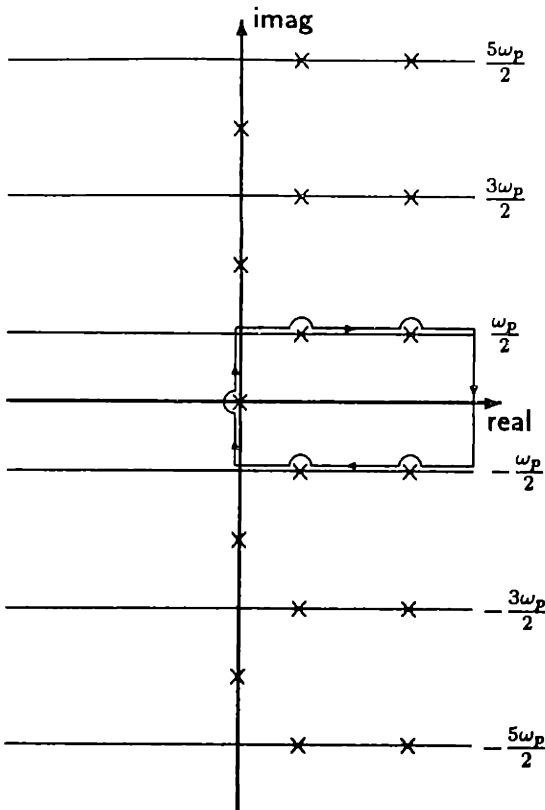
Figure 4.4: The LTP Nyquist contour in the s-plane. The Nyquist path is denoted by $\bar{N}_f$. The "×" denote the poles of $\widehat{\mathcal{G}}(s)$. Appropriate indentations are shown such that poles in the RHP fundamental strip are considered unstable.

the Hill determinant can then be counted, and stability determined, for the given value of feedback gain. However, this computation must be performed for each value of feedback gain of interest. In contrast, the zeroes of the closed loop Hill determinant can be computed quite readily using truncated determinants as is common practice in the literature, so that the closed loop pole locations are easily obtained. As in the integral operator case, a method of determining closed loop stability for a parameterization of feedback gain is desired, so that a Nyquist diagram based on eigenloci will be developed. Also, note that the above theorem provides the fundamental connection between the Hill theory and the Nyquist criterion developed earlier using the integral operator approach. □

4.4.2 Numerical method using eigenloci of the HTF

It is a simple matter to compute the eigenloci of the truncated harmonic transfer function using standard eigenvalue routines on the computer. Stability can then be determined by

counting encirclements of the $-\frac{1}{k}$ point by the eigenloci of the harmonic transfer function. Thus, closed loop stability can be determined for a parameterization of feedback gain. The harmonic transfer function captures all of the behavior of the LTP system, since it is simply a transformation of the integral operator transfer function, so that the eigenloci of the HTF provide an excellent numerical alternative to the eigenloci of the integral operator transfer function.

Although the Nyquist test will not be rigorously proven using the harmonic theory, heuristic arguments are presented to motivate the numerical method. The eigenloci of the HTF are parameterized by $s \in \bar{N}_f$. The Hill determinant $\left| \mathcal{I} + k\widehat{\mathcal{G}}(s) \right|$ can be expressed in terms of the eigenvalues of the harmonic transfer function

$$\left| \mathcal{I} + k\widehat{\mathcal{G}}(s) \right| = \prod_{n=-\infty}^{\infty} [1 + k\lambda_n(s)] \quad s \in \bar{N}_f \qquad (4.69)$$

However, it is difficult to count encirclements of this infinite product, so that it will be truncated as done previously.

Recall that the eigenvalues, $\lambda_i(z)$, of the integral operator transfer function, $\widehat{G}(z)$, converge uniformly to the origin on $\bar{N}_1$. If we consider only those eigenloci of the HTF generated on the Nyquist contour $s \in \bar{N}_f$, then the same may be said for the eigenloci of $\widehat{\mathcal{G}}(s)$ since $\widehat{\mathcal{G}}(s)$ is isomorphic to $\widehat{G}(z)$, so that the $\lambda_n(s)$ converge uniformly to the origin on $\bar{N}_f$ as n grows large. Thus, it is not necessary to consider the infinite product above, but only a finite number of terms, say those terms corresponding to including N eigenloci in the analysis, defined by the set of integers $Z_N = \{-N, \cdots, -1, 0, 1, \cdots, N\}$. Thus, the infinite product can be expressed as the product below:

$$\left| \mathcal{I} + k\widehat{\mathcal{G}}(s) \right| = \prod_{n \in Z_N} [1 + k\lambda_n(s)] \prod_{n \notin Z_N} [1 + k\lambda_n(s)] \quad s \in \bar{N}_f \qquad (4.70)$$

Now, the infinite product in the above expression corresponds to the eigenloci for all $|n| > N$ that remain inside a disk, say D_ϵ centered on the origin. Therefore, all of the eigenloci corresponding to $|n| > N$ cannot contribute to encirclements of the $-\frac{1}{k}$ point as long as $\left| \frac{1}{k} \right| \gg \epsilon$. The eigenloci that exit D_ϵ may not form closed loops due to the truncation of the infinite product, but these may be closed arbitrarily within the disk D_ϵ, in order to count encirclements. Hence, we count encirclements of

$$\angle \left| \mathcal{I} + k\widehat{\mathcal{G}}(s) \right| \approx \angle \prod_{n \in Z_N} [1 + k\lambda_n(s)] \quad s \in \bar{N}_f \qquad (4.71)$$

148

This equation is similar to that of the LTI case, so that the results in Desoer [21] can be applied directly. Thus, for closed loop stability, the eigenloci of the truncated HTF must produce n_p CCW encirclements of the $-\frac{1}{k}$ point, where $\left|\frac{1}{k}\right| \gg |\epsilon|$ and n_p is the number of closed RHP fundamental strip poles enclosed by the Nyquist path, $s \in \bar{N}_f$, counting multiplicities.

The above discussion then forms the basis for the numerical method. In summary, the eigenloci of the truncated HTF are computed along the imaginary axis in the fundamental strip and plotted in the complex plane. Then, some eigenloci may connect to form closed loops, and some may not. Those that do not form closed loops may have to be closed arbitrarily within the disk D_ϵ. The argument principle can then be applied to the Nyquist diagram constructed using the eigenloci of the truncated HTF, that is, for closed loop stability, the eigenloci of the HTF must encircle the $-\frac{1}{k}$ point, n_p times where n_p is the number of open loop poles (counting multiplicity) enclosed by the Nyquist contour $\bar{N}_f$ or the number of right half plane poles in the fundamental strip.

In the next section, the harmonic balance methods will be applied to the lossy Mathieu and lossy Meissner equations in order to illustrate the use of the Nyquist test.

4.5 Application of the Nyquist Criterion

Several stability criteria applicable to LTP systems have been presented in the literature. Primarily Floquet and Lyapunov theory have been most successfully applied. But every stability analysis technique presented suffers from the limitation that closed loop stability can be determined only for a specific value of gain. The primary objective of this section is to present some comparative discussion of the Nyquist criterion to examples of Floquet type analyses in the literature, and to illustrate the benefits of the Nyquist criterion. In addition, several sufficient conditions available in the literature are compared to the Nyquist analysis results, and numerical issues associated with computation of the eigenloci using the harmonic transfer function are discussed.

4.5.1 The lossy Mathieu equation

The most widely studied LTP system model is the Mathieu equation [72,83], and so it is appropriate that it be treated as our first example. The canonical form of the lossy

(damped) Mathieu equation is

$$\ddot{x}(t) + 2\zeta\dot{x}(t) + (a - 2q\cos\omega_p t)x(t) = 0 \tag{4.72}$$

where classically the *pumping frequency*, $\omega_p = 2$, implying a *pumping period* of $T = \pi$. Here, a represents the constant portion of the time periodic coefficient of $x(t)$, and q represents the amplitude of the time periodic variation. Clearly, the Mathieu equation reduces to a dissipative simple harmonic oscillator for $q = 0$. The parameter q is often referred to as the *pumping amplitude* or the *amplitude of parametric excitation*. The lossy Mathieu equation has been used extensively to describe the physical behavior of many types of engineering systems, as discussed in Chapter 1.

Stability criteria

The first stability criterion to be examined is, of course, that due to Floquet, which is necessary and sufficient. The solid lines in Figure 4.5, were produced using the Floquet Theorem, and illustrate the stability boundaries of the lossy Mathieu equation for $\zeta = 0.2$. In this classical stability (Strutt) diagram [96], the stability boundaries correspond to the contours in the (q, a) plane for which the solutions of the lossy Mathieu equation are periodic. The stability boundaries were produced using the following procedure. The monodromy matrix, $\Phi(T, 0)$, was determined by integrating its defining ODE for a mesh of points in the (q, a) plane. The integration technique used was a variable step Runge-Kutta-Fehlberg algorithm with a step error tolerance of 1×10^{-6}. At each point in the mesh, the maximum absolute value of the eigenvalues of the monodromy matrix was saved in a table. A contour plot was then drawn through this table where the maximum absolute value of the eigenvalues equals one, thus indicating where a single eigenvalue is on the unit circle.

Classically, the method of Hill determinants has been used to determine the stability boundaries shown in the Strutt diagram. The values of (q, a) for which the Hill determinant vanishes provides the same contours as illustrated in Figure 4.5. Regardless of the method used in producing the Strutt diagram, these methodologies only permit determination of stability for a specific choice of (q, a); or equivalently, a specific value of gain.

Several sufficient stability conditions have been developed for the lossy Mathieu equation. First, the LTI version of the Small Gain Theorem [64, page 23] can be applied. The simulation diagram is shown in Figure 4.6. The stiffness in the lossy Mathieu equation can
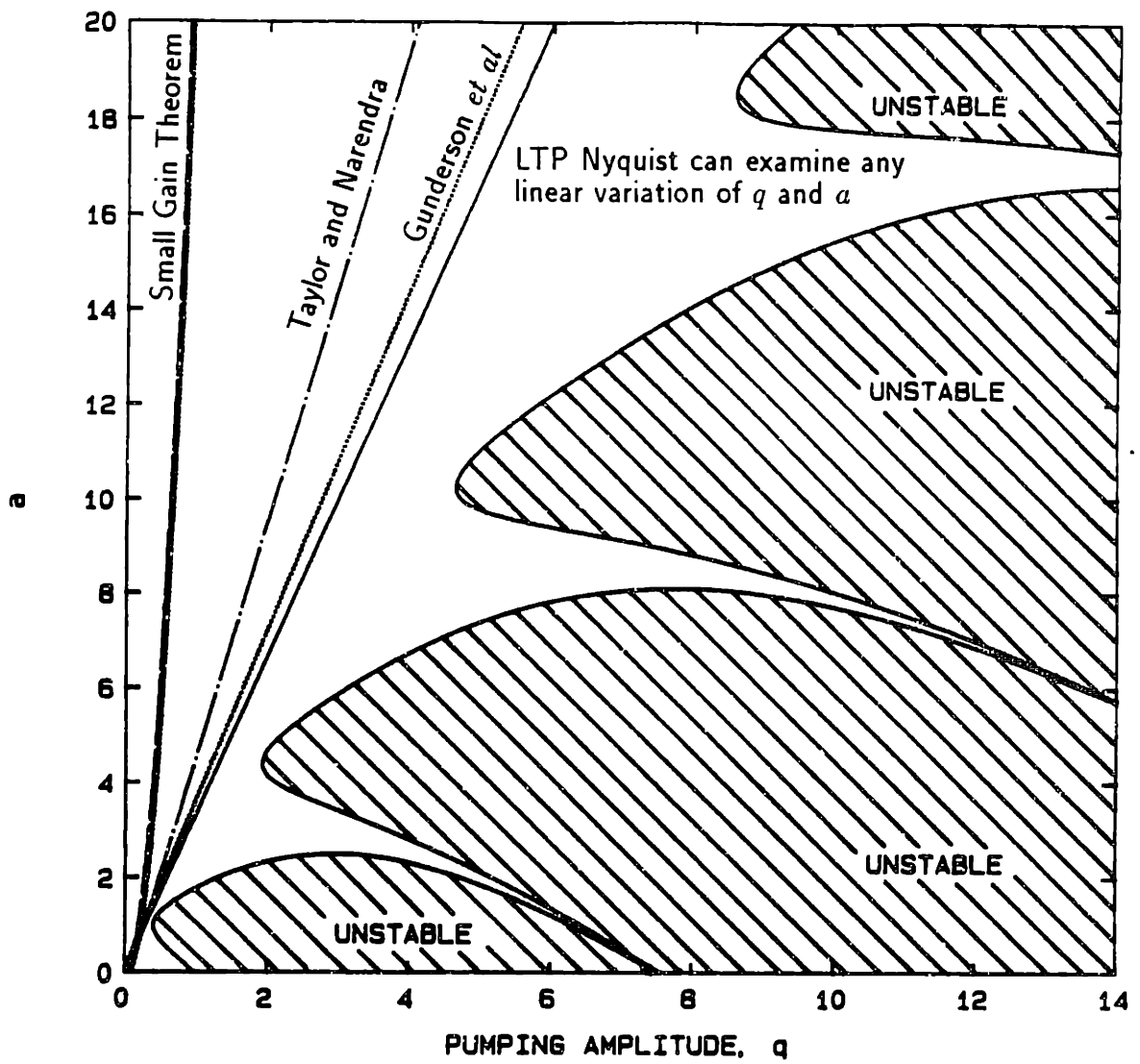
Figure 4.5: Stability conditions for the lossy Mathieu equation with $\zeta = 0.2$**.** The solid contour lines are obtained using the (necessary and sufficient) Floquet Theorem and correspond to purely periodic solutions of the lossy Mathieu equation, that is, eigenvalues of the monodromy matrix with unit magnitude. Also shown are the stability criteria due to application of the small gain theorem, of Taylor and Narendra [102], and Gunderson *et al* [39].
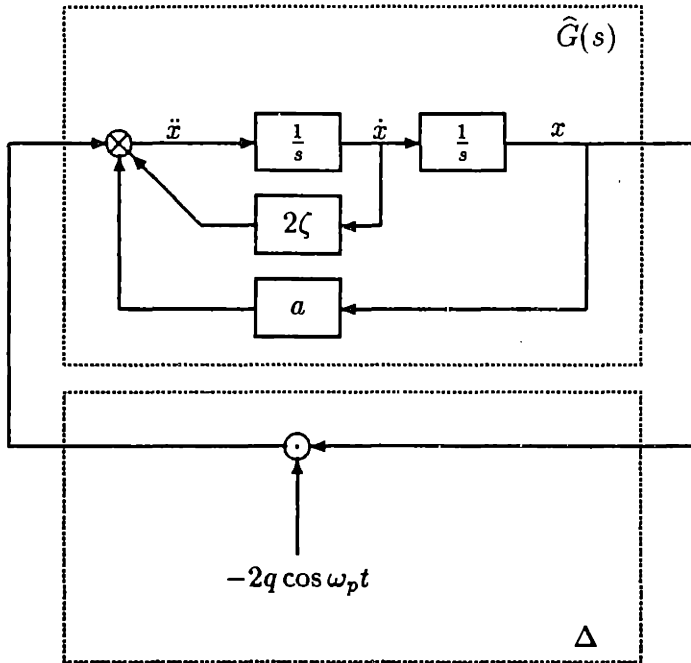
Figure 4.6: The lossy Mathieu equation with internal time periodic feedback gain. Stability of the above feedback loop is guaranteed if the product of $\left\|\widehat{G}\right\|_\infty$ and $\|\Delta\|_\infty$ is less than one.

be expressed as the sum of a time invariant term, a, and a time periodic term, $-2q\cos\omega_p t$. In the simulation diagram, the time periodic portion of the stiffness is interpreted as an operator in the feedback loop, $\Delta(s)$, and the time invariant feedback terms are lumped with the forward loop to construct an LTI transfer function $\widehat{G}(s)$, as below:

$$\widehat{G}(s) \;=\; \frac{1}{s^2 + 2\zeta s + a}$$

$$\Delta \;=\; -2q\cos\omega_p t$$

The lossy Mathieu equation can then be represented by a closed loop system with the LTI oscillator in the forward loop, and a time periodic perturbation in the feedback loop, as shown in **Figure 4.6**. The Small Gain Theorem [64] guarantees stability if the product of the $\|\cdot\|_\infty$ of each of the above quantities is less than unity. It should be noted that $\|\cdot\|_\infty$ is simply the maximum magnitude.

Thus,

$$\left\|\hat{G}(s)\right\|_\infty \;=\; \frac{1}{2\zeta\sqrt{a-\zeta^2}}$$

$$\|\Delta\|_\infty \;=\; 2q$$

152

so that the lossy Mathieu equation is stable if the product

$$\left\|\hat{G}(s)\right\|_\infty \|\Delta\|_\infty = \frac{q}{\zeta\sqrt{a - \zeta^2}} < 1 \tag{4.73}$$

The stability condition predicted by the Small Gain Theorem is thus given by

$$q \leq \zeta\sqrt{a - \zeta^2} \tag{4.74}$$

which is plotted in Figure 4.5. The Small Gain Theorem stability boundary is the closest to the vertical a axis and is the most conservative of the sufficient stability conditions. The Small Gain Theorem is also a necessary condition if Δ is permitted to be an arbitrary perturbation, which is not the case here.

Taylor and Narendra [76,102] have determined two sufficient conditions for stability:

$$q \leq \zeta\sqrt{a} \tag{4.75}$$

$$q \leq \zeta\sqrt{a(1 + a)} \tag{4.76}$$

In addition, an approximate criterion for $\zeta \ll 1$, $a \gg \zeta$ and $a > 1$ was developed,

$$q \leq \frac{\pi}{2}a\zeta \tag{4.77}$$

The stability boundaries from (4.75–4.76) are illustrated in Figure 4.5. Although the sufficient condition in (4.75) is less conservative than the Small Gain Theorem stability condition, it overlays the Small Gain Theorem result in Figure 4.5. The sufficient condition in (4.76) is much less conservative than both the Small Gain Theorem stability boundary and the sufficient condition in (4.75). Both of these sufficient conditions show some improvement over the Small Gain Theorem result, but are still conservative.

Gunderson *et al* [39] also produced two sufficient conditions for stability of the lossy Mathieu equation:

$$q \leq \frac{1}{2}(a - \zeta^2)\tanh\pi\zeta \tag{4.78}$$

$$q \leq \zeta\sqrt{a} + \zeta^2 \tag{4.79}$$

These two stability boundaries are shown in Figure 4.5. However, the more conservative of the two sufficient conditions (4.79) overlays the Small Gain Theorem stability condition in Figure 4.5. It is clear from Figure 4.5 that (4.78) is the least conservative of the above sufficient conditions.

All of the above stability conditions are sufficient conditions. In contrast, the Nyquist test can treat arbitrary linear variations of a with q, that is, the Nyquist test is necessary and sufficient. The advantages of the Nyquist methodology will be demonstrated in the sequel.

Nyquist stability analysis

Defining the parameter, $\beta = q/a$, the lossy Mathieu equation can be rewritten as

$$\ddot{x}(t) + 2\zeta\dot{x}(t) + a[1 - 2\beta\cos\omega_p t]x(t) = 0 \tag{4.80}$$

Here, the meaning of β is clear. For $\beta \ll 1$, the periodic effects are small, so that the behavior of the time periodic system will not vary much from that of the LTI oscillator. For large values of β, the periodic effects must be incorporated into the analysis.

Using the Nyquist methodology, we can determine stability for linear variations of q with a in a necessary and sufficient sense. If the feedback control law,

$$u(t) = -ax(t) \tag{4.81}$$

is applied to the open loop system

$$\ddot{x}(t) + 2\zeta\dot{x}(t) = [1 - 2\beta\cos\omega_p t]u(t) \tag{4.82}$$

then the lossy Mathieu equation in (4.80) results. Thus, the lossy Mathieu equation can be represented by the simple block diagram configuration shown in Figure 4.7. In the figure, the "plant" transfer function, determined by applying the Laplace transform to the LTI dynamics in (4.82),

$$\widehat{G}(s) = \frac{1}{s(s + 2\zeta)} \tag{4.83}$$

has an input that is amplitude modulated by the time periodic signal, $1 - 2\beta\psi(t)$, where

$$\psi(t) = \cos\omega_p t \tag{4.84}$$

The states of (4.82) are $x^T(t) = [x(t) \quad \dot{x}(t)]$. The parameter a can now be thought of as the feedback gain, k. Selecting $x(t)$ as the measurement leads to the open loop dynamics expressed by the state space model

$$\begin{aligned} \dot{x}(t) &= Ax(t) + B(t)u(t) \\ y(t) &= Cx(t) \end{aligned} \tag{4.85}$$

154
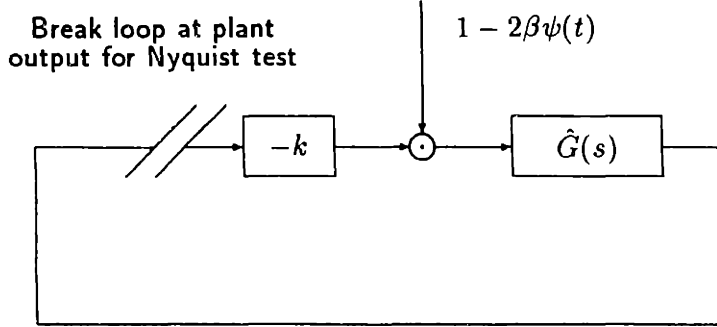
Figure 4.7: System block diagram. Block diagram illustrating system configuration examined in the lossy Mathieu and Meissner equation examples. The input, $u(t)$, to the plant, $\hat{G}(s)$, is amplitude modulated by a time periodic signal. This block diagram is a simple representation of a second order damped Hill equation with time periodic stiffness.

where

$$
A = \begin{bmatrix} 0 & 1 \\ 0 & -2\zeta \end{bmatrix}
$$

$$
B(t) = \begin{bmatrix} 0 \\ 1 - 2\beta\cos\omega_p t \end{bmatrix}
$$

$$
C = \begin{bmatrix} 1 & 0 \end{bmatrix} \tag{4.86}
$$

Clearly, A and C are time invariant. However, $B(t)$ is T-periodic and can be expanded in a complex Fourier series as

$$
\begin{aligned}
B(t) &= \{\cdots,0,B_{-1},B_0,B_1,0,\cdots\} \\
&= \left\{\cdots,0,\begin{bmatrix} 0 \\ -\beta \end{bmatrix},\begin{bmatrix} 0 \\ 1 \end{bmatrix},\begin{bmatrix} 0 \\ -\beta \end{bmatrix},0,\cdots\right\}
\end{aligned} \tag{4.87}
$$

Now, following the procedure outlined in Example 3.2 yields the harmonic transfer function

$$\hat{\mathcal{G}}(s) = \begin{bmatrix} \ddots & \vdots & \vdots & \vdots & \vdots & \vdots & \\ \cdots & G_{-2} & -\beta G_{-2} & 0 & 0 & 0 & \cdots \\ \cdots & -\beta G_{-1} & G_{-1} & -\beta G_{-1} & 0 & 0 & \cdots \\ \cdots & 0 & -\beta G_0 & G_0 & -\beta G_0 & 0 & \cdots \\ \cdots & 0 & 0 & -\beta G_1 & G_1 & -\beta G_1 & \cdots \\ \cdots & 0 & 0 & 0 & -\beta G_2 & G_2 & \cdots \\ & \vdots & \vdots & \vdots & \vdots & \vdots & \ddots \end{bmatrix} \qquad (4.88)$$

where for all $n \in Z$,

$$\begin{aligned} G_n &= G(s + jn\omega_p) \\ &= C[(s + jn\omega_p)I - A]^{-1}B_0 \\ &= \frac{1}{(s + jn\omega_p)(s + jn\omega_p + 2\zeta)} \end{aligned} \qquad (4.89)$$

The stability (Strutt) diagram for the lossy Mathieu equation with $\zeta = 0.2$ is shown in Figure 4.8. This diagram was obtained using the Floquet Theorem, using the same software that produced Figure 4.5. The rays emanating from the origin correspond to the contours of constant β that will be used in the Nyquist test.

The inverse Nyquist diagram is plotted for the values $\beta = \{0, 0.4, 0.5, 0.75\}$. Figure 4.9a shows the LTP inverse Nyquist diagram for $\beta = 0$, which recovers the inverse Nyquist diagram for $\hat{G}(s)$. Recall that the gain, k, in this context is simply the value of a in the lossy Mathieu equation. In order to compare the Nyquist results to those of classical stability analyses, radial contours of constant β have been plotted as dashed lines in the Strutt diagram for the Mathieu equation in Figure 4.8. As z travels around the unit circle in CCW fashion (or up the imaginary axis in the fundamental strip and then clockwise around the Nyquist path $\bar{N}_f$), the loops in the inverse Nyquist diagram travel in CCW fashion. There is a single open loop pole outside the open unit disk in the z-plane, so that we require a single CCW encirclement of the $-k$ point in order for the closed loop system to be stable. The Nyquist diagram is closed at the far left in CCW fashion, so that it forms a CCW loop about the negative real axis. Thus, by counting encirclements of the $-k$ point, we conclude that $k > 0$ (that is, those points on the negative real axis) produces stable closed loop configurations and $k < 0$ (that is, those points on the positive real axis)

156
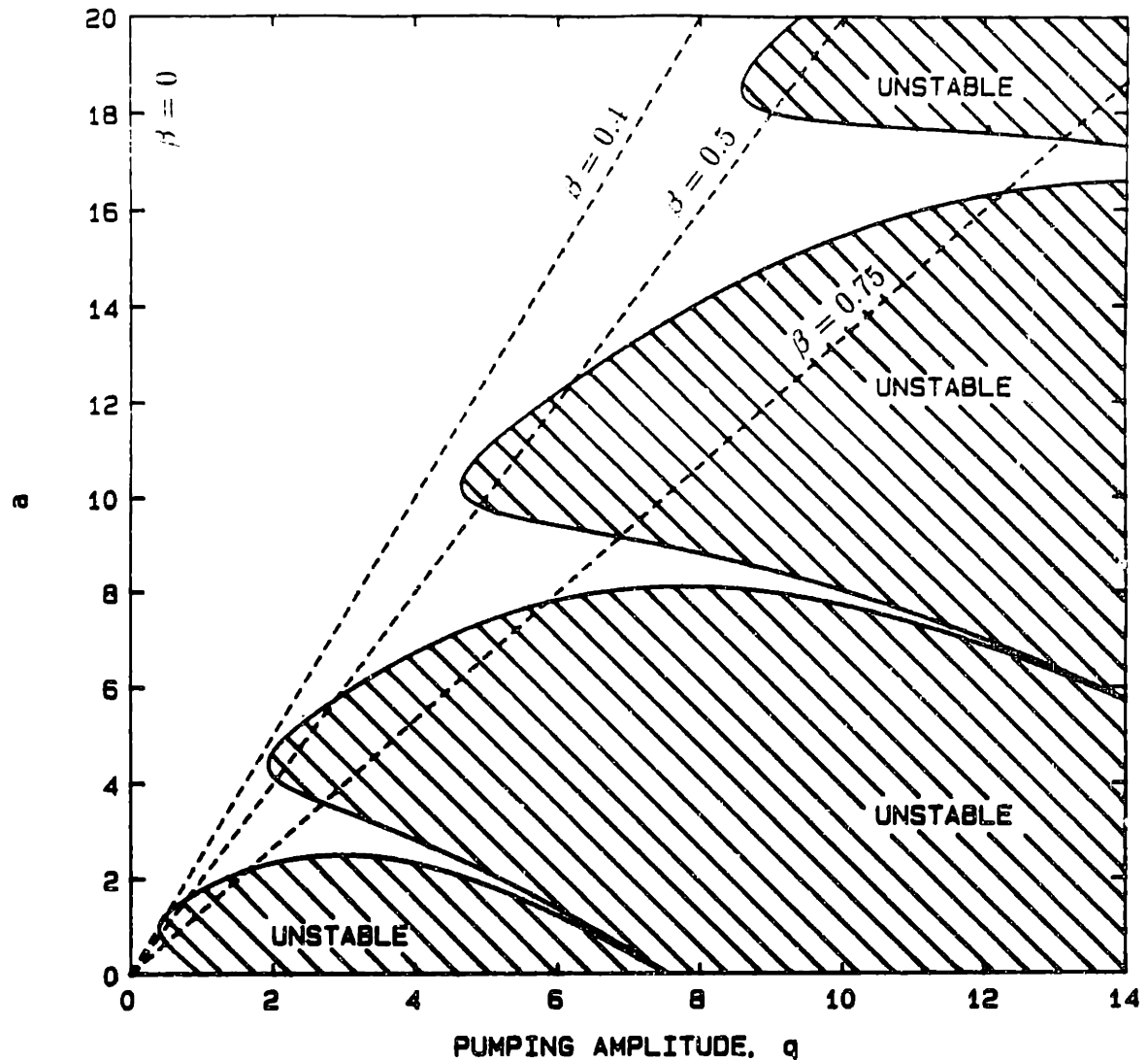
Figure 4.8: Classical stability (Strutt) diagram for the lossy Mathieu equation with damping ratio $\zeta = 0.2$. The contour lines correspond to purely periodic solutions of the lossy Mathieu equation, that is, eigenvalues of the monodromy matrix with unit magnitude. The rays emanating from the origin are lines of constant $\beta = q/a$ used in the Nyquist test.
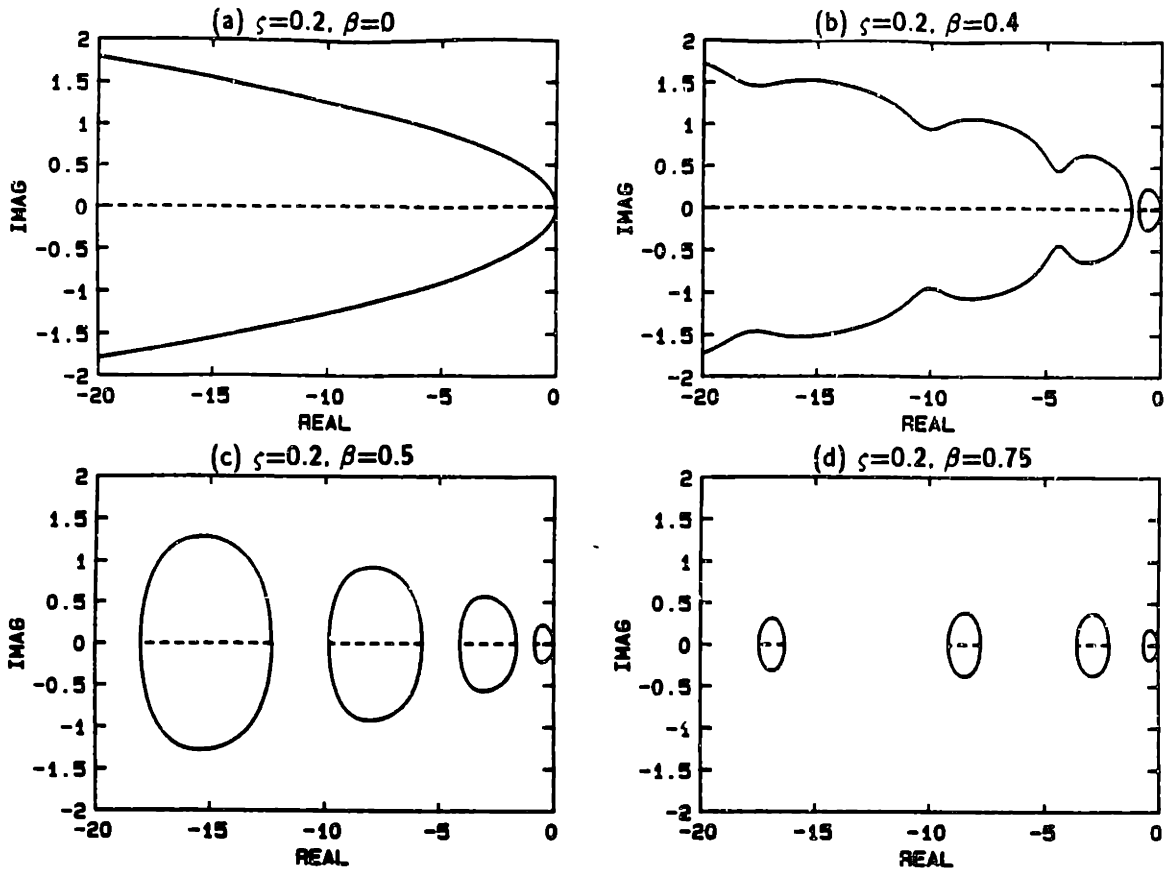
Figure 4.9: LTP inverse Nyquist diagram for the lossy Mathieu equation. Here, the damping ratio is $\zeta = .2$. When $\beta = 0$, the LTI inverse Nyquist diagram is recovered. As β is increased, so that the periodic effects grow stronger, the Nyquist diagram starts to ripple, and eventually a single closed CCW circuit is formed ($\beta \approx 0.4$). For larger values of β, the inverse eigenloci form a finite number of CCW circuits, each of which is symmetrical about the real axis.

produces unstable configurations. As β increases, the Nyquist diagram starts to ripple until approximately $\beta = 0.4$ where a single CCW circuit is formed. As β is increased further, a finite number of closed CCW circuits are formed that are symmetrical about the real axis. As before, those points on the real axis enclosed by a CCW circuit produce stable solutions of the lossy Mathieu equation, while those points on the real axis not enclosed by a CCW circuit produce unstable solutions of the lossy Mathieu equation. It interesting to note that portions of the positive real axis in the complex plane were also enclosed by CCW circuits, so that the Nyquist test predicts stable configurations of the lossy Mathieu equation for $a < 0$. These same stable regions are predicted using the Floquet theory and are illustrated in Strutt diagrams elsewhere [83].

Comparison of Floquet and Nyquist

It is relatively straightforward to compute the stability boundaries using either Floquet or Nyquist techniques. In Table 4.1, the values of a at the stability boundaries are compiled for the three non-zero values of $\beta = \{0.4, 0.5, 0.75\}$ used in the Nyquist test.

The Floquet stability boundaries were determined by constructing a function that computed the maximum absolute value of the two Floquet poles determined from the monodromy matrix calculation for a constant value of β. In this case the monodromy matrix, $\Phi(T, 0)$, was determined by integration of its defining ODE using a variable step Runge-Kutta-Fehlberg algorithm with a step error tolerance of 1×10^{-10}. A secant root finding technique was then applied to this function minus unity, thus, determining when the Floquet poles left the open unit disk in the z-plane. The accuracy imposed on the root finding procedure was 1×10^{-12}. These values are listed as the Floquet results in Table 4.1.

The stability boundaries were also determined using the Nyquist test by observing that the stability boundaries are simply the real axis crossings of the closed CCW contours in the Nyquist diagrams. If, in fact, these closed CCW contours crossed the negative axis, this occurred when $\omega = \pm\omega_p/2$ and/or $\omega \to 0$. In Table 4.1, twenty harmonics, $N = 20$, were included in the harmonic transfer function when computing the eigenloci used in the Nyquist diagram. Excellent agreement is obtained from comparison of the Nyquist and Floquet results. They agree, in general, to nine decimal places using the techniques described above for the stability boundaries shown in the table. Note, however, that the Nyquist test provides a stability analysis for a line in the (q, a) plane (that is, a parameterization of feedback gain), while the Floquet analysis provides a stability analysis for only a single point in the (q, a) plane.

Effects of truncation

Usually, the stability boundaries are sought for specific ranges of a and q such as shown in Figure 4.8. However, there are two sources of error due to truncation that will affect the accuracy of the computed stability boundaries in the given region of the (q, a) plane. Truncation of the harmonic transfer function in the sense of the main diagonal (that is, upper left to lower right) corresponds to a truncation of the Fourier series expansions of the steady state solutions of the state, control and measurement signals. On the other

Table 4.1: Comparison of Floquet and Nyquist analyses for the Lossy Mathieu equation. Here, the damping ratio is $\zeta=0.2$. The values of a, or of feedback gain k, are presented at each point a stability boundary is encountered. The Nyquist diagram was constructed with eigenloci computed using $N=20$ harmonics in the harmonic transfer function, implying a 41×41 eigenvalue problem at each value of frequency in the fundamental strip.

β	Analysis Type	Stability Boundary			
		First Unstable	Second Stable	Second Unstable	Third Stable
0.4	Nyquist	1.01038396671	1.27956036846	—	—
	Floquet	1.01038396648	1.27956036870	—	—
0.5	Nyquist	0.84768955928	1.60021555487	4.09897619802	5.72109930334
	Floquet	0.84768955918	1.60021555496	4.09897619769	5.72109930364
0.75	Nyquist	0.67079159348	2.17981504798	3.60843864899	7.74951351337
	Floquet	0.67079159341	2.17981504796	3.60843864881	7.74951351333

Table (continued)

β	Analysis Type	Stability Boundary			
		Third Unstable	Fourth Stable	Fourth Unstable	Fifth Stable
0.4	Nyquist	—	—	—	—
	Floquet	—	—	—	—
0.5	Nyquist	9.82428898738	12.31516144551	18.01986769151	21.37896847826
	Floquet	9.82428898670	12.31516144613	18.01986769033	21.37896847938
0.75	Nyquist	9.16171180645	16.31771540226	17.45768806959	27.71569830669
	Floquet	9.16171180614	16.31771540216	17.45768806919	27.71569830651

hand, truncation of the harmonic transfer function in the sense of the skew diagonal (that is, lower left to upper right) corresponds to a truncation of the Fourier series expansions of the system parametric excitation. Each of these sources of error is present to a certain extent, however, the truncation error in the skew sense is reduced in significance if the harmonic transfer function is banded, that is, the parametric excitation can be described by a truncated complex Fourier series.

The time periodic modulation in the lossy Mathieu equation, which consists of a cosinusoid at the pumping frequency and a bias, can be described exactly by a complex Fourier series with only three terms, as shown in (4.87). This leads to a harmonic transfer function that is a doubly infinite *tridiagonal or banded* complex matrix at every value of frequency in the fundamental strip. Therefore, the error in this case is due entirely to truncation in the main diagonal sense, which cannot be avoided since the truncation is a pragmatic necessity. Thus, the truncated HTF will be a tridiagonal complex valued matrix of dimension

$(2N+1)m \times (2N+1)m$ at every frequency $\omega \in (-\omega_p/2, \omega_p/2]$. Intuitively, we would expect the eigenloci of the harmonic transfer function to accurately predict the real axis crossings with relatively few harmonics, since the harmonic content of the parametric excitation, or LTP state space model, consists of only the zeroth and first harmonic.

In Table 4.2, the stability boundaries have been computed along a contour of constant $\beta = 0.5$, using both Nyquist and Floquet. The eigenloci of the harmonic transfer function were computed for several different values of the number of harmonics, N, included in the HTF. It is assumed in this case that the Nyquist results are the more accurate of the Floquet and Nyquist results due to the inevitably large errors accrued in the integration used to obtain the monodromy matrix. The step error tolerance imposed on the Runge-Kutta-Fehlberg integration was 1×10^{-10}, requiring very long processing times to complete the Floquet analyses for a single value of β (on the order of a few hours), even on a 20MHz Intel 386/7 personal computer. Imposing a smaller step error tolerance would have been impractical from a computational standpoint. To render the table easier to read, where the Floquet and Nyquist results disagree, an italic font is used. Also, the insignificant figures in the Floquet results, which are due to the step error tolerance in the integration routine, are italicized. The Nyquist and Floquet results agree, in general, to nine decimal places for the first few stability boundaries, with as few as ten harmonics, $N = 10$, included in the HTF. Therefore, the Nyquist test provides an excellent characterization of the stability boundaries, even though few harmonics are included in the HTF. On the other hand, the Floquet theory, which requires the integration of the monodromy matrix for every choice of (q, a) of interest is much more tedious.

Approximate Nyquist analysis for Mathieu equation

Although the lossy Mathieu equation was considered above, the LTP Nyquist diagram of the undamped Mathieu equation can be approximated by computing the eigenloci for a very small value of damping ratio, say $\zeta = 1 \times 10^{-4}$. The Strutt diagram is plotted in Figure 4.10. Here, the same values of β are selected for the Nyquist analyses.

As before, the LTP inverse Nyquist diagram will be plotted instead of the Nyquist diagram for convenience and ease of interpretation, therefore, encirclements of the $-k$ point will be counted, instead of the $-\frac{1}{k}$ point as would be the case for the Nyquist diagram. Recall that the gain, k, in this context is simply the value of a in the lossy Mathieu equation. In

Table 4.2: Comparison of Floquet and Nyquist stability boundaries for the Lossy Mathieu equation with $\zeta=0.2$ and $\beta=0.5$. To illustrate convergence of the stability boundaries computed using the Nyquist test, different numbers of harmonics were included in the harmonic transfer function until the stability boundaries converged. The Nyquist results are more accurate due to performance limitations of the integration routine used to apply the Floquet theory.

Analysis Type	Stability Boundary			
	First Unstable	Second Stable	Second Unstable	Third Stable
$N=1$	0.84931502823884	1.69902068898176	4.35075774975293	7.64924225024706
$N=2$	0.84768881849881	1.60054689628544	4.10025416414121	5.75291633918666
$N=3$	0.84768955891037	1.60021574730962	4.09897755870427	5.72125189624481
$N=4$	0.84768955928208	1.60021555490968	4.09897619823156	5.72109953399966
$N=5$	0.84768955928210	1.60021555487723	4.09897619802353	5.72109930348669
$N=6$	0.34768955928210	1.60021555487723	4.09897619802366	5.72109930334153
$N=7$	0.84768955928210	1.60021555487723	4.09897619802366	5.72109930334149
$N=8$	0.84768955928210	1.60021555487723	4.09897619802363	5.72109930334153
$N=9$	0.84768955928210	1.60021555487723	4.09897619802367	5.72109930334144
$N=10$	0.84768955928210	1.60021555487723	4.09897619802366	5.72109930334147
$N=15$	0.84768955928210	1.60021555487723	4.09897619802365	5.72109930334151
$N=20$	0.84768955928210	1.60021555487723	4.09897619802369	5.72109930334144
$N=25$	0.84768955928210	1.60021555487723	4.09897619802362	5.72109930334154
$N=30$	0.84768955928210	1.60021555487723	4.09897619802370	5.72109930334150
Floquet	0.84768955918250	1.60021555496816	4.09897619769419	5.72109930364319

Table (continued)

| Analysis Type	Stability Boundary			
	Third Unstable	Fourth Stable	Fourth Unstable	Fifth Stable
$N=1$	—	—	—	—
$N=2$	10.14279785549181	15.94516693598970	—	23.60802644997851
$N=3$	9.83856920190253	12.44902531812798	18.24447338455505	22.49677971167218
$N=4$	9.82438324457189	12.31725115247109	18.02357169148811	21.41712350587179
$N=5$	9.82428918313354	12.31517249073162	18.01989064401156	21.37944952865552
$N=6$	9.82428898754685	12.31516147034193	18.01986775542407	21.37897112579982
$N=7$	9.82428898738309	12.31516144554065	18.01986769159854	21.37896848577490
$N=8$	9.82428898738302	12.31516144551221	18.01986769150748	21.37896847828377
$N=9$	9.82428898738304	12.31516144551220	18.01986769150838	21.37896847826903
$N=10$	9.82428898738304	12.31516144551219	18.01986769150837	21.37896847826958
$N=15$	9.82428898738304	12.31516144551222	18.01986769150669	21.37896847827154
$N=20$	9.82428898738304	12.31516144551221	18.01986769151144	21.37896847826602
$N=25$	9.82428898738304	12.31516144551221	18.01986769150484	21.37896847827336
$N=30$	9.82428898738304	12.31516144551222	18.01986769150885	21.37896847827307
Floquet	9.82428898670343	12.31516144619940	18.01986769033023	21.37896847938900
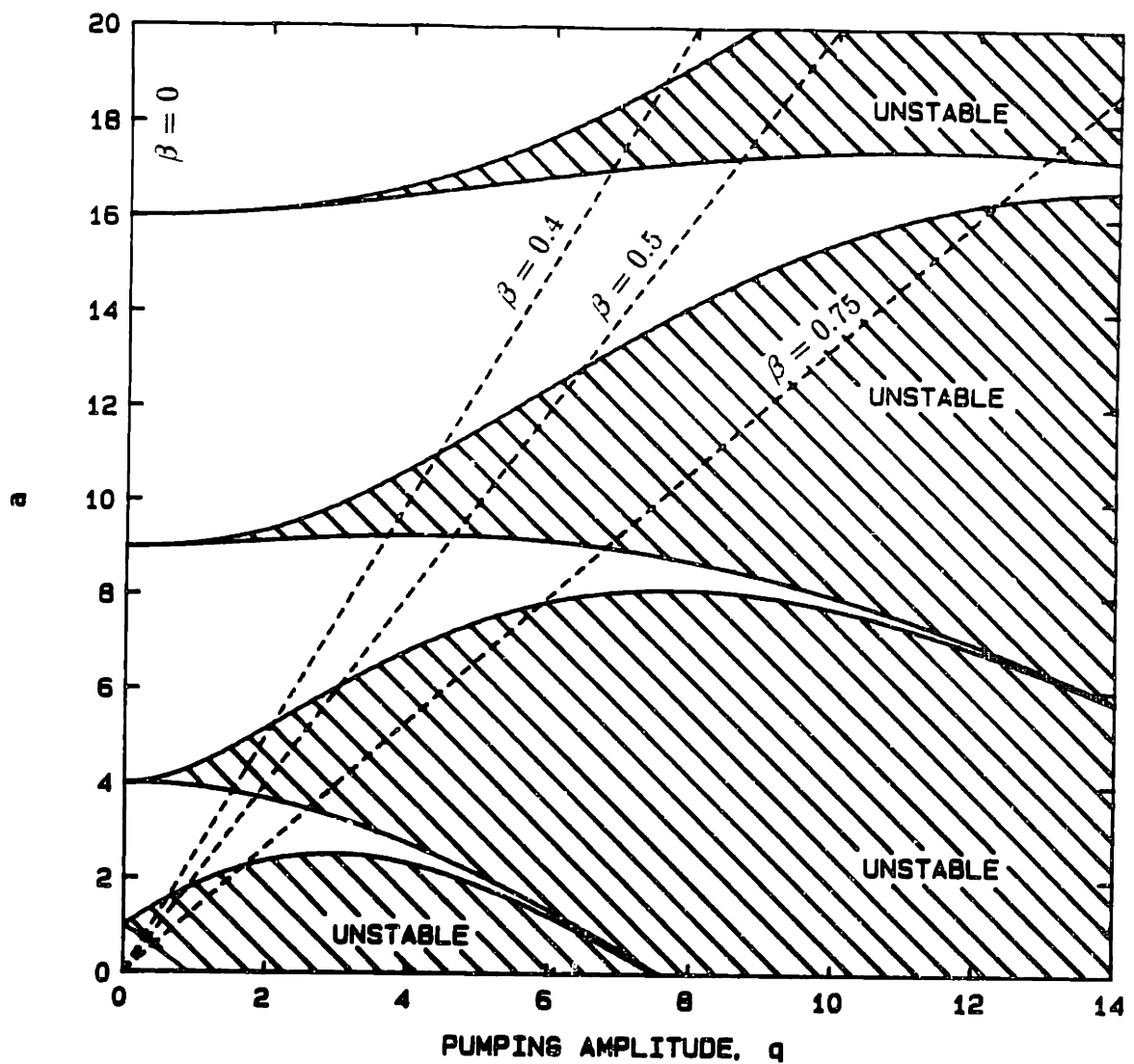
Figure 4.10: Classical stability (Strutt) diagram for the Mathieu equation. The Strutt diagram is symmetrical about the a axis, and the unstable regions are labeled as such. This diagram was produced from data in Appendix 2 of [72]. The radial contours of constant β corresponding to the proportional variation of gain used in the Nyquist test cases, are plotted.

order to compare the Nyquist results to those of classical stability analyses, radial contours of constant β have been plotted as dashed lines in the Strutt diagram for the Mathieu equation in Figure 4.10. Figure 4.9a shows the LTP inverse Nyquist diagram for $\beta = 0$, which corresponds to the LTI inverse Nyquist diagram for the transfer function $\hat{G}(s)$. Recall also that due to the single pole outside the unit circle, a single CCW encirclement of the $-k$ point is required for closed loop stability.

As z travels CCW around the unit circle (or equivalently, ω varies from $\omega = -\omega_p/2$ to $\omega = \omega_p/2$), which corresponds to traveling CW around the Nyquist path $\bar{N}_1$, the Nyquist diagram forms the CCW circuit shown in Figure 4.11a. For all $k > 0$, that is, the negative real axis, the closed loop system is stable, since there is a CCW encirclement of the $-k$ point. For all $k < 0$, that is, points of the positive real axis, the closed loop system is unstable since there is no CCW encirclement of the $-k$ point. Thus, the LTI Nyquist diagram can be viewed as a special case of the LTP Nyquist diagram, since Figure 4.11a is identical to the LTI inverse Nyquist diagram. As β increases, an infinite number of CCW closed circuits are formed, each of which is symmetric about the negative real axis, as shown in Figure 4.11b–d. The values of $-k$ within each of these CCW circuits leads to a value of gain that stabilizes the closed loop system, that is, the Mathieu equation. In the figures, stable portions of the real axis are labeled by dashed lines. As β increases, the stable regions dwindle in size. A comparison of the inverse Nyquist diagrams with the Strutt diagram in Figure 4.10, shows perfect agreement for the values of k or a, along a contour of constant β, for which the closed loop system is stable.

It should be noted that even though a finite number of closed CCW circuits are shown in Figure 4.11b-d, there are an infinite number of closed CCW circuits in the LTP inverse Nyquist diagram for the Mathieu equation emanating outward from the origin into the left half plane. This is in contrast to the lossy Mathieu equation for which a finite number of CCW circuits were formed for a specific value of β.

Alternative stability diagram computation

An alternative method for the computation of the Strutt diagram for the (lossy) Mathieu equation can be deduced using these results. The CCW circuits from the inverse eigenloci were symmetric about the real axis, and the real axis crossovers occurred only for frequencies $\omega = 0$ and/or $\omega = \pm 1$ when evaluating the eigenloci of the harmonic transfer function. Thus,
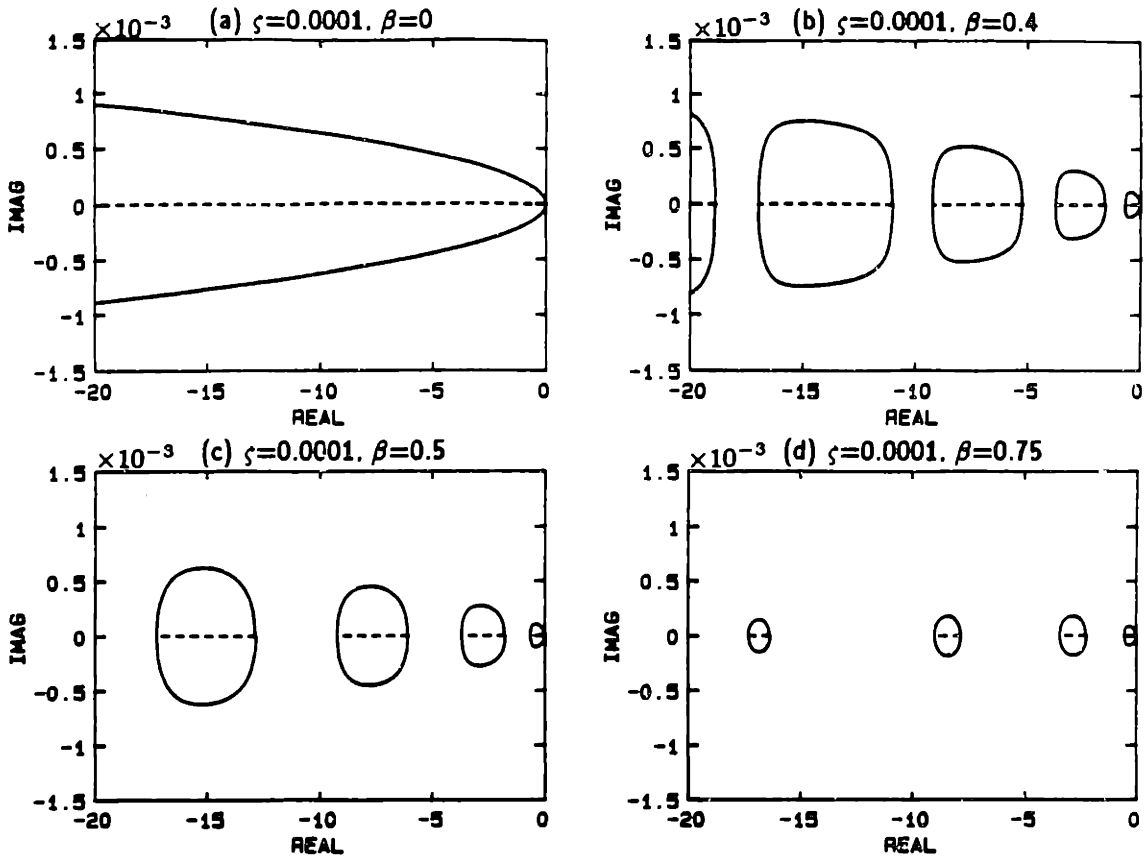
Figure 4.11: LTP inverse Nyquist diagram for the Mathieu equation. Here, a small amount of damping ($\zeta = .0001$) has been added to the system so that the inverse eigenloci do not lie completely on the real axis. When $\beta = 0$, the LTI inverse Nyquist diagram is recovered. As β is increased, so that the periodic effects grow stronger, an infinite number of loops emanating outward from the origin into the left half plane are formed from the eigenloci, each of which is CCW and symmetrical about the real axis.

a simple algorithm suggests itself for determining the stability boundaries. For a given value of β, determine the real axis crossings by computing the eigenvalue problem for the HTF at both $\omega = 0$, and at $\omega = -1$ or $\omega = 1$, and place these eigenvalues in an augmented vector. Eliminate those eigenvalues for which the imaginary part is above a given threshold (this is necessary because some of the closed CCW circuits may be formed from more than one eigenlocus). Sort the remaining eigenvalues in ascending order. This provides the stability boundary crossings for a given value of β, so that the stability diagram can be constructed for a parameterization of β, in the regions ($q > 0, a > 0$), and ($q < 0, a < 0$). The remaining two quadrants are obtained by noting that the Strutt diagram for the (lossy) Mathieu equation is symmetrical about the a axis.

This algorithm was, in fact, utilized to construct Table 4.1 and Table 4.2. The method relies on a series of eigenvalue problems and a final sort to construct the stability diagram, which are readily handled by a computer. The Floquet based methods require a much larger number of integrations to obtain the monodromy matrix for a mesh of points in the (q, a) plane. The Hill determinant method requires a large number of determinant calculations based on an iteration scheme on the Hill determinant, which also requires much more computation. In addition, the method is much more reliable than the approximate Floquet methods advocated by Richards [83,85] in close proximity to the stability boundaries.

4.5.2 The lossy Meissner equation

In 1918, Meissner [74] presented an important paper on the stability of time periodic systems that dealt with instabilities in the side rods of locomotives. This investigation led to an equation of the Hill type,

$$\ddot{x}(t) + 2\zeta\dot{x}(t) + [a - 2q\psi(t)]x(t) = 0 \qquad (4.90)$$

in which the periodically time varying parameter, $\psi(t)$, is a unit rectangular waveform as shown in Figure 4.12. It is a well known fact that the complex Fourier series associated with the rectangular waveform cannot be truncated, that is, an infinite number of Fourier coefficients are required to describe the rectangular wave. In addition, the complex Fourier series that describes the rectangular waveform converges very slowly (relative to the parametric excitation in the Mathieu equation), so that substantial errors result if the Fourier series is truncated. In fact, the effect of this slow convergence is the well-known *Gibbs phenomenon*, which is a consequence of the fact that the Fourier series of a discontinuous waveform on $L_2[0,T]$ does not converge uniformly.

In this example, the lossy form of the Meissner equation will be considered, which can be described by two LTI systems over alternating intervals,

$$
\begin{aligned}
\ddot{x}(t) + 2\zeta\dot{x}(t) + (a - 2q)x(t) &= 0 \quad t \in [0,\tau] \\
\ddot{x}(t) + 2\zeta\dot{x}(t) + (a + 2q)x(t) &= 0 \quad t \in [\tau,T]
\end{aligned} \qquad (4.91)
$$

with the usual convention of $T = \pi$ and $\omega_p = 2$. The lossy Meissner equation has the virtue that a closed form solution is easily obtained, unlike the lossy Mathieu equation. The availability of a closed form solution allows extremely accurate determination of the stability

166
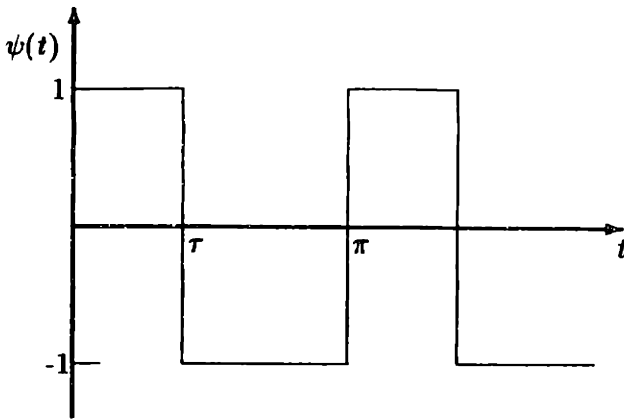
Figure 4.12: The unit rectangular waveform coefficient for the lossy Meissner equation.

boundaries using the Floquet theory, so that comparison of the Nyquist results can be accomplished with confidence. Determination of the monodromy matrix is straightforward using a property of the state transition matrix,

$$
\begin{aligned}
\Phi(T,0) &= \Phi(T,\tau)\Phi(\tau,0) \\
&= e^{A_a(T-\tau)}e^{A_b\tau}
\end{aligned}
\tag{4.92}
$$

where

$$
A_a = \begin{bmatrix} 0 & 1 \\ -(a-2q) & -2\zeta \end{bmatrix}
$$

$$
A_b = \begin{bmatrix} 0 & 1 \\ -(a+2q) & -2\zeta \end{bmatrix}
\tag{4.93}
$$

Thus, stability boundaries can be easily determined in this case using the Floquet theorem. The computation of the monodromy matrix is simple, requiring no integration routine, so that the stability diagram for the lossy Meissner equation can be readily obtained using a slightly different algorithm than that described for the lossy Mathieu equation. Setting $\tau = \frac{T}{2}$, that is, the parametric excitation is assumed to be a unit square wave, the stability diagram shown in Figure 4.13 can be determined. The stability diagram is a contour plot, for a table of values in the (q,a) plane consisting of the maximum absolute value of the eigenvalues of the monodromy matrix, for which a single eigenvalue of the monodromy matrix is on the unit circle in the z-plane. The rays emanating from the origin correspond to the contours of constant β that will be used in the Nyquist analyses.

167
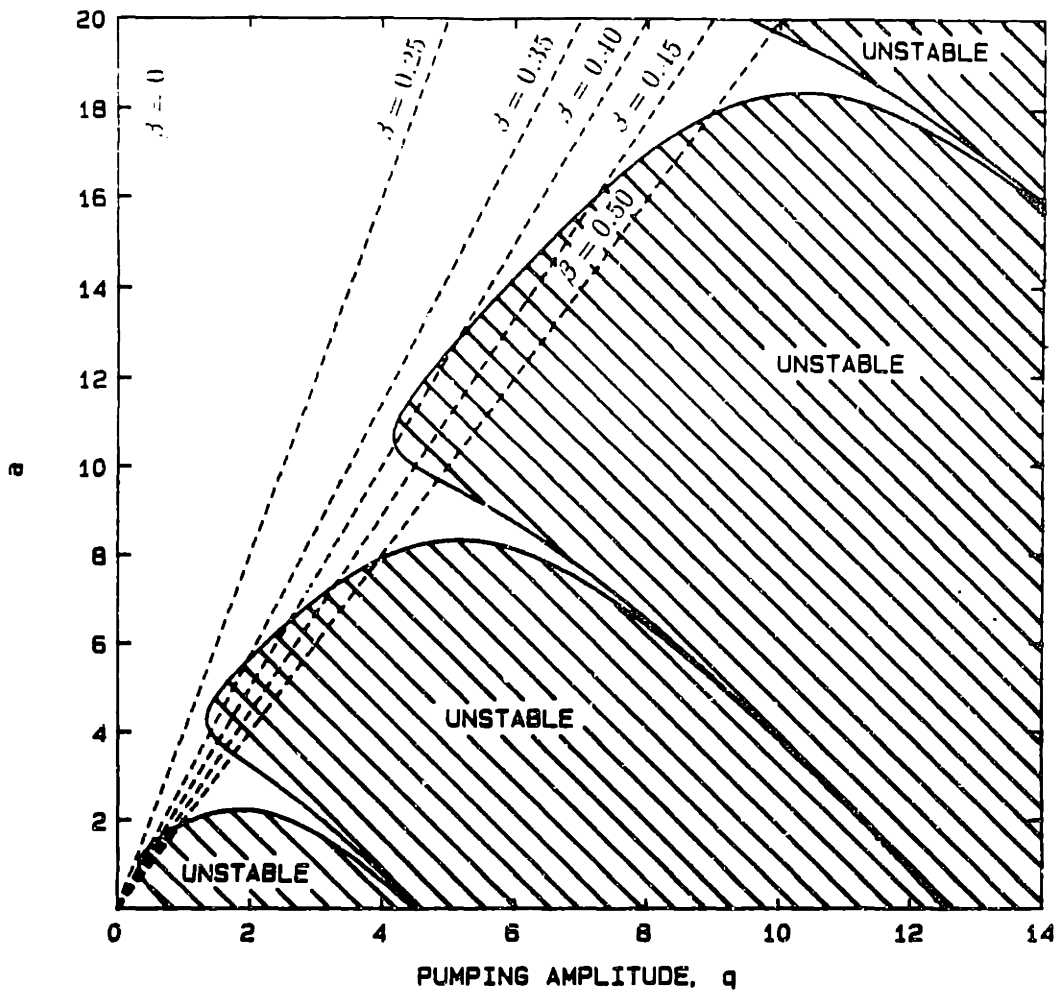
Figure 4.13: Stability (Strutt) diagram for the lossy Meissner equation with damping ratio $\zeta=0.2$. The contour lines correspond to purely periodic solutions of the lossy Meissner equation, that is, unit magnitude eigenvalues of the monodromy matrix.

In the same manner as for the lossy Mathieu equation example, stability of the lossy Meissner equation can be determined for linear variations of q with a, that is, for constant values of $\beta = q/a$. Introducing the feedback control law, $u(t) = -ax(t)$, into the open loop system

$$\ddot{x}(t) + 2\zeta\dot{x}(t) = [1 - 2\beta\psi(t)]u(t) \tag{4.94}$$

produces the lossy Meissner equation in (4.90). The parameter a can now be treated as the feedback gain. Thus, by applying the Nyquist methodology to the above open loop system, the stability of the lossy Meissner equation, that is, the closed loop system, can be determined. As before, selecting the state vector to be $x^T(t) = [x(t), \dot{x}]$, and $x(t)$ as the

168

measurement (or output), leads to the state space model below:

$$A = \begin{bmatrix} 0 & 1 \\ 0 & -2\zeta \end{bmatrix} \quad B(t) = \begin{bmatrix} 0 \\ 1 - 2\beta\psi(t) \end{bmatrix} \quad C^T = \begin{bmatrix} 1 \\ 0 \end{bmatrix} \quad (4.95)$$

Here, $B(t)$ can be expanded in a complex Fourier series,

$$\begin{aligned} B(t) \quad &\rightarrow \quad \{B_n | n \in Z\} \\ &\rightarrow \quad \begin{cases} \begin{bmatrix} 0 \\ 1 - 2\beta\psi_0 \end{bmatrix} & n = 0 \\ \begin{bmatrix} 0 \\ -2\beta\psi_n \end{bmatrix} & n \in Z, \; n \neq 0 \end{cases} \end{aligned} \quad (4.96)$$

where the general unit rectangular waveform for $\tau \in [0, T]$ has nonzero Fourier coefficients at all harmonics,

$$\psi_n = \begin{cases} \frac{2\tau - T}{T} & n = 0 \\ \frac{1}{jn\pi}\left[1 - e^{-jn\omega_p\tau}\right] & n \in Z, \; n \neq 0 \end{cases} \quad (4.97)$$

Here it is assumed that the time periodic parametric excitation is a unit square wave, so that $\tau = \frac{T}{2}$ and all of the even harmonics vanish,

$$\psi_n = \begin{cases} \frac{2}{jm\pi} & m = 2n + 1, n \in Z \\ 0 & \text{otherwise} \end{cases} \quad (4.98)$$

Thus, define the Fourier coefficients of the control distribution matrix as

$$\begin{aligned} B(t) &= \{\cdots, 0, B_{-3}, 0, B_{-1}, B_0, B_1, 0, B_3, 0, \cdots\} \\ &= \{\cdots, 0, -\beta_{-3}B_0, 0, -\beta_{-1}B_0, B_0, -\beta_1 B_0, 0, -\beta_3 B_0, 0, \cdots\} \end{aligned} \quad (4.99)$$

where $\beta_n = 2\beta\psi_n$. The harmonic transfer function in this case is

$$\hat{\mathcal{G}}(s) = \begin{bmatrix} \ddots & \vdots & \vdots & \vdots & \vdots & \vdots & \\ \cdots & G_{-2} & -\beta_{-1}G_{-2} & 0 & -\beta_{-3}G_{-2} & 0 & \cdots \\ \cdots & -\beta_1 G_{-1} & G_{-1} & -\beta_{-1}G_{-1} & 0 & -\beta_{-3}G_{-1} & \cdots \\ \cdots & 0 & -\beta_1 G_0 & G_0 & -\beta_{-1}G_0 & 0 & \cdots \\ \cdots & -\beta_3 G_1 & 0 & -\beta_1 G_1 & G_1 & -\beta_{-1}G_1 & \cdots \\ \cdots & 0 & -\beta_3 G_2 & 0 & -\beta_1 G_2 & G_2 & \cdots \\ & \vdots & \vdots & \vdots & \vdots & \vdots & \ddots \end{bmatrix} \quad (4.100)$$

where for all $n \in Z$,

$$
\begin{aligned}
G_n &= G(s + jn\omega_p) \\
&= C[(s + jn\omega_p)I - A]^{-1}B_0 \\
&= \frac{1}{(s + jn\omega_p)(s + jn\omega_p + 2\zeta)}
\end{aligned}
\tag{4.101}
$$

Interpretation of the Nyquist diagrams

Again, the inverse eigenloci are plotted instead of the eigenloci in the LTP Nyquist diagram for ease of interpretation, so that encirclements of the $-k$ point will be counted instead of the $-\frac{1}{k}$ point. In Figure 4.14, the eigenloci are shown for $a \in [0, 20]$, the same range of values of a as shown in Figure 4.13. In this case, the open loop transfer function has a single pole inside the unit circle, and a pole on the unit circle, so that to guarantee closed loop stability, a single CCW encirclement of the $-k$ point is required. In Figure 4.14a, the Nyquist diagram constructed from the inverse eigenloci is shown for $\beta = 0$, which recovers the LTI inverse Nyquist diagram, as was the case for the lossy Mathieu equation. The loop is closed at the far left in CCW fashion, so that every value of $-k$ on the negative real axis corresponds to a CCW encirclement. Thus, we conclude that closed loop configurations for which $k > 0$ (that is, points on the negative real axis) are stable, and unstable configurations are produced for $k < 0$ (or point on the the positive real axis for which the Nyquist diagram is not shown).

As β increases, the Nyquist diagram begins to ripple, as shown in Figure 4.14b until closed CCW circuits, symmetrical about the real axis, are formed. As before, the portions of the real axis enclosed by a CCW circuit lead to stable configurations of the lossy Meissner equation. The first closed CCW circuit is formed at approximately $\beta = 0.31$. As β is increased further, the portions of the real axis enclosed by CCW circuits are diminished. The CCW circuits are roughly ellipsoidal in the interval $a \in [0, 20]$. However, if the Nyquist diagram is plotted for the expanded interval of interest, $a \in [0, 100]$, as shown in Figure 4.15, it is clear that the nature of the LTP inverse Nyquist diagram for the lossy Meissner equation is much different than that of the lossy Mathieu equation. In the lossy Mathieu equation, the CCW circuits formed very regular closed convex curves symmetrical about the real axis. However, in the lossy Meissner example, the shapes of the CCW circuits can be very irregular and not convex, although the symmetry of the CCW circuits about the real axis
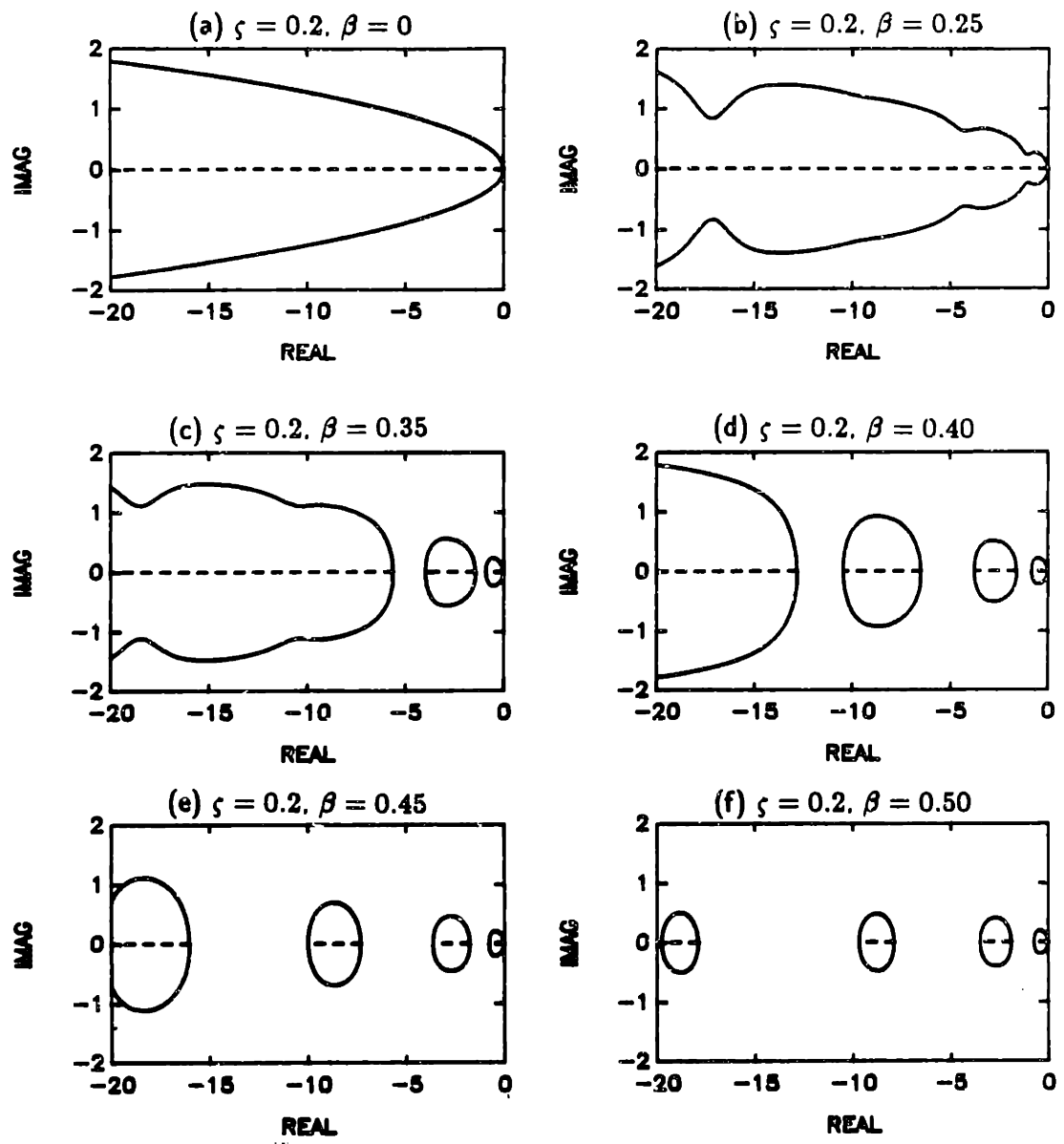
Figure 4.14: LTP Inverse Nyquist diagram for the lossy Meissner equation for $a \in [0, 20]$. Here, the damping ratio is $\zeta = .2$. The inverse Nyquist diagrams are plotted for the same range of gain shown in the stability diagram in Figure 4.13. When $\beta = 0$, the LTI inverse Nyquist diagram is recovered. As β is increased, so that the periodic effects grow stronger, the diagram starts to ripple until eventually a single CCW circuit is formed ($\beta \approx= .31$). For larger values of β, the inverse eigenloci form circuits that are symmetrical about the real axis. All circuits are CCW. The dashed lines correspond to values of stabilizing feedback gain.

is maintained. This irregularity in the CCW circuits suggests more complex interactions between the harmonic content of the parametric excitation and closed loop stability of the lossy Meissner equation. It should be noted that when the CCW circuits approach, but do not touch, the real axis, the contour of constant β in Figure 4.13 is close to a stability boundary.

Comparison of Floquet and Nyquist

The stability boundaries can be computed in straightforward fashion using either Floquet or Nyquist techniques. In Table 4.3, the values of a (or k) at the stability boundaries are compiled for four non-zero values of $\beta = \{0.35, 0.4, 0.45, 0.5\}$ used in the Nyquist test.

The Floquet stability boundaries were determined by constructing a function that computed the maximum absolute value of the two Floquet poles determined from the monodromy matrix calculation for a constant value of β. In this case the monodromy matrix, $\Phi(T,0)$, was determined numerically using (4.92). A function was then constructed that computed the maximum absolute value of the two eigenvalues of the monodromy matrix. A secant root finding technique was then applied to this function minus unity, thus, determining when either of the Floquet poles left the open unit disk in the z-plane. The accuracy imposed on the root finding procedure was 1×10^{-12}. These values are listed as the Floquet results in Table 4.3.

The stability boundaries were also determined using the Nyquist test by observing that the stability boundaries are simply the real axis crossings of the closed CCW contours in the Nyquist diagrams. If, in fact, these closed CCW circuits crossed the negative axis, this occurred when $\omega = \pm\omega_p/2$ and/or $\omega \to 0$. In Table 4.3, eighty harmonics, $N = 80$, were included in the harmonic transfer function when computing the eigenloci used in the Nyquist diagram in order to achieve results accurate to a minimum of six significant figures for the stability boundaries considered in the table. Excellent agreement is obtained from comparison of the Nyquist and Floquet results from nine significant figures for the first unstable region to six significant figures for the fifth stable boundary using the techniques described above. In general, the accuracy of the stability computation decreases as the gain, $a = k$ is increased. It is interesting to note that the Nyquist test predicted the first unstable boundary to two decimal places even though only a single harmonic was included in the harmonic transfer function. Thus, the Floquet and Nyquist results compare very

172
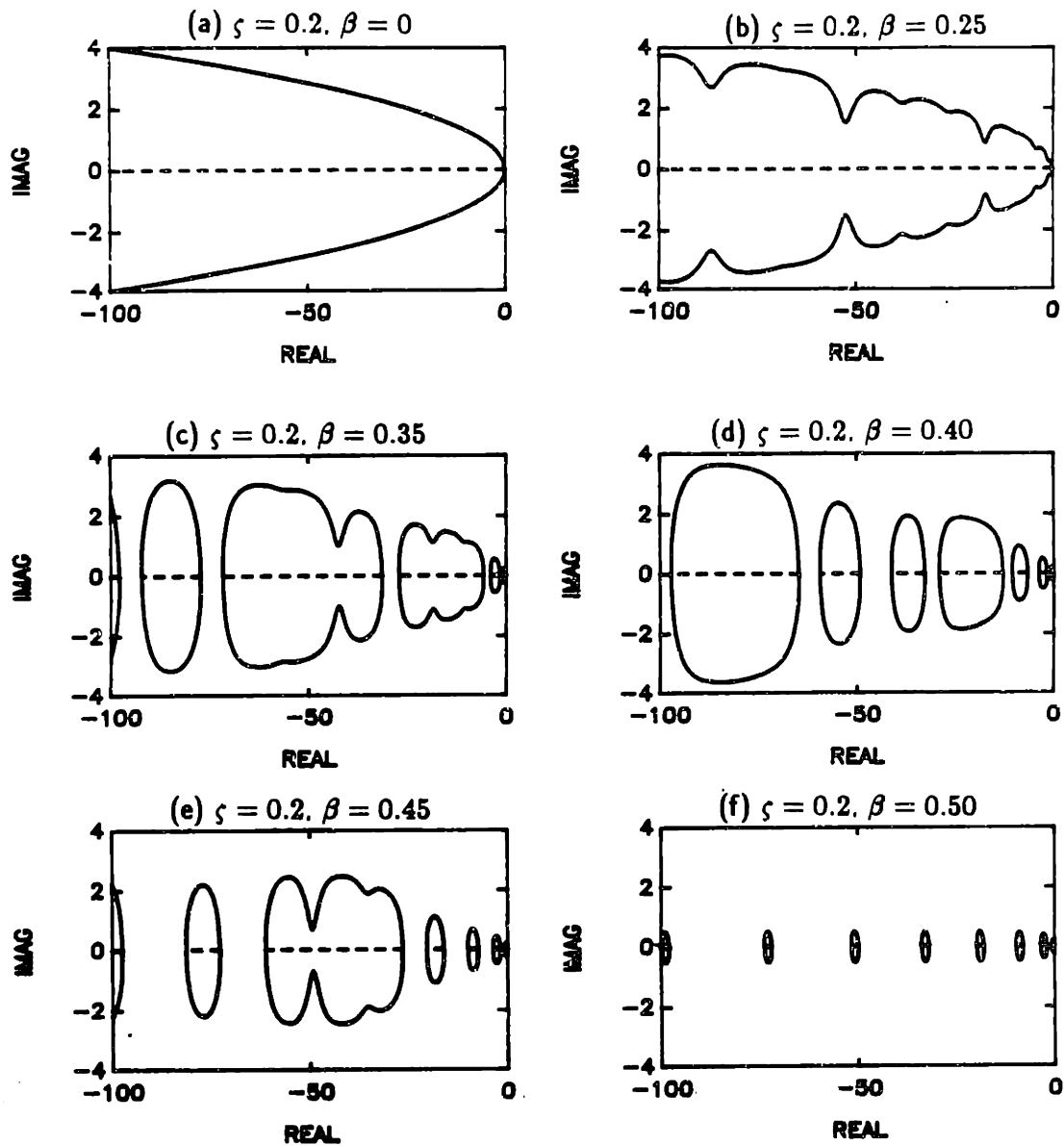
Figure 4.15: LTP inverse Nyquist diagram for the lossy Meissner equation for $a \in [0, 100]$. Here, the damping ratio is $\zeta = .2$. All circuits are CCW. The dashed lines correspond to stabilizing feedback gains.

well. However, it must be remembered that the Nyquist test provides a stability analysis for a line in the (q, a) plane, while the Floquet analysis provides a stability analysis for only a single point in the (q, a) plane.

Effects of truncation

The time periodic parametric excitation in the lossy Meissner equation consisting of a square wave at the pumping frequency and a bias must be described by a complex Fourier series with an infinite number of terms. The harmonic transfer function is a doubly infinite complex matrix at every value of frequency along the imaginary axis in the fundamental strip. The HTF is truncated for pragmatic reasons, so that the HTF will be a complex valued matrix of dimension $(2N + 1) \times (2N + 1)$. Since the parametric excitation cannot be described by a truncated complex Fourier series, we would expect that the truncation error in the skew diagonal sense will be much more significant than in the lossy Mathieu equation example. Thus, many more harmonics of the parametric excitation must be included in the harmonic transfer function in order for the eigenloci to accurately predict the real axis crossings, and hence the stability boundaries.

In Table 4.4, the stability boundaries are computed along a contour of constant $\beta = 0.45$ using the eigenloci of the harmonic transfer function for several different values of N, the number of harmonics included in the HTF. Up to eighty harmonics were included in the computation of the stability boundaries of the lossy Meissner equation. In addition, the insignificant figures in the values of the stability boundaries obtained using Nyquist are italicized in the table. Clearly, many more harmonics must be included in the harmonic transfer function in order to obtain good results using Nyquist. This is due primarily to the fact that a truncated complex Fourier series is always insufficient to describe the parametric excitation in the lossy Meissner equation, resulting in an HTF that is not even banded. In contrast, the lossy Mathieu equation example required fewer harmonics for accurate results because the HTF was tridiagonal.

4.6 Conclusions

The classical stability analysis methods of Floquet and Hill can only determine closed loop stability for a specific value of feedback. The objective of this chapter was to develop a

Table 4.3: Comparison of Floquet and Nyquist analyses for the Lossy Meissner equation. Here, the damping ratio is $\zeta=0.2$. The values of a, or of feedback gain k, are presented at each point a stability boundary is encountered. In computing the eigenloci of the harmonic transfer function used in the Nyquist test, $N=80$ harmonics were included, implying an 161×161 eigenvalue problem at each frequency in the fundamental strip. The Floquet results should be regarded as the most accurate.

β	Analysis Type	Stability Boundary			
		First Unstable	Second Stable	Second Unstable	Third Stable
0.35	Nyquist	0.916275394791	1.430344329145	3.994303942260	5.622542822018
	Floquet	0.916275392220	1.430344174990	3.994303031002	5.622541932449
0.40	Nyquist	0.838272386733	1.603488613760	3.790488659706	6.492752546826
	Floquet	0.838272378784	1.603488371110	3.790487746346	6.492749854334
0.45	Nyquist	0.781711391370	1.755194149193	3.635654220460	7.303324920163
	Floquet	0.781711380876	1.755193782656	3.635653228399	7.303319413106
0.50	Nyquist	0.736046949977	1.888570967911	3.502777366334	7.895167480647
	Floquet	0.736046937790	1.888570448777	3.502776293377	7.895158923405

Table (continued)

β	Analysis Type	Stability Boundary			
		Third Unstable	Fourth Stable	Fourth Unstable	Fifth Stable
0.35	Nyquist	27.105441587100	31.346851739408	71.677465782886	77.218816682875
	Floquet	27.105410124760	31.346805215793	71.677347279928	77.218418854017
0.40	Nyquist	10.479953102209	12.831286620816	29.029399365639	32.634589890584
	Floquet	10.479942204328	12.831285373380	29.029393154682	32.634480449978
0.45	Nyquist	9.997742160250	16.025042300979	20.411663584393	26.413218616094
	Floquet	9.997732066636	16.025020314574	20.411614962233	26.413192433889
0.50	Nyquist	9.694555628043	17.896259027615	19.755565795585	31.896716278049
	Floquet	9.694544791229	17.896214809522	19.755515993965	31.896574347522

Table (continued)

β	Analysis Type	Stability Boundary			
		Fifth Unstable	Sixth Stable	Sixth Unstable	Seventh Stable
0.35	Nyquist	92.179564710410	97.771229141740	140.095409745532	141.263667625460
	Floquet	92.178904223607	97.771133148987	140.098851204862	141.258480617433
0.40	Nyquist	41.168829156735	49.121759903864	59.424989627358	64.701911890927
	Floquet	41.168712348994	49.121601684323	59.424608159416	64.701899141958
0.45	Nyquist	61.231622550791	72.716662363453	81.328896079068	97.290349030582
	Floquet	61.231386364849	72.716050503113	81.328208064986	97.289407248244
0.50	Nyquist	33.780885109680	49.897091773143	51.793637254281	71.897571284968
	Floquet	33.780731199126	49.896739069338	51.793263426506	71.896828105506

Table 4.4: Comparison of Floquet and Nyquist stability boundaries for the Lossy Meissner equation with $\zeta=0.2$ and $\beta=0.45$.

Analysis Type	Stability Boundary			
	First Unstable	Second Stable	Second Unstable	Third Stable
$N=1$	0.784778308552	1.961511810761	4.251998358417	11.394911703320
$N=2$	0.781697054704	1.792781307360	3.915559368162	6.581839620784
$N=3$	0.781851701546	1.760571490676	3.651847347139	7.439159777596
$N=4$	0.781758273680	1.758720402824	3.646939331738	7.422006671156
$N=5$	0.781743977399	1.756435304828	3.639363472236	7.326149938819
$N=6$	0.781729975699	1.756167556187	3.638577327368	7.323420401267
$N=7$	0.781723985623	1.755665189484	3.637040721310	7.311307583235
$N=8$	0.781720107194	1.755591412866	3.636814428835	7.310476266290
$N=9$	0.781723985623	1.755665189484	3.637040721310	7.311307583235
$N=10$	0.781716093189	1.755393569475	3.636226948445	7.306701951427
$N=15$	0.781712810258	1.755245045025	3.635798382009	7.304121562908
$N=20$	0.781712022039	1.755217866103	3.635719988233	7.303694632020
$N=30$	0.781711575138	1.755200835080	3.635672598422	7.303427392543
$N=40$	0.781711463665	1.755196740594	3.635661277610	7.303364379979
$N=50$	0.781711443508	1.755195291847	3.635657318131	7.303342276831
$N=60$	0.781711405639	1.755194654005	3.635655548818	7.303332703386
$N=80$	0.781711391370	1.755194149193	3.635654220460	7.303324920162
Floquet	0.781711380875	1.755193782656	3.635653228398	7.303319413105

Table (continued)

Analysis Type	Stability Boundary			
	Third Unstable	Fourth Stable	Fourth Unstable	Fifth Stable
$N=1$	19.724074973292	—	—	—
$N=2$	10.206776284175	21.625685477367	26.479667953751	—
$N=3$	10.524562970155	16.436710894150	21.786466878626	33.454790194722
$N=4$	10.449750895792	15.180746424928	20.099322981774	25.373691168752
$N=5$	10.050767917606	16.230839037022	21.221572458489	25.629476575519
$N=6$	10.045015071094	16.161425232679	21.145793955103	25.401331798664
$N=7$	10.014804262325	16.073452934689	20.537427253762	26.477246751649
$N=8$	10.013481426774	16.058695494491	20.523545615071	26.411374797367
$N=9$	10.014804262325	16.073452934689	20.537427253762	26.477246751649
$N=10$	10.004915762426	16.039991519662	20.455296186322	26.414004071216
$N=15$	9.999296617796	16.028651567498	20.420153263102	26.417690509922
$N=20$	9.998468656908	16.026495513104	20.415403259608	26.414094398864
$N=30$	9.997937669983	16.025444718447	20.412636765055	26.413559037709
$N=40$	9.997816326430	16.025197682052	20.412027651479	26.413369214018
$N=50$	9.997744473888	16.025110752819	20.411820919276	26.413290058118
$N=60$	9.997756331166	16.025072538635	20.411732394000	26.413251260700
$N=80$	9.997742160249	16.025042300979	20.411669584393	26.413218616093
Floquet	9.997732066636	16.025020314574	20.411614962232	26.413192433889

method that would permit determination of closed loop system stability using only open loop information. that is, a Nyquist test for LTP systems. It was determined that the MIMO Nyquist criterion for LTI systems could be extended to the LTP case using the notions of the LTP integral operator transfer function and the harmonic transfer function developed in Chapter 3. The Nyquist criterion provides a method of determining closed loop system stability for a parameterization of feedback gain, by plotting the eigenloci of the open loop LTP transfer function.

Although the examples used to illustrate the multivariable Nyquist test were single input single output cases, a completely general multivariable LTP Nyquist test was presented. The Nyquist methodology presented here was shown to be a powerful alternative to the classical stability notions of Floquet and Hill, and should ultimately prove useful in the general study of the control of linear time periodic systems.

[Page Left Blank]

Chapter 5

Stability Robustness and Feedback Control Design

The introduction of the linear operator theoretic framework for LTP systems has thus far led to a frequency domain interpretation for LTP systems. To reiterate, poles, zeroes, principal gain, phase, and all of the associated directional properties, as well as a Nyquist diagram and criterion, have been developed.

An important notion in the linear operator theory is the Small Gain Theorem, which leads to several useful and important analysis techniques in the linear time invariant control theory. Central to the Small Gain Theorem are operator norms that quantify the gain of an operator. In this chapter, the Small Gain Theorem is reviewed, and norms appropriate for LTP systems are described. Essentially all of the Small Gain Theorem results can be extended to LTP systems with a slight change of notation, and computations performed using the harmonic balance procedures developed in this thesis. Therefore, instead of attempting to transcribe all of the various theorems that rely on the Small Gain Theorem, some example–driven analyses are developed that illustrate the uses of the Small Gain Theorem. First, the stability robustness properties (that is, gain and phase margins) of steady state periodic solutions of the linear quadratic regulator are examined. Second, a compensation methodology is presented for weakly periodic systems that treats the periodic parametric excitation as a modeling error. This approach permits LTI compensators to be designed for weakly periodic systems using the familiar tools of the LTI control theory.

5.1 Preliminaries

The Small Gain Theorem [111,112] has proven to be extremely useful in a multitude of applications for LTI multivariable control systems. Most of the stability robustness results [60, for example] can be directly or indirectly attributed to the original Small Gain Theorem due to Zames [111,112]. Zames took a very broad perspective to interconnected systems, and essentially required that only two criteria be satisified for acceptable behavior of an input–output systems:

1) bounded input must produce bounded outputs,

2) outputs must not be sensitive to small variations in the input signal, for example, noise.

The above two statements form the basis of the definition of stability presented by Zames, and lead to the Small Gain Theorem. First, let us consider some preliminaries.

5.1.1 Operator norms

In Chapter 3, the principal gains were introduced in order to describe the amplification of a GP input signal into a GP output signal. These principal gains were computed using the SVD of the truncated harmonic transfer function. However, it is sometimes more useful to have a global measure of the gain of the LTP transfer function, that is, a single number. In the literature of LTI control theory [64], this is accomplished through the notions of the operator norm $\|\cdot\|_2$, or the L_2/H_2 norm, and the operator norm $\|\cdot\|_\infty$, or the L_∞/H_∞ norm. Here, we present preliminary definitions for the L_2/H_2 and L_∞/H_∞ operator norms, and describe some frequency domain function spaces that are analoguous to the frequency domain function spaces commonly used in the LTI control theory.

Definition 5.1 *P denotes the space of all LTP transfer functions determined using the integral operator formulation, determined from proper LTP state space models.*

First, let us consider the operator norm, $\|\cdot\|_2$.

Definition 5.2 (L_2/H_2 **operator norm,** $\|\cdot\|_2$) *Let $\widehat{G}(z)$ be a proper LTP transfer function with no poles on the unit circle. The L_2/H_2 operator norm of $\widehat{G}(z)$ is defined as*

$$\left\|\widehat{G}\right\|_2 = \left\{ \frac{1}{2\pi} \int_{-\pi}^{\pi} \mathrm{Tr}\left[\hat{G}^*(e^{j\theta})\hat{G}(e^{j\theta}) \right] d\theta \right\}^{\frac{1}{2}} \tag{5.1}$$

180

Thus, we define two function spaces.

a) PL_2 *denotes the frequency domain function space consisting of all LTP transfer functions with no poles on the unit circle, and with finite L_2 norm.*

b) PH_2 *denotes the frequency domain function space consisting of all functions in PL_2 that have no poles outside the unit circle. Alternatively, if*

$$\left\|\widehat{G}\right\|_2 = \left\{ \frac{1}{2\pi} \int_{-\pi}^{\pi} \mathrm{Tr}\left[\widehat{G}^*(re^{j\theta})\widehat{G}(re^{j\theta}) \right] d\theta \right\}^{\frac{1}{2}} \tag{5.2}$$

is bounded for $r < 1$, then $\widehat{G}(z)$ is a member of the class PH_2. □

This is an extension of the standard definition of H_2 functions as described in Grenander [38]. The trace is introduced because the integral operator transfer function is multi-input multi-output. Thus, an H_2 optimization theory comparable to that of the LTI case can be developed on the basis of the above H_2 norm. The H_2 optimization for LTI systems produces the LQG design methodology. The LQG design methodology has also been fully developed for the LTP case, and consists of a linear quadratic regulator (LQR) and a linear quadratic estimator (LQE). The stability rol istness properties of the LQR will be examined in the sequel.

To compute the H_2 norm, we again resort to the harmonic transfer function, and propose that the H_2 norm be computed using

$$\left\|\widehat{G}\right\|_2 = \lim_{N\to\infty} \left\{ \frac{1}{2\pi} \int_{-\frac{\omega_p}{2}}^{\frac{\omega_p}{2}} \mathrm{Tr}\left[\widehat{\mathcal{G}}_N^*(j\omega)\widehat{\mathcal{G}}_N(j\omega) \right] d\omega \right\}^{\frac{1}{2}} \tag{5.3}$$

as long as the limit converges. The H_2 norm certainly deserves further study, but is not of much use in the context of stability robustness as discussed in this chapter, and the complete H_2 theory for LTP systems is left for future research.

In the context of stability robustness to perturbations in the plant model, we are more concerned with the greatest possible magnification of an input signal by the LTP transfer function. Hence, the $\|\cdot\|_\infty$ is defined.

Definition 5.3 (L_∞/H_∞ **operator norm,** $\|\cdot\|_\infty$) *Let $\widehat{G}(z)$ be a proper LTP transfer function with no poles on the unit circle. The L_∞/H_∞ operator norm of $\widehat{G}(z)$ is defined as*

$$\left\|\widehat{G}\right\|_\infty = \sup_{\theta\in(-\pi,\pi]} \sigma_{max}\left\{ \widehat{G}(e^{j\theta}) \right\} \tag{5.4}$$

Thus, we define two function spaces.

a) PL_∞ denotes the frequency domain function space consisting of all LTP transfer functions with no poles on the unit circle (or finite L_∞ norm).

b) PH_∞ denotes the frequency domain function space consisting of all functions in PL_∞ that have no poles outside the unit circle. □

Recall that a numerical method was developed to compute the singular values of the LTP transfer function in Chapter 3. Therefore, an algorithm to compute the H_∞ norm is given by the formula below

$$\left\|\widehat{G}\right\|_\infty = \lim_{N\to\infty} \sup_{\omega\in(-\frac{\omega_p}{2},\frac{\omega_p}{2}]} \sigma_{max}\left\{\mathcal{G}_N(j\omega)\right\} \tag{5.5}$$

as long as the limit exists.

The above operator norms satisfy the usual properties of a norm, namely,

1. $\left\|\widehat{G}\right\| > 0$, and $\left\|\widehat{G}\right\| = 0$ if and only if $\widehat{G}(z) \equiv 0$

2. $\left\|\alpha\widehat{G}\right\| = |\alpha|\left\|\widehat{G}\right\|$ for all scalar α, and

3. $\left\|\widehat{G} + \widehat{H}\right\| \leq \left\|\widehat{G}\right\| + \left\|\widehat{H}\right\|$, that is, the *triangle inequality*.

The $\left\|\widehat{G}\right\|_\infty$ operator norm satisfies an additional property,

$$\left\|\widehat{G}\widehat{H}\right\|_\infty \leq \left\|\widehat{G}\right\|_\infty \left\|\widehat{H}\right\|_\infty \tag{5.6}$$

which is derivative of the properties of singular values. Also note that the above inequality is not satisfied by the $\left\|\widehat{G}\right\|_2$ operator norm.

5.1.2 Another closed loop stability result

In Chapter 4, the Nyquist criterion for LTP systems was presented using the Fredholm determinant of the LTP transfer function, and provides a necessary and sufficient condition for stability of a closed loop system even if the plant and the compensator are unstable. The Small Gain Theorem applies to any operator with a sensible definition of an operator norm that describes the maximum amplification of a signal from an input signal space to an output signal space, where the space of input signals equals the space of output signals.

Clearly, the GP input and output signals satisfy the latter requirement, and the H_∞ norm defined above satisfies the former requirement. However, in stating the Small Gain
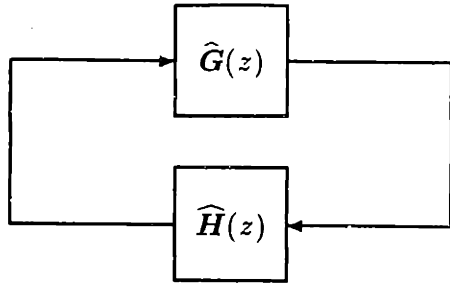
Figure 5.1: A closed loop system.

Theorem below, we are omitting many of the details associated with extended normed linear spaces, which is required to prove the general case. In addition, the Small Gain Theorem is a conservative, but very simple method for determining closed loop stability using only information from the open loop system. Consider the feedback loop in Figure 5.1.

Theorem 5.4 (The Small Gain Theorem) *The system in Figure 5.1 is internally stable, when both $\widehat{G}(z)$ and $\widehat{H}(z)$ are PH_∞ functions, that is, stable, and*

$$\left\| \widehat{G} \right\|_\infty \left\| \widehat{H} \right\|_\infty < 1 \tag{5.7}$$

or, in terms of singular values,

$$\sigma_{max} \left[\widehat{G}(e^{j\theta}) \right] \sigma_{max} \left[\widehat{H}(e^{j\theta}) \right] < 1 \quad \theta \in (-\pi, \pi] \tag{5.8}$$

Proof: The proof is a direct application of the Small Gain Theorem by Zames [111]. □

Thus, closed loop stability can be determined for a feedback loop composed of stable elements in a sufficient sense by computing the H_∞ operator norm of every element in the loop, and requiring that the product of the H_∞ norms be less than one. The Small Gain Theorem will prove useful in the sequel in determining stability robustness (especially gain margins) of closed loop systems.

The second aspect of stability required in Zames' notion of stability, that is, tolerance of small perturbations, can now be examined. If the transfer function in the feedback loop, $\widehat{H}(z)$, is thought of as a perturbation, say $\Delta(z)$, then the stability of the loop in Figure 5.1 is guaranteed if

$$\sigma_{max} \left[\widehat{G}(e^{j\theta}) \right] < \frac{1}{\sigma_{max} \left[\Delta(e^{j\theta}) \right]} \quad \forall\, \theta \in (-\pi, \pi] \tag{5.9}$$

The above statement forms the basis for much of the stability robustness analysis, originally developed by Lehtomaki [60] and others. Other forms of the above equation will be developed in the sequel that are more useful from a control design standpoint.

5.2 Optimal Linear Quadratic Control

The *linear quadratic Gaussian* (LQG) design methodology has proven to be one of the most useful feedback control design techniques for LTI systems. In this section, the LQG design methodology is examined in the context of the theoretical framework developed for LTP systems in previous chapters. The underlying *linear quadratic regulator* (LQR) and *linear quadratic estimator* (LQE) procedures are well established, however, the majority of the material presented here is new.

The section is organized as follows. The LQR problem is defined, and its solution presented, in order to establish terminology. The LQR solution requires solving the usual matrix Riccati differential equation. A harmonic balance form of the solution is then proposed. Finally, the stability robustness properties of the steady state periodic solutions of the time periodic LQR problem are described.

5.2.1 The linear quadratic regulator

The linear quadratic regulator for LTP systems is a well known design methodology which is well suited for several performance goals.

Definition 5.5 (Linear quadratic regulator for LTP systems) *Consider the LTP state space model*

$$\dot{x}(t) = A(t)x(t) + B(t)u(t) \tag{5.10}$$

with the usual assumptions that $A(t)$ and $B(t)$ are T-periodic, with initial state condition,

$$x(0) = \xi_0 \tag{5.11}$$

The controlled variable is

$$z(t) = M(t)x(t) \tag{5.12}$$

where $M(t + T) = M(t)$. Consider also the quadratic cost

$$J(0, t_f) = \int_0^{t_f} \left\{ z^T(t)R(t)z(t) + u^T(t)R_c(t)u(t) \right\} dt + x^T(t_f)P_f x(t_f) \tag{5.13}$$

184

where the controlled variable weighting, $R(t)$, and the weighting on the control effort, $R_c(t)$, are uniformly positive definite, T-periodic, symmetric matrices for all $t \in [0, T]$. The constant matrix, P_f, is also positive definite and symmetric. Then, the problem of determining the input $u(t)$ for $t \in [0, t]$ for which the cost J is minimized is called the **time periodic deterministic linear quadratic regulator problem.**

Remark: Usually, the LQR weighting functions are assumed to be general uniformly positive definite time varying functions. However, the scope of the LQR problem has been limited to the case where $M(t)$, $R(t)$, and $R_c(t)$, are all T-periodic, although the general problem need not be restricted in this way. $\square$.

The solution of the linear quadratic regulator problem for LTP systems is well known, and can be derived using the elementary calculus of variations as shown in [59] and elsewhere. The result is summarized in the following theorem.

Theorem 5.6 (Linear quadratic regulator for LTP systems) *The optimal input for the time periodic deterministic linear quadratic regulator problem is generated by the linear feedback control law*

$$u(t) = -G(t)x(t) \tag{5.14}$$

where the optimal full state feedback gains, $F(t)$, are given by

$$G(t) = R_c^{-1}(t)B^T(t)P_c(t) \tag{5.15}$$

The symmetric nonnegative definite matrix $P_c(t)$ satisfies the **control matrix Riccati differential equation** *(CMRDE)*

$$-\dot{P}_c(t) = P_c(t)A(t) + A^T(t)P_c(t) + Q_c(t) - P_c(t)B(t)R_c^{-1}(t)B^T(t)P_c(t) \tag{5.16}$$

with terminal condition

$$P_c(t_f) = P_f \tag{5.17}$$

Here,

$$Q_c(t) = M^T(t)R_c(t)M(t) \tag{5.18}$$

For the optimal solution the terminal cost is given by

$$J(t, t_f) = x^T(t)P_c(t)x(t) \tag{5.19}$$

Proof: See Kwakernaak and Sivan [59]. $\square$

5.2.2 Steady state properties of the LQR

Many authors have been concerned with the determination of the asymptotic properties of the CMRDE, especially in the search for asymptotic solutions as $t_f \rightarrow \infty$. The two important results are summarized below:

1) As the terminal time, $t_f \rightarrow \infty$, the solution of the CMRDE, $P_c(t)$, with the terminal condition

$$P_c(t_f) = P_f \qquad (5.20)$$

generally approaches a *steady state solution* that is independent of the terminal condition, P_f.

2) The steady state control law results, in general, in an asymptotically stable closed loop system.

It is a well known fact that the above results hold if the state space model is either exponentially stable or both uniformly controllable and uniformly reconstructible [59]. In addition, a periodic solution of the CMRDE exists at steady state, $P_c(t+T) = P_c(t)$, if these same conditions hold [4]. It is this periodic solution that is of interest in determining the stability robustness properties of the LQR.

5.2.3 Harmonic balance form of the CMRDE

In previous chapters, the harmonic balance methodology invariably led to additional insight into the implications of results derived using the integral operator approach. Here, the harmonic balance approach will be used to transform the CMRDE to an algebraic form that leads to additional insights into the behavior of LQR solutions.

Much of the geometric theory of the time periodic version of the CMRDE has focused on the development of periodic generators, that is, the determination of an initial condition for the Riccati matrix, $P_c(t)$, that produces the correct time periodic solution by direct integration of the Hamiltonian system associated with the Riccati equation [4,87]. However, by applying the Toeplitz transform to the CMRDE, assuming that a periodic solution is to be found, an analogous infinite dimensional algebraic Riccati equation can be determined.

Recall the CMRDE,

$$- \dot{P}_c(t) = P_c(t)A(t) + A^T(t)P_c(t) + Q_c(t) - P_c(t)B(t)R_c^{-1}(t)B^T(t)P_c(t) \qquad (5.21)$$

186

Here, time periodic solutions are being sought in the steady state sense. Thus, at steady state, it is required that

$$P_c(t + T) = P_c(t) \tag{5.22}$$

or that $P_c(t)$ is T-periodic. The remaining matrices in the CMRDE are T-periodic by assumption, so that all of the matrices in (5.21) are T-periodic. Taking the Toeplitz transform of both sides of (5.21),

$$-(\mathcal{N}\mathcal{P}_c - \mathcal{P}_c\mathcal{N}) = \mathcal{P}_c\mathcal{A} + \mathcal{A}^*\mathcal{P}_c + \mathcal{Q}_c - \mathcal{P}_c\mathcal{B}\mathcal{R}_c^{-1}\mathcal{B}^*\mathcal{P}_c \tag{5.23}$$

so that

$$0 = \mathcal{P}_c(\mathcal{A} - \mathcal{N}) + (\mathcal{A} - \mathcal{N})^*\mathcal{P}_c + \mathcal{Q}_c - \mathcal{P}_c\mathcal{B}\mathcal{R}_c^{-1}\mathcal{B}^*\mathcal{P}_c \tag{5.24}$$

The above equation is the harmonic balance form of the CMRDE, which is denoted the *control matrix Riccati harmonic balance equation* (CMRHBE). This leads to the following lemma.

Lemma 5.7 *A T-periodic solution of the CMRDE given by $P_c(t)$, satisfies the CMRHBE in (5.24).*

The CMRHBE will prove useful in determining the stability robustness properties of the LQR problem.

Solving the CMRDE using unitary transformations

The CMRHBE is an infinite dimensional equation that can be studied by examining its finite truncation, just as the many other properties developed in this thesis were studied. Unfortunately, the finite truncation of the CMRHBE is a complex algebraic Riccati equation (ARE). The usual ARE equation solvers use real arithmetic (such as *are.m* in MATLAB), but can be utilized in this instance by following a procedure nearly identical to that developed for circulant/Toeplitz systems [105,49, for example]. This is advantageous since the ARE solvers are very accurate and numerically robust, so that an ARE solver using complex arithmetic is not necessary using the procedure described below.

Define the augmented matrices

$$\mathcal{A}_2 = \begin{bmatrix} \mathrm{Re}(\mathcal{A}) & \mathrm{Im}(\mathcal{A}) \\ -\mathrm{Im}(\mathcal{A}) & \mathrm{Re}(\mathcal{A}) \end{bmatrix} \tag{5.25}$$

187

and similarly for $\mathcal{B}_2$, $\mathcal{P}_{c2}$, $\mathcal{Q}_{c2}$, and $\mathcal{R}_{c2}$. Finally, by noting that

$$\text{Re}(\mathcal{N}) = 0 \tag{5.26}$$

then

$$\mathcal{N}_2 = \begin{bmatrix} 0 & -j\mathcal{N} \\ j\mathcal{N} & 0 \end{bmatrix} \tag{5.27}$$

Thus, all of the augmented matrices defined above are strictly real.

As an aside, these two representations of $\mathcal{A}$ are strongly related by a simple unitary (similarity) transformation [78], which preserves the eigenvectors as well as the eigenvalues of $\mathcal{A}$. To illustrate this, consider the similarity transformation matrix

$$\mathcal{T}_2 = \frac{1}{\sqrt{2}} \begin{bmatrix} \mathcal{I} & \mathcal{I} \\ j\mathcal{I} & -j\mathcal{I} \end{bmatrix} \tag{5.28}$$

where, due to the fact that the transformation is unitary,

$$\mathcal{T}_2^{-1} = \mathcal{T}_2^* \tag{5.29}$$

Then the following relationship holds:

$$\begin{bmatrix} \mathcal{A} & 0 \\ 0 & \mathcal{A}^* \end{bmatrix} = \mathcal{T}_2^* \mathcal{A}_2 \mathcal{T}_2$$

$$= \mathcal{T}_2^* \begin{bmatrix} \text{Re}(\mathcal{A}) & \text{Im}(\mathcal{A}) \\ -\text{Im}(\mathcal{A}) & \text{Re}(\mathcal{A}) \end{bmatrix} \mathcal{T}_2 \tag{5.30}$$

This is a common stratagem in dealing with Hermitian systems and has been found useful in applications such as Toeplitz/circulant systems [49] and in dealing with complex conjugate modes in the standard eigenstructure assignment problem for linear time invariant systems.

Thus, the augmented Riccati equation

$$0 = \mathcal{P}_{c2}(\mathcal{A}_2 - \mathcal{N}_2) + (\mathcal{A}_2 - \mathcal{N}_2)^T \mathcal{P}_{c2} + \mathcal{Q}_{c2} - \mathcal{P}_{c2}\mathcal{B}_2 \mathcal{R}_{c2}^{-1} \mathcal{B}_2^T \mathcal{P}_{c2} \tag{5.31}$$

is an infinite dimensional ARE using real arithmetic. As before, a limiting process is implied in that the various quantities are truncated to contain N harmonics, and a limiting solution is sought as N grows large. Pragmatically, an ARE of order $2(2N+1)n$ will be solved on the computer.

Solving the CMRDE using similarity transformations

One problem with the above procedure is that the dimensionality of the problem is doubled. This is an undesirable feature of the procedure since memory on a computer is invariably limited. Thus, a different approach that does not double the dimensionality of the truncated ARE would be of interest.

A second method can be applied here to render all of the matrices in the CMRHBE strictly real without increasing the dimensionality of the truncated Riccati equation. Recall that the principle of harmonic balance originally used in developing the harmonic state space model was applied to the set of complex exponentials, $\{e^{jn\omega_p t} | n \in Z\}$. In addition, the state was represented by the doubly infinite vector, x, which was composed of the complex Fourier coefficients of the state. Both u and y were defined in similar fashion. However, the harmonic balance could just as easily have been performed over the set of functions

$$1, \ \cos\omega_p t, \ \sin\omega_p t, \ \cos 2\omega_p t, \ \sin 2\omega_p t, \cdots \qquad (5.32)$$

This leads to the similarity transformations

$$
\begin{aligned}
x &= T_n \tilde{x} \\
u &= T_m \tilde{u} \\
y &= T_p \tilde{y}
\end{aligned}
\qquad (5.33)
$$

Here

$$
\tilde{x} = \begin{bmatrix} \vdots \\ x_{2s} \\ x_{1s} \\ x_0 \\ x_{1c} \\ x_{2c} \\ \vdots \end{bmatrix}, \quad
\tilde{u} = \begin{bmatrix} \vdots \\ u_{2s} \\ u_{1s} \\ u_0 \\ u_{1c} \\ u_{2c} \\ \vdots \end{bmatrix}, \quad
\tilde{y} = \begin{bmatrix} \vdots \\ y_{2s} \\ y_{1s} \\ y_0 \\ y_{,c} \\ y_{2c} \\ \vdots \end{bmatrix}, \qquad (5.34)
$$

The transformation matrix is given by

$$
\mathcal{T}_n = \begin{bmatrix}
\ddots & \vdots & \vdots & \vdots & \vdots & \vdots & \\
\cdots & -j I_n & 0 & 0 & 0 & I_n & \cdots \\
\cdots & 0 & -j I_n & 0 & I_n & 0 & \cdots \\
\cdots & 0 & 0 & I_n & 0 & 0 & \cdots \\
\cdots & 0 & j I_n & 0 & I_n & 0 & \cdots \\
\cdots & j I_n & 0 & 0 & 0 & I_n & \cdots \\
& \vdots & \vdots & \vdots & \vdots & \vdots & \ddots
\end{bmatrix}
\tag{5.35}
$$

where I_n is the identity matrix of dimension $n \times n$. The inverse of this matrix is easily obtained

$$
\mathcal{T}_n^{-1} = \begin{bmatrix}
\ddots & \vdots & \vdots & \vdots & \vdots & \vdots & \\
\cdots & -\frac{1}{2j} I_n & 0 & 0 & 0 & \frac{1}{2j} I_n & \cdots \\
\cdots & 0 & -\frac{1}{2j} I_n & 0 & \frac{1}{2j} I_n & 0 & \cdots \\
\cdots & 0 & 0 & I_n & 0 & 0 & \cdots \\
\cdots & 0 & \frac{1}{2} I_n & 0 & \frac{1}{2} I_n & 0 & \cdots \\
\cdots & \frac{1}{2} I_n & 0 & 0 & 0 & \frac{1}{2} I_n & \cdots \\
& \vdots & \vdots & \vdots & \vdots & \vdots & \ddots
\end{bmatrix}
\tag{5.36}
$$

The transformation matrices $\mathcal{T}_m$ and $\mathcal{T}_p$, and their respective inverses, are defined in similar fashion.

Using the above transformations, the harmonic state space model

$$
\begin{aligned}
s\mathcal{X} &= (\mathcal{A} - \mathcal{N})\mathcal{X} + \mathcal{B}u \\
y &= \mathcal{C}\mathcal{X} + \mathcal{D}u
\end{aligned}
\tag{5.37}
$$

can be similarity transformed to another harmonic state space model of the form

$$
\begin{aligned}
s\tilde{\mathcal{X}} &= (\tilde{\mathcal{A}} - \tilde{\mathcal{N}})\tilde{\mathcal{X}} + \tilde{\mathcal{B}}\tilde{u} \\
\tilde{y} &= \tilde{\mathcal{C}}\tilde{\mathcal{X}} + \tilde{\mathcal{D}}\tilde{u}
\end{aligned}
\tag{5.38}
$$

where

$$
\tilde{\mathcal{A}} = \mathcal{T}_n^{-1} \mathcal{A} \mathcal{T}_n
$$

190

$$\tilde{\mathcal{N}} = \mathcal{T}_n^{-1}\mathcal{N}\mathcal{T}_n$$

$$\tilde{\mathcal{B}} = \mathcal{T}_n^{-1}\mathcal{B}\mathcal{T}_m$$

$$\tilde{\mathcal{C}} = \mathcal{T}_p^{-1}\mathcal{C}\mathcal{T}_n$$

$$\tilde{\mathcal{D}} = \mathcal{T}_p^{-1}\mathcal{D}\mathcal{T}_m \tag{5.39}$$

All of the matrices $(\tilde{\cdot})$, are real infinite dimensional matrices.

If these similarity transforms are applied to the CMRHBE, then a modified form of the CMRHBE results,

$$0 = \tilde{\mathcal{P}}_c(\tilde{\mathcal{A}} - \tilde{\mathcal{N}}) + (\tilde{\mathcal{A}} - \tilde{\mathcal{N}})^T\tilde{\mathcal{P}}_c + \tilde{\mathcal{Q}}_c - \tilde{\mathcal{P}}_c\tilde{\mathcal{B}}\tilde{\mathcal{R}}_c^{-1}\tilde{\mathcal{B}}^T\tilde{\mathcal{P}}_c \tag{5.40}$$

where

$$\tilde{\mathcal{P}}_c = \mathcal{T}_n^*\mathcal{P}_c\mathcal{T}_n$$

$$\tilde{\mathcal{Q}}_c = \mathcal{T}_m^*\mathcal{Q}_c\mathcal{T}_m$$

$$\tilde{\mathcal{R}}_c = \mathcal{T}_n^*\mathcal{R}_c\mathcal{T}_n \tag{5.41}$$

The modified CMRHBE is composed of completely real matrices and the Riccati solution obtained is also a real matrix. Thus, a real ARE solver can be utilized in this instance without doubling the dimensionality of the CMRHBE. The resulting feedback gain matrix is then composed of the Fourier sine and cosine coefficients of the time periodic LQR gains, and is obtained via

$$\tilde{\mathcal{G}} = \tilde{\mathcal{R}}_c\tilde{\mathcal{B}}^T\tilde{\mathcal{P}}_c \tag{5.42}$$

The Fourier sine and cosine coefficients of the trigonometric Fourier series expansion of the time periodic LQR feedback gains are then obtained from the center block row of $\tilde{\mathcal{G}}$.

As before, a limiting process is implied in that the various quantities are truncated to contain N harmonics, and a limiting solution is sought as N grows large. Pragmatically, an ARE of order $(2N + 1)n$ will be solved on the computer. The above method was used to determine the time periodic LQR gains for the examples in this chapter, and proved to be very convenient.

5.2.4 Stability robustness of the steady state LQR

An important omission from the LQR theory for LTP systems is an indication of just how well the LQR compensation performs in terms of gain and phase margins, and if the plant

191

remains stable, in the face of plant uncertainty (as in unmodeled dynamics or uncertainty in the plant model). In the classical LTI theory, gain and phase margins are used to quantify this stability robustness. Until the frequency response notions in this thesis were developed, notions of stability robustness for LTP systems were not available, so that this important aspect of the design process could not be evaluated, nor even analyzed in any systematic way. In the following discussion, the stability robustness properties of the steady state LQR compensator will be examined using the tools developed thus far in this thesis. Essentially, the Kalman frequency domain inequality is derived for LTP systems.

From previous discussion, the harmonic balance form of the CMRDE was determined,

$$0 = \mathcal{P}_c(\mathcal{A} - \mathcal{N}) + (\mathcal{A} - \mathcal{N})^*\mathcal{P}_c + \mathcal{Q}_c - \mathcal{P}_c\mathcal{B}\mathcal{R}_c^{-1}\mathcal{B}^*\mathcal{P}_c \tag{5.43}$$

so that the feedback gains can be determined using the formula

$$\mathcal{G} = \mathcal{R}_c^{-1}\mathcal{B}^*\mathcal{P}_c \tag{5.44}$$

Now, add and subtract $s\mathcal{P}_c$ from the harmonic balance form of the CMRDE,

$$0 = -\mathcal{P}_c(s\mathcal{I} - \mathcal{A} + \mathcal{N}) - (-s\mathcal{I} - \mathcal{A}^* + \mathcal{N}^*)\mathcal{P}_c + \mathcal{Q}_c - \mathcal{P}_c\mathcal{B}\mathcal{R}_c^{-1}\mathcal{B}^*\mathcal{P}_c \tag{5.45}$$

Define

$$\mathcal{Q}_c = \mathcal{M}^*\mathcal{M} \tag{5.46}$$

Premultiply the above equation by $\mathcal{B}^*(-s\mathcal{I} - \mathcal{A}^* + \mathcal{N}^*)^{-1}$ and postmultiply by $(s\mathcal{I} - \mathcal{A} + \mathcal{N})^{-1}\mathcal{B}$ to obtain

$$\begin{aligned}
0 = {} & -\mathcal{B}^*(-s\mathcal{I} - \mathcal{A}^* + \mathcal{N}^*)^{-1}\mathcal{P}_c(s\mathcal{I} - \mathcal{A} + \mathcal{N})(s\mathcal{I} - \mathcal{A} + \mathcal{N})^{-1}\mathcal{B} \\
& -\mathcal{B}^*(-s\mathcal{I} - \mathcal{A}^* + \mathcal{N}^*)^{-1}(-s\mathcal{I} - \mathcal{A}^* + \mathcal{N}^*)\mathcal{P}_c(s\mathcal{I} - \mathcal{A} + \mathcal{N})^{-1}\mathcal{B} \\
& +\mathcal{B}^*(-s\mathcal{I} - \mathcal{A}^* + \mathcal{N}^*)^{-1}\mathcal{Q}_c(s\mathcal{I} - \mathcal{A} + \mathcal{N})^{-1}\mathcal{B} \\
& -\mathcal{B}^*(-s\mathcal{I} - \mathcal{A}^* + \mathcal{N}^*)^{-1}\mathcal{P}_c\mathcal{B}\mathcal{R}_c^{-1}\mathcal{B}^*\mathcal{P}_c(s\mathcal{I} - \mathcal{A} + \mathcal{N})^{-1}\mathcal{B}
\end{aligned} \tag{5.47}$$

Many of the above terms cancel, so that

$$\begin{aligned}
0 = {} & -\mathcal{B}^*(-s\mathcal{I} - \mathcal{A}^* + \mathcal{N}^*)^{-1}\mathcal{P}_c\mathcal{B}\mathcal{R}_c^{-1}\mathcal{R}_c \\
& -\mathcal{R}_c\mathcal{R}_c^{-1}\mathcal{B}^*\mathcal{P}_c(s\mathcal{I} - \mathcal{A} + \mathcal{N})^{-1}\mathcal{B} \\
& +\mathcal{B}^*(-s\mathcal{I} - \mathcal{A}^* + \mathcal{N}^*)^{-1}\mathcal{M}^*\mathcal{M}(s\mathcal{I} - \mathcal{A} + \mathcal{N})^{-1}\mathcal{B} \\
& -\mathcal{B}^*(-s\mathcal{I} - \mathcal{A}^* + \mathcal{N}^*)^{-1}\mathcal{G}_c^*\mathcal{R}_c\mathcal{G}_c(s\mathcal{I} - \mathcal{A} + \mathcal{N})^{-1}\mathcal{B}
\end{aligned} \tag{5.48}$$

192

Finally

$$
\begin{aligned}
0 = \; & -\mathcal{B}^*(-s\mathcal{I} - \mathcal{A}^* + \mathcal{N}^*)^{-1}\mathcal{G}_c^*\mathcal{R}_c \\
& -\mathcal{R}_c\mathcal{G}_c(s\mathcal{I} - \mathcal{A} + \mathcal{N})^{-1}\mathcal{B} \\
& +\mathcal{B}^*(-s\mathcal{I} - \mathcal{A}^* + \mathcal{N}^*)^{-1}\mathcal{M}^*\mathcal{M}(s\mathcal{I} - \mathcal{A} + \mathcal{N})^{-1}\mathcal{B} \\
& -\mathcal{B}^*(-s\mathcal{I} - \mathcal{A}^* + \mathcal{N}^*)^{-1}\mathcal{G}_c^*\mathcal{R}_c\mathcal{G}_c(s\mathcal{I} - \mathcal{A} + \mathcal{N})^{-1}\mathcal{B}
\end{aligned} \tag{5.49}
$$

Identify the following harmonic transfer functions,

$$
\begin{aligned}
\widehat{\mathcal{G}}_{LQR}(s) &= \mathcal{G}_c(s\mathcal{I} - \mathcal{A} + \mathcal{N})^{-1}\mathcal{B} \\
\widehat{\mathcal{G}}_{LQR}^*(s) &= \mathcal{B}^*(-s\mathcal{I} - \mathcal{A}^* + \mathcal{N}^*)^{-1}\mathcal{G}_c^*
\end{aligned} \tag{5.50}
$$

and

$$
\begin{aligned}
\widehat{\mathcal{G}}_c(s) &= \mathcal{M}(s\mathcal{I} - \mathcal{A} + \mathcal{N})^{-1}\mathcal{B} \\
\widehat{\mathcal{G}}_c^*(s) &= \mathcal{B}^*(-s\mathcal{I} - \mathcal{A}^* + \mathcal{N}^*)^{-1}\mathcal{M}^*
\end{aligned} \tag{5.51}
$$

By substituting the above into (5.49), the following result is obtained:

$$
0 = -\widehat{\mathcal{G}}_{LQR}^*(s)\mathcal{R}_c - \mathcal{R}_c\widehat{\mathcal{G}}_{LQR}(s) + \widehat{\mathcal{G}}_c^*(s)\widehat{\mathcal{G}}_c(s) - \widehat{\mathcal{G}}_{LQR}^*(s)\mathcal{R}_c\widehat{\mathcal{G}}_{LQR}(s) \tag{5.52}
$$

The first, second, and last terms can be grouped together,

$$
0 = \mathcal{R}_c - \left[\mathcal{I} + \widehat{\mathcal{G}}_{LQR}(s)\right]^* \mathcal{R}_c \left[\mathcal{I} + \widehat{\mathcal{G}}_{LQR}(s)\right] + \widehat{\mathcal{G}}_c^*(s)\widehat{\mathcal{G}}_c(s) \tag{5.53}
$$

The above equation is the LTP analog of the LTI version of the above equation, which was first introduced by MacFarlane [62]. The following inequality holds:

$$
\left[\mathcal{I} + \widehat{\mathcal{G}}_{LQR}(s)\right]^* \mathcal{R}_c \left[\mathcal{I} + \widehat{\mathcal{G}}_{LQR}(s)\right] \geq \mathcal{R}_c \tag{5.54}
$$

If we set $\mathcal{R}_c = \rho\mathcal{I}$, then the above equation simplifies to

$$
\left[\mathcal{I} + \widehat{\mathcal{G}}_{LQR}(s)\right]^* \left[\mathcal{I} + \widehat{\mathcal{G}}_{LQR}(s)\right] \geq \mathcal{I} \tag{5.55}
$$

Furthermore, it follows that

$$
\sigma_{min}\left\{\mathcal{I} + \widehat{\mathcal{G}}_{LQR}(s)\right\} \geq 1 \tag{5.56}
$$

From the isomorphism between the integral operator transfer function and the harmonic transfer function, we have that

$$
\sigma_{min}\left\{\mathcal{I} + \widehat{\mathcal{G}}_{LQR}(z)\right\} \geq 1 \tag{5.57}
$$

193

This result implies that none of the eigenloci of the LQR transfer function penetrate the unit circle centered on the -1 point in the Nyquist diagram. Thus, we can state the following lemmas concerning multiloop phase and gain margins of the LQR compensator.

Lemma 5.8 ($\pm 60°$ multiloop phase margin for steady state LQR for LTP systems) If $Q_c(t)$ is uniformly positive definite and T-periodic, and $R_c = \rho I$, and a phase shift of $\|\phi_i\| \leq 60°$ is introduced in each of the feedback loops associated with the ith control signal, $u_i(t)$, then the LQR compensated LTP system will remain asymptotically stable.

Proof: This follows directly from (5.57), and that the eigenloci of $\widehat{G}_{LQR}(z)$ do not penetrate the unit circle centered on the -1 point in the Nyquist diagram. □

We also obtain a gain margin property for the steady state LQR problem for LTP systems.

Lemma 5.9 (Multiloop infinite upward gain margin and one half downward gain margin for the steady state LQR for LTP systems) If $Q_c(t)$ is uniformly positive definite and T-periodic, and $R_c = \rho I$, then the insertion of linear constant gains $k_i \geq \frac{1}{2}$ in each of the feedback loops $u_i(t)$ of the LQR compensated LTP system will leave the closed loop system asymptotically stable.

Proof: Again, this follows directly from (5.57), and that the eigenloci of $\widehat{G}_{LQR}(z)$ do not penetrate the unit circle centered on the -1 point in the Nyquist diagram.

Remark: These results are completely analogous to the gain and phase margin properties of the LQR determined for LTI systems by Safonov and Athans [88]. □

In practice, the assumption that $R_c = \rho I$ is not a limiting assumption since scaling can always be introduced by setting $B(t) \rightarrow B(t)R_c(t)^{\frac{1}{2}}$ and $R_c(t) = I$ in the CMRDE.

5.2.5 Stabilization of the lossy Mathieu equation

In this section, the lossy Mathieu equation will be examined as the open loop plant, and the stability robustness properties of two different compensation schemes will be determined. In the first case, the control law will be a static (time invariant) output feedback of the displacement measurement. In the second case, an LQR compensation scheme will be implemented.

Stabilization using displacement feedback

In many instances, static output feedback is used to stabilize a system. A simple way to design such a compensation scheme is direct application of the Nyquist criterion. The following example will illustrate how the Nyquist diagram can be used to design a static output feedback law, and how to evaluate the gain and phase margins.

Consider the lossy Mathieu equation, for which

$$
\begin{aligned}
A(t) &= \begin{bmatrix} 0 & 1 \\ -(a - 2q\cos\omega_p t) & -2\zeta \end{bmatrix} \\
B &= \begin{bmatrix} 0 \\ 1 \end{bmatrix} \\
C &= \begin{bmatrix} 1 & 0 \end{bmatrix}
\end{aligned}
\tag{5.58}
$$

Here, the parameter values will be $a = 5$, $q = 4$, $\omega_p = 2$, and $\zeta = 0.2$. The open loop z–plane poles are given by $z_1 = 3.4380$ and $z_2 = 0.0828$. The corresponding open loop s–plane poles are given by $s_1 = 0.3931$ and $s_2 = -0.7931$. We wish to design a feedback law, using displacement feedback, of the form

$$
y(t) = - \begin{bmatrix} k_d & 0 \end{bmatrix} x(t)
\tag{5.59}
$$

that stabilizes the above system. Thus, if the Nyquist test is applied, a stabilizing value of feedback gain will be given by those portions of the real axis enclosed by a CCW encirclement in the Nyquist diagram. In this example, the design will be driven by gain and phase margin specifications. In particular, minimal specifications of downward gain margin $\underline{\text{GM}} < \frac{1}{2}$ upward gain margin $\overline{\text{GM}} > 2$, and phase margin PM > 45 degrees, are to be satisfied.

The Nyquist diagram for this case is shown in Figure 5.2. The negative real axis is enclosed by a CCW encirclement for $-\frac{1}{k} \in [-0.59, 0]$. Thus, negative values of stabilizing feedback are given by $k \in [1.68, \infty)$. In order to achieve reasonable values of gain margin, the feedback gain chosen is $k_d = 5$. This choice of feedback gain produces an upward gain margin of $\overline{\text{GM}} \to \infty$ and a downward gain margin of $\underline{\text{GM}} = \frac{1}{3}$. These values of gain margin are deduced by considering how much gain can be introduced without destabilizing the closed loop system (that is, without losing the required CCW encirclement of the $-\frac{1}{k}$ point). However, the phase margin for this system is very poor. The phase margin is
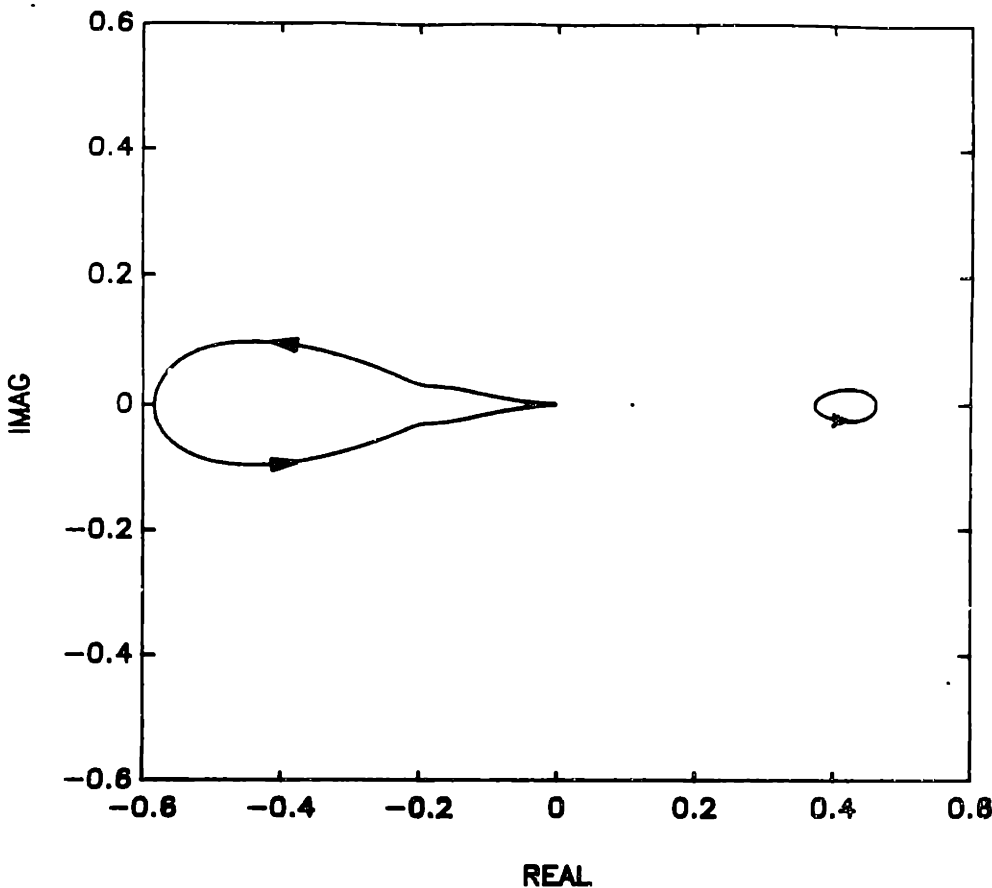
Figure 5.2: Nyquist diagram for lossy Mathieu equation with displacement feedback.

---

evaluated by first drawing a circle centered at the origin, of radius $\frac{1}{k_d}$. Then the point on this circle that intersects the Nyquist diagram, say p_0, is determined. The angle from the negative real axis to the line segment drawn from the origin to p_0 is the value of the phase margin, PM. Usually, compensation is added to the system, so that the closed loop system will have phase margin in the range of 45 to 60 degrees. In this case, the phase margin is PM = 8.2 degrees, which is insufficient.

Therefore, an alternative design strategy should be applied to enhance the phase margin specification.

Stabilization using displacement and rate feedback

In developing the stability robustness properties of the steady state LQR for LTP systems, it was determined that the LQR provided at least 60 degrees of phase margin and good gain margins, that is, infinite upward gain margin and downward gain margin of at least one half.

196

In addition, the LQR problem provides a systematic way of incorporating rate feedback. In this example, the LQR gains are determined using the harmonic balance methods described earlier. In addition, the gain and phase margins of the LQR design are evaluated.

The state weighting matrix is selected to be

$$Q = \begin{bmatrix} 1 & 0 \\ 0 & 0.1 \end{bmatrix} \tag{5.60}$$

and the control weight is selected to be $\rho = 0.01$. The resulting LQR gains are shown in Figure 5.3. The numerical method described above that exploited the unitary transformation was used. In this case, $N = 10$ harmonics proved to be sufficient for the first six harmonics of the control gain matrix to converge to four decimal places. The Fourier coefficient associated with the seventh harmonic of the LQR gain matrix, $G(t)$, was less than 1×10^{-4}, so that the Fourier series associated with the LQR gains was truncated after six terms.

The Nyquist diagram of the LQR transfer function, obtained from the LTP state space model, $S = [A(t), B(t), G(t)]$, is plotted in Figure 5.4. For values of feedback gain on the negative real axis, the Nyquist diagram does not penetrate the unit circle centered on the -1 point, so that the phase margin is at least 60 degrees, there is downward gain margin of at least one half, and (ideally) infinite upward gain margin. The actual value of the phase margin is 77 degrees, which is more than adequate. The downward gain margin is $\underline{GM} = \frac{1}{9}$. The upward gain margin is infinite, but only in an ideal sense due to physical limitations.

5.3 LTI Compensation for Weakly Periodic Systems

The time periodic parametric excitation in an LTP system is often a small effect. Thus, in this situation, it would be desirable to design a compensator without having to account for the periodic effects in the design plant model. In this section, a compensation technique is described that lumps the weakly periodic effects into a modeling error. In this way, the stability of the closed loop system can be determined, in terms of the modeling error, using the Small Gain Theorem. The design plant model is the LTI state space model embedded in the LTP state space model (that is, the average state space model), so that LTI design procedures can be applied.

197
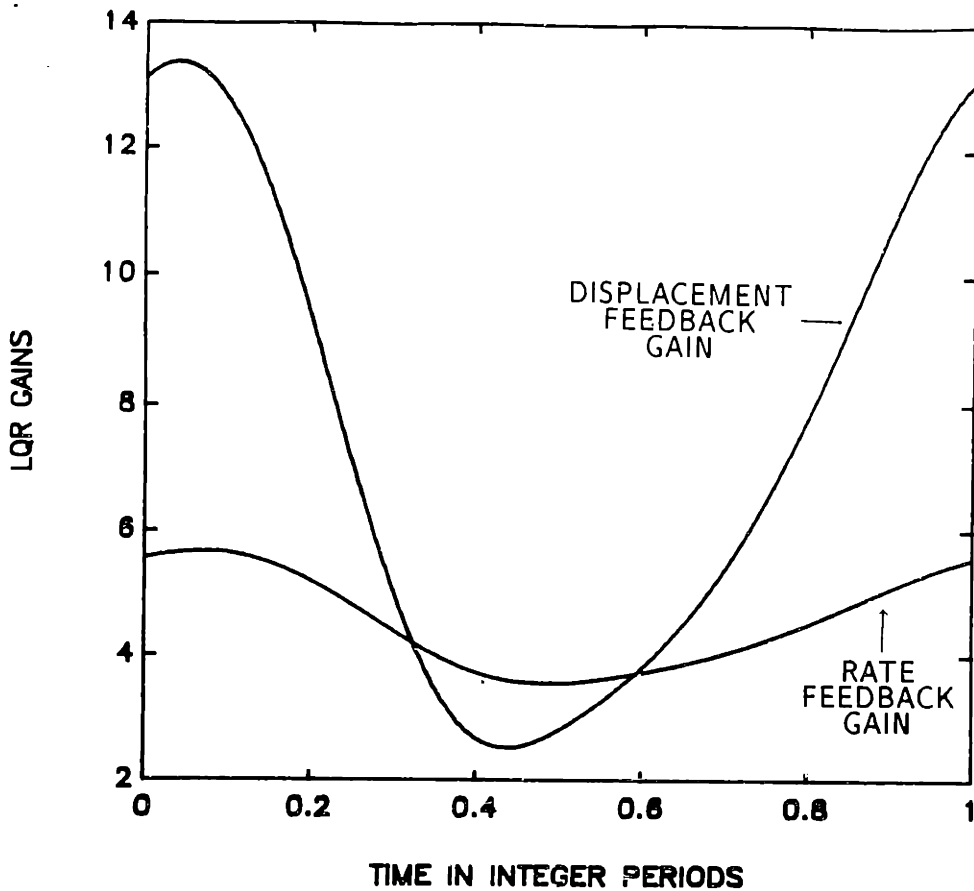
Figure 5.3: LQR gains for lossy Mathieu equation. The LQR methodology provides a systematic method for determining time periodic feedback gains.

5.3.1 Design plant model and modeling error

Here, we consider the state space model of a linear time periodic system, $S = [A(t), B(t), C(t)]$. However, the design plant model, to which the control design techniques are to be applied, will be time invariant. The embedded LTI model, that is, the average state space model over a period, will be designated as the design plant model, and will be denoted by $S_0 = [A_0, B_0, C_0]$. Thus, the average state space model consists of the zeroth Fourier coefficients of the LTP state space model. However, the average state space model is not unique, since a similarity transformation may change the average value of the system matrices for the transformed states. Of course, the design plant model must satisfy the usual requirements of controllability/stabilizability, and observability/detectability.

It should be noted that the embedded LTI model may in fact be nonsensical in some instances. For example, if the control distribution matrix, $B(t)$, consisted solely of sinu-
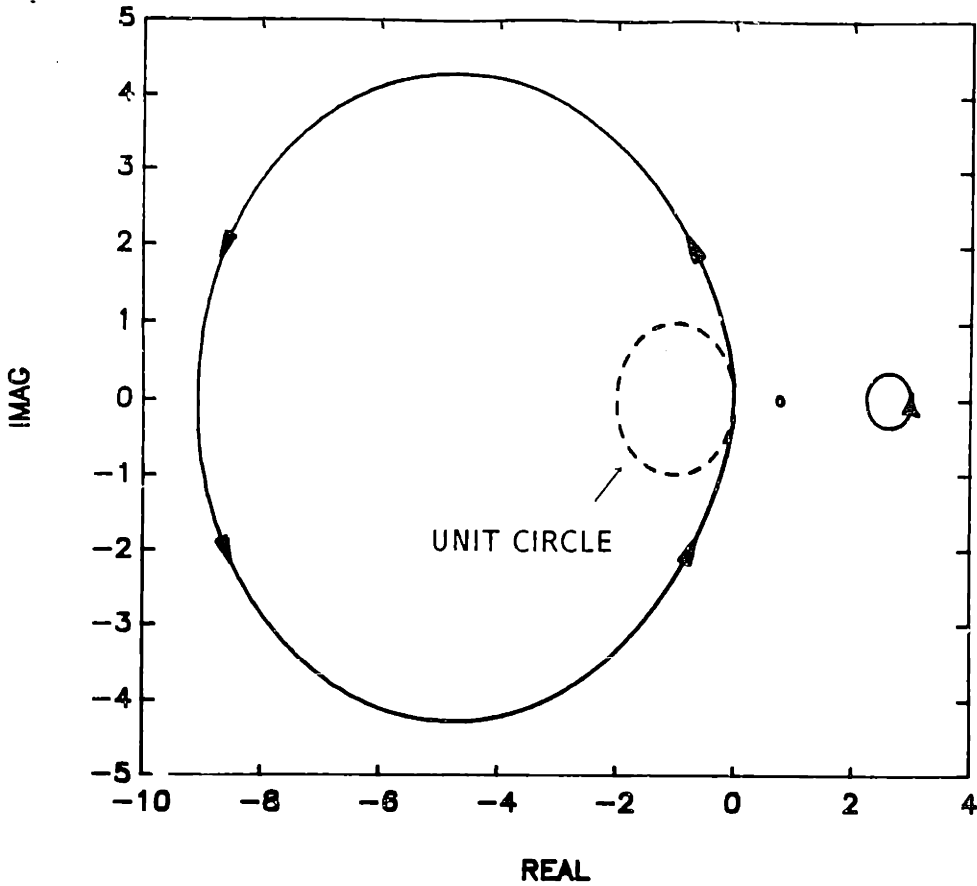
Figure 5.4: Nyquist diagram of LQR transfer function for lossy Mathieu equation. The Nyquist diagram does not penetrate the unit circle centered on the −1 point. This diagram demonstrates that the LQR design provides at least 60 degrees of phase margin, infinite upward gain margin, and a downward gain margin of at least one half.

soids, then the average control distribution matrix would be a zero matrix. Therefore, the embedded LTI model would be uncontrollable. This situation can occur in the control of blade pitch of a helicopter rotor, when the control effort is the lateral and longitudinal cyclic blade pitch, which introduces sine and cosine modulations in the control distribution matrix. This situation has in fact occurred in research performed by the author [43].

Hence, the implication here is that the embedded LTI model, or the average state space model, must account for all of the important behavior of the system. However, how does one quantify the "importance" of various dynamic effects? A simple way to characterize the importance of the time periodic effects is to treat them as a modeling error. This error can be either additive or multiplicative (which is usually more convenient because the resulting stability robustness boundaries, or uncertainty templates, do not depend on

the compensator). Then using a small gain argument, the impact of the modeling error on closed loop bandwidth and gain can be characterized. In this way, LTI compensation can be applied to the design plant model or embedded LTI model, and stability guaranteed (in a sufficient sense) in the face of the periodic dynamics that were omitted from the design plant model.

In the sequel, this type of modeling error will be treated as an unstructured uncertainty.

5.3.2 Unstructured uncertainty and templates

In the LTI control theory, the notion of unstructured uncertainty plays a central role in the study of stability robustness. Uncertainty can be unstructured in that it is expressed as a bound on the magnitude (or of the phase in some cases) of possible perturbations, but does not attempt to identify the specific element of the plant that produces the perturbation. The notion of unstructured uncertainty can be easily extended to LTP systems.

Unstructured uncertainty is commonly expressed in three forms. If we denote the actual plant by $\widehat{G}(z)$, and the design plant model by $\widehat{G}_0(z)$, then the LTP transfer function can be expressed in one of the following ways:

$$
\begin{aligned}
\widehat{G}(z) &= \widehat{G}_0(z) + \Delta_a(z) \\
\widehat{G}(z) &= \widehat{G}_0(z)\left[\check{I} + \Delta_i(z)\right] \\
\widehat{G}(z) &= \left[\check{I} + \Delta_o(z)\right]\widehat{G}_0(z)
\end{aligned}
\tag{5.61}
$$

Here, $\Delta_a(z)$ is referred to as an *additive perturbation*, $\Delta_o(z)$ is referred to as the *output multiplicative perturbation*, and $\Delta_i(z)$ is referred to as the *input multiplicative perturbation*. The only restriction placed on these perturbations is on their size, which is given by $\|\Delta(z)\|_\infty$. Of course, this is computed using the SVD of the truncated harmonic transfer function. The following results are simple extensions of the LTI results developed in part by Lehtomaki [60], with a more comprehensive treatment in a textbook by Maciejowski [65].

The additive error can be utilized to guarantee stability in the face of modeling error. We consider a compensator denoted by $\widehat{K}(z)$, that stabilizes the design (nominal) plant model. In addition, we require that the design and the actual plant have the same number of unstable poles. Since the loop is stable for $\Delta_a(z) = 0$, then the loop will remain stable as long as no eigenloci of the open loop transfer function passes through the -1 point. This

is equivalent to requiring that the Fredholm determinant satisfy

$$\left| \tilde{I} + \widehat{G}(e^{j\theta})\widehat{K}(e^{j\theta}) \right| \neq 0 \tag{5.62}$$

for all $\theta \in (-\pi, \pi]$. This is equivalent to saying that

$$\sigma_{min}\left[\tilde{I} + \widehat{G}(e^{j\theta})\widehat{K}(e^{j\theta}) \right] > 0 \tag{5.63}$$

for $\theta \in (-\pi, \pi]$. Then

$$\sigma_{min}\left[\tilde{I} + \widehat{G}_0(e^{j\theta})\widehat{K}(e^{j\theta}) + \Delta_a(e^{j\theta})\widehat{K}(e^{j\theta}) \right] > 0 \tag{5.64}$$

so that

$$\sigma_{min}\left[\tilde{I} + \widehat{G}_0(e^{j\theta})\widehat{K}(e^{j\theta}) \right] > \sigma_{max}\left[\Delta_a(e^{j\theta})\widehat{K}(e^{j\theta}) \right] \tag{5.65}$$

Thus, if the above inequality holds for all $\theta \in (-\pi, \pi]$, then the system remains stable in the face of the additive perturbation. The RHS of the above inequality is referred to as the *stability robustness boundary* or *template* for the additive perturbation. But, the compensator transfer function shows up in both sides of the above equation (which is the usual case for additive errors, see [60, pages 80–88]). It should also be noted that the above stability robustness condition is sufficient, but not necessary. From an engineering standpoint, we would rather have a method leading to separate evaluation of a stability robustness boundary, or template, that can be computed *a priori*, so that subsequent design iterations can be compared against the template.

The output multiplicative error can be used in such a manner. Again, we consider a compensator denoted by $\widehat{K}(z)$, that stabilizes the design plant model. In addition, we require that the nominal and the actual plant have the same number of unstable poles. Since the loop is stable for $\Delta_o(z) = 0$, then the loop will remain stable as long as no eigenloci of the open loop transfer function passes through the -1 point. This is equivalent to requiring that the Fredholm determinant satisfy

$$\left| \tilde{I} + \widehat{G}(e^{j\theta})\widehat{K}(e^{j\theta}) \right| \neq 0 \tag{5.66}$$

where $\theta \in (-\pi, \pi]$. This is equivalent to saying that

$$\sigma_{min}\left[\tilde{I} + \widehat{G}(e^{j\theta})\widehat{K}(e^{j\theta}) \right] > 0 \tag{5.67}$$

for $\theta \in (-\pi, \pi]$. Now, the above can be expanded in terms of the output multiplicative perturbation,

$$\sigma_{min} \left[\tilde{I} + \widehat{G}_0(e^{j\theta})\widehat{K}(e^{j\theta}) + \Delta_o(e^{j\theta})\widehat{G}_0(e^{j\theta})\widehat{K}(e^{j\theta}) \right] > 0 \qquad (5.68)$$

or

$$\sigma_{min} \left\{ \left[\tilde{I} + \left(\Delta_o(e^{j\theta})\widehat{G}_0(e^{j\theta})\widehat{K}(e^{j\theta}) \right)^{-1} + \Delta_o^{-1}(e^{j\theta}) \right] \Delta_o(e^{j\theta})\widehat{G}_0(e^{j\theta})\widehat{K}(e^{j\theta}) \right\} > 0 \quad (5.69)$$

This implies that

$$\sigma_{min} \left[\tilde{I} + \left(\Delta_o(e^{j\theta})\widehat{G}_0(e^{j\theta})\widehat{K}(e^{j\theta}) \right)^{-1} + \Delta_o^{-1}(e^{j\theta}) \right] > 0 \qquad (5.70)$$

and grouping terms

$$\sigma_{min} \left\{ \tilde{I} + \left[\left(\widehat{G}_0(e^{j\theta})\widehat{K}(e^{j\theta}) \right)^{-1} + \tilde{I} \right] \Delta_o^{-1}(e^{j\theta}) \right\} > 0 \qquad (5.71)$$

Recall a property of the $\|\cdot\|_\infty$ operator norm,

$$\max(0, \sigma_{min}(Q) - 1) \le \sigma_{min}(Q + I) \le \sigma_{min}(Q) + 1 \qquad (5.72)$$

so that the lower bound yields

$$\sigma_{min} \left\{ \left[\tilde{I} + \left(\widehat{G}_0(e^{j\theta})\widehat{K}(e^{j\theta}) \right)^{-1} \right] \Delta_o^{-1}(e^{j\theta}) \right\} > 1 \qquad (5.73)$$

Then

$$\sigma_{min} \left[\tilde{I} + \left(\widehat{G}_0(e^{j\theta})\widehat{K}(e^{j\theta}) \right)^{-1} \right] \sigma_{min} \left[\Delta_o^{-1}(e^{j\theta}) \right] > 1 \qquad (5.74)$$

which implies that

$$\sigma_{max} \left[\tilde{I} + \left(\widehat{G}_0(e^{j\theta})\widehat{K}(e^{j\theta}) \right)^{-1} \right] \sigma_{max} \left[\Delta_o(e^{j\theta}) \right] < 1 \qquad (5.75)$$

The above statement is just another way of stating the Small Gain Theorem. A more useful form of the above equation is given by

$$\sigma_{max} \left[\tilde{I} + \left(\widehat{G}_0(e^{j\theta})\widehat{K}(e^{j\theta}) \right)^{-1} \right] < \frac{1}{\sigma_{max}\left[\Delta_o(e^{j\theta}) \right]} \quad \forall\, \theta \in (-\pi, \pi] \qquad (5.76)$$

Thus, if the above inequality holds for all $\theta \in (-\pi, \pi]$, the system remains stable in the face of the output multiplicative perturbation. Again, the RHS of the above equation is the *stability robustness boundary* (SRB) or *template* for the output multiplicative perturbation. A useful property of the above template is that it is independent of the choice of compensator. Thus,

202

the SRB can be plotted on a principal gain diagram *a priori*, so that all subsequent design iterations can be compared against it in order to guarantee stability in the face of the output multiplicative perturbation. It is usually more convenient to use a different but equivalent form of (5.76) given by

$$\sigma_{max}\left[\widehat{G}_0(e^{j\theta})\widehat{K}(e^{j\theta})\left(\check{I} + \widehat{G}_0(e^{j\theta})\widehat{K}(e^{j\theta})\right)^{-1}\right] < \frac{1}{\sigma_{max}\left[\Delta_o(e^{j\theta})\right]} \quad \forall\, \theta \in (-\pi, \pi] \quad (5.77)$$

Clearly, the LHS is the closed loop transfer function, so that the above formula is an equivalent statement of the Small Gain Theorem.

The input multiplicative perturbation could have been used to develop a similar stability robustness rule. The comparable result is

$$\sigma_{max}\left[\check{I} + \left(\widehat{K}(e^{j\theta})\widehat{G}_0(e^{j\theta})\right)^{-1}\right] < \frac{1}{\sigma_{max}\left[\Delta_i(e^{j\theta})\right]} \quad \forall\quad \theta \in (-\pi, \pi] \quad (5.78)$$

Thus, if the above inequality holds for all $\theta \in (-\pi, \pi]$, then the system remains stable in the face of the input multiplicative perturbation. The above inequality is equivalent to

$$\sigma_{max}\left[\left(\check{I} + \widehat{K}(e^{j\theta})\widehat{G}_0(e^{j\theta})\right)^{-1}\widehat{K}(e^{j\theta})\widehat{G}_0(e^{j\theta})\right] < \frac{1}{\sigma_{max}\left[\Delta_i(e^{j\theta})\right]}\forall\quad \theta \in (-\pi, \pi] \quad (5.79)$$

where the LHS is just the maximum closed loop transfer function gain.

The sufficient stability conditions presented above are special cases of the Small Gain Theorem, which states that a feedback loop consisting of stable operators will remain stable if the product of the induced infinity norm of each operator is less than one.

5.3.3 LTI compensation for the lossy Mathieu equation

In this section, we consider the LTI compensation of a linear time periodic system for which the periodic dynamic dynamic effects are small, that is, a weakly periodic system. Consider a stable configuration of the the lossy Mathieu equation in (5.58), for which the following parameters are selected: $a = 10$, $q = \frac{3}{4}$, $\omega_p = 2$, and $\zeta = 0.2$. The objective here is to design a regulator that rejects output disturbances. Since the value of the pumping amplitude, q, is quite small, it is reasonable to expect that an LTI compensation technique, such as the LQR compensator, could be applied, and that reasonable results would be obtained. Here, the periodic effects will be treated as an output multiplicative error, and the LTI compensation will be designed to maintain stability robustness.

The actual plant will be denoted by $\widehat{G}(z)$. The design plant model (or nominal plant) in this case will be the average state space model, $S_o = [A_o, B_o, C_o]$, which corresponds

to the LTP transfer function, $\widehat{G}_0(z)$. These two transfer functions differ by the additive perturbation

$$\widehat{G}(z) = \widehat{G}_0(z) + \Delta_a(z) \tag{5.80}$$

so that

$$\widehat{G}(z) = \left(\check{I} + \Delta_a(z) \widehat{G}_0^{-1}(z) \right) \widehat{G}_0(z) \tag{5.81}$$

Thus, the output multiplicative perturbation is given by

$$
\begin{aligned}
\Delta_o(z) &= \Delta_a \widehat{G}_0^{-1}(z) \\
&= \left(\widehat{G}(z) - \widehat{G}_0(z) \right) \widehat{G}_0^{-1}(z) \\
&= \widehat{G}(z) \widehat{G}_0^{-1}(z) - \check{I}
\end{aligned}
\tag{5.82}
$$

Thus, the maximum singular values of the output multiplicative perturbation can be computed *a priori*, and a compensation technique applied to the embedded LTI system represented by the design plant model. Thus, the LTI compensation can be designed using the stability robustness rule in (5.76). It should be noted that the various principal gain diagrams are computed using the respective harmonic transfer functions.

In Figure 5.5a, the uncertainty template for the output multiplicative perturbation is plotted. From the figure, it is clear that the closed loop LTP transfer function can have a maximum principal gain of 0 dB. Therefore we can expect good performance from a regulator design. The stability robustness rule from (5.76) states that none of the closed loop principal gain loci can be greater than this uncertainty template. The open loop LTP principal gain diagram is plotted in Figure 5.5b, and from it we conclude that we can increase the gain by reducing the peak magnitude. Since the uncertainty template is periodic in frequency, a LTI Bode gain diagram can be constructed where the uncertainty template is plotted over all frequencies, as shown in Figure 5.5c. The Bode gain diagram of the average state space model or the LTI design plant model is also shown. The LTI Bode gain diagram is simply the unfolded version of the LTP principal gain diagram of the LTI design plant model.

Thus, as long as the closed loop Bode gain does not exceed the uncertainty template in Figure 5.5c, then the system will remain stable even though no periodic effects were included in the design plant model. A set of LQR feedback gains was computed for the
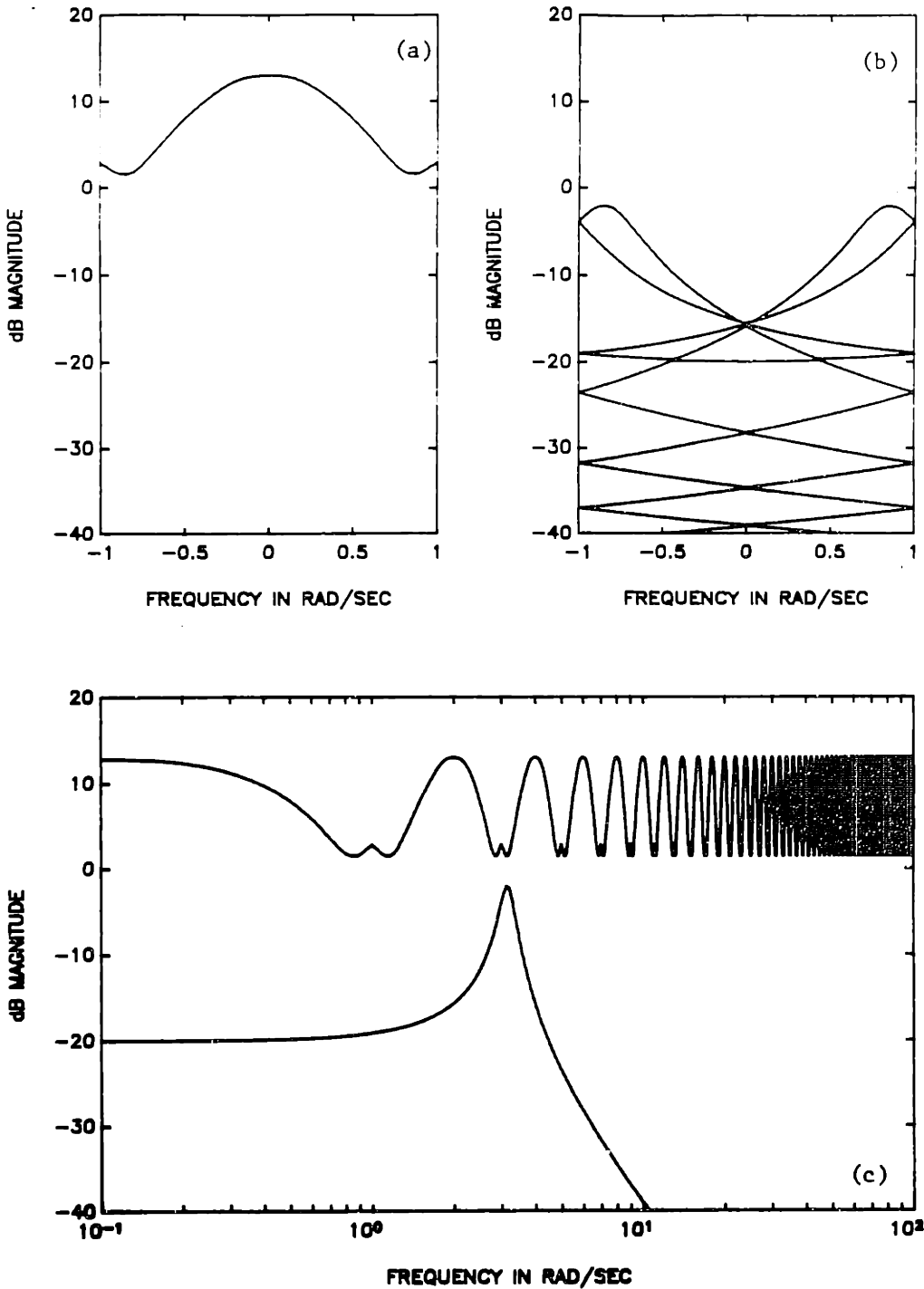
**Figure 5.5:** Uncertainty template and open loop principal gain diagram for lossy Mathieu equation (a) Uncertainty template for output multiplicative perturbation that includes all periodic effects. (b) Open loop principal gain diagram for embedded LTI model or average state space model. (c) Since the uncertainty template is periodic, the LTI Bode gain diagram can be compensated by unfolding the LTP principal gain diagram.
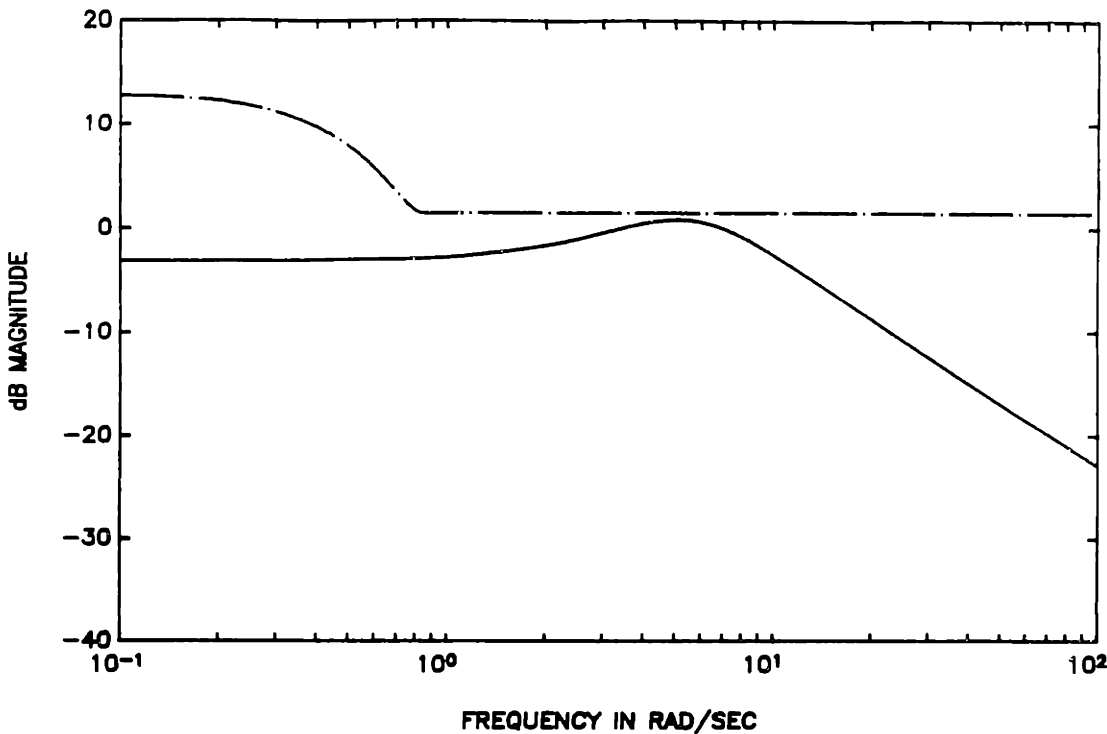
Figure 5.6: Lossy Mathieu equation compensated using time invariant formulation of the LQR The uncertainty template has been simplified to be the dashed line. Time invariant LQR provides satisfactory design in terms of stability robustness to time periodic effects.

design plant model by selecting

$$Q_c = \begin{bmatrix} 10 & 0 \\ 0 & 0.1 \end{bmatrix}, \quad \rho = 0.01 \tag{5.83}$$

to produce the feedback gain matrix

$$G_o = \begin{bmatrix} 23.16 & 7.12 \end{bmatrix} \tag{5.84}$$

The LTI Bode gain diagram is plotted in Figure 5.6. A simplified uncertainty template is also shown in Figure 5.6 as a dashed line. Figure 5.6 illustrates that the LQR transfer function will remain stable in the face of the time periodic effects, since the maximum singular value of the LQR transfer function is less than the uncertainty template for all frequency.

The Nyquist diagram of the LQR transfer function of the actual system, $S_{LQR} = [A(t), B(t), G_o]$, is plotted in Figure 5.7. The Nyquist diagram of the compensated LTP

system does not penetrate the unit circle centered on the -1 point, therefore, we conclude that the phase and gain margins are excellent. In fact, the phase margin is PM = 72 degrees. The LTP system compensated using time invariant LQR gains also has (ideally) infinite upward gain margin, and the downward gain margin is zero (this is because the open loop system was stable). Thus, it is clear that the time invariant LQR design was a conservative compensation technique due to the application of the stability robustness rule. There is still plenty of gain and phase margin that could be exploited in terms of improving time responses, and other design criterion not considered here.

5.3.4 Truncation of harmonics in the LTP state space model

The above procedure can be applied when the number of harmonics in the design plant state space model is truncated. In this case, the design plant, $\widehat{G}_o(z)$, would correspond to a state space model where the Fourier series associated with each system matrix was truncated to N terms. The additive perturbation, $\Delta_a(z)$, would contain the remaining terms, and the output multiplicative perturbation could be computed in the same way as shown above. The design of an LTP controller could then be carried out for a state space model with N harmonics, and stability guaranteed even though all of the periodic behavior was not included in the design plant model.

5.4 Summary

In this chapter, some stability robustness ideas from the LTI control theory were applied to LTP systems. This was possible to do in this case because the Small Gain Theorem was directly applicable to LTP systems due to the operator theoretic framework developed in Chapter 3 and due to the Nyquist criterion developed in Chapter 4. Two applications of the Small Gain Theorem were developed. The first was an examination of the gain and phase margins of the steady state LQR problem for LTP systems. The second was a compensation technique for weakly periodic systems.

In summary, the steady state LQR problem for LTP systems was shown to exhibit excellent gain and phase margin properties. The ideal steady state LQR problem guarantees a minimum of 60 degrees of phase margin, infinite upward gain margin, and a downward gain margin of at least one half. This result is identical to that for the LTI case. In addition,
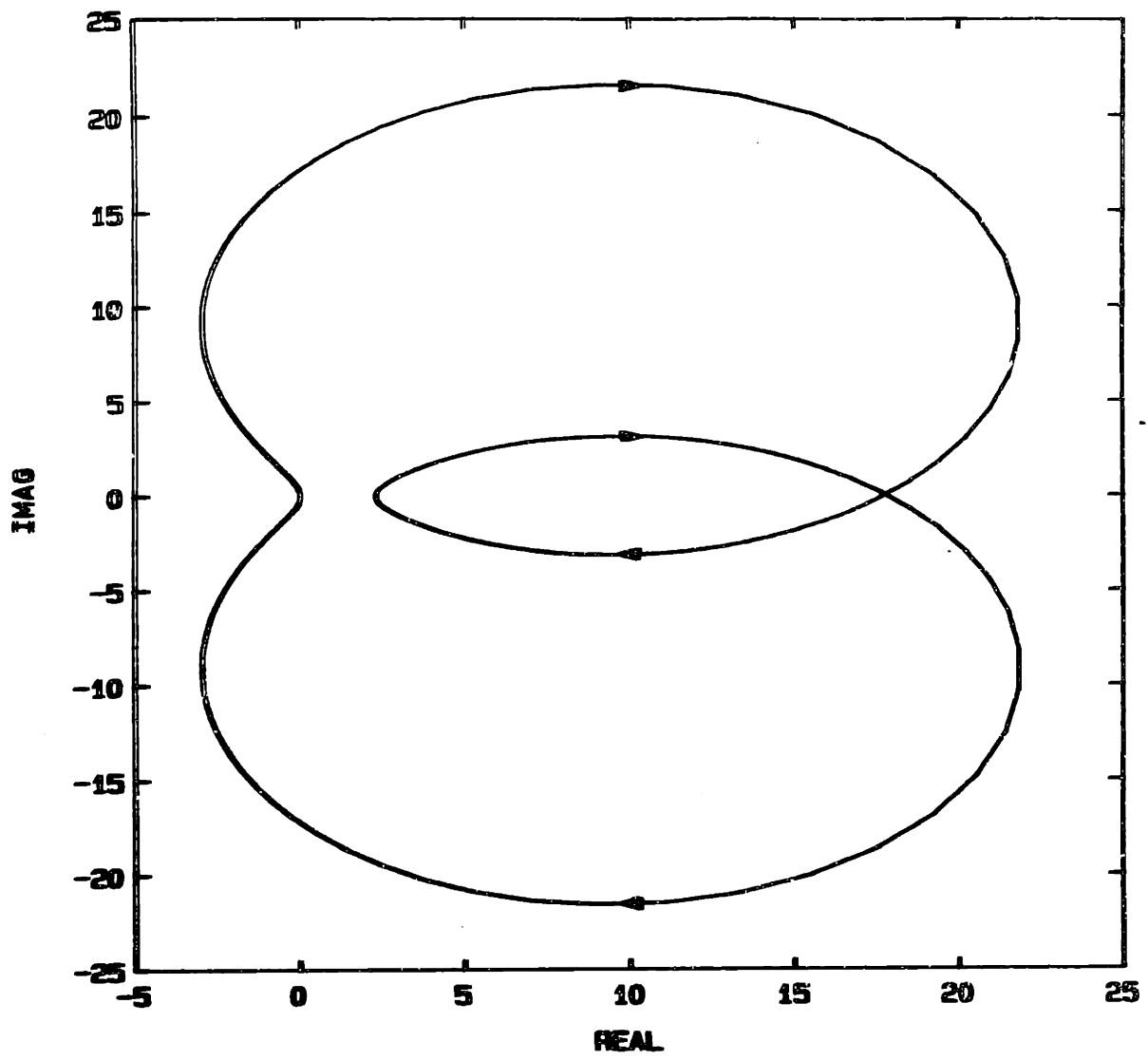
Figure 5.7: LTP Nyquist diagram of lossy Mathieu equation with time invariant LQR compensation. The time invariant LQR compensated lossy Mathieu equation has at least 60 degrees of phase margin and excellent gain margins.

a new method for computing the LQR gains was discussed, using the harmonic balance methodology and the Toeplitz transform. The Nyquist methodology was then applied to an unstable SISO configuration of the lossy Mathieu equation. It was shown that the eigenloci of the LQR transfer function did not penetrate the unit circle centered on the -1 point in the Nyquist diagram, thereby demonstrating the stability robustness properties of the LQR problem for LTP systems.

A compensation technique was developed that treats the periodic effects in the LTP state space model as a perturbation of the average state space model. This permits an LTI compensation technique to be applied to the average state space model, although it was shown that this approach results in a very conservative treatment of the periodic effects.

[Page Left Blank]

Chapter 6

Conclusion

Prior to this research, a relatively complete open loop stability analysis theory was available for LTP systems in the Floquet and Hill Theory (harmonic balance). In addition, there was a relatively complete LQG design procedure for LTP systems based on a calculus of variations approach, although no frequency domain interpretation of the LQG properties was available. In this thesis, a frequency domain interpretation for LTP systems was provided in a linear operator framework, and the transfer properties of the resulting operators were developed. This research bridges the gap between the classical results of Floquet and Hill, and the modern results of the LQG theory for LTP systems, with frequency domain notions for LTP systems that are analogous to those for multivariable LTI systems.

In this chapter, the results of this thesis are reviewed briefly, and some directions for future research are suggested.

6.1   Summary and Conclusions

The primary objective of this thesis was to introduce a linear operator for LTP systems that is analogous to the transfer function for LTI systems. In Chapter 3, a frequency domain theory for LTP systems was sought that is comparable to frequency response notions for LTI systems (with certain caveats concerning directional properties in the multivariable case).

First, the fundamentally important signal space of geometrically periodic (GP) signals was identified, using insight gleaned from the Floquet theory. The input test signal was then defined to be bounded and to have the property that the signal varied geometrically

from the beginning of one period to the beginning of the next period. It was determined that if a GP test input signal were injected at the input of an LTP plant, the steady state and steady output response were also GP signals. In addition, the transient responses to a GP signal were determined. Since the objective was to determine a transfer function, a linear map between the input signal space and the output signal space was required. The linear operator that described this linear map was the integral operator transfer function, $\widehat{G}(z)$, which was the steady output response to a GP signal.

An associated integral operator state space model was then defined, that described the evolution of the state, $\tilde{x}_k$, from the beginning of the kth period to the beginning of the $(k+1)$st period, $\tilde{S} = [\tilde{A}, \tilde{B}, \tilde{C}, \tilde{D}]$. The integral operator state space model provided a concise representation of the integral operators describing the system behavior. Using the the integral operator/linear operator framework, notions of poles, zeroes, principal gains, and phase, along with their directional properties, were developed.

Although the integral operator approach provided a clear and concise conceptual framework for the study of LTP systems, the integral operator approach does not provide numerical techniques directly. In the integral operator theory, most authors resort to a time discretization of the integral operator kernel in order to develop numerical techniques. In this thesis, a different approach is advocated. Since the time periodic parametric excitation in most engineering systems can be described by a truncated complex Fourier series, an approach called the harmonic balance methodology or Hill theory was used that exploited this tendency.

Essentially the periodic portion of the GP signal is expanded in a complex Fourier series. The exponentially modulated periodic (EMP) signal is a complex exponential modulation of a complex Fourier series, and is a series expansion of the GP signal. The transient and steady state responses were then developed using the EMP test input signal. The steady output response was also an EMP signal, so that EMP signals induce a one-to-one map at steady state. The steady output response was then modified, by applying the principle of harmonic balance, to obtain a linear operator called the harmonic transfer function (HTF).

The HTF, denoted by $\hat{\mathcal{G}}(s)$, maps the Fourier coefficients of the EMP test input signal to the Fourier coefficients of the EMP output signal. The associated harmonic state space model, $\mathcal{S} = [(\mathcal{A}\text{-}\mathcal{N}), \mathcal{B}, \mathcal{C}, \mathcal{D}]$, was proposed as an alternative to the LTP state space model, where $\mathcal{A}$ is the infinite dimensional block Toeplitz matrix associated with the Fourier coef-

ficients of $A(t)$. Notions of poles, zeroes, principal gains, phase, and all of their associated directional properties were then developed. By truncating the infinite dimensional eigenvalue problems, numerical methods were developed that were easily implemented on the computer. The directional properties of the LTP system were found to be manifested in the multivariable (multi–input multi–output) nature of the LTP state space model, as well as in the infinite number of Fourier coefficients required to describe an arbitrary periodic signal.

All of the above techniques were developed because there was no theoretical framework that provided the basic open loop analysis tools required to examine the behavior of an LTP system. In fact, no other research has ever appeared that attempts to describe the explicit input–output relationship between signals of fundamental importance to LTP systems, such as is done in this thesis.

Therefore, in Chapter 3 several contributions were made in understanding the transfer properties of LTP systems using the integral operator formulation of the LTP transfer function:

a) Formal definition of the geometrically periodic (GP) signal as the test input signal of interest for LTP systems and its relation to the Floquet theory. The alternative representation of the GP signal called an exponentially modulated periodic signal and its connection to the Hill theory and harmonic balance.

b) The integral operator or LTP transfer function, which describes the explicit input–output relationship between GP input and GP output at steady state, and the associated integral operator state space model.

c) The definition of LTP poles as locations in the z-plane where the LTP transfer function loses analyticity. The associated z-plane pole eigenvalue problem, and its replication of the Floquet poles.

d) The definition of transmission zeroes of the LTP system, and the physical interpretation of the zeroes as having the transmission blocking property. The associated z–plane transmission zero eigenvalue problem was developed.

The integral operator formulation was found to be useful in an analytical context, but a set of numerical procedures was necessary to compute these transfer properties. Thus, a

213

set of numerical procedures was developed using harmonic balance or Hill theory. These contributions are listed below:

a) Development of the harmonic transfer function, and the associated harmonic state space model.

b) Definition of poles as locations in the s-plane where he harmonic transfer function loses analyticity. The s-plane pole eigenvalue problem was developed to compute the s-plane poles and the mode shapes (as periodic functions). The connection of this eigenvalue problem with the Hill determinant methodology.

c) Definition of s-plane zeroes and the development of the s-plane transmission zero eigenvalue problem.

Finally, the singular values or principal gains, and their associated directional properties were developed. Notions of range and domain spaces were presented, and the principal gain diagram was developed.

In Chapter 4, a Nyquist stability criterion for LTP systems was presented. First, a stability theorem was stated based on encirclements of the origin by the Fredholm determinant, $\mathcal{D}_{\widehat{G}(z)}(\mu)$. It was determined that the eigenloci of the LTP transfer function could be used to generate a Nyquist diagram along a suitable Nyquist contour. However, this does not lead to a useful Nyquist stability criterion because the integral operator approaches do not lead directly to numerical techniques. Then, the connection between the Hill theory and the Nyquist theory was developed by developing a harmonic theory analog to the Nyquist criterion developed using the Fredholm determinant. Thus, the eigenloci of the LTP transfer function were computed using the eigenloci of the truncated harmonic transfer function. The eigenloci of the truncated harmonic transfer function can be computed using standard software, such as MATLAB.

The Nyquist methodology was applied to the lossy Mathieu and Meissner equations, and the results are compared to the classical Strutt diagrams. The stable regions correspond in both the Nyquist and Strutt diagrams, and an extensive numerical analysis was discussed to show the effects of truncation.

The Nyquist methodology was shown to be very effective at determining closed loop stability and alleviates difficulties associated with the classical stability methods of Floquet and Hill. Although the examples used to illustrate the multivariable Nyquist test were single

input single output cases, a completely general multivariable Nyquist test was presented. The Nyquist methodology presented here was shown to be a powerful alternative to the classical stability notions of Floquet and Hill, and should prove ultimately prove useful in the general study of the control of linear time periodic systems.

In Chapter 5, the notions of stability robustness from the LTI control theory were discussed in terms of their appli-ability to LTP systems. It was noted that the Small Gain Theorem is a completely general result that applies to any operator for which the input signal space is equal to the output signal space, and for which a suitable H_∞ could be defined. Since the LTP transfer function satisfied both of these conditions, the Small Gain Theorem approaches work for LTP systems as well. Two applications of the Small Gain Theorem were considered in this chapter.

The first example was an examination of the stability robustness properties of the steady state linear quadratic regulator to LTP systems. It was shown that the LQR for LTP systems has the same stability robustness properties, that is, gain and phase margins, as for the LQR applied to time invariant systems. Thus, the linear quadratic regulator has ±60 degrees of phase margin, infinite upward gain margin, and one half downward gain margin for both the LTI and LTP case.

The second example examined in Chapter 5 involved the application of stability robustness rules in the design of LTI controllers for weakly periodic systems. It was shown that the notions of additive and multiplicative perturbations, and their associated stability robustness rules apply equally well in the LTP context. To design the LTI compensator for the weakly periodic system, the time periodic effects were lumped into an output multiplicative perturbation, and the time invariant LQR gains were computed using the average state space model. Satisfying the stability robustness rule ensured that the time periodic effects would not destabilize the weakly periodic system with the time invariant LQR gains. This approach was shown to be conservative, so that the Small Gain Theorem approach tends to overestimate the importance of the time periodicity in the LTP state space model.

6.2   Recommendations for Future Research

Many issues were not examined in the course of this thesis that deserve further study.

In this thesis, the properties of the LTP system were studied numerically using trun-

cations of quasi–Toeplitz forms. Adequate convergence criteria were not developed in the course of this research, in order to understand when the various numerical methods (based on harmonic balance) will converge *a priori*. Instead, convergence was checked numerically. However, it is common in the spectral theory of Toeplitz forms to study the convergence of eigenvalue problems of circulant forms, that is, the finite dimensional truncation of the Toeplitz form [38]. It may be possible to extend the spectral theory associated with Toeplitz forms to doubly infinite block Toeplitz matrices, and then to extend the spectral theory to the quasi–Toeplitz case developed in this thesis. This development would enable the harmonic theory to serve more capably as a computational tool since the study of the convergence properties of the various harmonic balance procedures could begin in earnest.

In Chapter 5, the L_2/H_2 norm was defined. In the LTI theory, optimization of the L_2/H_2 norm provided useful interpretations of the LQG methodology. A similar body of work should prove useful for LTP systems. In addition, a definition of the L_∞/H_∞ norm was proposed. An H_∞ optimization theory comparable to that under current investigation in the LTI theory should prove to be interesting. A solution to this problem has been proposed by Tadmoor [100] using the maximum principle. However, his approach does not address the optimization of the H_∞ norm of an LTP operator directly.

Although all of the procedures developed in this thesis are applicable to multivariable systems, all of the examples in this thesis were of the lossy Mathieu equation or lossy Meissner equation. This was partly by design, since nearly every paper in the literature on LTP systems deals with the Mathieu equation or very minor modifications of the Mathieu equation. The motivating problem in this thesis is the helicopter vibration control problem. Some analytical models are available in a textbook by Johnson [52], however, these models are no more complicated than the Mathieu equation unless complex aerodynamic effects are modeled. Therefore, an unanswered question, at this point, is how well the methods developed in this thesis will work for complex aerodynamic systems such as the helicopter rotor.

Bibliography

[1] A. Allievi and A. Soudack. Ship stability via the Mathieu equation. *International Journal of Control*, 51(1):139–167, 1990.

[2] M. Araki and K. Yamamoto. Multivariable multirate sampled–data systems: state space description, transfer characteristics, and Nyquist criterion. *IEEE Transactions on Automatic Control*, AC-31:145–154, 1986.

[3] J. F. Barman and J. Katzenelson. A generalized Nyquist type stability criterion for multivariable feedback systems. *International Journal of Control*, 20(4):593–622, 1974.

[4] E. C. Bekir and R. S. Bucy. Periodic equlibria for matrix Riccati equations. *Stochastic*, 2(1):1–104, 1976.

[5] J. J. Belletrutti and A. G. J. MacFarlane. Characteristic loci techniques in multivariable systems. *Proceedings of the Institution of Electrical Engineers*, 118:1291–1297, 1971.

[6] R. Bellman, J. Bentsman, and S. M. Meerkov. Stability of fast periodic systems. *IEEE Transactions on Automatic Control*, AC-30(3):289–291, 1985.

[7] S. Bittanti and P. Bolzern. Reachability and controllability of discrete–time linear periodic systems. *IEEE Transactions on Automatic Control*, AC-30(4):399–401, 1985.

[8] S. Bittanti, P. Colaneri, and G. Guardabassi. Periodic solutions of periodic Riccati equations. *IEEE Transactions on Automatic Control*, AC-29(7):665–667, 1984.

[9] V. V. Bolotin. *The Dynamic Stability of Elastic Systems*. Holden–Day, Inc., San Francisco, 1964.

[10] R. W. Brockett. *Finite Dimensional Linear Systems*. John Wiley and Sons, 1970.

[11] R. S. Bucy. The problem of Hill for systems. In *International Conference for Differential Equations*, 1975.

[12] A. J. Calise, M. E. Wasikowski, and D. P. Schrage. Optimal output feedback for linear time periodic systems. In *Proceedings of the 1989 AIAA Guidance, Navigation, and Control Conference*, pages 1232–37, 1989. Paper no. 89–3574–CP.

[13] F. M. Callier and C. A. Desoer. A graphical test for checking the stability of a linear time invariant feedback system. *IEEE Transactions on Automatic Control*, AC–17(12):773–780, 1972.

[14] F. M. Callier and C. A. Desoer. On simplifying a graphical stability criterion for linear distributed feedback systems. *IEEE Transactions on Automatic Control*, AC-21(2):128–129, 1976.

[15] K. C. Chu. Optimal decentralized regulation for a string of coupled systems. *IEEE Transactions on Automatic Control*, AC-19(3):243–246, 1974.

[16] R. V. Churchill. *Fourier Series and Boundary Value Problems*. McGraw-Hill, 1963.

[17] J. A. Cochran. *The Analysis of Linear Integral Equations*. McGraw-Hill, 1972.

[18] H. D'Angelo. *Linear Time-Varying Systems: Analysis and Synthesis*. Allyn and Bacon, 1970.

[19] J. H. Davis. Encirclement conditions for stability and instability of feedback systems with delays. *International Journal of Control*, 15:793–799, 1972.

[20] P. H. Dawson. *Quadrupole Mass Spectrometry*. Elsevier, 1976.

[21] C. A. Desoer and Y. T. Wang. On the generalized Nyquist stability criterion. *IEEE Transactions on Automatic Control*, AC-25(2):105–114, 1980.

[22] J. Dieudonné. *Foundations of Modern Analysis*. Academic Press, 1969.

[23] J. Doyle, K. Glover, P. Khargonekar, and B. Francis. State space solutions to standard H_2 and H_∞ control problems. *IEEE Transactions on Automatic Control*, AC-34(8):831–847, 1989.

[24] R. W. Du Val, C. Z. Gregory Jr., and N. K. Gupta. Design and evaluation of a state-feedback vibration controller. *Journal of the American Helicopter Society*, 29(3):30–37, 1984.

[25] R. W. Du Val and H. Saberi. Active vibration control of the RSRA/X-Wing vehicle using a time domain approach. In *Proceedings of the 44th Annual Forum of the American Helicopter Society*, 1988.

[26] J. Dugundji and V. Mukhopadhyay. Lateral bending torsion vibrations of a thin beam under parametric excitation. *Journal of Applied Mechanics*, 40:693–698, September 1973.

[27] J. Dugundji and J. H. Wendell. Some analysis methods for rotating systems with periodic coefficients. *AIAA Journal*, 21(6):890–897, June 1983.

[28] N. J. Finizio. Stability of columns subjected to periodic axial forces of impulsive type. *Quarterly of Applied Mathematics*, 31:455–465, 1974.

[29] G. Floquet. Sur les équations différentielles linéaires a coefficients périodiques. *Annales de L'Ecole Normale Supérieure*, 12:47–89, 1883.

[30] A. R. Forsyth. *Theory of Differential Equations*. Volume 3, Dover, 1959.

[31] B. A. Francis. *A Course in H_∞ Control Theory*. Volume 88 of *Lecture Notes in Control and Information Sciences*, Springer-Verlag, 1986.

[32] J. S. Freudenberg and D. S. Looze. *Frequency Domain Properties of Scalar and Multivariable Feedback Systems.* Volume 104 of *Lecture Notes in Control and Information Sciences*, Springer-Verlag, 1986.

[33] P. Friedmann, C. E. Hammond, and Tze-Hsin Woo. Efficient numerical treatment of periodic systems with application to stability problems. *Inter. J. for Numerical Methods in Engineering*, 11(7):1117–1136, 1977.

[34] F. R. Gantmacher. *Theory of Matrices.* Chelsea Publishing, 1977.

[35] A. Gelb and W. E. Vander Velde. *Multiple-Input Describing Functions and Nonlinear System Design.* McGraw-Hill, 1968.

[36] M. A. Gockel. Practical solution of linear equations with periodic coefficients. *Journal of the American Helicopter Society*, 17(1):2–10, 1972.

[37] H. P. Greenspan and D. J. Benney. *Calculus: An Introduction to Applied Mathematics.* McGraw-Hill, 1973.

[38] Ulf Grenander and Gabor Szegö. *Toeplitz Forms.* Chelsea Publishing Co., second (textually unaltered) edition, 1958. Reprinted 1984.

[39] H. Gunderson, H. Rigas, and F. S. Van Vleck. A technique for determining stability regions for the damped Mathieu equation. *SIAM Journal of Applied Mathematics*, 26(2):345–349, 1974.

[40] N. K. Gupta. Frequency-shaped cost functionals: extension of LQG design approach. *AIAA Journal of Guidance, Control, and Dynamics*, 3(6):529–535, 1980.

[41] S. R. Hall and N. M. Wereley. Linear control issues in the higher harmonic control of helicopter vibrations. In *Proceedings of the 45th Annual Forum of the American Helicopter Society*, pages 955–972, 1989.

[42] N. D. Ham, N. M. Wereley, and K. D. von Ellenrieder. *Active Control of Gust- and Interference-Induced Vibration of Tilt-Rotor Aircraft.* Technical Report VTL TR 198-2, VTOL Technology Laboratory, Dept. of Aeronautics and Astronautics, Massachusetts Institute of Technology, November 1989. Prepared under NASA Cooperative Agreement No. NCC 2-477.

[43] N. D. Ham, N. M. Wereley, and K. D. von Ellenrieder. Active control of gust- and interference-induced vibration of tilt-rotor aircraft. In *Proceedings of the 45th Annual Forum of the American Helicopter Society*, pages 641–654, 1989.

[44] C. E. Hammond. An application of Floquet theory to prediction of mechanical instability. *Journal of the American Helicopter Society*, 19(4):14–23, 1974.

[45] V. Hernandez and L. Jodar. Boundary problems and periodic Riccati equations. *IEEE Transactions on Automatic Control*, AC-30(11):1131–1133, 1985.

[46] G. W. Hill. On the part of the lunar perigee which is a function of the mean motions of the sun and the moon. *Acta Mathematica*, 8:1–36, 1886.

[47] G. W. Hill. Researches in lunar theory. *American Journal of Mathematics*, 1:129–147, 245–260, 1878.

[48] H. Hochstadt. *Integral Equations*. John Wiley and Sons, 1973.

[49] J. P. How. *Local control design methodologies for a hierarchic control architecture*. Master's thesis, Dept. of Aeronautics and Astronautics, M.I.T., 1990.

[50] P. C. Hughes. *Geometrical Properties in State Space of Linear Differential Equations with Periodic Coefficients*. Technical Report 127, University of Toronto Institute for Aerospace Studies, July 1968.

[51] P. C. Hughes. *Spacecraft Attitude Dynamics*. John Wiley and Sons, 1968.

[52] W. Johnson. *Helicopter Theory*. Princeton University Press, 1980.

[53] T. Kailath. *Linear Systems*. Prentice-Hall, 1980.

[54] H. Kano and T. Nishimura. Controllability, stabilizability, and matrix Riccati equations for periodic systems. *IEEE Transactions on Automatic Control*, AC-30(11):1129–1131, 1985.

[55] H. Kano and T. Nishimura. Periodic solutions of matrix Riccati equations with detectability and stabilizability. *International Journal of Control*, 29:471–487, 1979.

[56] G. Kern. Linear closed-loop control in linear periodic systems with application to spin stabilized bodies. *International Journal of Control*, 31(5):905–916, 1980.

[57] D. W. King. *Design and analysis of a micromechanical tuning fork gyroscope*. Master's thesis, Dept. of Aeronautics and Astronautics, M.I.T., May 1989.

[58] G. A. Korn and T. M. Korn. *Mathematical Handbook for Scientists and Engineers*. McGraw-Hill, 1968.

[59] H. Kwakernaak and R. Sivan. *Linear Optimal Control Systems*. John Wiley and Sons, 1972.

[60] N. A. Lehtomaki. *Practical Robustness Measures in Multivariable Control Systems Analysis*. PhD thesis, Dept. of Electrical Engineering and Computer Science, M.I.T., 1981. Report No. LIDS-TH-1093.

[61] A. Leonhard. The describing function method applied for the investigation of parametric oscillations. In *Proceedings of the 2nd IFAC World Congress*, pages 21–28, Basle, Switzerland, 1963.

[62] A. G. J. MacFarlane. The return–difference and return–ratio matrices and their use in the analysis and design of multivariable feedback control systems. *Proceedings of the Institution of Electrical Engineers*, 117:2037–49, 1970.

[63] A. G. J. MacFarlane and I. Postlethwaite. Generalized Nyquist stability criterion and multivariable root loci. *International Journal of Control*, 25(1):81–127, 1977.

[64] D. C. MacFarlane and K. Glover. *Robust Controller Design Using Normalized Coprime Factor Plant Descriptions*. Volume 138 of *Lecture Notes in Control and Information Sciences*, Springer-Verlag, 1989.

[65] J. M. Maciejowski. *Multivariable Feedback Design*. Addison-Wesley, 1989.

[66] W. Magnus and S. Winkler. *Hill's Equation*. John Wiley and Sons, 1966.

[67] W. Magnus and S. Winkler. *Hill's Equation: Part II. Transformations, Approximations, Examples.* Technical Report No. BR–38, New York University, Institute of Mathematical Sciences, 1961.

[68] E. Mathieu. Mémoire sur le mouvement vibratoire d'une membrane de forme elliptique. *Journal de Mathématiques Pures et Appliquées*, 13:137–203, 1868.

[69] F. J. McHugh and J. Shaw. Helicopter vibration reduction with higher harmonic blade pitch. *Journal of the American Helicopter Society*, 23(4):26–34, 1978.

[70] R. M. McKillip Jr. *Periodic Control of the Individual-Blade-Control Helicopter Rotor.* PhD thesis, Dept.of Aeronautics and Astronautics, M.I.T., 1984.

[71] R. M. McKillip Jr. Periodic control of the individual-blade-control helicopter rotor. *Vertica*, 9(2):199–225, 1985.

[72] N. W. McLachlan. *Theory and Application of Mathieu Functions*. Oxford University Press, 1947. Reprinted by Dover, New York, 1964.

[73] L. Meirovitch. *Analytical Methods in Vibration.* MacMillan Publishing Company, 1967.

[74] E. Meissner. Über Schüttelerscheinungen im System mit periodisch veränderlicher Elastizitat. *Verlag der Schweiz, Bauzeitung*, 72:95–98, 1918.

[75] S. M. Melzer and B. C. Kuo. Optimal regulation of systems described by a countably infinite number of objects. *Automatica*, 7(3):359–366, 1971.

[76] K. S. Narendra and J. H. Taylor. *Frequency Domain Criteria for Absolute Stability.* Academic Press, 1973.

[77] A. H. Nayfeh and D. T. Mook. *Nonlinear Oscillations. Pure and Applied Mathematics*, John Wiley and Sons, 1979.

[78] B. Noble and J. W. Daniel. *Applied Linear Algebra.* Prentice-Hall, 1977.

[79] H. Nyquist. Regeneration theory. *Bell Systems Technical Journal*, 11:126–147, 1932.

[80] L.A. Pipes. Matrix solutions of equations of the Mathieu-Hill type. *Journal of Applied Physics*, 24:902–910, 1953.

[81] S. Pradeep and S. K. Shrivastava. On the stability of the damped Mathieu equation. *Mechanics Research Communications*, 15(6):353–359, 1988.

[82] C. S. Rees, S. M. Shah, and C. V. Stanojevic. *Theory and Applications of Fourier Analysis.* Volume 59 of *Pure and Applied Mathematics*, Marcel Dekker, New York, 1981.

[83] J. A. Richards. *Analysis of Periodically Time Varying Systems. Communications and Control Engineering Series*, Springer-Verlag, 1983.

[84] J. A. Richards. Modelling parametric processes – a tutorial review. *Proceedings of the IEEE*, 65:1549–57, 1977.

221

[85] J. A. Richards. Stability diagram approximation for the lossy Mathieu equation. *SIAM Journal of Applied Mathematics*, 30:240–7, 1976.

[86] J. Rodriguez-Canabal. Geometry of the Riccati equation. *Stochastic*, 1(2):129–149, 1974.

[87] J. Rodriguez-Canabal. Periodic geometry of the Riccati equation. *Stochastic*, 1(4):432–440, 1974.

[88] M. G. Safonov and M. Athans. Gain and phase margin for multiloop LQG regulators. *IEEE Transactions on Automatic Control*, AC-22(2):173–179, 1977.

[89] H. B. Schechter. Dumbbell librations in elliptic orbits. *AIAA Journal*, 2(6):1000–1003, 1964.

[90] G. Schweizer. The analysis of systems with periodically time varying parameters. In *Proceedings of the Fourth Joint Automatic Control Conference*, pages 347–362, Minneapolis, Minnesota, 1963.

[91] G. Schweizer. Eine allgemeine Methode zur Untersuchung von Systemen mit periodisch sich ändernden Koeffizienten. *Archiv der Elektrischen Uebertragung*, 19(9):469–482, 1965.

[92] J. Shaw and N. Albion. Active control of rotor blade pitch for vibration reduction: a wind tunnel demonstration. *Vertica*, 4(1):3–11, 1980.

[93] J. Shaw, N. Albion, E. J. Hanker Jr., and R. S. Teal. Higher harmonic control: wind tunnel demonstration of fully effective vibratory hub force suppression. *Journal of the American Helicopter Society*, 34(1):14–25, 1989.

[94] D. L. Shen. *Effects of Tower Motion on the Dynamic Response of Windmill Rotors*. Technical Report Volume VII, Dept. of Aeronautics and Astronautics, M.I.T., September 1978.

[95] R. Sivaramakrishnan and C. Venkatesan. Rotor/fuselage vibration isolation studies by a Floquet-harmonic iteration technique. *AIAA Journal of Aircraft*, 27(1):81–89, 1990.

[96] M. J. O. Strutt. Der charakteristische Exponent der Hillschen Differentialgleichung. *Math. Ann.*, 101:559–569, 1929.

[97] Y. Sun and I. T. Frish. A general theory of commutated networks. *IEEE Transactions on Circuit Theory*, CT-16:502–508, 1969.

[98] V. Szebehely. *Theory of Orbits*. Academic Press, 1967.

[99] W. Szemplińska-Stupnicka. The generalized harmonic balance method for determining the combination resonance in the parametric dynamic systems. *Journal of Sound and Vibration*, 58(3):347–361, 1978.

[100] G. Tadmoor. *The standard H_∞ problem and the maximum principle: the general linear case*. Technical Report, University of Texas at Dallas, Dept. of Mathematics, May, 1989.

[101] K. Takahashi. An approach to investigate the instability of the multiple degree of freedom parametric dynamic systems. *Journal of Sound and Vibration*, 78(4):519–529, 1981.

[102] J. H. Taylor and K. S. Narendra. Stability regions for the damped Mathieu equation. *SIAM Journal of Applied Mathematics*, 17(2):343–352, 1969.

[103] G. C. Temes and S.K. Mitra (Eds.). *Modern Filter Theory and Design*. John Wiley and Sons, 1973.

[104] M. Vidyasagar. *Nonlinear Systems Analysis*. Prentice-Hall, 1978.

[105] J. E. Wall Jr. *Control and Estimation for Large-Scale Systems Having Spatial Symmetry*. PhD thesis, Dept. of Electrical Engineering and Computer Science, M.I.T., 1978.

[106] S. G. Webb, R. A. Calico, and W. E. Wiesel. Time periodic control of a multi–blade helicopter. In *Proceedings of the 1989 AIAA Guidance, Navigation, and Control Conference*, pages 214–220, August 14–16 1989. Paper No. 89-3449-CP.

[107] E. T. Whittaker and G. N. Watson. *A Course of Modern Analysis*. Cambridge University Press, fourth edition, 1927. Reprinted 1962.

[108] W. Wiesel and W. Shelton. Modal control of an unstable periodic orbit. *Journal of the Astronautical Sciences*, 31(1):63–76, 1983.

[109] C. S. Wolf. *Pole placement for time periodic systems*. Master's thesis, Air Force Institute of Technology, 1982.

[110] L. A. Zadeh and C. A. Desoer. *Linear System Theory: The State Space Approach*. McGraw-Hill, 1963.

[111] G. Zames. On input–output stability of time–varying nonlinear feedback systems – Part I: conditions using concepts of loop gain, conicity, and positivity. *IEEE Transactions on Automatic Control*, AC–11(2):228–238, 1966.

[112] G. Zames. On input–output stability of time–varying nonlinear feedback systems – Part II: conditions involving circles in the frequency plane and sector nonlinearities. *IEEE Transactions on Automatic Control*, AC–11(3):465–476, 1966.